EVALUATION OF REDUNDANCY IN COMPOSITE TWIN-TUB-GIRDER BRIDGES WITH FINITE ELEMENT ANALYSIS

by

Cem Korkmaz

A Dissertation

Submitted to the Faculty of Purdue University

In Partial Fulfillment of the Requirements for the degree of

Doctor of Philosophy

Lyles School of Civil Engineering

West Lafayette, Indiana

May 2018

THE PURDUE UNIVERSITY GRADUATE SCHOOL
STATEMENT OF COMMITTEE APPROVAL

Dr. Robert J. Connor, Co-Chair

Lyles School of Civil Engineering, Purdue University

Dr. Amit H. Varma, Co-Chair

Lyles School of Civil Engineering, Purdue University

Dr. Mark D. Bowman

Lyles School of Civil Engineering, Purdue University

Dr. Karl H. Frank

Department of Civil, Architectural and Environmental Engineering, University of Texas at Austin (Professor Emeritus)

Dr. Brian M. Kozy

Office of Bridges and Structures, Federal Highway Administration

Approved by:

Dr. Dulcy M. Abraham

Head of the Graduate Program

ACKNOWLEDGMENTS

I would like to extend my sincere thankfulness to my advisor, Dr. Robert J. Connor for his endless support, immeasurable guidance, and remarkable patience in my entire development at Purdue University. It has been a great opportunity to study under a very knowledgeable and effective mentor in the steel bridge industry. Dr. Connor is more than an advisor, he is a true friend who always likes to spend time with his students and helps them. I truly believe that he is the best advisor, more than I could ever dream of.

I would also like to express my gratitude to my co-advisor, Dr. Amit H. Varma who generously shared his knowledge about concrete damage modeling for my shear stud study. I also appreciate valuable assistance and collaboration of my graduate committee members, Dr. Mark D. Bowman, Dr. Karl H. Frank, and Dr. Brian M. Kozy.

I would like to specially thank Dr. Francisco Bonachera, Dr. Zhichao Lai, Dr. Kadir Can Sener, Leslie Campbell and Curtis Schroeder for their wonderful friendship and immense support to accomplish my dissertation. It has been my privilege to study with these extraordinary colleagues.

The graduate study herein introduced is part of "Analytical Evaluation of the After-Fracture System Performance of Typical Steel Twin-tub-girder Bridges in the State of Wisconsin" and the NCHRP (National Collaborative Highway Research Program) Project 12-87a, "Fracture-Critical System Analysis for Steel Bridges". The funds from the Wisconsin Department of Transportation (WisDOT) made this graduate study possible. The cooperation of Mr. Scot Becker and Mr. Andrew Smith from WisDOT for very important for completing this research.

TABLE OF CONTENTS

LIST OF TABLES

LIST OF FIGURES

ABSTRACT

Author: Korkmaz, Cem, PhD
Institution: Purdue University
Degree Received: May 2018
Title: Evaluation of Redundancy in Composite Twin-Tub-Girder Bridges with Finite Element Analysis
Major Professor: Robert Connor

High torsional rigidity and attractive aesthetics in construction of twin-tub-girder bridges make them preferable for the design of curved bridges. However, according to the concepts associated with the term "Fracture Critical (FC)" that are in place today, all two-girder bridges are always classified as having FC members. For a steel bridge with FC members, the fracture of any of its members may result in complete catastrophic failure or significant loss of serviceability; hence, every two years twin-tub-girder bridges are subjected to very expensive hands-on field inspection.

Full-scale simple span twin-tub-girder bridge tests at University of Texas Austin have demonstrated excessive load capacity of a fractured simple span bridge. A significant number of twin-tub-girder bridges might be classified as redundant; however, this individual test is not adequate to define the comprehensive damage behavior of twin-tub-girder bridges in general.

In this dissertation, 3D non-linear (material and geometric) detailed finite element (FE) analysis procedures which have been calibrated from full-scale testing providing confidence in the results were developed. The FE models included all the plastic and damage behavior of reinforced concrete deck, brace connections, all steel components of the super structure, stages of construction, and the effects of the dynamic amplification of the bridge immediately following the fracture. Detail work was also performed to define comprehensive shear stud behavior.

In this research, 21 twin-tub-girder bridge units in the existing inventory of the Wisconsin Department of Transportation (WisDOT) were evaluated for the case where one of the two tub girders fails due to brittle fracture. The evaluation was completed using finite element model procedures and the failure criteria described in NCHRP (National Collaborative Highway Research Program) Project 12-87a, "Fracture-Critical System Analysis for Steel Bridges". The analysis has concluded that all bridges analyzed possess considerable reserve strength in the faulted state and that the steel tub girders do not meet the definition of a fracture critical member. Additional analyses were also performed for some bridges with higher load factors than proposed in NCHRP 12-87a in order to investigate the expected failure mode. Additionally, three other typical designs commonly used by other owners were also analyzed; however, none of them has sufficient reserve strength in the faulted state. The effect of section dimensions, bridge continuity, before-fracture dead load displacement and intermediate diaphragms are discussed. Characteristics of bridges which perform well in the faulted stated, which appear to improve the after-fracture system performance of typical steel twin-tub-girder bridges, are presented.

CHAPTER 1 INTRODUCTION

1.1 Motivation

Superior torsional stiffness and attractive aesthetics of twin-tub-girder bridges make them preferable for the design of curved bridges. Along with these features, they are also offer favorable advantages during construction due to their considerable stability and high structural efficiency. However, many bridge owners are not in favor of constructing this type of structure, since twin-tub-girder bridges are classified as fracture critical. According to the concepts associated with the term "Fracture Critical (FC)" that are in place today (2018), all two-girder bridges (including twin-tub-girder bridges) are automatically classified as having FC members (FCMs). For a steel bridge with FCMs, the fracture of any of its members is expected to result in complete catastrophic failure or significant loss of serviceability. As a result, every two years twin-tub-girder bridges are subjected to very expensive hands-on field inspection that must be carried out for the life of the structure by law. Connor et al. (2005) [1] explained that the inspection cost was increased up to 500% more for fracture critical bridges due to the hands-on inspection requirements.

On the other hand, a number of two-girder bridges such as the *Lafayette St. Bridge* (Minneapolis, MN), *Neville Island Bridge* (Pittsburgh, PA), and *Diefenbaker Bridge* (Prince Albert, Canada) bridges did not collapse even when a full-depth fracture occurred in one of the two girders. In fact, in most documented cases, there has not been any considerable serviceability damage post-fracture under normal traffic loads, even though after-fracture system performance was not an explicit consideration during the design. Connor et al. (2007) [2] noted that none of the bridges in which full-depth girder fractures have been observed have collapsed, though in some cases there was considerable deflection. The research by Connor concluded that using more detailed analytical models could be used to evaluate the fracture-critical status of bridges with FCMs. In other words, to determine if a member meets the definition of an FCM using a quantitative engineering-based approach rather than classifying a component as an FCM simply based on the structural configuration (e.g., the girders of all two-girder bridges are FCMs).

Today, non-linear finite element (FE) analysis can be used as an efficient tool to understand the behavior of these bridges in faulted state. With a simulated fracture case, it is possible to classify

the system redundancy of the bridge. Furthermore, to understand the governing damage behavior in the faulted state, additional computational studies can be performed. However, while advanced analytical tools can be used to evaluate the condition of a bridge in the faulted stated, no codified guidance exists regarding such efforts. (*In this document the term "faulted state" refers to the condition in which one of the primary members, traditionally classified as an FCM, has been assumed to have failed.*) For example, while several studies have been performed, there is limited information in the literature which could be used to establish the level of analysis required for performing such an evaluation. Also, there are no universal performance requirements for a bridge in the faulted state. Finally, there is only limited design criteria which can be utilized to improve the after-fracture system performance of twin-tub-girder bridges.

1.2 Research Objective

Recent tests, one at the University of Texas, Austin (UT) (Neuman (2009) [3]) on a simple span twin-tub-girder bridge and research conducted by Purdue University [4] on a simple span truss bridge, have demonstrated the significant reserve capacity of two bridges traditionally classified as FC. However, the number of full-scale experiments is not adequate to define damage behavior of "all" twin-tub-girder bridges. Clearly, the high cost of a full-size test makes the number of experiments that will ever be conducted limited. Fortunately, when properly calibrated, the response of the structure following a member failure can be economically and reliably investigated with 3-D non-linear (material and geometric) detailed finite element analysis procedures.

The purpose of this dissertation is to evaluate the performance of typical twin-tub-girder bridges in the faulted state using FE analysis. The results will be used to suggest new simplified classifications to improve after-fracture system performance of typical steel twin-tub-girder bridges. Bridges meeting the proposed classification would not be classified as having FCMs even though complex non-linear FE analysis (FEA) has not been completed. The FE models include all the plastic and damage behavior of the reinforced concrete deck, brace connections, steel components of the superstructure, stages of construction, and the effects of the dynamic amplification of the bridge immediately following the fracture. In order to more accurately approximate the composite behavior after fracture, comprehensive shear stud damage FE models

were performed. The numerical results were used to improve a simplified methodology to estimate the shear stud strength, stiffness, and ductility.

In this research, twenty-one (21) twin-tub-girder bridge units from the existing inventory of the Wisconsin Department of Transportation (WisDOT) and three other typical designs commonly used by other owners were evaluated for the case where one of the two tub girders fails due to brittle fracture. The evaluation was completed using the finite element model procedures and the failure criteria described in NCHRP Project 12-87a "Fracture-Critical System Analysis for Steel Bridges" [5], of which the author was part of the research team. The analysis has concluded that all bridges analyzed from WisDOT possess considerable reserve strength in the faulted state and that the steel tub girders do not meet the current definition of a FCM. On the other hand, none of bridges analyzed from other owners has sufficient reserve strength in the faulted state such that they meet the performance criteria of NCHRP 12-87a. The effect of section dimensions, bridge continuity, before-fracture dead load displacement and intermediate diaphragms are discussed. Additional analyses were also performed using higher load factors for two bridges which met the performance criteria of NCHRP 12-87a in order to investigate the expected failure mode. Another major outcome of the research is the development of a robust methodology to account for and model the effects of shear stud damage behavior in the faulted stated. Finally, a new simplified classification to improve after-fracture system performance of typical steel twin-tub-girder bridges are suggested.

1.3 Existing Fracture-Critical or Redundant Box-Girder Bridges in the USA

While it is difficult to determine the exact number of fracture-critical box-girder bridges due to variations in how states "code" their bridges in the NBI database [6], a quick examination reveals there appears to be more than 500 as of 2017. Interestingly, almost 40% of these bridges are located in Florida or Texas. The name of U.S. states corresponding to their minimum reported numbers of fracture critical steel box girder bridges are shown in Table 1.

Table 1 The minimum reported numbers of fracture critical steel box girder bridges of U.S. states

U.S. state	Number of Fracture Critical Steel Box Girder Bridges	U.S. state	Number of Fracture Critical Steel Box Girder Bridges
Florida	98	Pennsylvania	8
Texas	81	Rhode Island	5
Massachusetts	41	Idaho	4
Alaska	37	Delaware	3
Colorado	36	Iowa	3
Oregon	24	Missouri	3
Wisconsin	23	Nebraska	3
Connecticut	22	New Jersey	3
Louisiana	21	Kentucky	2
California	20	Mississippi	2
Maryland	19	Arkansas	1
Tennessee	17	Kansas	1
West Virginia	17	Maine	1
Illinois	16	Utah	1
New York	16	Vermont	1
Washington	14	Virginia	1

In the database, the following items are categorized according to "Recording and Coding Guide for the Structure Inventory and Appraisal of the Nation's Bridges" [7].

- Item 41 Structure Open, Posted, or Closed to Traffic: "Open, no restriction (A)"
- Item-43A Kind of material and/or design: "Steel" or "Steel continuous"
- Item-43B Type of design and/or construction: "Box Beam or Girders – Multiple" or "Box Beam or Girders – Single or Spread".
- Item-92A Fracture Critical Details: "Y (Yes)"

The first documented redundancy study focused on twin-tub-girder bridges was performed by Milwaukee Transportation Partners (2005) [8]. As a result of the analysis conducted during that project, it was agreed to classify ten twin-tub-girder bridges (shown in Table 2 from Highway Structures Information System (HSI) [9]) as redundant structures by the Wisconsin DOT and FHWA. It is noted that there was no detailed discussion regarding how shear stud tensile failure was modeled and accounted for nor how it potentially influenced the observed behavior. In full-scale simple span twin-tub-girder bridge tests at University of Texas Austin (Neuman (2009) [3]), researchers have observed significant amount of shear stud concrete break-out failure after the fracture was simulated. Thus, accurately capturing this failure mode is of importance when performing such system analysis.

Table 2 Twin-tub-girder bridges classified as redundant by Milwaukee Transportation Partners

Structural Number	Bridge Name	Year of Construction
B40-1122	Marquette Interchange Ramp-SE	2008
B40-1123-1	Marquette Interchange South to West Ramp Unit 1	2008
B40-1123-2	Marquette Interchange South to West Ramp Unit 2	2008
B40-1131	Marquette Interchange Ramp-SP	2006
B40-1221-1	Marquette Interchange North to East Ramp Unit 1	2008
B40-1221-2	Marquette Interchange North to East Ramp Unit 2	2008
B40-1321	Marquette Interchange West to South Ramp	2006
B40-1421-2	Marquette Interchange Ramp-EN	2008
B40-1422-1	Marquette Interchange Ramp-ES Unit 1	2008
B40-1422-2	Marquette Interchange Ramp-ES Unit 2	2008

1.4 Research Impact

The research project is intended to expand the knowledge on shear stud concrete break-out failure, the evaluation of the fracture critical status of twin-tub-girder bridges, and new simplified classification criteria to improve after-fracture system performance of typical steel twin-tub-girder bridges.

Almost all twin-tub-girder bridges are considered as having FCMs; hence, they have to be inspected with an arm's length inspection method. However, many of these bridges may possess a significant amount of redundancy. The behavior of the tub girder bridges in which an individual

tub is assumed to have completely fractured is presented in detail by this dissertation. Extension of the inspection periods or the use of a more economical inspection type may be performed for redundant twin-tub-girder bridges.

As a part of this research, the general procedures developed for redundancy evaluation were applied to Ramp TH over Interstate 43/894 in Milwaukee, Wisconsin. The approach was reviewed by Wisconsin DOT and the FHWA and was approved as satisfying the FHWA requirements for system analysis. Hence, this bridge is no longer classified as having FCMs, but rather has been classified as having SRMs as documented in a Memo to the Wisconsin DOT (dated April 19, 2016) [10]. As a result, arm's-length biennial field inspections are no longer required for this structure. The results of this study, which has now expanded to include many more bridges, has shown that many multi-span twin-tub-girder bridges in Wisconsin possesses sufficient reserve capacity even when one girder is completely severed. The impact of this work is significant, not only for the state of Wisconsin, but also for the many other states which use similarly designed and detailed twin tub structures as the would likely be classified as having SRMs and not FCMs. Doing so will result in more rational use of limited inspection funds as well as increase the safety for inspectors and the public since unneeded interruptions in traffic will not be required for unnecessary inspections.

CHAPTER 2 PRIOR RESEARCH AND BACKGROUND

Previous studies on the subject of tub-girder redundancy, shear stud concrete break-out, and fracture-critical system level redundancy are explained in this chapter. The review is divided into four parts. The first part discusses research about shear stud concrete break-out failure behavior. The second part focuses on the existing experimental studies about the fracture behavior of twin-tub-girder bridges. The next part gives information about previous FE model details related to this topic. The final part describes a study of fracture-critical system level redundancy evaluation.

2.1 Shear Stud Concrete Break-out Failure

2.1.1 Mouras et al. (2008) [12]

The concrete capacity design (CCD) approach in ACI 318-14 [11] provides the best approximation to calculate concrete break-out strength; however, this formulation does not consider the effects of the haunch. In Mouras et al. (2008) [12] study, it was shown that the deck with a haunch would have lower shear stud tensile capacity than the deck without a haunch, since the full concrete break-out cone was restricted by the edges between the studs and the haunch. Mouras et al. (2008) [12] developed a new modification factor for the CCD approach to consider the slab haunch effect. The existing methodology to account for the effect of the haunch is presented in the AASHTO LRFD Bridge Design Specifications (AASHTO LRFD BDS) [13] "Section 6.16.4.3-Shear Connectors". Comparing the available photographs of the small-scale experiments performed by Mouras et al. (2008) [12] to those from the full scale tests performed by Neuman (2009) [3], it appears to the author that there may have been less flexural cracking in the full-scale test (e.g., compare the behavior shown in Figure 1 and Figure 2). Comparing the figures, the bottom of the slab does not appear to have any flexural cracking, or at least very little when compared to the small-scale test. Both the large-scale and small-scale experiments used three transversely grouped 5-inch-tall shear studs, embedded in a 12-inch-wide and 3-inch-thick haunch. The studs were spaced longitudinally at approximately 2 feet. In Figure 1, the concrete break-out failure cone occurred during the fracture in the full-scale twin-tub-girder experiment is shown. Whereas in the small-scale experiment by Mouras et al. (2008) [12], it appears that flexural cracking at the corner of haunch

may have had a greater influence on the overall behavior. This would explain the horizontal haunch separation, and center haunch splitting as shown in Figure 2.

Figure 1 Neuman (2009) [3] concrete break-out failure geometry after second full-scale twin-tub-girder experiment performed

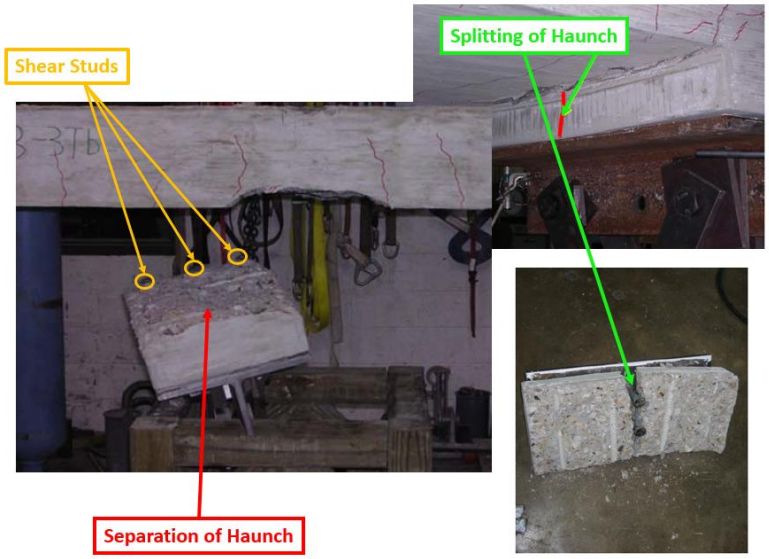

Figure 2 Mouras et al. (2008) [12] small-scale experiment failure geometry

While these subtle differences may appear trivial, it is possible that the effects of transverse flexural cracking were less pronounced in the large-scale test. However, if the spacing between the girders was much greater, as is the case in some of the bridges analyzed herein, the flexural effects could be underestimated. In summary, the methodology proposed by Mouras may result in conservative or unconservative estimates of the tensile capacity of a given shear stud arrangement as only a single geometry was considered. This will be discussed further in CHAPTER 4.

2.2 The Existing Experimental Studies

2.2.1 Neuman (2009) [3]

The purpose of this study was to demonstrate the redundancy of simple-span curved twin-tub-girder bridges using full-scale destructive tests. The full-scale specimen was originally in-service at the interchange between IH-10 and Loop 610 in Houston. Due to the road expansion at this interchange, the girder was removed. After the reconstruction process of the bridge, three full-scale destructive tests were performed. In the first experiment, the bottom tension flange at the exterior girder was fractured instantaneously in the middle of the simple span. The web remained fully intact. No major plasticity, no damage, and no crack initiation into the web was observed. In Test 2, the girder was supported with scissor jacks which were used to raise the bridge to its original position prior to Test 1 and the web was cut using a torch to a depth 10" below the top flange surface. Once all cutting was completed, the scissor jacks were quickly removed (again using a shape-charge mechanism); hence, the partial web and complete bottom flange fracture was simulated. It is noted that since the girder was effectively cut, with the exception of the top flange, no strain energy was released from the steel girder itself. Rather, the effects of removing the support from a girder that was significantly cut were only simulated. A considerable amount of concrete break-out damage on the interior top flange of the cut girder was observed.

The object of the third and final test was to investigate the maximum loading capacity. As additional load was applied, the following conditions were observed: excessive shear stud failures (tensile pull out), parapet crushing, excessive deck reinforcement yielding, and excessive deformation. The bridge started to collapse when the applied load reached approximately 360 kips.

Overall, the UT tests showed that the twin-tub-girder bridge possessed a tremendous amount of reserve capacity, carrying loads far in excess of the original design loads even in the faulted state. However, during these experiments, the top flange was not severed, and it provided significant continuity through membrane action. While it may seem unlikely that the entire girder could suddenly fracture, such behavior was observed during the fracture on Hoan Bridge. According to Hoan Bridge Investigation [14], the web fracture propagated through top compression flanges in two of three girders. If full depth fracture had been performed during the UT test, the outcome of

the experiment would likely have been much different. In other words, the bridge might have collapsed in Test 1, assuming the entire tub girder was severed in the first step. Nevertheless, this project provided very important data since these three tests could be used to improve the FE methodology for twin-tub-girder bridges. It is noted that in Chapter 4 of this document, using the benchmarked FE methodology, the effects of a full-depth fracture in the UT test specimen were simulated and the results reported.

2.3 FE Model Details and Existing Parametric Studies for Twin-tub-girder Redundancy

2.3.1 Hunley (2008) [15]

The purpose of the study by Hunley (2008) [15] was to develop an FE model to evaluate the redundancy of twin box girder bridges. A parametric study was performed to investigate the effects of girder spacing, bridge continuity, curvature, location of girder damage, and type and spacing of external bracing on bridge redundancy. In order to determine the functional limit of the models, the ultimate load capacity methodology in NCHRP Report 406 (1988) [16] was utilized.

Detailed finite element models were performed with ANSYS/CivilFEM (2007) software. However, rigid elements were used for the shear studs; and there was no detailed information provided about how the potential failure of the shear studs was modeled and included in the study. On the other hand, Neuman (2009) [3] observed significant amount of shear stud concrete break-out failure after the web fractured. If the pull-out failure mode was prevented in the Hunley study, the FE model likely over predicted the reserve strength in the faulted state. In addition, the dynamic amplification factor of the sudden failure was not considered in the models. This is unconservative based on the full-scale UT twin-tub-girder test by Neuman (2009) [3] in which the average dynamic amplification factor was 0.3 and the Milton Madison in-situ fracture test by Diggelmann et al. [4] in which the dynamic amplification factors varied from 0.17 to 0.41.

In conclusion of this study, it was found that some twin-tub-girder bridges possess sufficient redundancy when using the procedures proposed in NCHRP 406. Use of external braces increased the redundancy. The braces provided alternative load paths; therefore, the displacement with the

corresponding loading was reduced. In addition, continuous bridges had higher redundancy factor because of their continuity effect.

2.3.2 Kim & Williamson (2015) [17]

Another finite-element bridge modeling methodology was improved by Kim & Williamson (2015) [17]. The developed FE model was validated with Neuman's (2009) [3] full-scale experimental results. The shear stud concrete break-out failure mechanism was also considered. In this research project, material inelasticity, concrete cracking, and deck haunch separation were determined and explained in detail. The results obtained from the improved FE analysis were close to the full-scale bridge fracture tests' results. The developed model consisted of the post-fracture behavior as well. However, the cast iron steel model was assigned for the concrete compression plasticity and the concrete crack modeling. The cast iron steel was very similar to elastic perfectly plastic behavior. Cast iron plasticity material parameters were determined according to corresponding experiment results which improved the concrete deck model, but only for this specific bridge. This deck model might not be capable to simulate other twin-tub-girder bridges; therefore, it was not recommended to perform a parametric study with this model.

2.4 Fracture-Critical System Level Redundancy Evaluation

2.4.1 Bonachera (2016) [18]

In Bonachera (2016) [18], a detailed finite-element bridge modeling methodology was improved. In particular, this study provided a guideline to apply concrete pouring sequence modeling. Furthermore, reliability-based load combinations and minimum performance criteria in the faulted state were utilized to evaluate redundancy of existing twin-tub-girder bridges. Chapter 5 includes more detailed information about the load combinations and minimum performance criteria developed by Bonachera (2016) [18] and explained in NCHRP Report 12-87a [5]. Bonachera was part of the research team for the study NCHRP 12-87a.

New load combinations and associated load factors were developed to evaluate the redundancy of a bridge in the faulted condition. Bonachera (2016) [18] use the statistical parameters of both load and resistance, and a specific target reliability index as well as input from an expert consensus panel to determine the load factors for two load combinations. These load combinations are

referred to as Redundancy I and II. The Redundancy I load combination is to be used at the instant fracture occurs and includes the effects of inertial dynamic amplification. As has been discussed, the bridge will likely continue carrying traffic during the time period after the fracture occurred but prior to its discovery. This interval is assumed to be between 5 and 50 years. In order to evaluate the performance of the bridge in the faulted state during this period of time, Redundancy II load combination is intended to be used, reflecting the greater variability in live load due to the longer exposure period.

Certain strength and serviceability limits are supposed to be used to evaluate the analyzed bridge whether it has adequate capacity in the faulted state; hence the safety of the traveling public can be provided. These strength criteria and several minimum serviceability requirements must be met to determine that the bridge is redundant.

Bonachera's study which is presented in NCHRP 12-87a provides the first codified methodology to systematically evaluate the redundancy of the most common types of steel bridges that possess FCMs. Further, it provides guidance on modeling, load combinations, and performance criteria in the faulted state.

CHAPTER 3 FINITE ELEMENT MODELING DETAILS

Properly calibrated 3-D detailed finite element analysis developed in the current study is the most suitable analysis tool to adequately evaluate the redundancy of the twin-tub-girder bridges. The FE solver utilized was Abaqus 2017. The analytical approach is summarized below.

3.1 Parts, Materials and Element Details

There are four major part components of the twin-tub-girder bridges that have been modeled in detail. The analysis included non-linear geometry and material models. Each component is described below along with information pertaining to the type of elements selected and material property models.

3.1.1 Reinforced concrete deck and parapet

The reinforced concrete deck was defined using four-node linear shell elements (S4R) with reduced integration (shown in Figure 3), finite membrane strains, and a minimum of five Simpson thickness integration points. The transverse and lateral reinforcement in the concrete deck was modeled as a part of the reinforced concrete shell section. The section orientation followed the radius of the curvature of the structure.

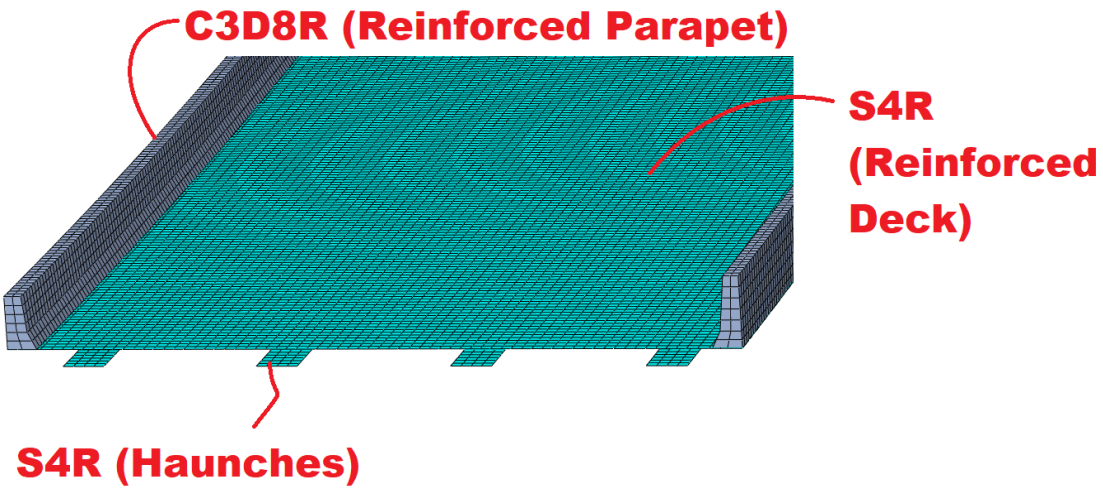

Figure 3 Finite element mesh of deck and parapet

Due to the fact that the shell elements are not capable of capturing shear cracking (when used in the concrete slab), the nominal shear capacity of the slab was also analyzed explicitly. The nominal shear capacity was calculated by using the formulation in ACI 318-14 [11] "Section 22.5.5.1". The transfer shear of the deck was measured directly from FE analysis. By referencing the approach defined in Barnard et al. (2010) [19], the adequate capacity was checked that the shear forces would be transferred through the deck. The element aspect ratio was held constant at 1.0 as much as possible. Using shell elements to model the composite deck greatly improves the efficiency of the model without compromising the fidelity. The mesh seed size was set to 6 inches.

The concrete parapet was defined using eight-node solid elements (C3D8R) with reduced integration (shown in Figure 3). The element aspect ratio was set to approximately 1. The transverse and lateral reinforcement in the concrete parapets was modeled using 2-node linear truss elements (T3D2). The average seed size of the truss elements was set equal to the average seed size of the solid concrete elements. The reinforcement between the deck and parapet was not included in the FE models. The equivalent shear stiffness between the deck and parapet was assumed to be infinitely high, whereas this stiffness depends on rebar stiffness and friction between the interfaces.

The well-known concrete damage plasticity (CDP) material model provided in Abaqus was utilized in order to define isotropic concrete compressive crushing and tensile cracking behavior. The CDP model was used to define inelastic behavior of the concrete. The CDP model is based on isotropic damaged elasticity which is coming from the combination of isotropic tensile and compressive plasticity. In the CDP model, the damage due to the concrete hardening and the tensile cracking is irrecoverable. The elastic modulus of concrete was defined according to ACI 318-14 [11] "Section 19.2.2.1". Poisson's ratio was set at 0.2 for all concrete. The compressive behavior of the concrete was assigned according to the empirical stress-strain curve proposed by Popovics (1973) [20]. Linear elastic behavior was assigned up to initial yielding, and then inelastic behavior was defined.

Figure 4 shows the compressive stress-strain ($f_c(\varepsilon)$) diagrams of the concrete with ultimate compressive strength (f_c'). ε is unit strain of concrete, $n_{concrete}\ and\ k$ is the experimental parameter.

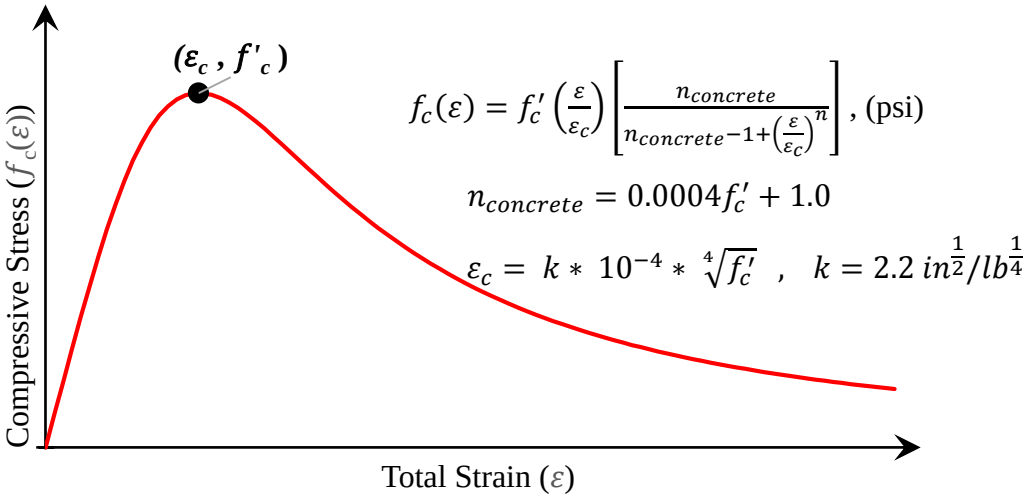

Figure 4 Concrete compression behavior according to Popovics (1973) [20]

The concrete tensile behavior is based on the fictitious crack model of Hillerborg et al. (1976) [21]. Cracking displacement was used instead of the cracking strain to reduce the mesh sensitivity for non-reinforced concrete. The tensile strength and tension stiffness were calculated in accordance with the fracture energy principles and empirical models noted in FIB Model Code 2010 [22]. Figure 5 shows the tensile stress-crack opening displacement ($f_t(\delta)$) bi-linear softening curve of the concrete with tensile strength (f_t (psi)). δ is crack opening displacement, G_t is the fracture energy of concrete, f_{cm} (psi) is mean compressive strength (known for experiment benchmarking), f_{ck} (psi) is design compressive strength (known from bridge design plans).

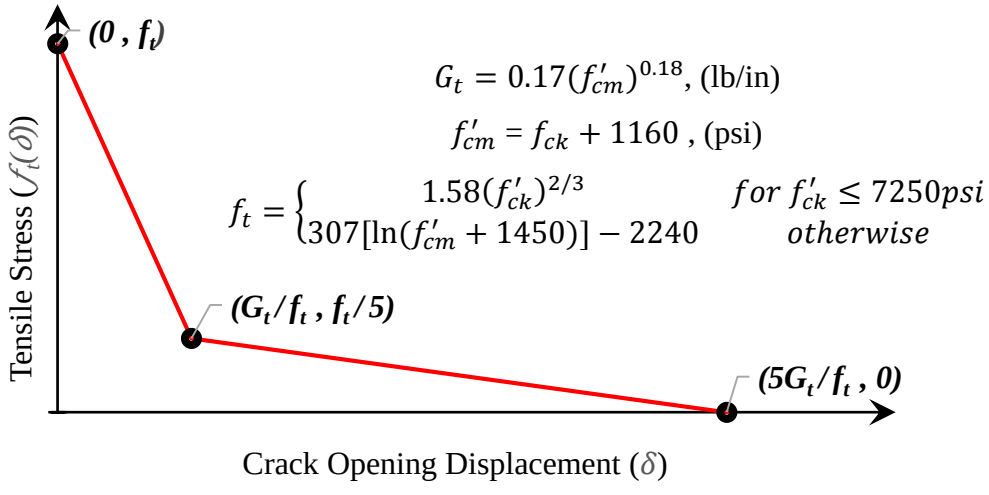

Figure 5 Concrete tensile softening behavior according to the FIB Model Code 2010

The dilation angle ψ which controls the amount of the volume change under shear plasticity was set to 31 in the bridge models, this is the most commonly recommended number by many researchers according to Genikomsou & Polak (2015) [23]. On the other hand, a higher dilation angle was preferred to be used for small scale shear stud experiments (CHAPTER 4) since the concrete under the shear stud head is significantly confined by the surrounding concrete. According to Abaqus 2017 Documentation [24] which is based on Lubliner et al. (1989) [25] experiments, the following terms were defined for the other plasticity parameters which are flow potential eccentricity (0.1), the ratio of initial biaxial compressive yield stress to initial uniaxial compressive yield stress (1.16) and, the ratio of the second stress invariant on the tensile meridian (0.667). The material models did not have the effect of strain rate on concrete tensile and compressive strength. In addition, the time-dependent behaviors of concrete sections such as creep, shrinkage, crack growth and concrete strength increase were not included in the FE models.

The yield strength (σ_y) of the stainless-steel bar reinforcement, Grade 60 was set to be 60 ksi with the ultimate tensile strength (σ_u) set equal to 90 ksi. The steel material is based on Von Mises yield surface, associated flow rule, and kinematic hardening. The defined steel has 29000 ksi elastic modulus (E_s) and 0.3 poisson's ratio. The failure strain was assumed to be 0.05. This is a conservative, but reasonable estimate of the limiting fracture strain. Figure 6 shows the stress-strain ($\sigma(\varepsilon)$) diagram. The assigned curve refers to Bonachera (2016) [18].

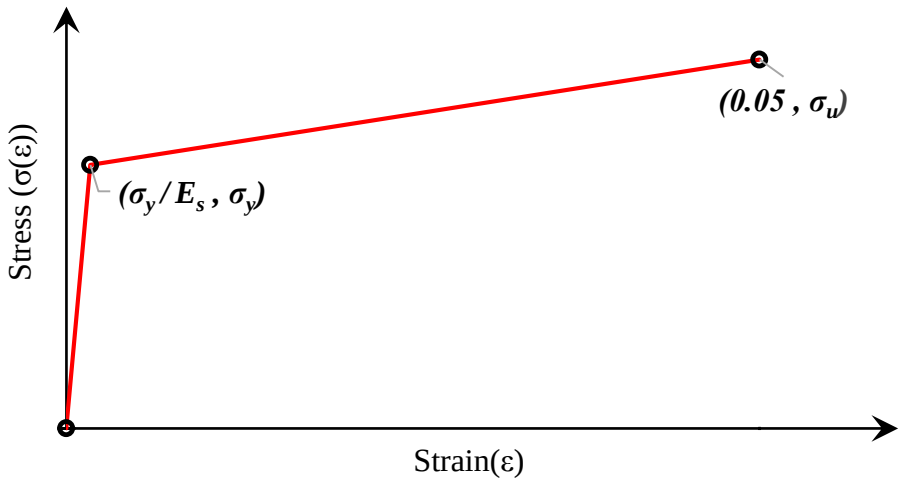

Figure 6 Steel stress-strain diagram

The minimum required number of integration points and element sizes were verified through a convergence study. In this study, a reinforced concrete slab under four-point bending (Figure 7) was simulated to compare the results from a solid slab incompatible mode element model which includes truss elements for its reinforcement (Figure 8) to a shell reduced integration element model (Figure 9). Top and bottom reinforcement were provided in the slabs. In the solid model, four elements through thickness was provided. In the shell model, the element size was approximately 6 in. which was same as the element size used in the twin-tub-girder bridge models.

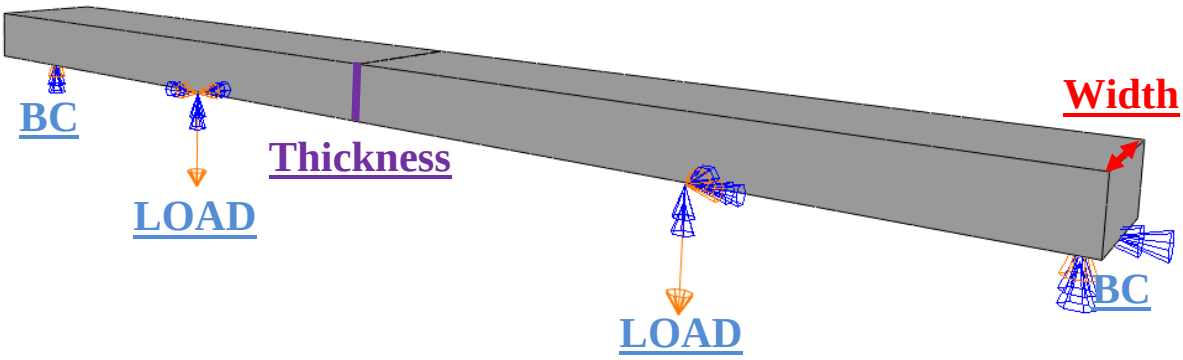

Figure 7 A reinforced concrete slab under four-point bending

The most common deck configurations of the twin-tub-girder bridges in CHAPTER 7 were used in this study. In total, twenty detailed non-linear finite element models were used to compare the flexural strength of the solid model and shell model to the calculation in ACI 318-14 [11] Chapter 22. The parameters included in the study were as follows:

- Concrete compressive strength: 4, 5, 6, or 7 ksi.
- Slab thickness: 8, 9.5, 10, 10.5, or 11 inches.
- Slab width: 20 or 28 inches.
- Top and bottom rebar size: #5 or #6.
- Spacing of rebars: 5 or 7 inches.
- Concrete clear cover for top reinforcement: 2, 2.5, or 3.5 inches.
- Concrete clear cover for bottom reinforcement: 2, 1.5, or 3.5 inches.

The moment capacities of solid, shell and ACI methodology were shown in Table 3. Note, no "phi" factors were used in the comparisons with the ACI predictions since a nominal capacity should be used for this comparison. The differences in moment capacity are within 10%; hence, the shell model can accurately and economically estimate the moment capacity of the slab.

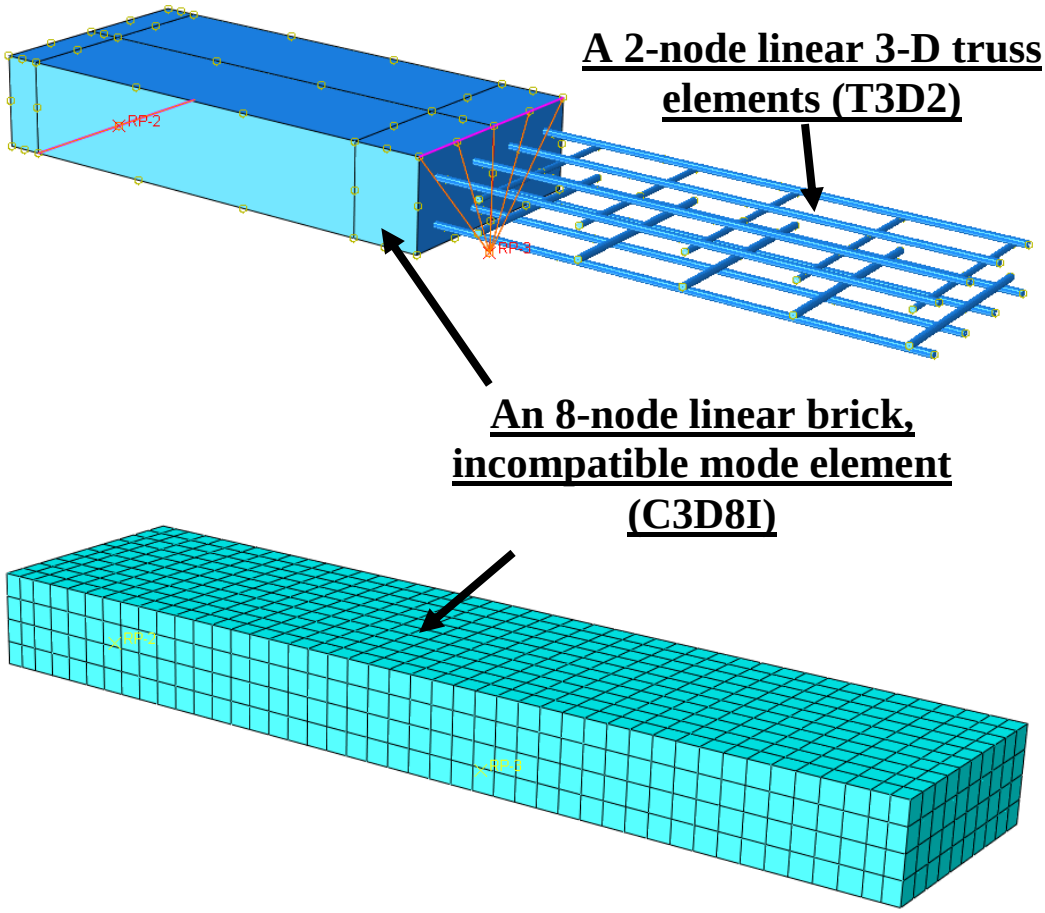

Figure 8 A solid slab mesh elements with incompatible modes

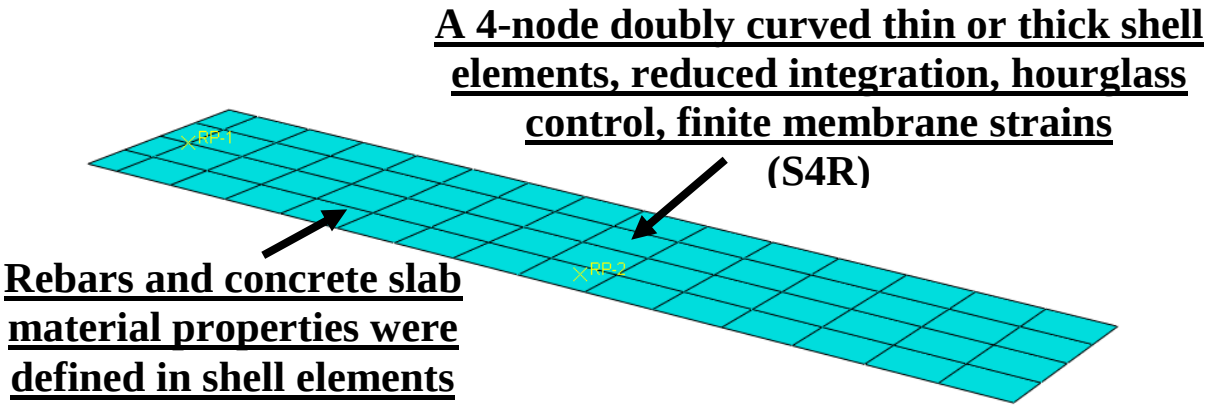

Figure 9 A shell slab mesh element with reduced integration

Table 3 The moment capacities of solid, shell and ACI methodology

Slab			Top Rebar			Bottom Rebar			Moment (kips.in)			Difference (%)	
Concrete Strength (ksi)	**Thickness (in)**	**Width (in)**	**Size (#)**	**Clear Cover (in)**	**Spacing (in)**	**Size (#)**	**Clear Cover (in)**	**Spacing (in)**	**Solid (C8)**	**Shell (S4)**	**Calc (AC)**	**1-S4/AC**	**1-S4/C8**
4	8	20	5	2.0	5	5	1.5	5	449	429	450	5	4
	9.5	28	5	3.5	7	5	1.5	7	740	681	740	8	8
	10	28	6	2.5	7	6	1.5	7	856	852	888	4	0
	10.5	28	6	3.5	7	6	1.5	7	979	964	1061	9	2
	11	28	6	2.5	7	6	1.5	7	997	973	993	2	2
5	8	20	5	2.0	5	5	1.5	5	477	456	476	4	4
	9.5	28	5	3.5	7	5	1.5	7	761	738	763	3	3
	10	28	6	2.5	7	6	1.5	7	891	911	939	3	-2
	10.5	28	6	3.5	7	6	1.5	7	1046	1031	1133	9	1
	11	28	6	2.5	7	6	1.5	7	1055	1041	1045	0	1
6	8	20	5	2.0	5	5	1.5	5	503	484	498	3	4
	9.5	28	5	3.5	7	5	1.5	7	768	800	778	-3	-4
	10	28	6	2.5	7	6	1.5	7	954	970	982	1	-2
	10.5	28	6	3.5	7	6	1.5	7	1143	1105	1164	5	3
	11	28	6	2.5	7	6	1.5	7	1066	1108	1087	-2	-4
7	8	20	5	2.0	5	5	1.5	5	525	509	516	1	3
	9.5	28	5	3.5	7	5	1.5	7	775	839	790	-6	-8
	10	28	6	2.5	7	6	1.5	7	984	1032	1016	-2	-5
	10.5	28	6	3.5	7	6	1.5	7	1180	1189	1187	0	-1
	11	28	6	2.5	7	6	1.5	7	1117	1203	1122	-7	-8

The load-displacement behavior from the solid and shell models was also compared, and the solid and shell model results are shown in Figure 11. The displacement was measured where the force was applied, this was 39 in. away from the support. The models were displaced up to when the rupture of the bottom reinforcement occurred; in other words, the total strain of the reinforcement was equal to 0.05. Even if crack displacement methodology reduces the mesh sensitivity for non-reinforced concrete, when the reinforcement is embedded in the concrete element, the relative strain of the reinforcement depends on the element mesh sizes. The smaller elements result in early rupture behavior. In the solid model, therefore, solid reinforcements were used in the concrete elements with a void in the concrete element where the reinforcement is located (Figure 10). The surfaces of the reinforcement were tied to surface of the concrete void. The load-displacement behavior (Figure 11) of an 8 in. thick 4 ksi concrete slab has a very good approximation between the models, and the shell model conservatively captured the rupture behavior.

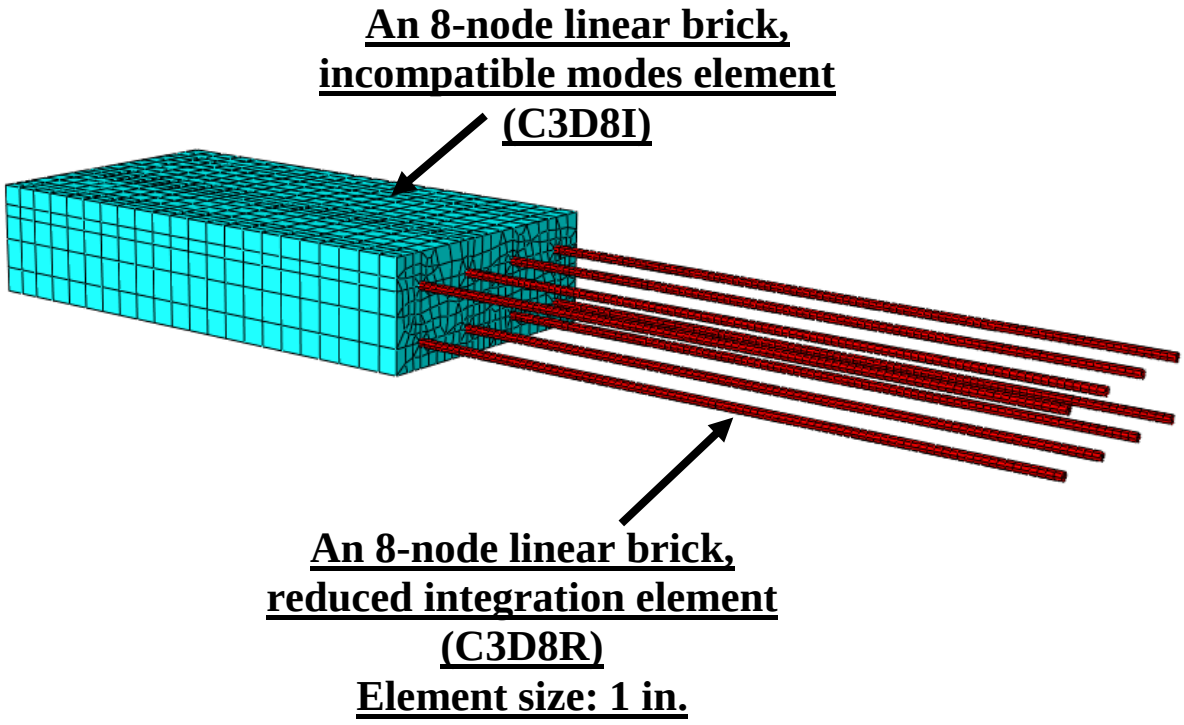

Figure 10 A solid slab mesh elements with solid reinforcement elements

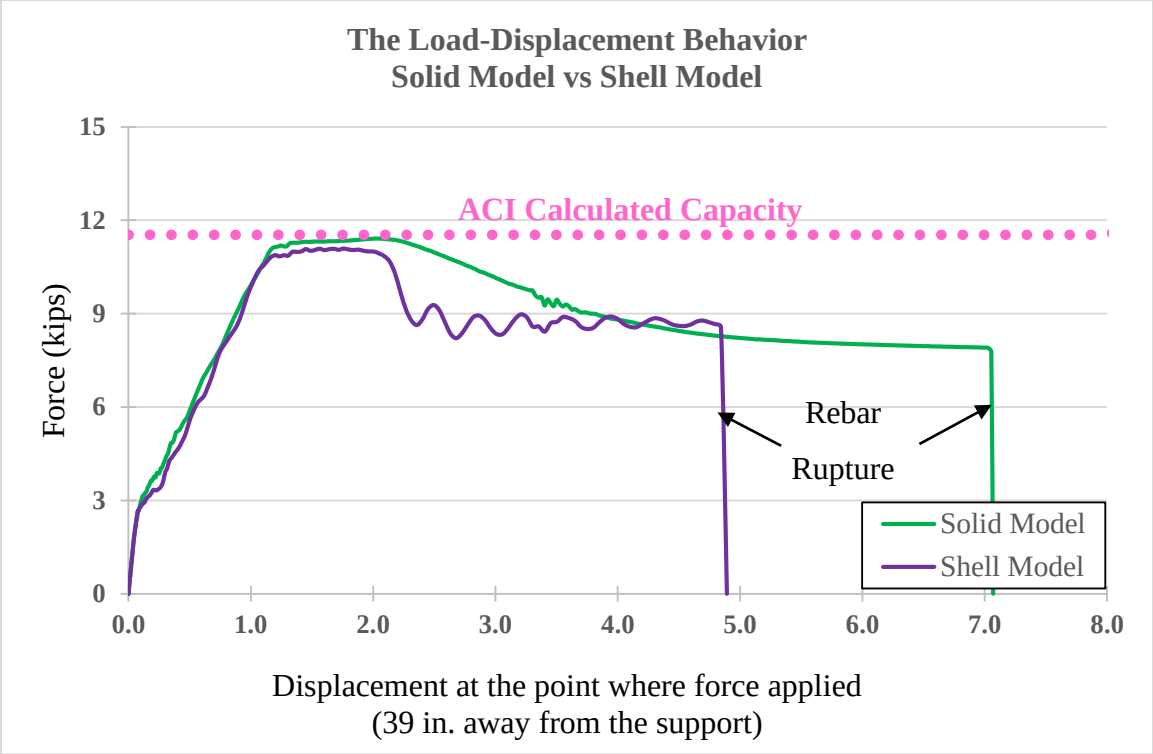

Figure 11 The load-displacement behavior of 8 in. thick 4 ksi concrete slab

Stages of deck placement are also included in the models. However, no staging of steel erection is modeled. The finite element analysis was divided into two parts. The first portion was performed using implicit static analysis for the construction sequence. The concrete pouring sequence modeling procedure refers to Bonachera (2016) [18]. In the approach recommended by Bonachera, only the factored self-weight of the steel girders and wet concrete was applied to the steel tub girders in the initial implicit step. The wet concrete and all reinforcement was modeled by assigning very low stiffness for the concrete and rebar. The wet concrete elements were tied to the top surface of the flanges, and as a result, the deck and rebar displace downward with the girders under dead load. Thus, unintended concrete settlement was avoided. After this step, the strain of the slab was reset to zero. In explicit dynamic analysis (the second portion), the deck was then "hardened" in the FE model by increasing the stiffness of the concrete and rebar. Then, the analysis continued by introducing the simulated fracture, assigning additional factored loads and evaluating the performance of the bridge in the faulted state.

3.1.2 Tub girders, web stiffeners, end diaphragms, and end diaphragm stiffeners

Figure 12 illustrates the steel components of the twin-tub-girder system. The steel tub girder system was defined using 4-node shell elements (S4R). These are general purpose reduced integration elements with hourglass control. At least five elements were used along the depth of the web and at least four elements were used across the width of the flange to obtain accurate estimates of possible buckling behavior. This approach was benchmarked using the data from brace experiments performed by Wang [26] at University of Texas, Austin. In Wang's study, it was observed that the buckling capacity and stiffness were governed by the effects of applied load eccentricity instead of the effects of material imperfection and residual stress.

Von Mises yield surface, associated flow rule, and kinematic hardening were also used to assign the steel material multiaxial behavior. The yield and ultimate stresses was assigned based on the material specified on the design plans. For example, ASTM A709 Grade HPS 50W has an assumed yield stress of 50 ksi and tensile stress of 70 ksi, and Grade HPS 70W has an assumed yield stress of 70 ksi and tensile stress of 85 ksi. Ultimate stress was conservatively set to correspond with a strain of 0.05. The elastic modulus was assumed to be 29,000 ksi and Poisson's ratio was set equal to 0.3. The assigned stress-strain curve follows the diagram in Figure 6.

The material models did not have the effect of strain rate on steel tensile and compressive strength. The time-dependent behaviors of steel sections such as corrosion were not included in the FE models. The effect of temperature was not considered. Residual stress and section imperfection was not included in the models. In order to simplify models, the details in the bridges which are human holes in the diaphragms, plate thickness transition section, vertical elevation differences, horizontal slope in alignment layout, and camber in plate section were neglected.

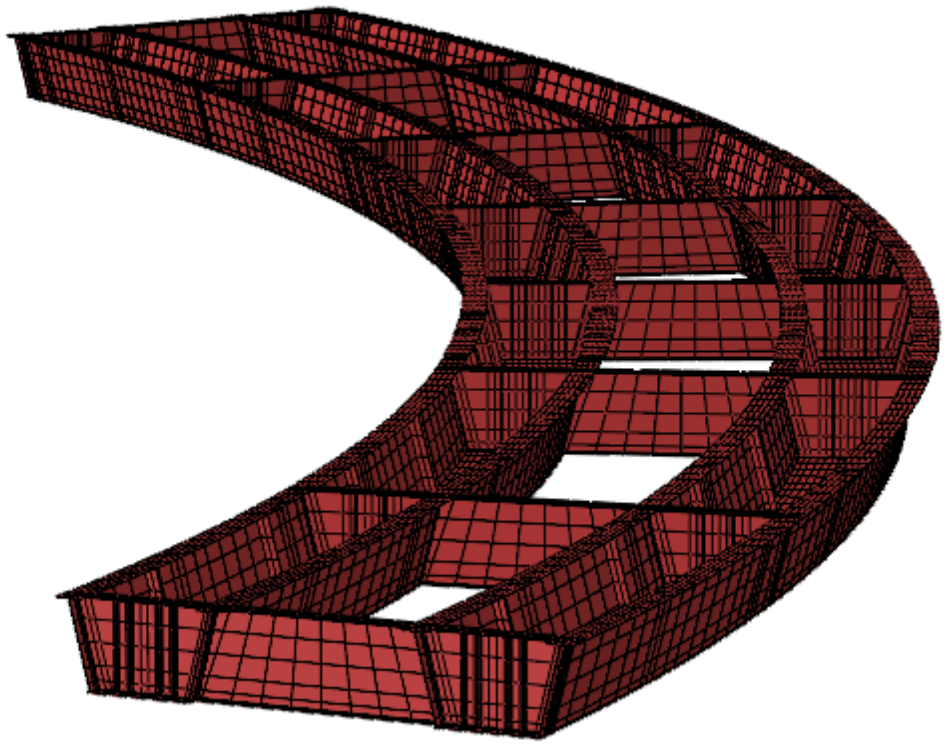

Figure 12 Shell model (S4R) of twin-tub-girder system

3.1.3 Internal cross frames, lateral braces and longitudinal stiffeners

All internal cross frames and lateral braces were modeled using traditional Timoshenko beam elements (B31). The gusset plates were defined using four-node linear shell elements (S4R) with reduced integration. In Figure 13, the blue and green colors show lateral brace locations and the white color denotes the location of the internal cross frames and struts. In Figure 14, an internal cross frame with connections is shown in detail.

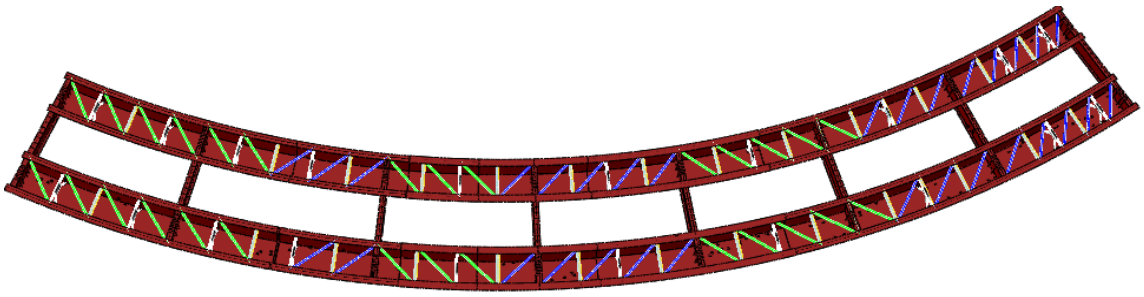

Figure 13 Top view of all braces

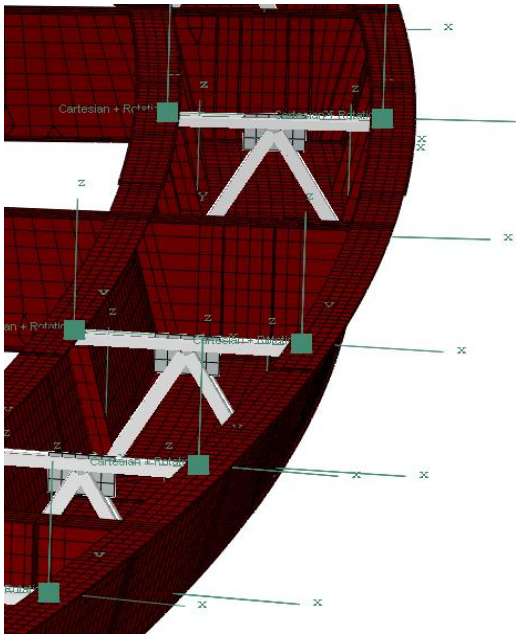

Figure 14 Internal cross frame & connection details

The eccentricity of the single bracing components significantly reduces the buckling capacity and stiffness of the brace. The eccentricity of each brace was specified in the section definition within the FE model as shown in Figure 15.

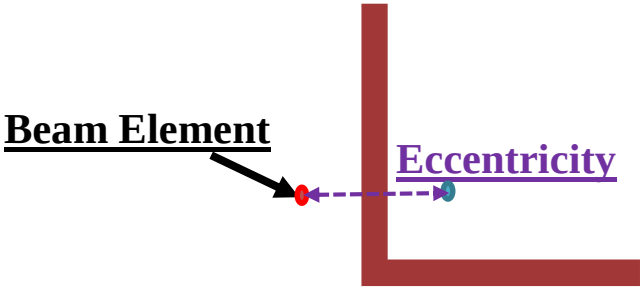

Figure 15 Eccentricity in beam element

The approach with an eccentricity was benchmarked and verified according to the experiments published by Wang [26]. For the analyzed bridges in CHAPTER 7, all internal cross frames have K-frame geometry. The following K-Frame geometry was used from Wang [26] for benchmark study.

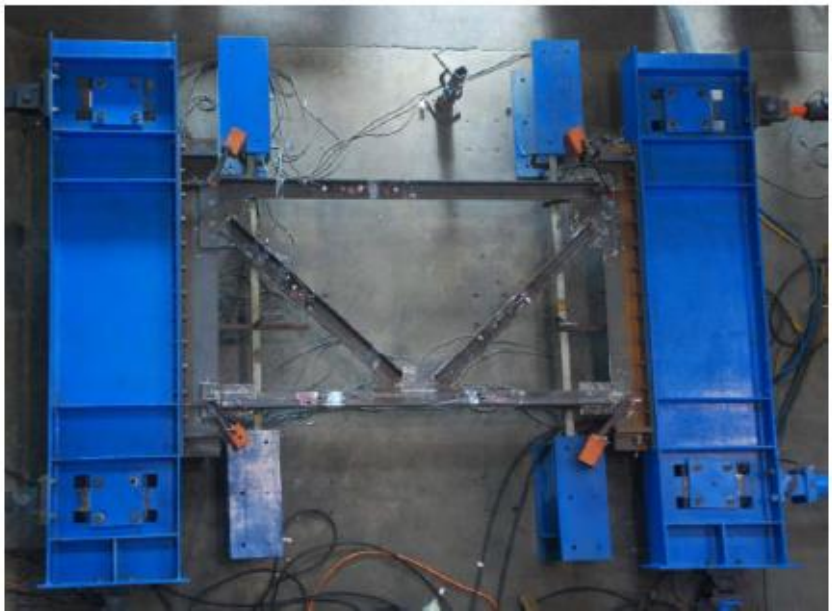

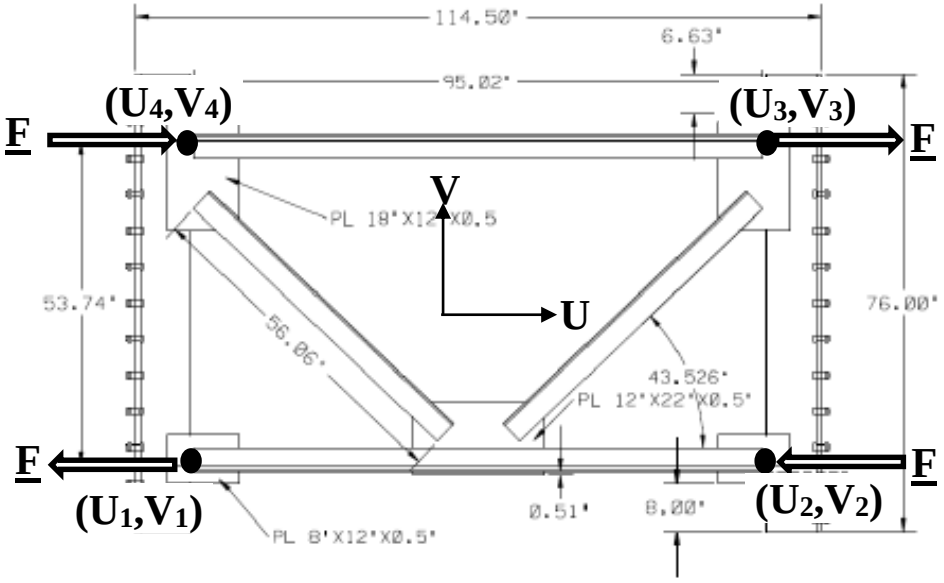

Figure 16 Single K-frame specimen details from Wang [26]

The specimens were loaded until buckling occured in the compression diagonal of the experiment (shown in Figure 17) and the FE models (shown in Figure 18). In the experiments, the yield

strength of the steel was 57 ksi. In FE model, elastic perfectly plastic material properties were assigned. All angles consisted of L4x4x3/8 sections. Gusset plate thicknesses were 0.5 in.

Figure 17 Buckling of the single angle K-frame from Wang[26]

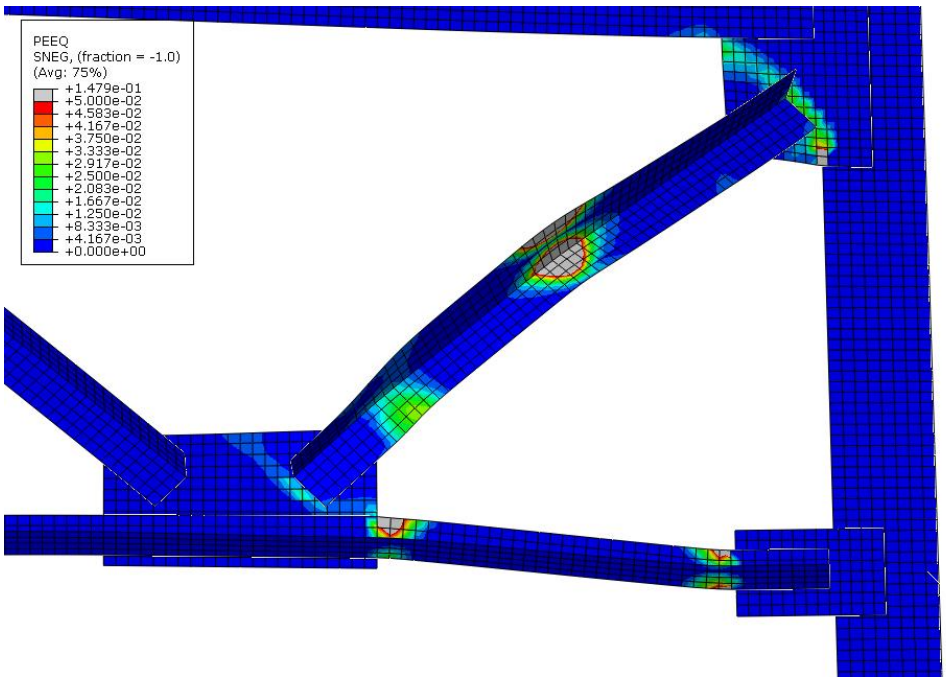

Figure 18 Buckling of the single angle K-frame from FE model

The applied moment, the deformational rotation angle and the stiffness are calculated by using force (F) and displacements (U and V) from Figure 16 as follows:

$$\text{Moment (M)} = 2(\text{F x } 53.74) \quad (kips.in)$$

$$\text{Angle } (\theta) = \frac{(U_3 - U_4) + (U_1 - U_2)}{53.74} + \frac{(V_3 - V_2) + (V_1 - V_4)}{95.02} \quad (rad)$$

$$\text{Stiffness (K)} = \frac{\text{M}}{\theta} \quad (kips.in)$$

Wang [26] models made of 1 in. quadratic shell elements were able to estimate the buckling behavior of the K-frame successfully. The initial imperfection and residual stresses were also studied by Wang [26]; however, the effect of these on initial stiffness and total buckling capacity were found to be negligible according to the results in Table 4.

Table 4 The result comparisons between experiments and Wang [26] models

	Stiffness K (kips.in)	**Stiffness Difference (%) 1 – EXP/Wang**	**Force F (kips)**	**Force Difference (%) 1 – EXP/Wang**
Experiment (EXP)	760027	-	62.70	-
Wang [26] quadratic shell element model without imperfection and residual stresses	781000	2.76	56.00	-10.69
Wang [26] quadratic shell element model with only initial imperfection of the member length	781000	2.76	56.00	-10.69
Wang [26] quadratic shell element model with only residual stresses (maximum 30% of yielding strength)	781000	2.76	53.00	-15.47

In this dissertation, first, the shell models were created according to the procedures defined in Wang[26]. The welds were assigned as tie constrains. 1 in. sized quadratic, linear and reduced integration shell elements used for the stiffeners, angles, and gusset plates can estimate the overall behavior successfully; however, these models require too much computational time.

Table 5 The result comparisons between experiments and FE shell models

	Stiffness K (kips.in)	Stiffness Difference (%) 1 – EXP/FEA	Force F (kips)	Force Difference (%) 1 – EXP/FEA
Experiment (EXP)	760027	-	62.70	-
Shell model with quadratic elements	807458	6.24	63.25	0.88
Shell model with linear elements	813700	7.06	63.87	1.86
Shell model with reduced integration elements	796258	4.77	62.55	0.26

In this dissertation, second, the models made of Timoshenko beam elements (B31 in Abaqus) with eccentricity were created for all angles. In addition, the gusset plates and the stiffeners consisted of 4 in. shell elements with reduced integration (S4R) as shown in Figure 19. The FE model with 10 in. beam element size and minimum six elements through the angle length is able to reasonably, conservatively and economically estimate both capacity and initial stiffness according to the results in Table 6, the load displacement curves shown in Figure 20 and the failure geometry in Figure 21. Therefore, this approach was used in twin-tub-girder bridge models.

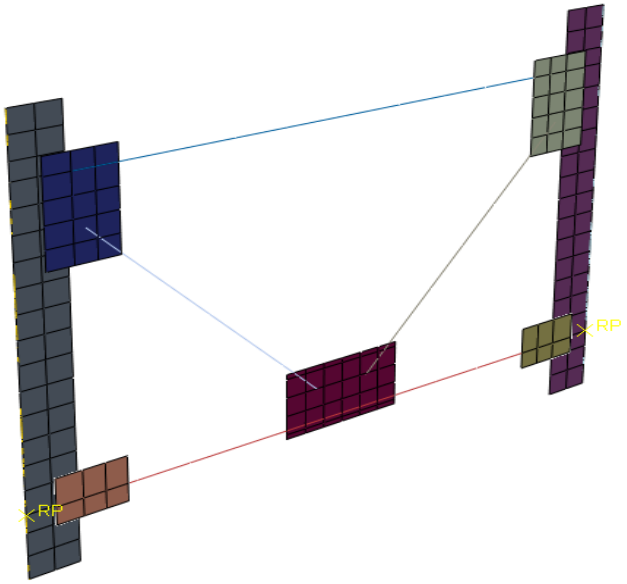

Figure 19 FE mode detail of the single angle K-frame

Table 6 The result comparisons between experiments and FE beam models

	Stiffness K (kips.in)	Stiffness Difference (%) 1 – EXP/FEA	Force F (kips)	Force Difference (%) 1 – EXP/FEA
Experiment (EXP)	760027	-	62.70	-
Timoshenko beam model Element size: 0.1 in.	796080	4.52	59.22	-5.88
Timoshenko beam model Element size: 1.0 in.	777700	2.27	57.91	-8.27
Timoshenko beam model Element size: 10.0 in. Minimum 6 elements through the angle length	619090	-22.77	49.15	-27.57

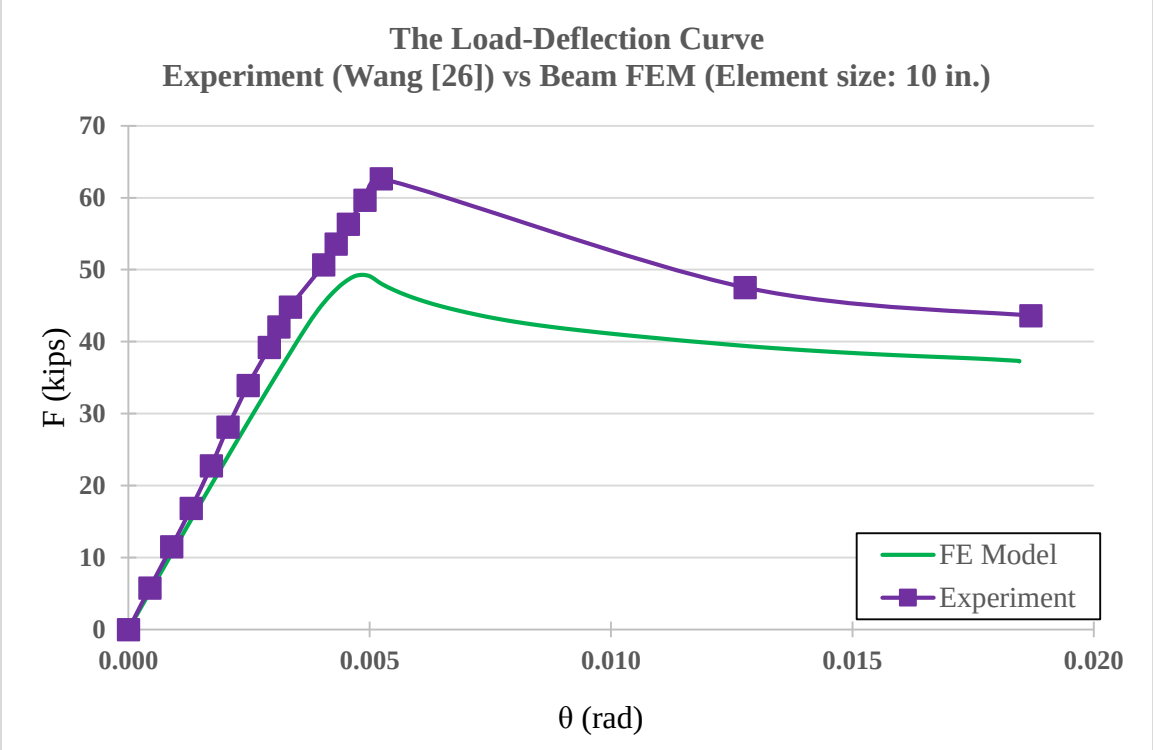

Figure 20 The load-displacement curve comparison between the experiment and FE model

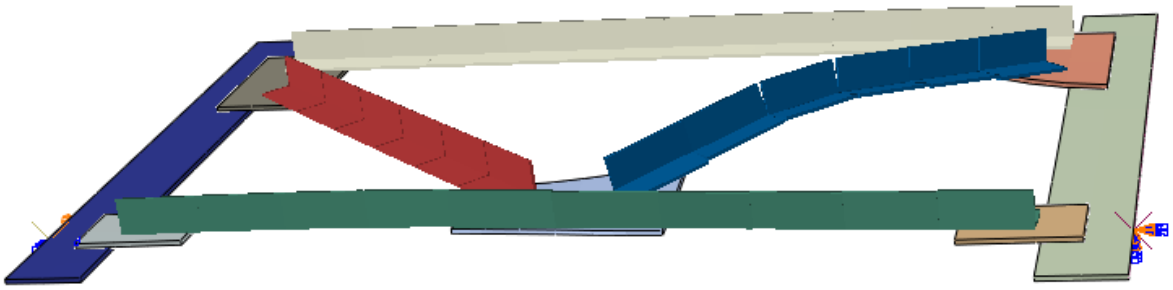

Figure 21 Buckling of the single angle K-frame from FE beam model

The connections of the braces were defined using connector elements (CONN3D2) for a fastener group as shown in Figure 14. The shear and bearing strength of the connections were obtained according to "Sections 6.13.2.7 and 6.13.2.9" of the current AASHTO LRFD Bridge Design Specifications [13].

The equivalent stiffness per connection was obtained from the shear stiffness of the bolt and the bearing stiffness of the plates based on the formulation in Eurocode 3 [27] as it is a well-accepted approach to estimating the stiffness of a connection. Serial spring summations were used to calculate equivalent stiffness per connection, and total equivalent stiffness for multiple bolts was obtained by multiplying one fastener stiffness by the number of fasteners as a parallel spring summation. However, exterior fasteners would carry higher load than interior bolts according to the stiffness of each fastener and where it is located within the connections. In other words, if a fastener is stiffer, the ratio of the load carried by exterior fasteners to interior fasteners would be higher. Eccentricity of the single shear connection was defined inside the beam element and hence the effects of eccentricity were indirectly included in the connection model. While the stiffness of the connection is not a concern in typical design, when modeling the system behavior, the stiffness of the connection must be included in the model. The behavior was assumed to be elastic-perfectly plastic. The maximum recommended deformation was set to 2.5 times of the displacement at the start of yielding. This approach was also benchmarked against the experimental connection failure behavior published in NCHRP 12-84, Appendix C [28], which focused on gusset plate behavior following the collapse of the I-35W bridge.

Longitudinal stiffeners were also defined using four-node linear shell elements (S4R) with reduced integration as shown in Figure 22. The longitudinal stiffeners increased the buckling capacity of the bottom flanges significantly.

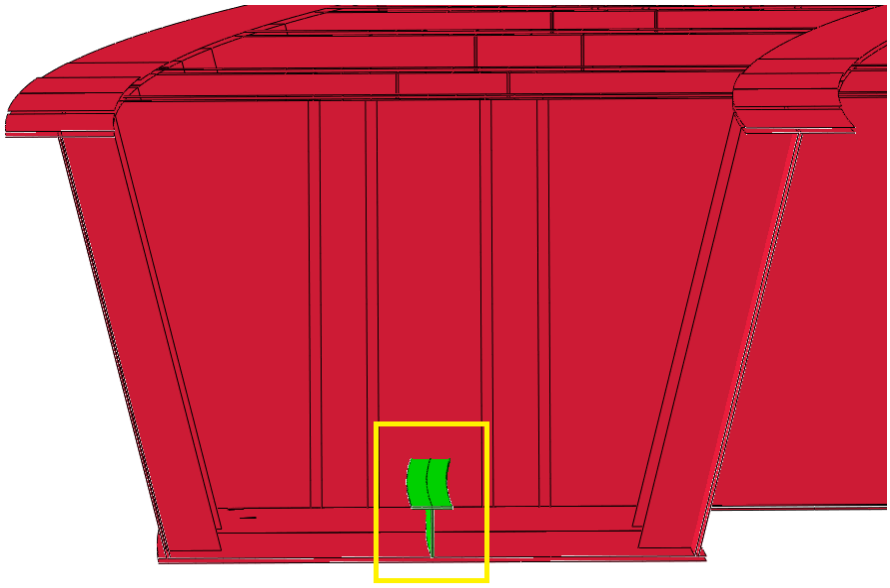

Figure 22 Longitudinal stiffeners

Similar to the steel properties used in the main girders, the assigned stress-strain curve follows the diagram in Figure 6.

3.1.4 Shear studs

The tensile and shear behavior of shear studs is critical in the load transfer between the steel members and the concrete slab in composite steel bridges, as they help provide additional load paths after the failure of a primary steel member. The superior ability of composite steel bridges to transfer load was shown by Neuman (2009) [3], who performed full-scale experiments in a simple span twin-tub-girder bridge that underwent failure of the bottom flange and web of one of the tub girders. Therefore, given their essential role in composite action, the behavior of shear studs needs to be properly modeled to capture the transfer of load from a faulted composite member to the rest of the structure. To this end, a methodology was developed in this dissertation (which is also incorporated into NCHRP Project 12-87a [5]) to implement shear, tensile, and combined shear and tensile behavior of shear studs in finite element models of steel bridges. The suggested methodology is valid for up to three transversely grouped shear studs.

The primary focus of the shear stud behavior study was the development of a method to calculate tensile stiffness, strength, and inelastic behavior of transversely grouped shear studs. Shear studs under high tensile load may fail due to one of three modes: steel rupture of the shear studs' shaft, pull-out of the shear studs from the concrete slab (and/or haunch), or break-out of a section of the concrete slab (and/or haunch). The tensile force-displacement relations for shear stud groups is dependent upon these failure modes and requires different definitions of the inelastic response of the shear stud group as well as different expressions for the calculation of the initial stiffness, nominal tensile strength, and maximum cumulative tensile displacement.

In general, concrete break-out strength is lower than the steel rupture strength or concrete pull-out strength, hence becoming the governing failure mode. The concrete capacity design (CCD) approach in ACI 318-14 [11] provides the best approximation to calculate concrete break-out strength; however, this formulation does not consider the effects of the haunch. Mouras et al. (2008) [12] developed a new modification factor for the CCD approach that considers the slab haunch effect. The existing methodology for the slab haunch effect is presented in the AASHTO LRFD BDS "Section 6.16.4.3-Shear Connectors" [13]. Nonetheless, Mouras et al. (2008) [12] performed very limited number of experiments which may not be enough to develop an accurate modification factor. Further, the approach does not consider the statistical variations that are inherent in the existing procedures based on the ACI 355 database [29]. In other words, they did not treat their data statistically and hence, did not address the fact that their data represent a mean value and not a 5% fractile, as implied in their approach. Moreover, neither ACI 318-14 nor AASHTO LRFD BDS include any information about shear stud tensile stiffness and load-displacement behavior.

The CCD approach needed to be enhanced and made suitable for implementation in finite element analysis procedures for steel bridges developed herein. With that goal, a calibrated finite element analysis methodology was developed to estimate the effect of several parameters on the concrete tensile break-out strength, stiffness, and ductility of several shear stud configurations. First, detailed finite element models were calibrated and benchmarked to the full-scale sub-assembly testing of shear studs noted in the ACI 355 database [29] and performed by Mouras et al. (2008) [12]. The finite element analysis procedures developed during the benchmark process were then utilized to conduct a parametric study in which the effects of several parameters on the tensile

behavior of transversely grouped shear studs were assessed. In the parametric study the tensile behavior was influenced by the following parameters: (1) concrete compressive strength, (2) shear stud height, (3) stud spacing in longitudinal direction, (4) stud spacing in transverse direction, (5) top flange width, (6) top flange thickness, (7) haunch thickness, and (8) number of shear studs in a group.

A total of eighty finite element models were analyzed in the parametric study to develop load-displacement relationships. Based on the results of the parametric study, tensile force-displacement relationships dependent upon the dominant failure mode were developed. When the failure mode is tensile rupture of the shear stud shafts, the behavior is initially linear elastic until the tensile yield strength of the shear stud shaft is reached, followed by plasticity with linear hardening. As yielding continues, failure is assumed to occur when the tensile rupture strength of the shear stud shaft is reached at a maximum axial displacement equal to 5% of the effective stud height (i.e., height of shaft). A triangular load-displacement curve is characteristic of concrete break-out and shear stud pull-out failure modes; the behavior is initially linear elastic until the concrete break-out strength or the shear stud pullout strength is reached, followed by linear softening until the axial ductility of the shear stud group is exhausted.

In this dissertation, the following provisions to model the behavior of shear connectors were developed:

- Simple equations to calculate the initial stiffness of transversely grouped shear studs that account for the combined effect of the flexibility of the shear stud shaft, the concrete section, and the bending stiffness of the flange.
- Modification factors for the calculation of concrete break-out strength that account for the haunch effect to be applied to the CCD expressions in ACI 318-14 [11].
- Modification factors applied to the expressions in ACI 318-14 to calculate steel rupture strength and concrete pull-out strength. These factors incorporate the effect of unequal load distribution among transversely grouped shear studs.
- Maximum tensile displacement values dependent upon the governing failure mode and the number of shear studs in the group.

In addition to the tensile load-displacement relations studied, it is necessary to define the shear behavior of transversely grouped shear studs to completely capture the behavior of the shear stud "group". The shear force-displacement relations developed by Ollgaard et al. (1971) [30] were employed in the current research and subsequently recommended. The nominal shear strength, non-linear shear force-displacement behavior, and maximum shear displacement at failure are determined according to Ollgaard's model, which is also prescribed in AASHTO LRFD BDS to calculate the shear resistance of shear studs. Ollgaard's shear force-displacement relations are combined with the tensile force-displacement relationships develop in this current study through the shear-tension interaction equation in AASHTO LRFD BDS 6.16.4.3 [13].

To implement the shear stud behavior in finite element models of composite steel bridges, it is necessary to use connector elements. These elements are basically multi-dimensional springs for which coupled force-displacement curves can be assigned which allow the Engineer to characterize the stiffness, capacity, and ductility of the shear stud group at discrete locations. Linear or nonlinear force-displacement curves need to be assigned for each relative motion component. In Abaqus, the axial and interfacial shear interaction between the shear studs and the concrete deck was defined using CONN3D2 connector elements, and mesh independent fasteners were used as stud connections to transfer load from the girder to the deck. The implementation of the shear stud modeling methodology in finite element models of composite steel bridges was also benchmarked against the full-scale experiments conducted by Neuman (2009) [3]. Specific details on the research conducted regarding shear stud behavior, as well as comprehensive explanations of the application procedures to implement coupled shear and tensile load-displacement relations in finite element models of composite steel bridges are presented in CHAPTER 4.

3.2 Interaction

Friction (based on isotropic Coulomb friction) and hard contact interaction behavior was defined between the surfaces at expansion joints in the parapets (when present), and between the bottom of the deck haunches and the top surface of the top flange. The interaction model between the haunch of the concrete deck and the top flange of the tub girders is shown in Figure 23. In general, the mesh density was similar to the one utilized for the steel elements. At the locations in contact with steelwork (e.g., bottom slab haunches) the mesh density was higher than the mesh density of

the steelwork to ensure proper enforcement of the contact interaction and minimize penetrations between the element surfaces. Haunches were modeled with additional superimposed layers of shell elements. According to Lai et al. (2014) [31], Coulomb friction coefficient and shear stress limit carried by the interface are 0.55 and 0.06 ksi correspondingly.

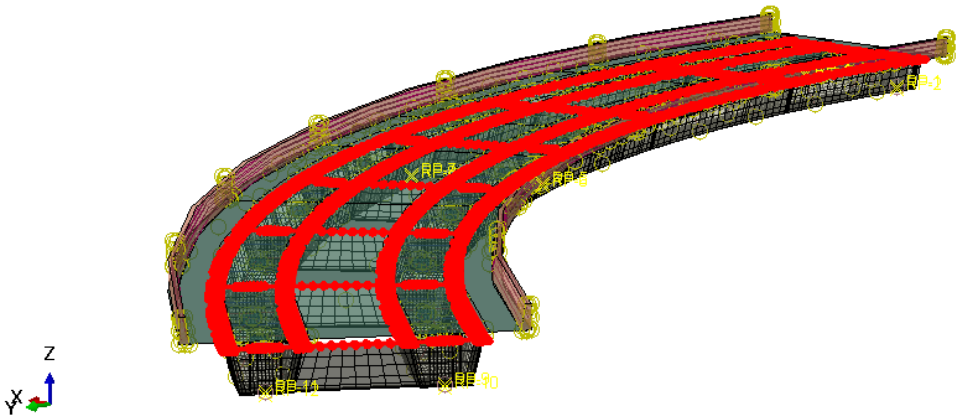

Figure 23 Interaction between deck haunches and top flanges

3.3 Long Bridge Simplification

In this dissertation, the bridges which have *more* than 3 spans were simplified to significantly reduce computational time. Only 2.5 spans of the full bridge were modeled, and a symmetry boundary condition was provided at the end of the center span (shown in Figure 24). For example, in Figure 24, the bridge *B40-786-Unit2* (additional details about this bridge included in Chapter 6.14) was modeled as both a 4 span continuous curved girder bridge and a 2.5 span symmetric bridge.

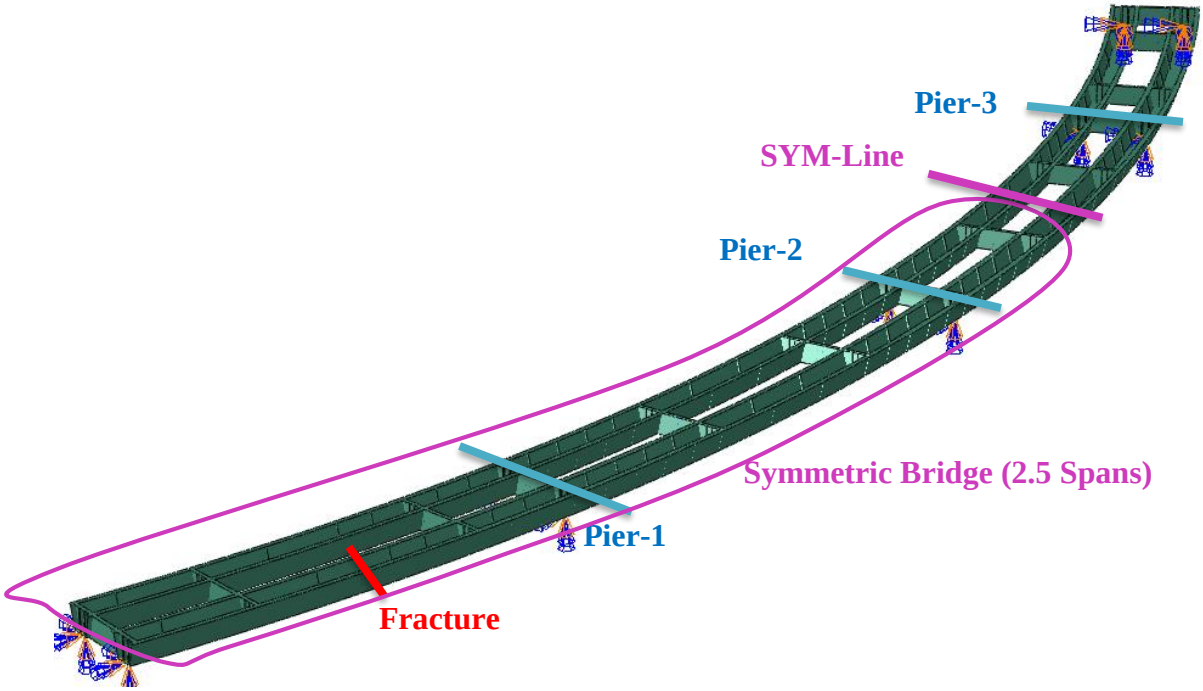

Figure 24 Full bridge and simplified bridge with symmetry

By comparing the stress and displacement results obtained from both models (Figure 25 through Figure 36), it was confirmed that the simplified model provides very similar results to the full bridge model, especially in fractured span where the results are almost the same. In the fractured span (includes both fractured girder and intact girder), the stress and the displacement differences are less than 1% for both bottom and top flanges. In the next span (adjacent to the fractured span), the stress and the displacement differences are not more than 5% in both bottom and top flanges. As a result, this approach will be used for cases in which there are many spans in order to improve the efficiency of the analysis without compromising the accuracy of the results.

Fractured girder bottom flange results:

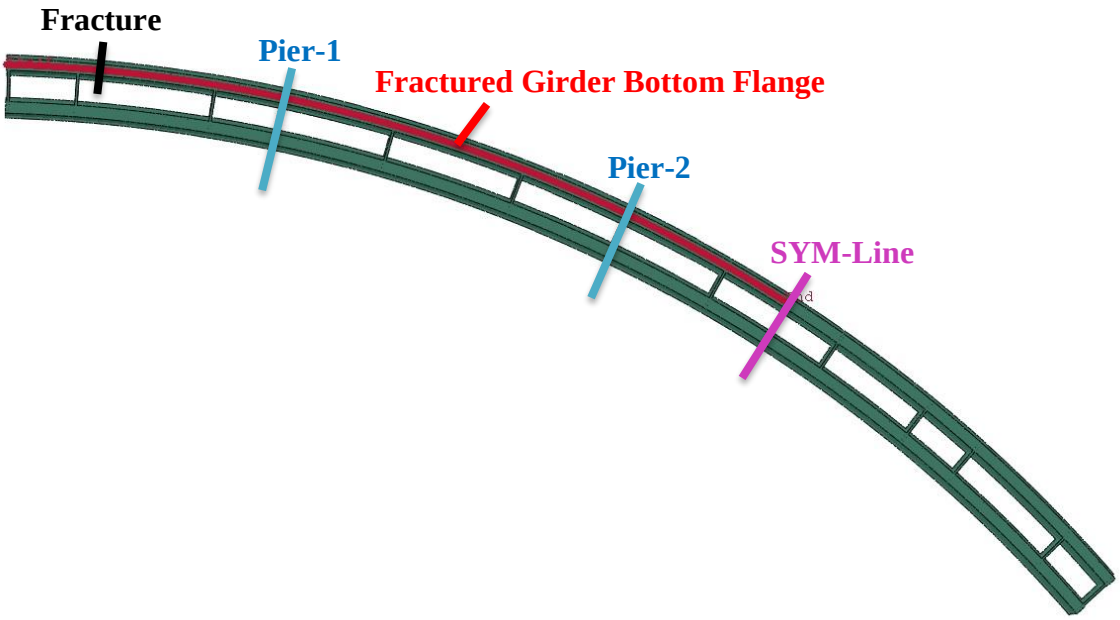

Figure 25 Fractured girder bottom flange (bottom view)

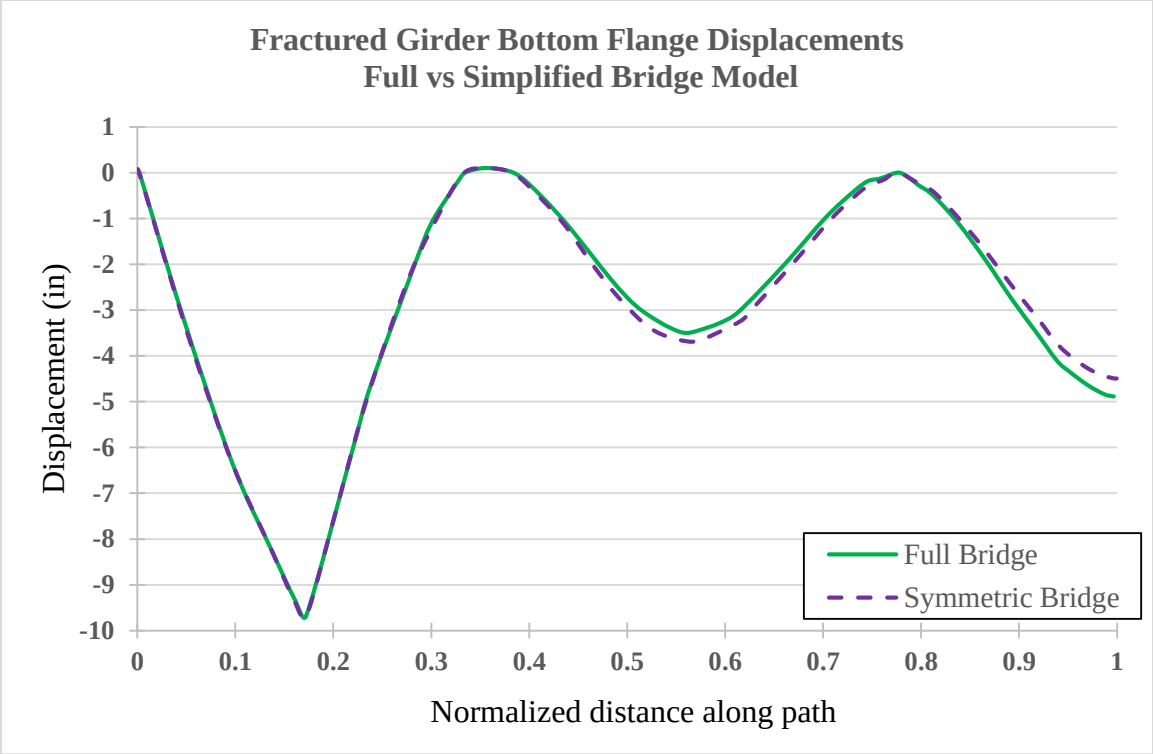

Figure 26 Fractured girder bottom flange displacements

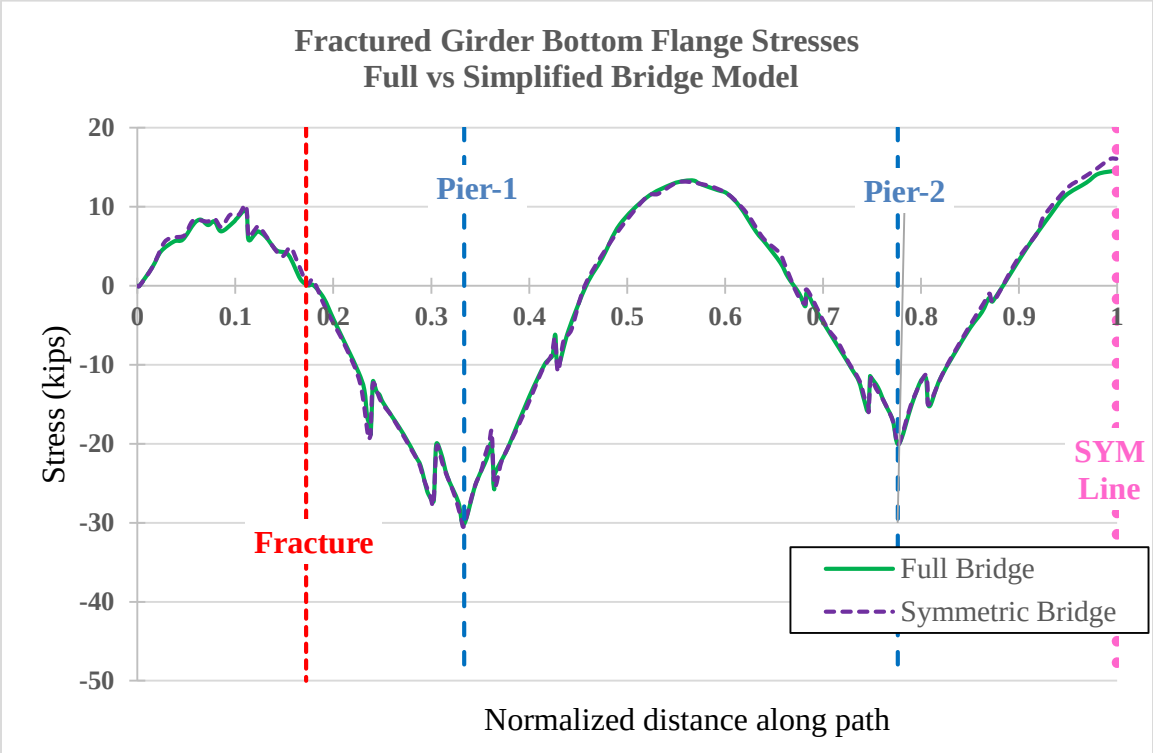

Figure 27 Fractured girder bottom flange stresses

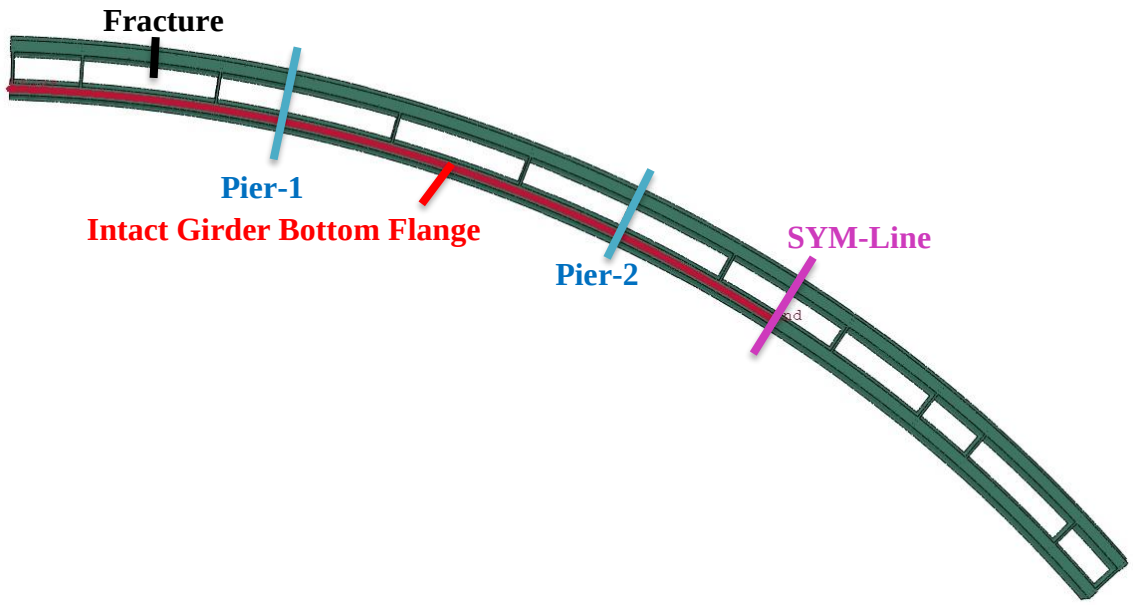

Figure 28 Intact girder bottom flange (bottom view)

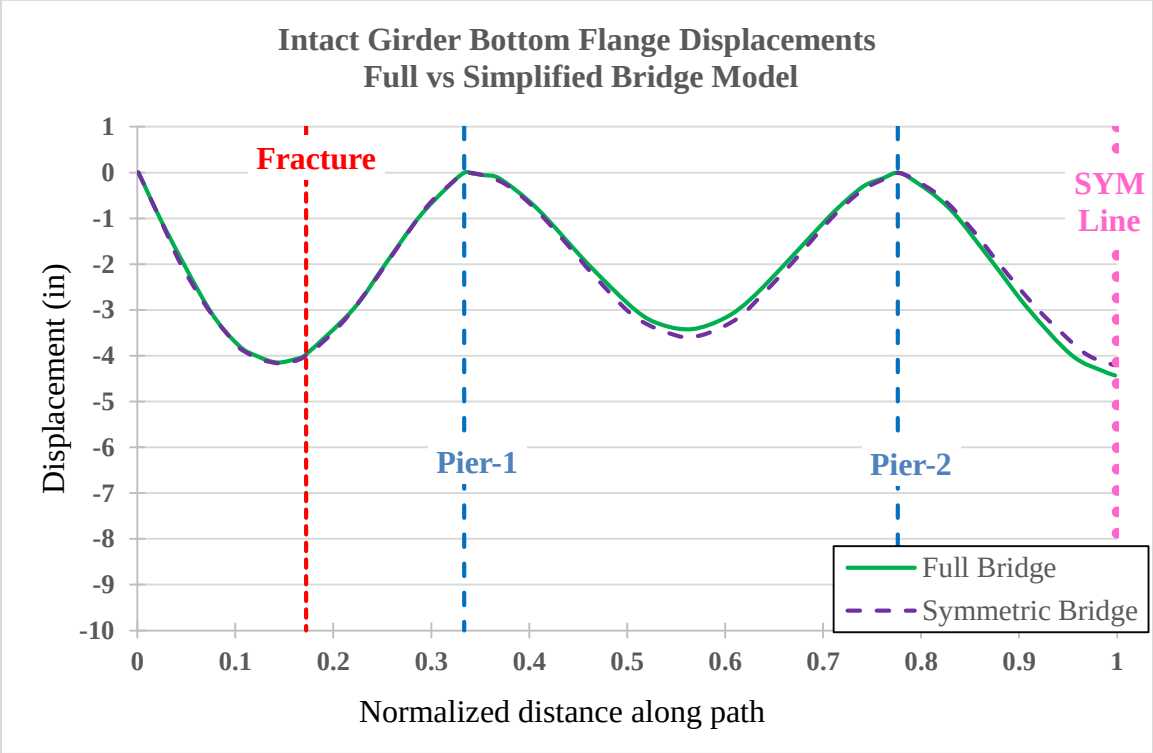

Figure 29 Intact girder bottom flange displacements

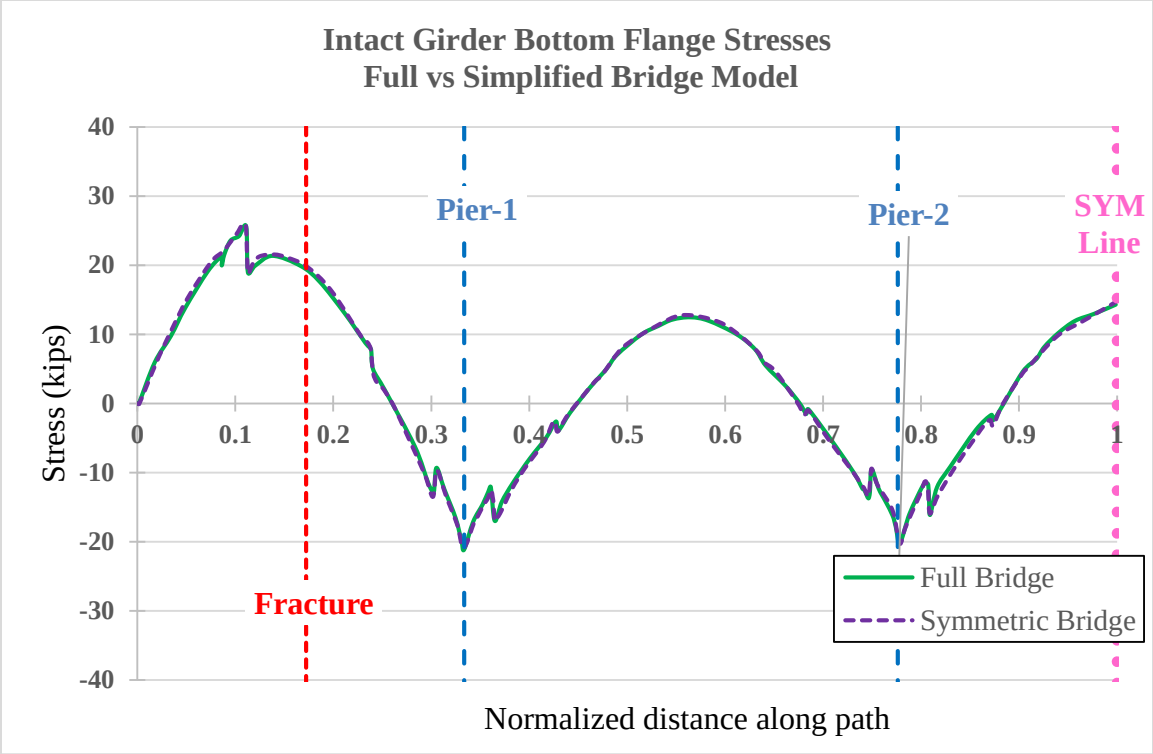

Figure 30 Intact girder bottom flange stresses

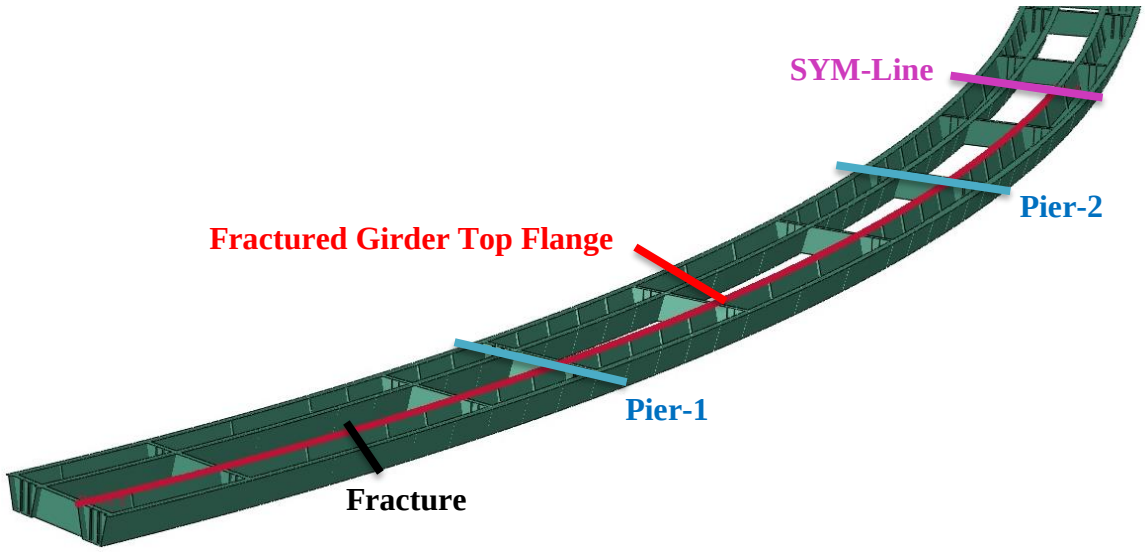

Figure 31 Fractured girder top flange (top view)

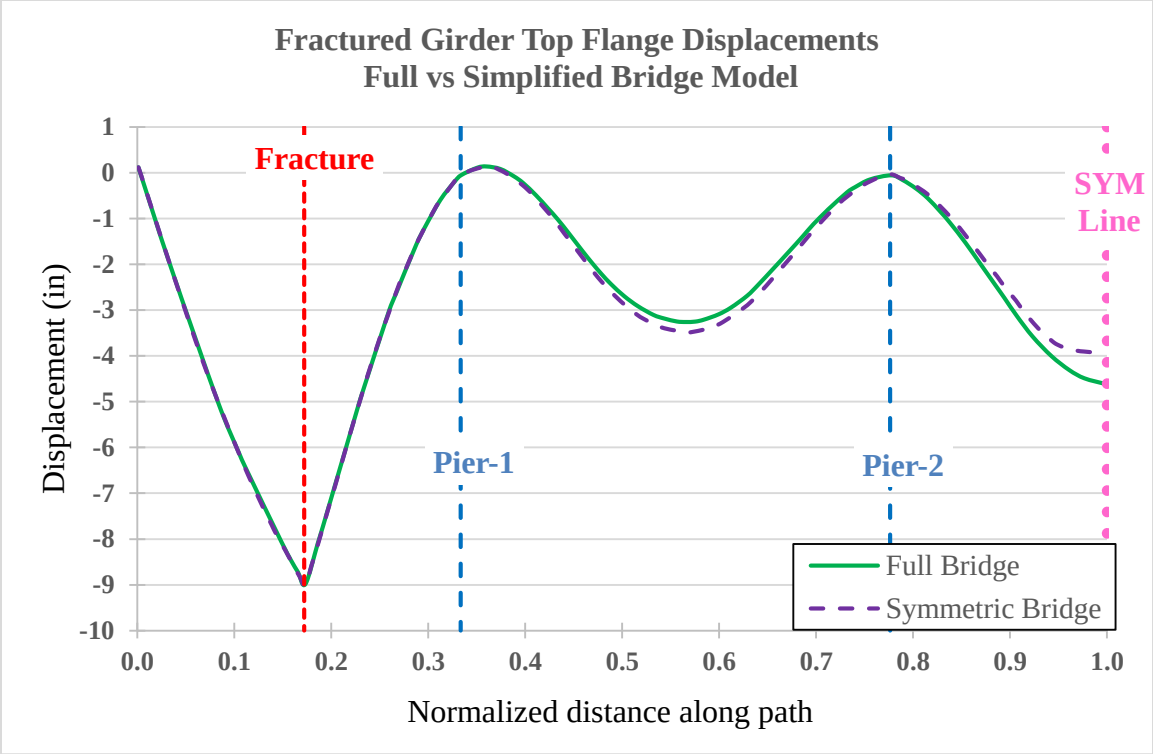

Figure 32 Fractured girder top flange displacements

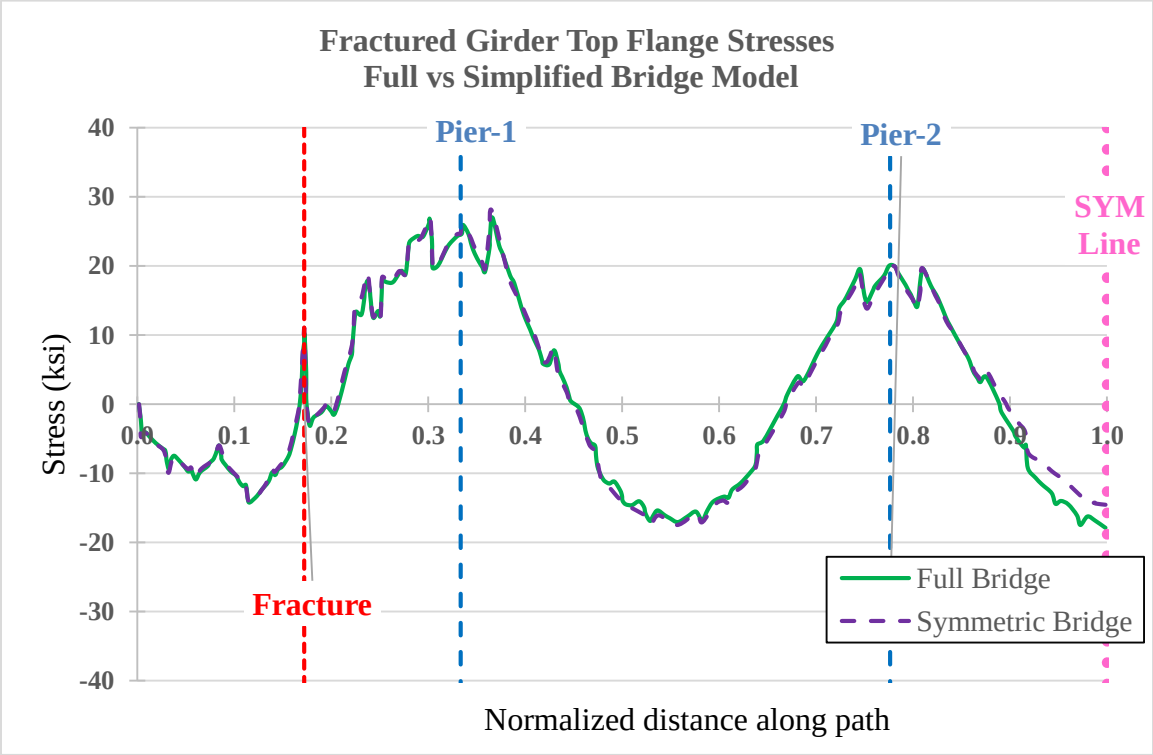

Figure 33 Fractured girder top flange stresses

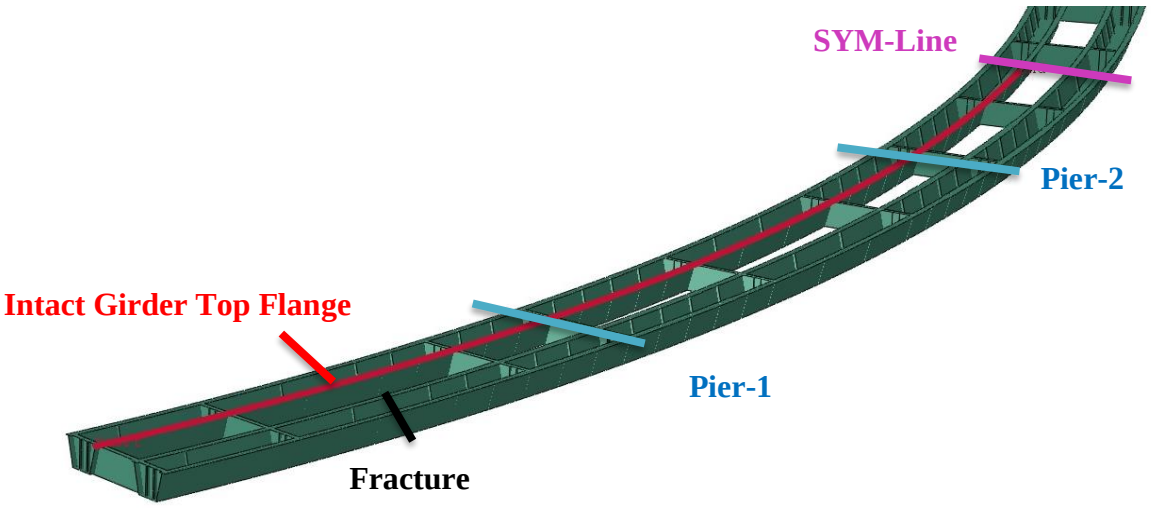

Figure 34 Intact girder top flange (top view)

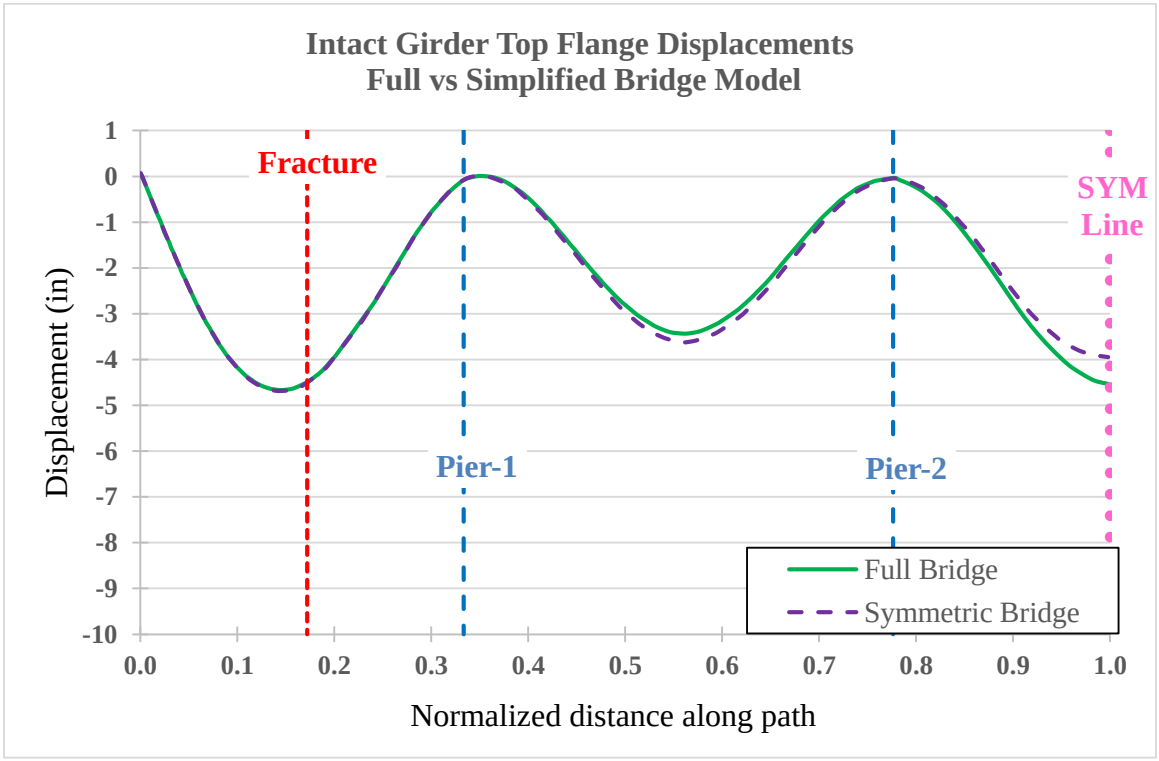

Figure 35 Intact girder top flange displacements

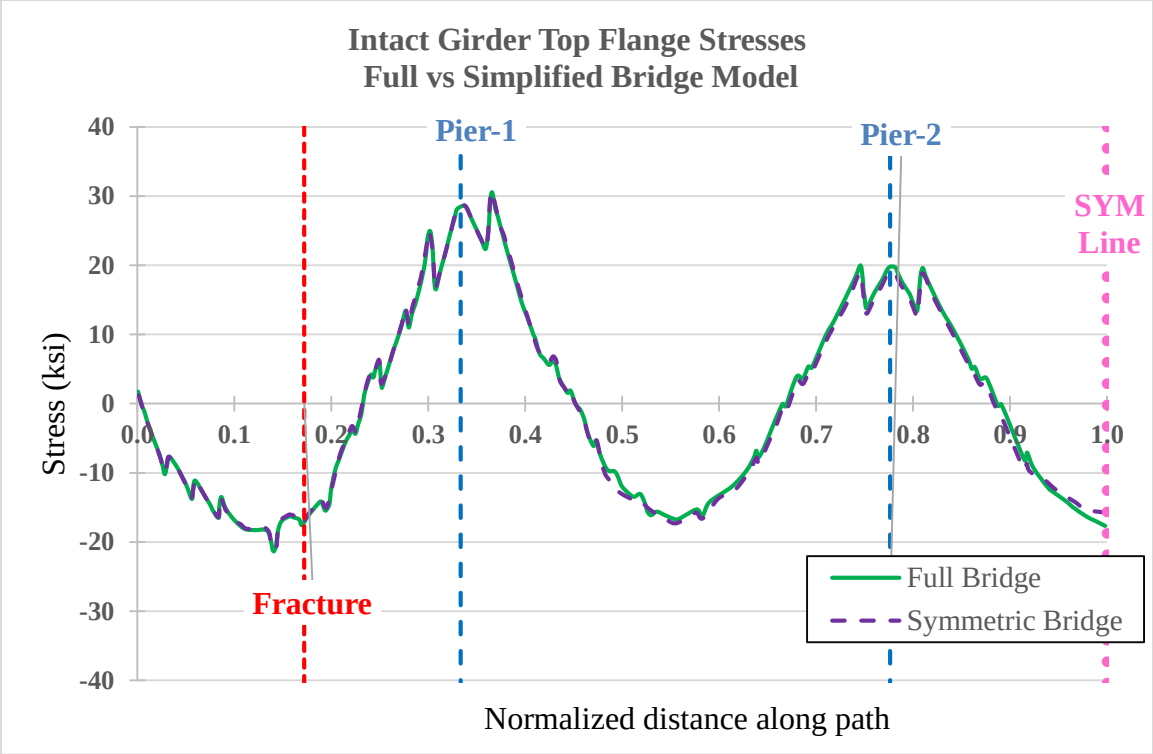

Figure 36 Intact girder top flange stresses

3.4 Dynamic Amplification Factor Calculation

The dynamic response of a twin-tub-girder bridge after the sudden simulated fracture of the web (Test-2 of Neuman (2009) [3]) was investigated during the large-scale experiment performed in UT Austin. The ratio between the peak stress following the sudden fracture to the final stress after the structure comes to rest minus 1 is called the dynamic amplification factor (DA_R) in this study. In Test-2 of Neuman (2009) [3], the average dynamic amplification factor was measured, and it was equal to 0.3. This dynamic behavior can be simulated successfully with a detailed finite element analysis by Bernard et al. (2010) [19] who performed FE models to benchmark the UT twin-tub-girder experiments and obtained very similar dynamic responses to experimental values.

This dynamic amplification factor definition is very similar to the definition of dynamic magnification in Eurocode [27] or impact factor in AASHTO LRFD BDS [13]. These factors or magnifications are used to apply the dynamic effects of traffic loads for strength limit states, serviceability limit states or fatigue assessments. AASHTO LRFD BDS [13] provides conservative dynamic impact factors to designers for their static analyses, because it is very complicated to perform a dynamic analysis for each design process. On the same purpose, in this

study, a conservative dynamic amplification factor was investigated for the effect of a sudden fracture. This conservative dynamic amplification factor provided in this study simplifies the redundancy analysis for twin-tub-girder bridges.

Dynamic amplification is calculated as the ratio of the peak stress in a given member in free vibration following the sudden fracture to the stress in that member after the structure comes to rest minus 1. The models that were developed are capable of predicting the dynamic behavior of a steel structure after sudden failure of a tension member. DA_R (like in Figure 37) through this research according to following figure and equation. σ_p is peak stress and σ_f is final stress when the kinetic energy is almost zero was calculated as follows:

$$DA_R = \frac{\sigma_p}{\sigma_f} - 1$$

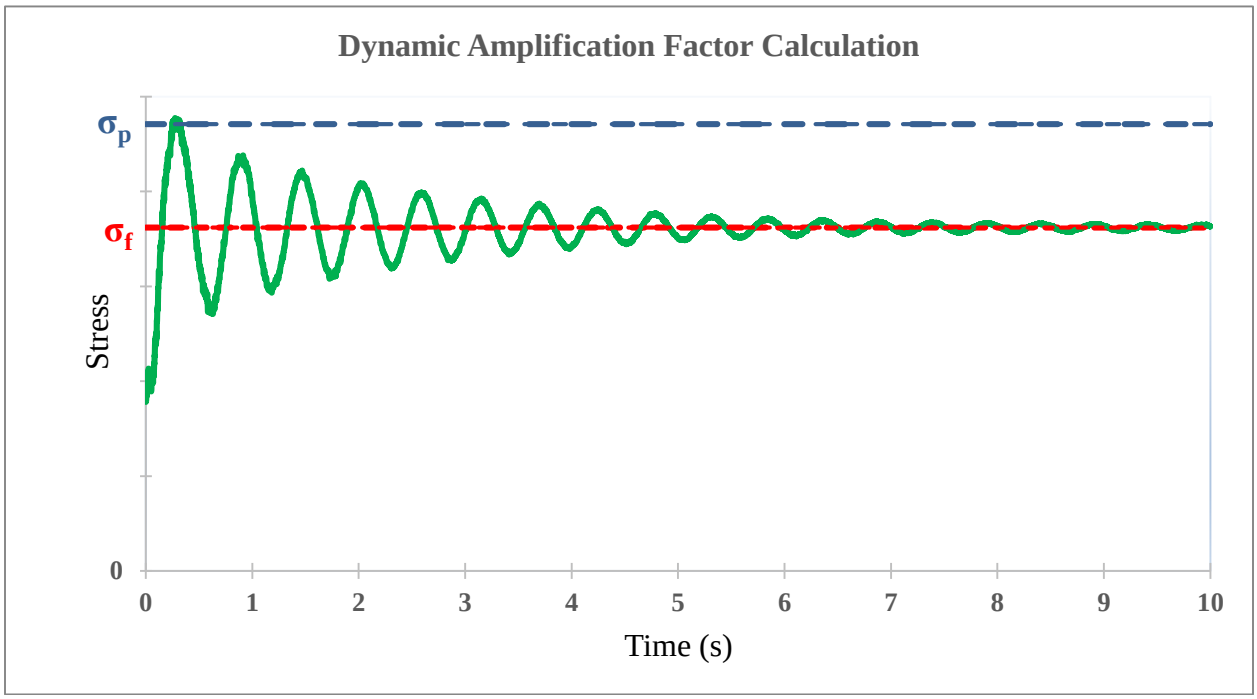

Figure 37 Dynamic amplification factor calculation

3.5 Loads and Boundary Conditions

Dead loads (gravity load, *Z axis*) and live loads (applied loads) were applied in FE models. In Abaqus, only material densities and gravitational acceleration were input. The product of density, gravitational constant and per section unit volume were assigned as body forces. Live loads were distributed over the specified surfaces with surface traction. The HL-93 vehicular live load, which includes design truck and design lane load were applied in FE models according to AASHTO LRFD BDS "Section 3.6.1.2-Design Vehicular Live Load" [13]. In detail, the wheel loads of the HS-20 truck were distributed over the rectangular tire contact surface which has 20.0 in width and 10.0 in length as noted in AASHTO LRFD BDS "Section 3.6.1.2.5-Tire Contact Area" [13]. In the analyses, design lane load per length (0.64 kips per ft.) was distributed over 10.0 ft wide surface as a surface traction. This methodology was based on AASHTO LRFD BDS "Section 3.6.1.2.4-Design Lane load" [13]).

Connector elements were used to describe boundary conditions. Infinite stiffness was defined only for the direction which is against to gravity; hence uplifts were allowed. Only one of the bearing supports was fixed to avoid overturning rotation *(Z axis)*, longitudinal and transverse direction *movement (X and Y axes)*, however X and Y axes rotation were allowed. Others were conservatively free to move all horizontal direction and rotate over all axes.

3.6 Brittle Fracture Assignment

The fractures were simulated by instantaneously removing or deleting elements. For example, in the parametric study described in CHAPTER 7, the bottom flange, web and both top flange elements were instantaneously deleted to simulate sudden brittle fracture. Energy dissipation due to plasticity, damage, friction and viscosity (introducing damping) was built into the model. Cracks were not "advanced" but rather, they were instantly introduced. In other words, a fracture was not initiated in one location and then analytically "grown" through the girder. It was assumed to have occurred instantly, similarly to how a real brittle fracture would propagate.

CHAPTER 4 SHEAR STUD MODELING STUDY AND RECOMMENDATIONS

In composite steel bridges, shear studs provide additional load paths to allow transfer of load from the failed steel members to the slab. Obviously, the load transfer between the steel members and the concrete slab is affected by the behavior of the shear studs. The shear stud behavior can be divided into two major components: tensile behavior, and shear behavior. Neuman (2009) [3] showed the superior ability of composite bridges to transfer load through the deck when shear studs were adequately embedded in the slab. In the second test of Neuman, although the fracture of the bottom flange and partial web of one of the tub girders resulted in failure of several shear studs, this did not result in collapse of the entire bridge. Thus, despite isolated failures, there was adequate number of shear studs to contribute to the redundant load transfer mechanisms. Shear studs have vital importance in the evaluation on redundancy for composite steel bridges with members designated as fracture critical members (FCMs). It is important to include proper shear stud properties which cover the shear, tensile, and combined shear and tensile behavior to prevent erroneous conclusions regarding redundancy. The methodology developed in this study to obtain the stiffness, strength, and ductility of transversely grouped shear studs is explained hereafter. The suggested methodology is valid for up to three transversely grouped shear studs.

4.1 Shear Behavior of Transversely Grouped Shear Studs

The model by Ollgaard et al. (1971) [30] is recommended to be utilized for the definition of shear force-displacement relations. The Ollgaard model provides all the parameters to determine nominal shear strength, non-linear force-slip behavior, and maximum cumulative shear displacement at failure. The shear strength of transversely grouped shear studs is based on the nominal shear resistance for a single stud embedded in concrete, Q_n, which is calculated per the AASHTO LRFD BDS [13] "Section 6.10.10.4.3". The nominal shear resistance for transversely grouped shear studs, $Q_{g,n}$, is calculated as follows:

$$Q_{g,n} = N_s Q_n$$

N_s is the number of transversely grouped shear studs.

The shear load-displacement relation, $Q_g(\delta_Q)$, is defined according to Ollgaard et al. (1971) [30] as follows:

$$Q_g(\delta_Q) = Q_{g,n}\left(1 - e^{-18\delta_Q}\right)^{\frac{2}{5}} \quad (kips)$$

where δ_Q is the shear displacement (inch). Ollgaard et al. (1971) [30] showed that the maximum shear displacement is approximately 0.2 inches, when 90% of the shear capacity has been reached. Hence, it is recommended that failure of the shear is introduced at a shear displacement equal to 0.2 inch, in other words the shear capacity goes to zero when the displacement is 0.2 inch.

4.2 Tensile Behavior of Transversely Grouped Shear Studs Modeling

When evaluating the redundancy of a composite bridge it is necessary to include the tensile behavior of shear studs. Shear studs under high tensile load may fail due to three different mechanisms: shear stud steel rupture, pullout from the concrete slab and/or haunch, or break-out of a section of the concrete slab and/or haunch. These different failure modes affect the initial stiffness, strength, and ductility of transversely grouped studs. This must be properly captured in order to define accurate tensile force-displacement relations for use as input into finite element models of composite steel bridges.

Additionally, Mouras et al. (2008) [12] noted that in transverse shear stud groups, the amount of load is not distributed to each shear stud equally. For example, in three transversely shear stud groups, the shear stud in the middle of the group carries more load than the exterior studs. This imbalance results in a reduction of the shear stud rupture strength and/or concrete pullout strength.

For a shear stud group, the concrete break-out strength is generally much lower than the pullout strength or the stud rupture strength, and, therefore, typically controls the behavior. The concrete capacity design (CCD) approach in ACI 318-14 [11] provides the best approximation to calculate concrete break-out strength (according to ACI 355 database [29]); however, this formulation does not to consider the effects of the haunch. Mouras et al. (2008) [12] developed a new modification factor for the CCD approach to consider the slab haunch effect. This methodology has been adopted in the AASHTO LRFD BDS [13] "Section 6.16.4.3-Shear Connectors". Mouras performed a large number of tests (48 in total). In the test matrix, there were 15 unique

configurations tested under static loading with a haunch and there were five in which there were replicates (i.e., a total of 20 individual tests). There were seven unique configurations in which a haunch was not used and two replicates of each, for a total of 14 individual tests. The objective of the two tests was to evaluate the effects of the haunch.

However, it is important to note that Mouras et al. (2008) [12] did not evaluate the data by considering any statistical affects, as is normally done for shear stud pull-out data. For example, the ACI database used for the development of shear stud concrete break-out utilizes the 5% fractile of all data prior to the application of the traditional "phi" or strength reductions factors due to the large scatter observed in the data set. The ratio between the "mean" and the 5% fractile is about 1.7. In other words, the mean of the data used to develop the ACI approach is 1.7 times greater than the 5% fractile value. Rather, Mouras et al. (2008) [12] compared the mean results from the tests in which there was no haunch with the 5% fractile value predicted by the ACI approach and concluded that the ACI equation was in agreement with the experimentally obtained data. In other words, the ACI equation could be used to estimate the strength for the case without a haunch. However, this was not appropriate since their data were not lower bound (i.e., not consistent with the 5% fractile approach). The author of this dissertation believes the reason the experimentally obtained data were in agreement with the lower bound is due to the reduction in capacity that occurs due to the flexural effects, discussed above. Recall that the ACI 355 database does not include any flexural affects as also discussed previously. While Mouras utilized the cracking modification factor included in ACI, this factor is not intended to account for flexural cracking, but rather for existing cracking (due to temperature or shrinkage). This is reflected by the fact that the modification factor is a constant, which if it was related to flexural effects, would likely vary with applied moment. The author believes that if a longer span had been used, Mouras would have obtained lower data, and vice-versa. It is likely a coincidence that the ACI prediction (i.e., the lower bound with cracking) agreed with the specific test geometry. (*As will be discussed in Section 4.2.2 and shown in Table 9 the effects of flexure are apparent in the results from the calibrated FEA parametric study, in which it is clear that span length, and hence flexure plays a significant role in the observed capacity.*).

The data obtained from the tests which included a haunch were also compared with the ACI estimates, which again are based on the ACI 355 database. It is noted that the data in ACI 355 do

not include specimens with a haunch and hence, there were not modification factors in ACI to account for the haunch. Mouras observed that there was an increase in the strength from specimens in which a haunch was present and developed a modification factor to account for this increase in his specific set of tests. The adjustment factor would be valid for his specific geometry, such as for 5 inch long studs, the specific span length, slab thickness, etc. It is not clear how it would predict the strength for say, 9 inch studs in a slab with a different thickness etc. For these reasons, the author developed the calibrated FEA model using Mouras data and selected data from the ACI 355 database to perform a larger parametric study to develop an improved method estimate the capacity.

Neither ACI 318-14 [11] nor AASHTO LRFD BDS [13] include any information about shear stud tensile load-displacement behavior. Hence, a calibrated finite element analysis (FEA) methodology with the mean CCD approach by Fuchs et al. (1995) [32] and Mouras et al. (2008) [12] experiments was developed to estimate the effect of several parameters on the concrete tensile break-out strength, stiffness, and ductility of several shear stud configurations. The results were used to modify the existing approaches in the AASHTO LRFD BDS [13] and develop an approach to more accurately estimate the strength, stiffness and ductility of concrete break-out failure for a range of typical shear stud/haunch/flange configurations.

4.2.1 Benchmarking of finite element models for concrete break-out failure

Three-dimensional non-linear finite element models utilizing solid elements were developed to benchmark the FEA approach. The results were compared with strength values calculated per the CCD approach by Fuchs et al. (1995) [32], and experimental results by Mouras et al. (2008) [12]. Abaqus 2016 was used to perform explicit quasi-static and displacement control finite element analyses. The concrete damage plasticity (CDP) model was used to capture cracking and confinement for the concrete under the head of the shear stud. FIB Model Code 2010 [22] concrete tensile strength–displacement approach and Popovics' (1973) [20] approach were used for the concrete tensile and compressive inelastic behavior, respectively. The dilation angle ψ which controls the amount of the volume change under shear plasticity was set to 40 during shear stud concrete model calibration. A higher dilation angle was preferred to be used since the concrete

under the shear stud head is significantly confined by the surrounding concrete. The following terms were defined for the other plasticity parameters:

- Flow potential eccentricity (0.1),
- The ratio of initial biaxial compressive yield stress to initial uniaxial compressive yield stress (1.16) and,
- The ratio of the second stress invariant on the tensile meridian (0.667).

The approach to model the material behavior of concrete is essentially mesh independent, but an overly coarse mesh can result in artificially higher estimated strengths as they increase the width of crack path. Therefore, a mesh refinement study was performed until a sufficiently fine mesh (less than 0.2 in.) was found to give a negligible difference in the predicted strength. Incompatible mode elements were used to reduce the artificial effects of distortion and hourglassing. The interactions between the concrete and shear studs were modeled through the specification of a frictional contact interaction.

Firstly, the CCD approach developed by Fuchs et al. (1995) [32] was compared with the experimental results published in ACI 355 database [29]. More than 150 experimental results obtained from the ACI 355 database [29] for shear studs utilized in the US were used in the comparison with the CCD approach. It was found that the CCD approach provided estimated strength values that agreed well with the experimental data. From the database, it was also observed that concrete compressive stress under the shear stud head did not have any significant effect on the concrete break-out strength.

The mean values of the strengths calculated per the CCD approach were then used to calibrate the FEA methodology for US type headed studs. The material parameters input in the concrete damaged plasticity material model utilized in the FEA were determined by benchmarking the model to the mean strength values calculated by the CCD approach.

The calibration of the FEA methodology is based on the empirically developed *mean* strength equations of the CCD approach. The mean concrete break-out strength of a single headed shear stud, N_{ns}, according to the CCD approach is as follows:

$$N_{ns} = 40\sqrt{f_c'}\left(h_{ef}\right)^{1.5} \quad (lbf)$$

and the mean concrete break-out strength of a shear stud group, N_{ng}, is as follows:

$$N_{ng} = \frac{A_N}{A_{No}} \psi_{ed,N} N_{ns} \quad (lbf)$$

where f_c' is the nominal compressive strength of concrete (psi), h_{ef} is the effective height of the shear stud, A_N is the combined projected area of the failure surface for a group of headed shear studs (in^2), A_{No} is the projected area of the failure surface for a single headed shear stud (in^2), and $\psi_{ed,N}$ is the edge effect modification factor.

The specimen section details were determined according to the experimental procedures defined by Eligehausen et al. (1992) [33] which geometries are shown in Figure 38. Based on the experimental results and the test specimen geometry, the edge effect modification factor, $\psi_{ed,N}$, is taken as 1.0, and the projected area of the failure surface for a single headed shear stud, A_{No}, is as follows:

$$A_{No} = 9(h_{ef})^2$$

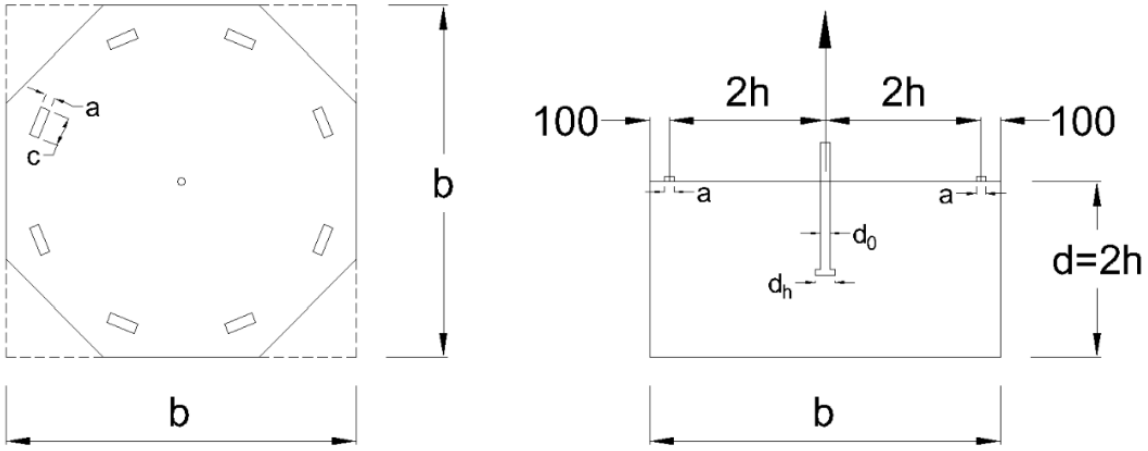

Figure 38 The experiment plan and section view of Eligehausen et al. (1992) [33].

Different shear stud heights, either single or in groups of four (two by two) spaced at a distance equal to h_{ef} were modeled. The comparison between the CCD and FEA results are shown in

Table 7. The finite element models were benchmarked by comparing the ratio between the concrete break-out strength calculated by FEA and the strength values computed by the CCD

approach. As shown in the Table 7, the ratio varied between 0.93 and 1.08 which implies that all results were within 10%, with most being within 5%.

Table 7 Concrete break-out strength comparison between FEA and CCD approach

Stud Height (inch)	Stud Combination	Concrete Strength (psi)	Strength (lb x 10^3)		FEA/CCD
			CCD	FEA	
5	Single	5100	28.41	28.64	1.01
		5900	30.56	30.55	1.00
		7500	34.46	34.02	0.99
	Group	5100	50.51	47.03	0.93
		5900	54.33	53.17	0.98
		7500	61.26	57.26	0.93
7	Single	5900	52.39	52.87	1.01
	Group		93.14	96.32	1.03
9	Single	5900	77.83	77.32	0.99
	Group		138.36	149.44	1.08

Furthermore, it is also critical that the FE model accurately captures the stud failure cone angle reported in Fuchs et al (1995) [32]. For example, the single stud failure cone angle obtained from the FE model is equal to 33 degrees (Figure 39) which is close to experimental average 35 degree reported by Fuch et al. (1995) [32]. The group failure is illustrated in Figure 40 which shows that the observed failure modes reported in the experimental database are captured by the FEA methodology.

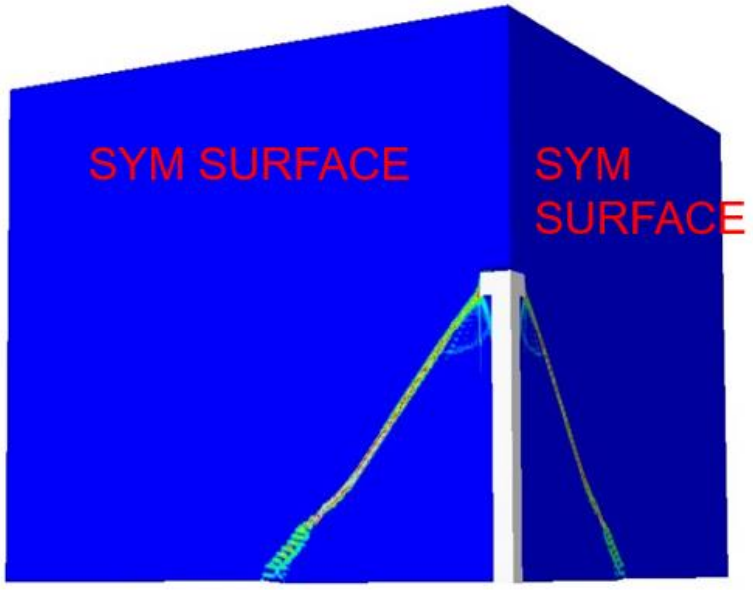

Figure 39 Concrete break-out cone for a single shear. Cracking angle is 33 degrees

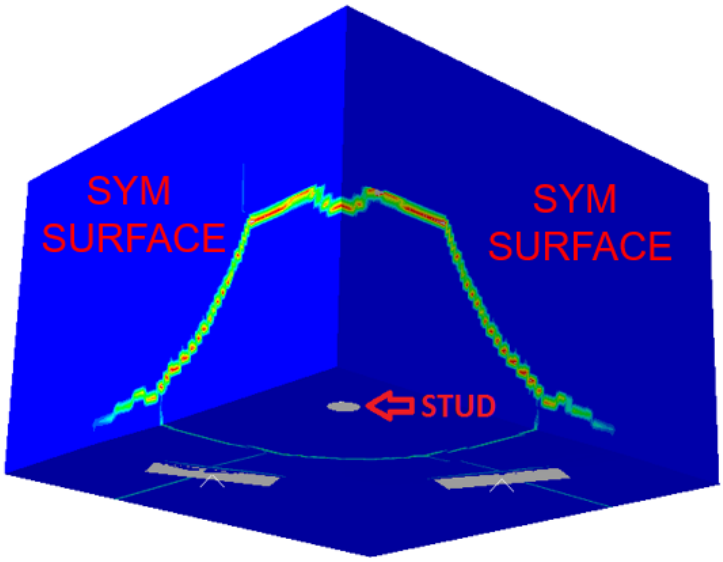

Figure 40 Concrete break-out cone for a shear stud group

A second benchmarking effort was carried out using the experimental data reported by Mouras et al. (2008) [12]. Using the FEA methodology previously defined, this additional benchmarking was performed to validate the ability of the model to accurately predict the load-displacement behavior. Such load-displacement data were not reported in the ACI 355 database [29], nor the CCD approach [32], but were reported by Mouras et al. (2008) [12]. It was also shown that when flexural loads are present, in addition to the formation of a failure cone originating at the head of the stud, flexural cracks form at the edge of the haunch. The interaction between these two cracks

for 5 inch shear studs is illustrated in Figure 41 alongside the results of the finite element model which accurately captured the failure mode shown by Mouras et al. (2008) [12].

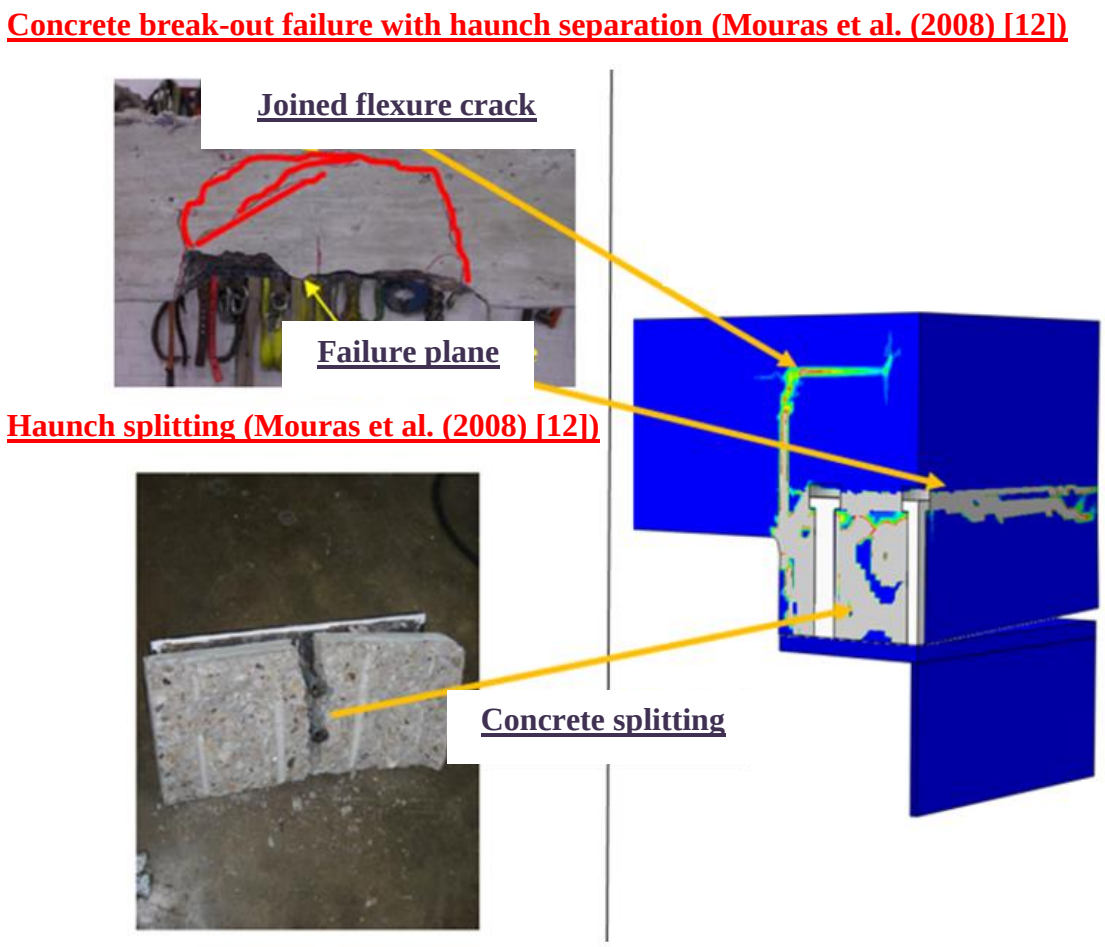

Figure 41 Concrete break-out failure mechanism under stud pulling and flexure (5-inch stud)

Additionally, Mouras et al. (2008) [12] reported that when longer shear studs (longer than 5 inches) were used in the experiments, horizontal cracks form below the top layer of reinforcement. This was captured by the finite element models, as shown in Figure 42 where a nine-inch stud is used.

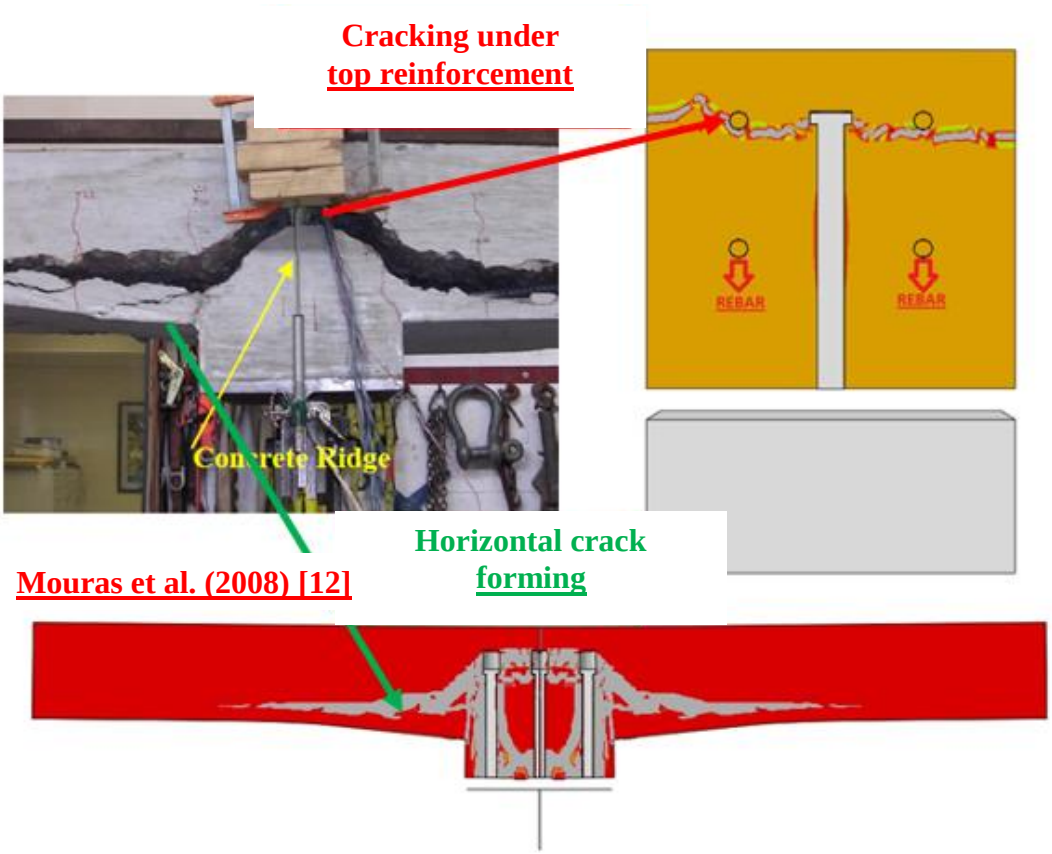

Figure 42 Concrete break-out failure mechanism under stud pulling and flexure (9 inch stud)

In the tests conducted by Mouras et al. (2008) [12], concrete slab segments 24 inches wide, 78 inches long and 8 inches thick were subjected to three point bending flexural tests by pulling on the shear studs. The shear studs were either 5 inches, 7 inches or 9 inches high, embedded in a 12-inch-wide and 3-inch-thick haunch (see Figure 43). Several shear stud configurations were tested, all of them longitudinally spaced at 24 inches, and transversely uniformly spaced within the 12-inch-wide haunch. The concrete compressive strength was 5.1 ksi for tests using 7 inch and 9 inch studs, and 5.9 ksi for tests using 5 inch transversely grouped shear studs.

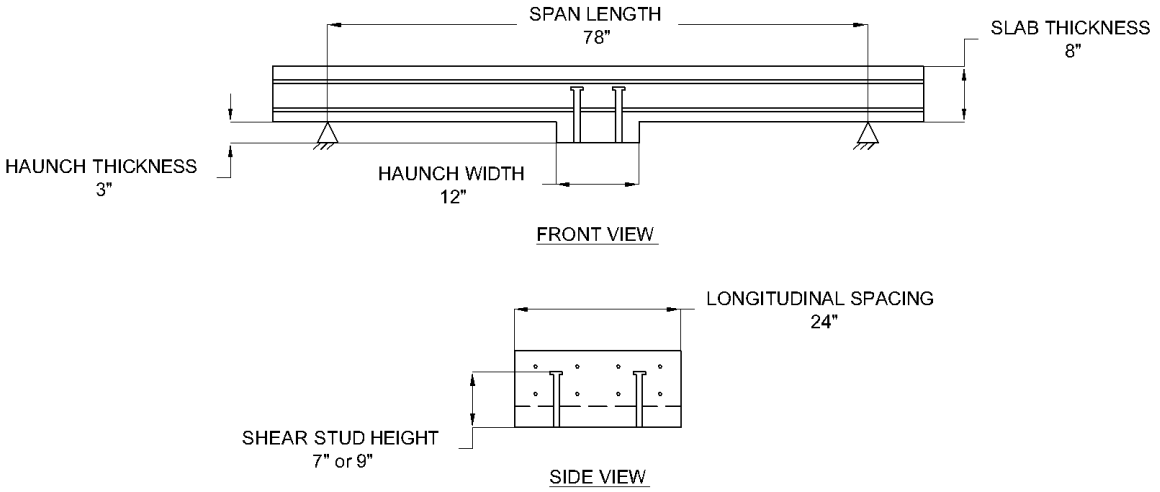

Figure 43 Dimensions of specimens tested by Mouras et al. (2008) [12]

A comparison among the experimental results from Mouras et al. (2008) [12], and the results from FEA is presented in Table 8. The concrete break-out strength computed by FEA is between 0.95 and 1.20 times the experimental values, which implied that all results are within 20%, with the majority of them within 10%.

Table 8 Comparison of experimental (Exp.) concrete break-out strength with results from FEA

Shear Stud Group Properties			Strength		FEA/Exp.
Height (in)	**Number**	**Spacing**	**Exp. (ksi)**	**FEA (ksi)**	
5	1	-	22.3	22.3	1.00
	2	Transverse (4 in)	19.2	21.4	1.11
	3	Transverse (4 in)	17.3	20.7	1.20
7.25	1	-	26.2	24.9	0.95
	2	Transverse (4 in)	25.1	24.9	0.99
	3	Transverse (4 in)	20.3	24.4	1.20
	2	Longitudinal (12 in)	27.2	30.0	1.10
	3	Longitudinal (8 in)	28.3	30.2	1.07
9.25	1	-	28.4	28.6	1.01
	2	Transverse (4 in)	27.7	29.2	1.05
	3	Transverse (4 in)	31.4	30.0	0.96
	2	Longitudinal (12 in)	29.5	30.5	1.03
	3	Longitudinal (8 in)	30.0	30.6	1.02

As stated, the load-displacement behavior from the experiments was compared to that predicted by the FEA and found to be in very good agreement. For example, as shown in Figure 44 and Figure 45, the analytical and experimental load-displacement behavior of the transversely grouped

7 inch shear studs and single 9 inch shear stud are compared. In both figures, the FEA results in a very good approximation of the corresponding experimentally obtained load-displacement curve.

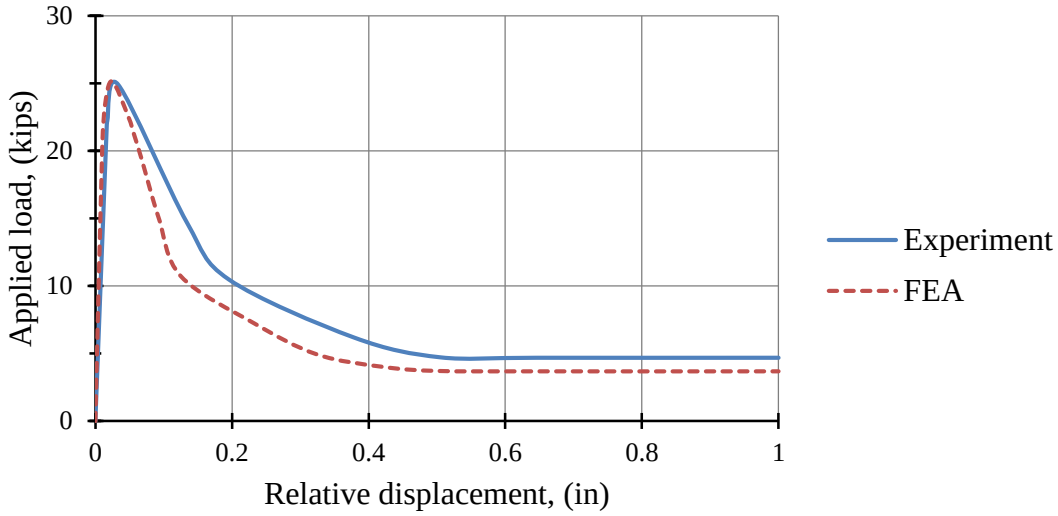

Figure 44 Experimental and FEA load-displacement relations for two transversely grouped 7-inch shear studs

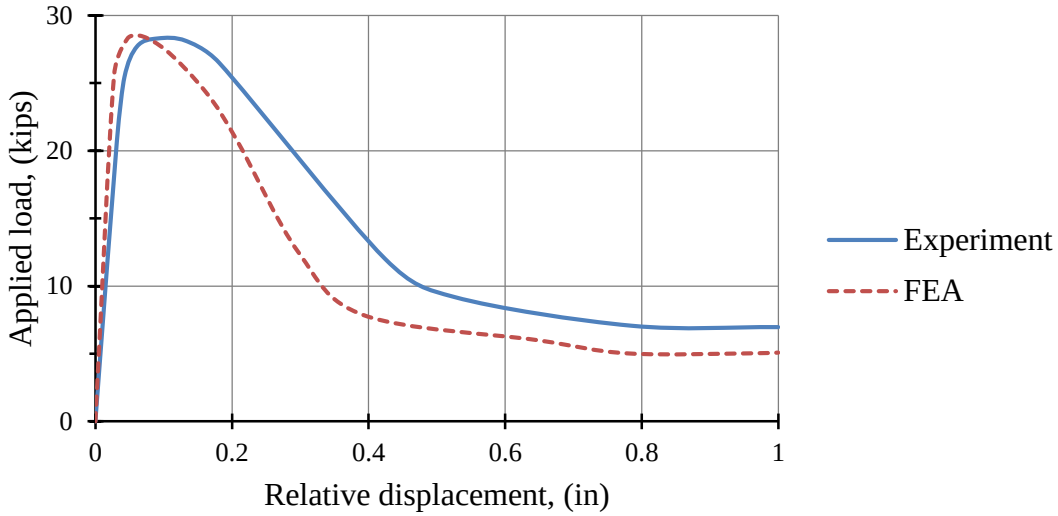

Figure 45 Experimental and FEA load-displacement relations for single 9-inch shear studs

Based on the results of the extensive benchmarking efforts, the following conclusions were reached:

- The CCD methodology [32] provides a reliable method to estimate the concrete break-out strength, based on a comparison with the experimental results reported in the ACI 355 database [29].
- The FEA methodology results in estimations of the concrete break-out strength of shear stud assemblies that are close to the mean concrete break-out strength values calculated per the CCD approach, and failure mechanisms coincident with those described by Fuch et al. (1995) [32].
- The FEA methodology replicates the behavior observed in the experiments conducted by Mouras et al. (2008) [12]. In this comparison, not only the strength values computed by the FEA were successfully benchmarked, but also the load-displacement relations, and failure mechanisms were reproduced as well.

Therefore, it is concluded that the FEA methodology developed herein can be reliable utilized to perform a parametric study to quantify how the tensile stiffness, strength, and ductility of transversely grouped shear studs is affected by various configurations typically used in composite steel bridges. The result of the parametric study can then be used to improve existing methodologies for the calculation of tensile strength of transversely grouped shear studs, as well as developing new methods to calculate the initial stiffness and ductility (i.e., tensile displacement at failure).

4.2.2 Comparison of full-scale test results to benchmarked FE predictions

As previously stated, the test performed by Mouras et al. (2008) [12] did not capture the failure modes that were observed by Neuman (2009) [3] in full-scale tests. Recall that in Figure 2, which illustrates the shear stud failure mechanism observed by Neuman (2009) [3] in a full-scale twin-tub-girder experiment, the failure cone characteristic of concrete break-out failure can be observed. On the other hand, Figure 1 illustrates the sub-assembly test specimen of Mouras et al. (2008) [12] which show flexural cracking at the corner of haunch, horizontal haunch separation, and center haunch splitting. In other words, the sub-assembly tests performed by Mouras et al. (2008) [12] predicted flexural failure combined with concrete break-out while in the full test failure was only

due to concrete break-out. Clearly, the behavior and therefore the observed strength, load-displacement, and ductility that would be estimated from the small-scale tests alone will not be in agreement with what would be expected in a real structure. To account for this error additional analysis was required.

During earlier benchmarking studies performed as a part of this dissertation on the full-scale twin-tub-girder test, FEA results showed that two-way bending in the slab occurs in the faulted state, primarily in the immediate region of the fracture, which is the critical location for stud pull out. In addition, the effects of continuity in both the longitudinal and transverse directions are significant.

As different configurations were investigated in the benchmarking process, it was found that by modifying the span length of the small-scale specimens modeled, the predicted failure mode varied. Since the FEA methodology was fully benchmarked, the analytical procedures previously described in Section 4.2.1 were utilized to develop a test geometry that best represented the conditions in the large-scale test performed by Neuman (2009) [3]. This ensures that the stiffness, strength, and ductility of the shear stud assembly that would take place in a real bridge are adequately estimated with a sub-assembly FE model.

As illustrated in Figure 2, the flexural cracking next to the edge of the haunch and the horizontal haunch separation reported by Mouras et al. (2008) [12] did not take place after the exterior tub girder fracture in the full-scale experiment conducted by Neuman (2009) [3]. Therefore, the failure mode in the full-scale experiment was concrete break-out without any observable interaction with other cracking due to flexure of the slab. Based on the full-scale experiment, it was concluded that the transverse moments that are developed at the edges of the haunch were not significant enough to affect the concrete-break strength of the shear studs. For the bridges analyzed in this study, the FEA showed that the load from the failed girder was transferred both longitudinally and transversely in the slab, and as well as through the intermediate diaphragms, resulting in a much lower moment at the edge of the haunch than if the load was transferred in the transverse direction only. This observation was verified after a finite element of the twin-tub-girder bridge used in the full-scale experiment was constructed.

Therefore, the moment that takes place at the edge of the haunch in the sub-assembly test is artificially increased since the span length selected by Mouras et al. (2008) [12] could have been based on the apparent assumption that the load was redistributed through transverse bending only. Further, the tests did not (and could not) include any longitudinal moments in the slab. To establish adequate dimensions for the sub-assembly FE model that accurately captures the behavior observed in the large-scale test, the span length was varied from six feet to two feet to identify a span length at which little to no flexural cracking was identified at the edge of the haunch edge. While span lengths less than two feet were investigated, there was little influence on the mean break-out strength below two feet. The results obtained by these models for the different span lengths are shown in Table 9 in which can be noted that while the initial stiffness and ductility are not affected, the span length inversely affects the mean strength. More importantly, it was found that at a span of two feet, the mode of failure was consistent with that observed in the full-scale test.

Table 9 Shear-stud sub-modeling results with different span lengths

Span Length (ft.)	**Mean Strength (kips)**	**Initial Stiffness (kips/in)**	**Failure Mode**
6’	21.6	2200	Flexural cracking w/ concrete break-out cone
4’	24.0	2200	
3’	26.2	2200	
2’	31.2	2200	Concrete break-out cone
<2’	32.0	2200	

In the model shown in Figure 46, in which the span was set at two feet, the concrete break-out failure cone geometry was similar to the failure in the full-scale experiment shown in Figure 1. In this sub-assembly model, the strength and initial stiffness were 31.2 kips and 2200 kips/in. Based on the above, the span length was set to 2ft and force-displacement curve was obtained for each of the small-scale FE models.

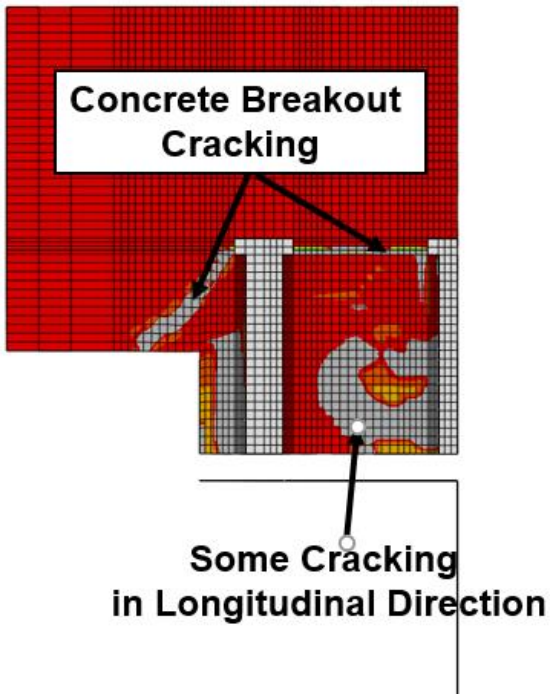

Figure 46 Concrete break-out failure geometry for a span length of 2 feet

After the shear stud sub-assembly modeling study was completed for the geometry used in the large-scale test, it was decided to model the second full-scale experiment of Neuman (2009) [3] but include the load-displacement curve obtained from the sub-assembly finite element model. This was performed in the following steps:

- Obtain load-displacement relations from the sub-assembly finite element model based on the configuration in the large-scale test.
- Apply the load-displacement relations obtained in the first step to a mesh independent connector element. (Details regarding the application procedure are discussed in Section 4.4).
- Analyze the full-scale model and compare the results to those reported by Neuman (2009) [3], including experimentally recorded stud failure observations, overall deflections, and other reported data.

Though all of the comparisons are not reported in detail herein, the agreement between the large-scale FE model and the experimental results was excellent, as shown by the following observations reported by Neuman (2009) [3] and that were replicated in the FEA of the full-scale test and shown in Figure 47:

A considerable amount of concrete break-out damage on the interior top flange of the fractured girder was observed.

- As much as 3.5 in. of separation was observed between the slab and the interior top flange of the failed girder.
- While a plot for the experimental crack separation on the exterior top flange of the fractured girder was not developed during the experimental work, Neuman (2009) [3] noted there were some concrete cracks over the exterior top flange.
- The damage zone extended up to thirty feet away for the mid span in each direction.
- The number and location of failed shear studs were reported by Neuman (2009) [3] were closely matched by the finite element model.

It is worth noting that in Figure 47, there is a modest difference in the number of shear studs which fail on the left-hand side of the plot. This is attributed to the fact that, in the full-scale test, the boundary conditions were symmetric and consisted of bearing pads, which can provide some restraint. In the FE model, the left side was modeled as an ideal "roller" while the right side was an ideal "pin". The roller support in the FE model provided no restraint to thrust and hence provided no restraint to the girder. As a result, the model with non-symmetric boundary conditions over-predicts the shear stud damage towards the left (roller) support. In this study, when the bridge was modelled with symmetric boundary conditions (two roller supports on each side of the fractured span), the FE model included symmetric concrete break-out behavior, but the length of the separation was over predicted. It is noted that in the same behavior was observed in the FEA results performed the UT researchers as well in Bernard et al. (2010) [19], though they did not provide an explanation as to the reason.

In summary the FEA methodology to model concrete break-out behavior in sub-assembly finite element models accurately predicts the stiffness, strength, and ductility of shear stud groups. Additionally, the tensile force-displacement relations obtained in sub-assembly finite element models can be reliably applied to full-scale models of composite steel bridges as supported by the benchmarking against the experimental observations by Neuman (2009) [3].

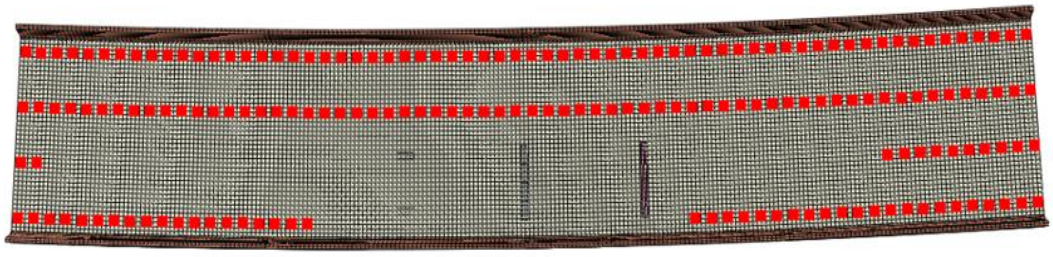

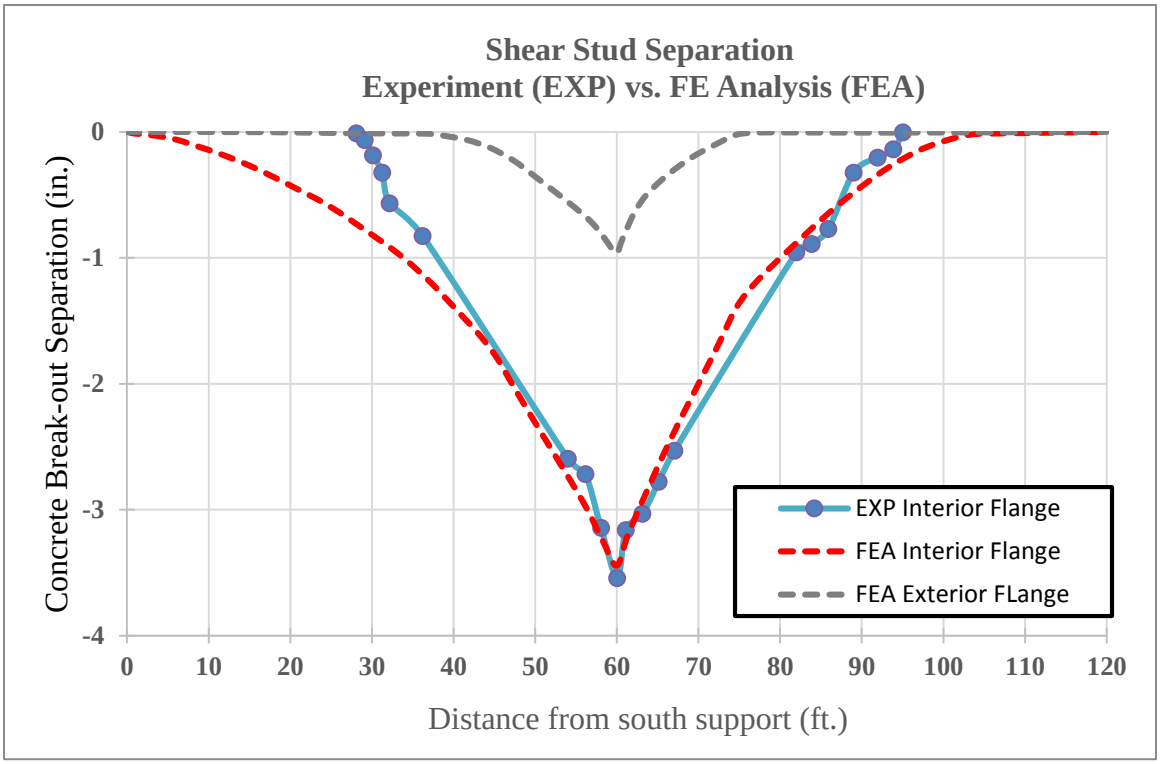

Figure 47 Experimental and analytical shear stud separation curves

4.2.3 Effect of dynamic strain rate

It is well known that at very high strain rates, increases in material strengths can be observed. This strength increase is common in very high strain rate conditions, such as blast and is often utilized in such applications. Mouras et al. (2008) [12] performed a limited number of shear stud concrete break-out experiments at loading rates that ranged from $8.7 \cdot 10^{-3}$ to $7.0 \cdot 10^{-2}$ in/in/sec. It was observed that dynamic resistance of the concrete break-out was 15% to 43% higher than the corresponding quasi-static experiments. However, in the actual large-scale experiment (second test) conducted by Neuman (2009) [3] the maximum strain rate at the intact girder bottom flange was only about $4 \cdot 10^{-3}$ to $5 \cdot 10^{-3}$ in/in/sec. Therefore, the strain rates due to sudden member fracture in a real bridge are lower than in the sub-assembly test, thus, the data obtained by Mouras et al.

(2008) [12] are not directly applicable to sudden failure of a primary steel tension member based on the large-scale experimental observations. According to TM 5-1300 [34] (Figure 48), at strain rates of $4 \cdot 10^{-3}$ to $5 \cdot 10^{-3}$ in/in/sec, the expected strength increase is less than 10%. It is also worth noting that different materials (steel or concrete) demonstrate different strength increases to a given strain rate. Further, different grades of steel respond differently as well. It is also well document that the effects are different under tensile strains as opposed to compressive strains. Incorporating such criteria into a specification would be very cumbersome and difficult to implement. Considering the variability associated with the data and the low strain rates, it was concluded that it would be reasonable and conservative to neglect any potential dynamic strength increases in the shear stud tensile and shear resistances.

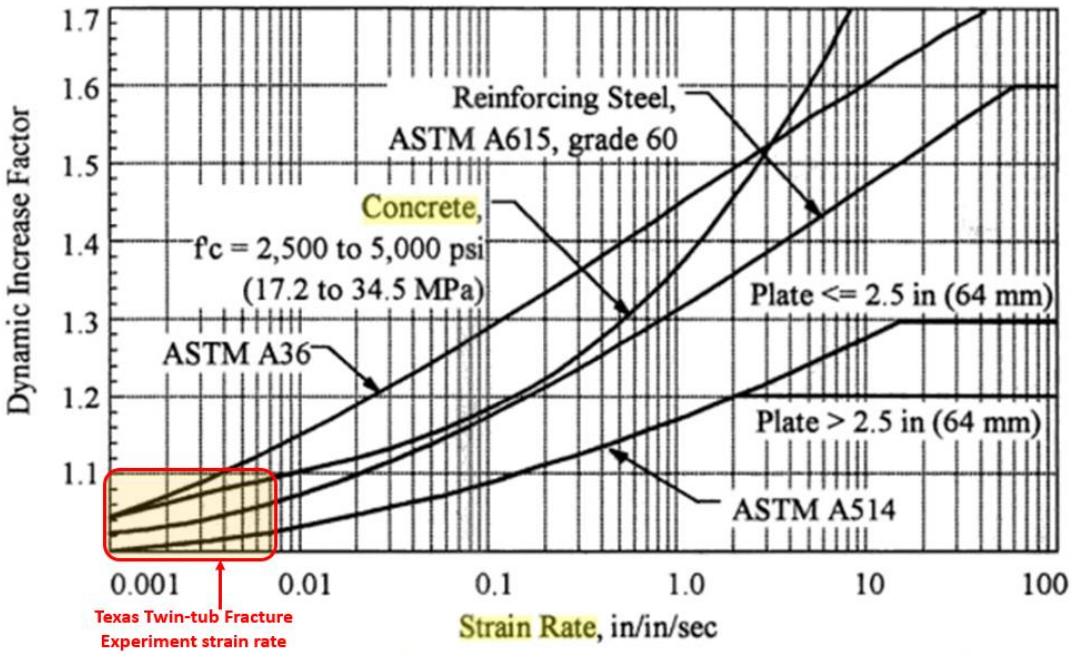

Figure 48 Effect of Strain Rate on Dynamic Material Strength (from TM 5-1300) [34]

4.2.4 Shear stud configurations and geometries considered in the parametric study for concrete break-out failure

While there are an infinite number of configurations that could be considered, only the most common configurations were considered in this study. Future research may be needed to address other configurations. Also, while many parameters were considered, some were quickly found to

have little to no impact on the overall performance, and others were limited to control the scope of the study. These are included in the list below:

- The thickness of the slab as the concrete break-out cone failure geometry is not dependent on the thickness of slab when flexural effects are not significant.
- Since it is the relative proportions of the haunch thickness as compared to the height of the stud that affects the behavior, the haunch thickness itself was not explicitly varied.
- The reinforcement was conservatively sized and positioned to ensure the ductility was not overestimated. In general, the presence of reinforcement below the head of the stud has the potential for increasing the ductility during break-out failure. However, it was not possible to include a number of reinforcement configurations significant enough so that their effects can be accounted for in the develop recommendation. Further, it is not practical to set design criteria based on the exact placement of rebar at various shear studs.

In total, eighty detailed non-linear finite element models were developed using the benchmarked FEA methodology to assess the effect of several parameters affecting the strength, stiffness and ductility of concrete break-out failure in shear stud assembly. The parameters included in the parametric study are shown in Figure 49. Specifically, the parameters and ranges were as follows:

- Concrete compressive strength: 4 ksi to 7 ksi.
- Shear stud height: 5 inches to 7 inches. Note that the effective stud height is equal to the shear stud height minus the height of the head (3/8 inch).
- Longitudinal spacing of shear studs: 10 inches to 18 inches.
- Top flange thickness: 1 inches to 3 inches.
- Haunch width: 12 inches to 20 inches:
    - For a 12-inch-wide flange/haunch, the span was 24 inches.
    - For a 20-inch-wide flange/haunch, the span was 32 inches.
- Number of transversely spaced shear studs: 1, 2, 3.
- For single shear stud, stud edge distance was half of the haunch width.
- For two transversely grouped shear studs, stud edge distance was quarter of the haunch width.
- For three transversely grouped shear studs, stud edge distance was 2 inches.

In the parametric study, all of the sub-assembly finite element models had a 8-inch thick slab with a 3-inch thick haunch. (Note, in this study this dimension is the distance between the top of the top flange and the bottom of the slab, as shown in Figure 49.)

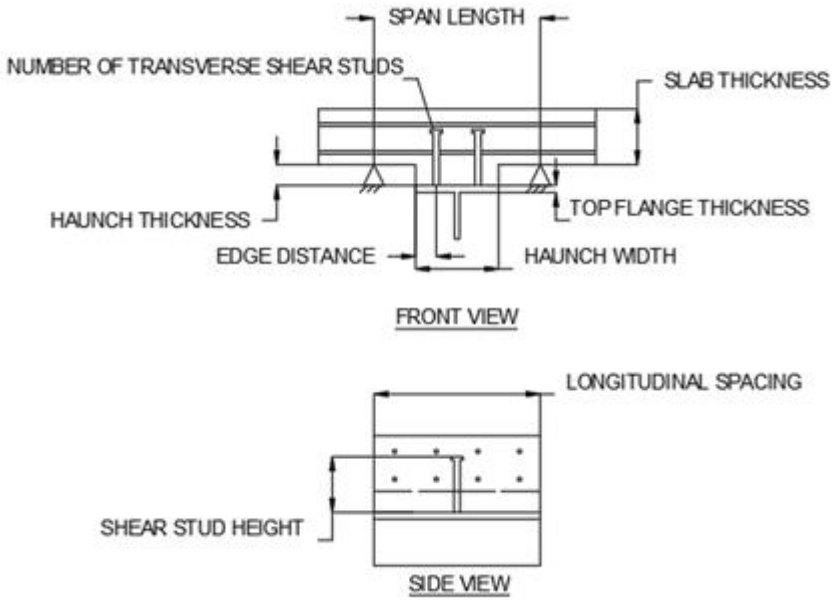

Figure 49 Geometrical parameters studied with FEA methodology

As stated, the main objective of the parametric study is to estimate the stiffness, strength, and ductility of different stud configurations. Additionally, the strength, stiffness, and ductility values computed by FEA are compared with the outcomes of suggested simplified methodology discussed in Section 4.2.5. These result comparisons are shown in the tables in Section 4.2.6.

4.2.5 Proposed methodology to estimate the tensile behavior of transversely grouped shear studs

4.2.5.1 *Initial tensile stiffness of transversely grouped shear studs*

The axial stiffness of a shear stud group depends on the *combined* effect of the stiffness of the shear stud shaft, the stiffness of the concrete section under the shear stud head, and the local transverse bending stiffness of the top flange. Although the stiffness is reduced as load increases and cracking develops around the shear stud assembly, the provisions in this section are used to

calculate a representative initial stiffness used in load-displacement relations that are applied to connector elements (further details regarding the application procedures are in Section 4.4).

The single stud steel stiffness, K_{s1} (kip/in), is based on axial stiffness due to elongation of the stud shaft, as follows:

$$K_{s1} = \frac{\pi E_s {d_s}^2}{4h_{ef}} = \frac{F_1}{\Delta_{s1}}$$

where E_s is the steel elastic modulus (ksi), F_1 is the applied force on the stud (kips), Δ_{s1} is the steel elongation (in), d_s is shear stud shaft diameter (in), and h_{ef} is shear stud effective height (in) (equal to height of the shear stud minus the height of the shear stud head) (as shown in Figure 50).

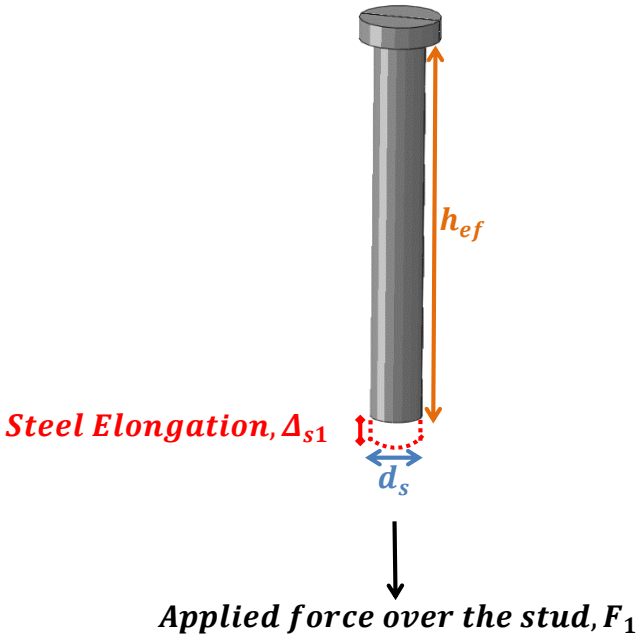

Figure 50 Single stud steel elongation and parameters

The overall axial stiffness of a single stud is also influenced by the contribution of the concrete stiffness, K_{c1} (kip/in) from the concrete compressive behavior under the head of the shear stud and also concrete crack initiation and propagation next to the stud head. The confinement under the head, i.e., hydrostatic pressure, is significantly high under the head of the shear stud, resulting in compressive stress than may be much greater than the concrete compressive strength as shown in the ACI 318-14 [11]. The under-head net area and the elastic modulus of the concrete were used

to developed K_{c1}; however in the stiffness formulation, it is difficult to determine the effective length L_u in order to obtain force over displacement relationship. L_u was developed empirically (as will be explained in Section 4.2.6.1) and is calculated as follows:

$$K_{c1} = \frac{\pi E_c \left({d_h}^2 - {d_s}^2\right)}{4L_u} = \frac{\pi E_c \left({d_h}^2 - {d_s}^2\right)}{5} = \frac{\mathrm{F_1}}{\Delta_{\mathrm{c1}}}$$

where E_c is the concrete elastic modulus (ksi), d_h is the shear stud head diameter (in), and d_s is the shear stud shaft diameter (in). Note, in the equation above, the value of $4L_u$ was found to be approximately 5, as will be discussed below. The number 4 comes from the calculation of the circular areas under the head of the stud.

The flange bending stiffness, K_{p1} (kip/in.), only affects the stiffness of two or more transversely spaced shear studs, since a single stud centered over the web is not affected by the flange bending. The calculation is based on the flexural stiffness of a cantilever plate with a fixed-end (web to top flange connection) and a free-end (stud to top flange connection), as follows:

$$K_{p1} = \frac{E_s l_s {t_f}^3}{4{s_o}^3} = \frac{\mathrm{F_1}}{\Delta_{\mathrm{p1}}}$$

where E_s is the steel elastic modulus (ksi), l_s is longitudinal stud spacing (in), h_{ef} is shear stud effective height (in) (equal to height of the shear stud minus the height of the shear stud head), t_f is top flange thickness (in), I is plate inertia (in^4), and s_o is the distance from the center of the flange to the outermost stud (in) (as shown in Figure 51).

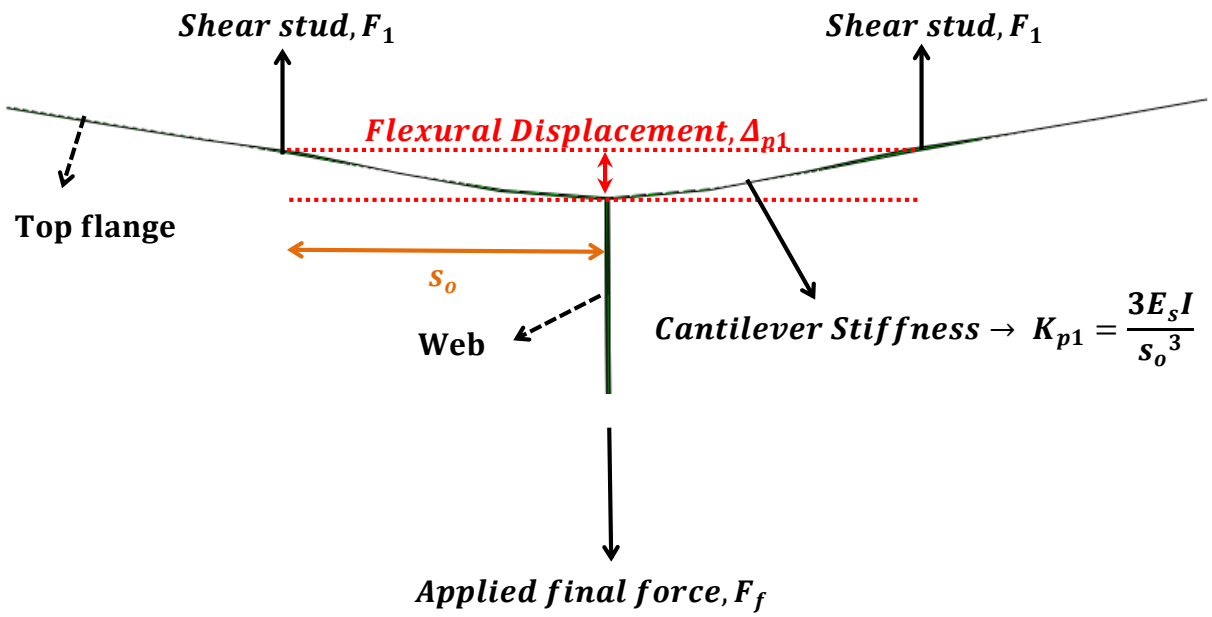

Figure 51 Cantilever stiffness of top flange

For the reason cited above, due to the fact that the stud is at the center of the flange, the effect of the flange bending stiffness is neglected for the case of a single shear stud is used. In this specific case, the total combined axial stiffness of a single stud, K_g (kip/in) can be calculated using the accepted approach associated with springs in parallel as follows:

$$K_g = \frac{1}{\frac{1}{K_{c1}} + \frac{1}{K_{s1}}}$$

The axial stiffness of two transversely grouped shear studs, K_g (kip/in) can be calculated as follows:

$$K_g = \frac{Number\ of\ Studs}{\frac{1}{K_{c1}} + \frac{1}{K_{s1}} + \frac{1}{K_{p1}}} = \frac{2}{\frac{1}{K_{c1}} + \frac{1}{K_{s1}} + \frac{1}{K_{p1}}}$$

For three transversely grouped shear studs, the amount of load is not distributed to each shear stud equally, and the distribution is dependent on the thickness of the flange. Outermost studs carry lower loads (F_o) than the applied load (F_c) on the stud at the center of the flange due to local flange bending as illustrated in Figure 52.

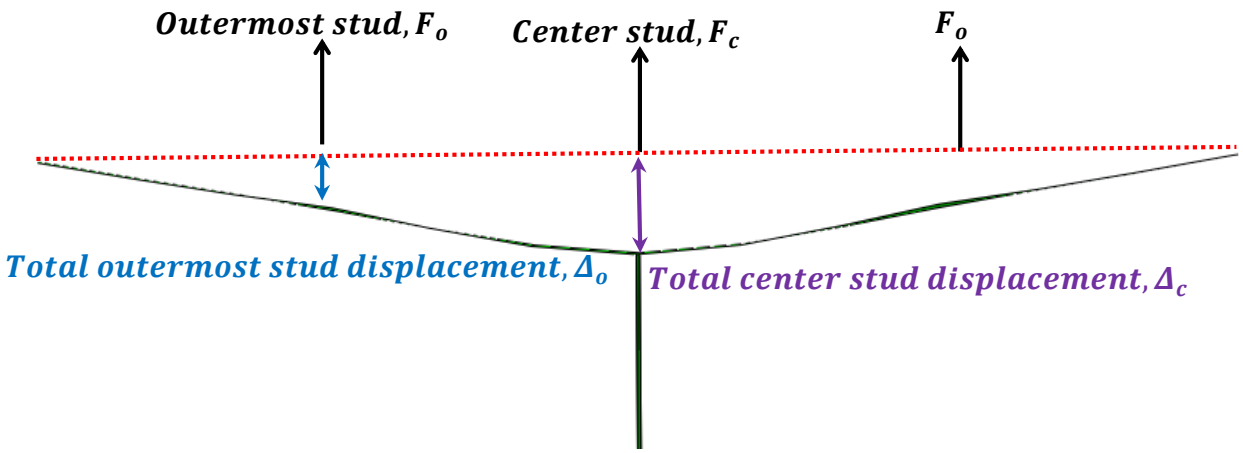

Figure 52 Load distribution of three transversely grouped shear studs

The cumulative stiffness depends on the load distribution ratio (R), which accounts for the flexibility of the flange. The load distribution ratio, R for three transversely grouped shear studs can be calculated as:

$$R = \frac{F_c}{F_o} = \frac{\mathrm{K_1} + \mathrm{K_{p1}}}{K_{p1}}$$

K_1 is the stiffness of a single shear stud neglecting flange flexibility effects (kip/in):

$$K_1 = \frac{1}{\frac{1}{K_{c1}} + \frac{1}{K_{s1}}}$$

The load distribution ratio formulation is obtained by the following steps:

$$\Delta_\mathrm{c} = \Delta_\mathrm{o} + \Delta_\mathrm{p1}$$

Δ_c is relative displacement of the stud at the center of the flange, Δ_o is relative displacement of the outermost studs, and Δ_p1 is the displacement from the flexural effect of the top flange:

$$\Delta_\mathrm{p1} = \frac{\mathrm{F_o}}{K_{p1}}, \qquad \Delta_\mathrm{o} = \frac{\mathrm{F_o}}{K_1}, \qquad \Delta_\mathrm{c} = \frac{\mathrm{F_c}}{K_1},$$

$$\frac{\mathrm{F_c}}{K_1} = \frac{\mathrm{F_o}}{K_{p1}} + \frac{\mathrm{F_o}}{K_1} \rightarrow \quad R = \frac{F_c}{F_o} = \frac{\mathrm{K_1 + K_{p1}}}{K_{p1}}$$

The axial stiffness of three transversely grouped shear studs, K_g (kip/in) can then be calculated as follows:

$$K_g = \frac{F_c + 2F_o}{\Delta_\mathrm{c}} = \frac{F_c}{\Delta_\mathrm{c}} + \frac{2F_c/R}{\Delta_\mathrm{c}} = K_1 \frac{R+2}{R}$$

4.2.5.2 ***Tensile strength of transversely grouped shear studs***

Shear studs under high tensile load may fail due to shear stud steel rupture, concrete pullout, or concrete break-out. For composite bridges, the nominal tensile resistance, $N_{g,n}$ (kip), of a shear stud group embedded in concrete shall be calculated as the minimum of the ultimate strength of the shear stud steel rupture failure, N_{sa} (kip), concrete pullout failure, N_{pn} (kip), or concrete break-out failure, N_{cb} (kip), as follows:

$$N_{g,n} = \min\left(N_{sa}, N_{pn}, N_{cb}\right)$$

The formulation noted in Section 17.4.1.2 of the ACI 318-14 [11] is used in this study to calculate the tensile rupture strength of transversely grouped shear studs, N_{sa} (kips) as follows:

$N_{sa} = N_s\, A_{se,N} f_{uta}$, for single or two transversely grouped shear studs

$A_{se,N}$ is the effective cross-sectional area of the shear stud shaft (in^2), f_{uta} is the ultimate tensile strength of the stud (ksi), and N_s is the number of transversely grouped shear studs.

Generally, in three transversely grouped shear studs, the shear stud in the middle of the group carries more load than the outermost studs. This results in a reduction of the shear stud steel rupture strength of transversely grouped shear studs than would be estimated assumed all three carry the same load, as discussed above. Hence, the formulation noted in Section 17.4.1.2 of the ACI 318-14 [11] was modified in this study. In steel, plastic deformation is much larger than elastic deformation, therefore the load inequality was considered only in the plastic range. The

tensile rupture strength of three transversely grouped shear studs, N_{sa} (kips) is calculated as follows:

$$N_{sa} = 3A_{se,N}f_{ya} + \frac{R+2}{R}\left(f_{uta} - f_{ya}\right)A_{se,N}$$, for three transversely grouped shear studs

f_{ya} is the yield tensile strength of the stud (ksi).

The pullout strength and concrete break-out equations are based on the 5% fractile calculations. The formulation noted in Section 17.4.3.4 of the ACI 318-14 [11] is used in this study to calculate the pullout strength of cast-in place shear studs, N_{pn}(kip) is calculated as follows:

$$N_{pn} = N_s\psi_{c,P}(8A_{brg}f_c')$$, for one or two transversely grouped shear studs;

A_{brg} is the under-head cross-sectional net area for single stud (in^2), f_c' is the specified concrete compressive strength (ksi), and $\psi_{c,P}$ is the cracking modification factor for pullout strength. When cracking is not expected at service levels, $\psi_{c,P}$ is equal to 1.4, otherwise it is equal to be 1.0, in agreement with the procedures in ACI 318-14 [11]. The Engineer may wish to conservatively take $\psi_{c,P}$ as 1.0 regardless of the presence of cracking at service levels.

The load distribution ratio reduces the pullout strength of transversely grouped shear studs; hence, the formulation noted in Section 17.4.3.4 of the ACI 318-14 [11] was modified in this study. The pullout strength of three transversely grouped shear studs, N_{pn}(kip) is calculated as follows:

$$N_{pn} = \frac{R+2}{R}\psi_{c,P}(8A_{brg}f_c')$$, for three transversely grouped shear studs

It is noted that when single stud pullout strength is higher than single stud steel tensile strength, there is no need to check pull-out strength. Stud pullout is not the governing failure mode when the following relation is true:

$$\psi_{c,P}\left(8A_{brg}f_c'\right) > A_{se,N}f_{uta}$$

As previously discussed, the concrete capacity design (CCD) approach in section 17.4.2 of the ACI 318-14 [11] provides the best approximation to calculate concrete break-out strength, however, this formulation does not consider the effects of the haunch. The CCD methodology was

improved in the course of the research with the modifications developed in this report. Specifically, an improved method to calculate the edge distance, c_1, was developed as shown below, to account for the behavior and cracking path which results when a haunch is present. As a result, the modified approach shown below is recommended to be used for the break-out capacity calculation under tensile loading in the presence of a haunch for studs in cast-in-place concrete. For this case, the concrete break-out strength of transversely grouped shear studs, N_{cb} (kips), can be calculated as follows:

$$N_{cb} = \frac{A_N}{A_{No}} \psi_{ed,N} \psi_{c,N} N_b \text{ from CCD approach [11]}$$

A_{No} (in^2) is the projected area of the failure surface for a single headed shear stud (in^2), A_N is the combined projected area of the failure surface for a group of headed shear studs (in^2), $\psi_{c,N}$ is the cracking modification factor for concrete break-out strength, $\psi_{ed,N}$ is the edge modification factor, and N_b is the single shear stud concrete break-out capacity (kips). When cracking is not expected at service levels, $\psi_{c,N}$ is equal to 1.25, otherwise it is equal to be 1.0, in agreement with the procedures in ACI 318-14 [11]. The Engineer may wish to conservatively take $\psi_{c,N}$ as 1.0 regardless of the presence of cracking at service levels. A_{No}, A_N, $\psi_{ed,N}$, and N_b are calculated as follows:

$$A_{No} = 9{h_{ef}}^2$$

$$A_N = 2l_s(c_1 + s_0) \leq 6h_{ef}(c_1 + s_0)$$

$$\psi_{ed,N} = 0.7 + 0.3\frac{c_1}{1.5h_{ef}} \leq 1.0 \text{ (CCD) from CCD approach [11]}$$

$$N_b = \frac{k}{1000}(1000f_c')^{0.5}{h_{ef}}^{1.5} \text{ from CCD approach [11]}$$

h_{ef} is the shear stud effective height (in) (equal to height of the shear stud minus the height of the shear stud head), l_s is the longitudinal stud spacing (in), c_1 is the edge distance (in), f_c' is the specified concrete compressive strength (ksi), and k is a constant which is taken as 24 representing a 5% fractile strength calculation, and s_o is the distance from the center of the flange to the outermost stud (in), which should be taken as zero for a single shear stud. The determination of

the edge distance, c_1, was developed in this study to account for the behavior and cracking path which results when a haunch is present.

If there is no flexural cracking at the corner of haunch as in Figure 53, the edge distance, c_1, which is the horizontal distance between the center of the outermost stud and location at which the concrete break-out cracking path intersects any edge of the slab is calculated as follows:

$$c_1 = \max\left(1.5\left(h_{ef} - t_h\right), 0.5w_h - s_o\right) \leq 1.5h_{ef}$$

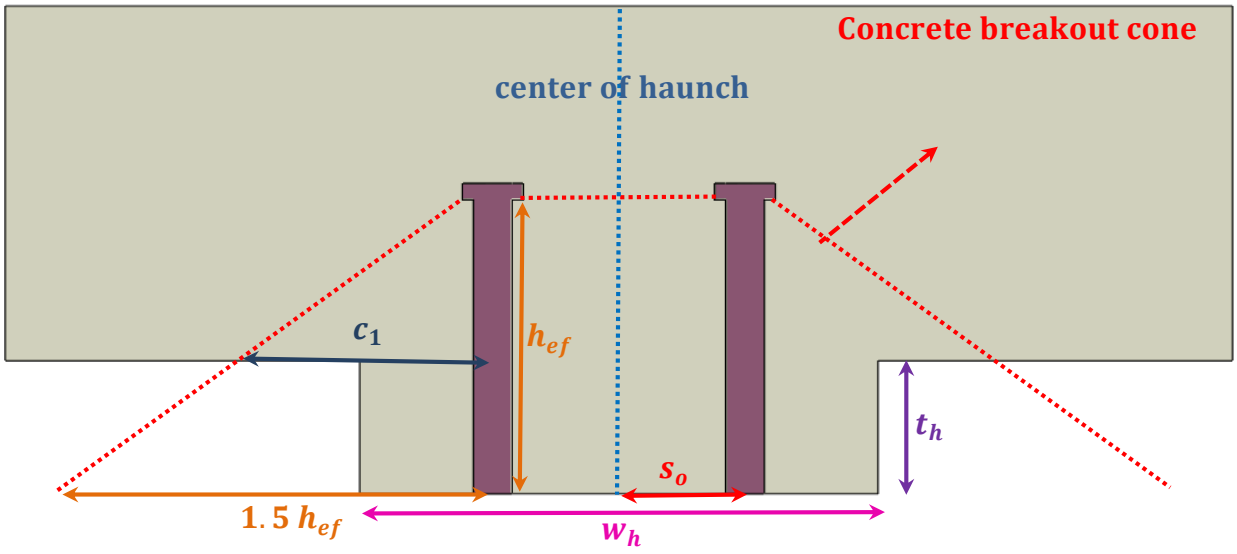

Figure 53 Concrete break-out cone geometry without flexural cracking

h_{ef} is the shear stud effective height (in), t_h is the thickness of the haunch (in), w_h is the width of the haunch (in), and s_o is the distance from the center of the flange to the outermost stud (in), which should be taken as zero for a single shear stud.

If there is flexural cracking at the corner of haunch, even if the flexural cracking at the corner of haunch does not combine with concrete break-out cracking, the edge distance, c_1, which is the horizontal distance between the center of outermost stud and flexural cracking path (shown in Figure 54) is conservatively calculated as follows:

$$c_1 = 0.5w_h - s_o \leq 1.5h_{ef}$$

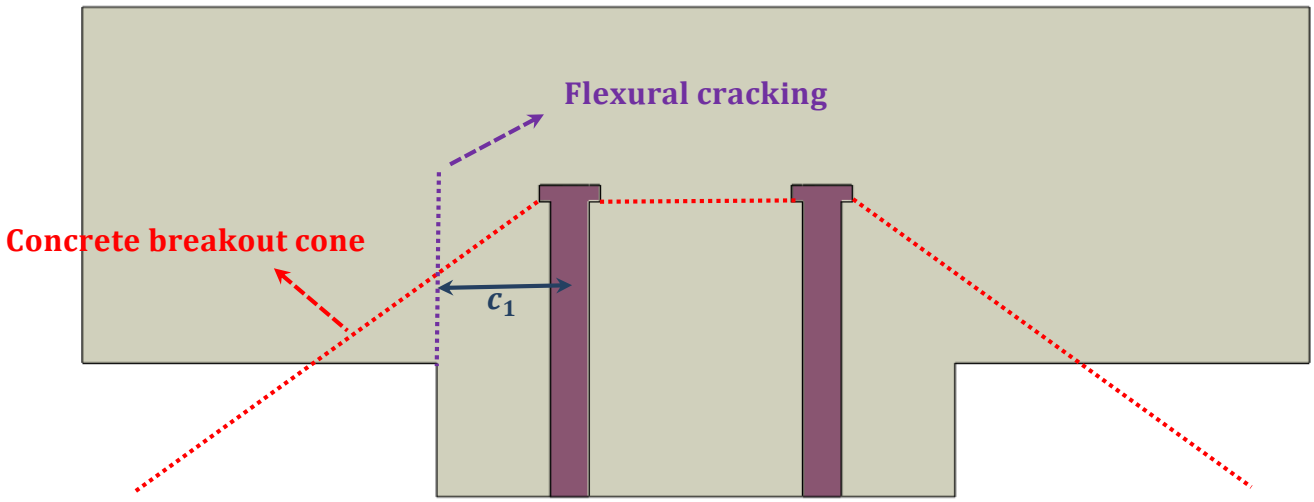

Figure 54 Concrete break-out cone geometry with flexural cracking

4.2.5.3 ***Load-displacement relationships of transversely grouped shear studs***

In order to properly define the tensile behavior of transversely grouped shear studs embedded in concrete, it is necessary to construct tensile load-displacement relations that are dependent upon the governing failure mode. Therefore, prior to developing the appropriate load-displacement relation it necessary to know the axial stiffness of a shear stud group, K_g, and the nominal tensile strength, $N_{g,n}$, as defined in Section 4.2.5.1 and Section 4.2.5.2, respectively.

If the governing failure mode is tensile rupture, i.e., $N_{g,n} = N_{sa}$, the tension force as a function of axial displacement for transversely grouped shear studs, $N_g(\delta_N)$, is initially linear elastic with stiffness equal to K_g. Once the tensile yield strength of transversely grouped shear studs, N_{ya}, is reached the relation is plastic with linear hardening until the nominal tensile strength, $N_{g,n}$, is reached. At this point the failure strain and hence the displacement is equal to 5% of the effective height of the shear stud, at which point failure of the shear stud group is conservatively assumed to take place.

Therefore, when the governing failure mode is tensile rupture, the tensile load-displacement relationship follows the steel stress-strain diagram in Chapter 3, and it can be explained as:

$$N_g(\delta_N) = \begin{cases} K_g\,\delta_N & for\ \ \delta_N \le \dfrac{N_{ya}}{K_g} \\ N_{ya} + \dfrac{\left(\delta_N - \dfrac{N_{ya}}{K_g}\right)\left(N_{g,n} - N_{ya}\right)}{0.05h_{ef} - \dfrac{N_{ya}}{K_g}} & for\ \ \dfrac{N_{ya}}{K_g} < \delta_N \le 0.05h_{ef} \end{cases}$$

The yield strength of transversely grouped shear studs, N_{ya}, is calculated as follows:

$$N_{ya} = N_s A_{se,N}\, f_{ya}$$

N_s is the number of transversely grouped shear studs, $A_{se,N}$ is the effective cross-sectional area of single shear stud (in^2), and f_{ya} is the nominal yield strength of the studs (ksi).

Once the tensile displacement reaches 5% of the effective height of the shear stud, ($\delta_N = 0.05h_{ef}$), failure of the transversely grouped shear studs shall be introduced. The suggested load-displacement behavior is shown in Figure 55.

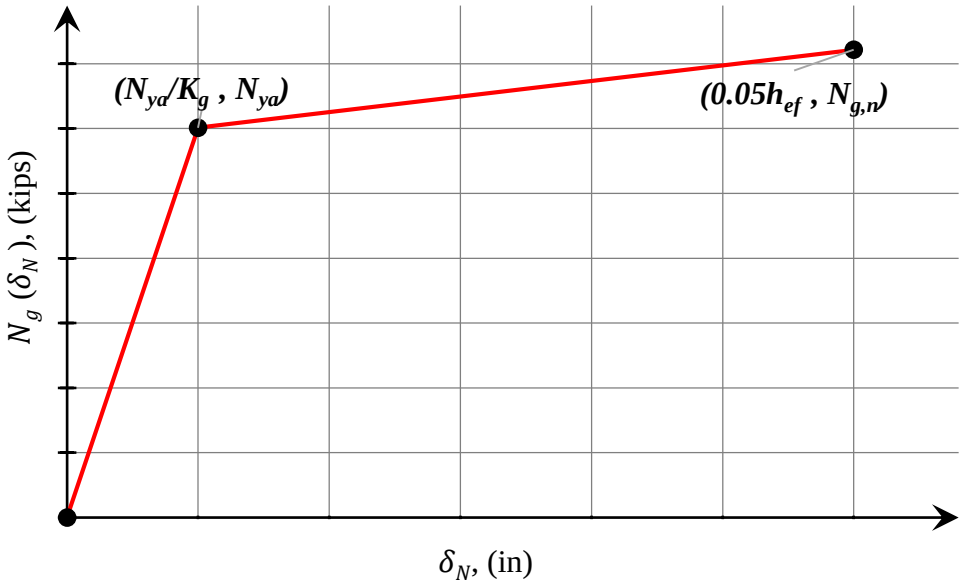

Figure 55 Steel rupture behavior of stud group

If the governing failure mode is concrete break-out or pullout, i.e., $N_{g,n} = N_{cb}$, or $N_{g,n} = N_{pn}$, the tension force as a function of axial displacement for transversely grouped shear studs, $N_g(\delta_N)$, is initially linear elastic with stiffness equal to K_g. Once the concrete break-out strength, N_{cb}, or the

pullout strength, N_{pn}, is reached the relation is characterized by linear softening until the tensile displacement of a shear stud group at failure, $\delta_{N,f}$, is reached, at which point the shear stud group has exhausted any tensile resistance.

Therefore, the tensile load-displacement relationship is based on the recommended behavior by Mouras et al. (2008) [12] with empirically developed displacement limits. When the governing failure mode is tensile rupture, the behavior is as follows:

$$N_g(\delta_N) = \begin{cases} K_g\ \delta_N & for\ \ \delta_N \leq \dfrac{N_{g,n}}{K_g} \\ K_g\ N_{g,n} \dfrac{\delta_{N,f} - \delta_N}{K_g \delta_{N,f} - N_{g,n}} & for\ \ \dfrac{N_{g,n}}{K_g} < \delta_N \leq \delta_{N,f} \end{cases}$$

Throughout the parametric study, the empirically developed tensile displacement of a shear stud group at failure for shear stud pullout or concrete break-out, $\delta_{N,f}$, is as follows:

For a single shear stud:

$$\delta_{N,f} = 20.0 \frac{N_{g,n}}{K_g}$$

For two transversely grouped shear studs:

$$\delta_{N,f} = 7.5 \frac{N_{g,n}}{K_g}$$

For three transversely grouped shear studs:

$$\delta_{N,f} = 6.4 \frac{N_{g,n}}{K_g}$$

The values of the constants (6.4, 7.5, 20.0) in the equations above were conservatively developed by using trial and error process in Section 4.2.6. The objective was to develop individual constants which best represented the results of the individual FE analysis. The suggested load-displacement behavior is shown in Figure 56.

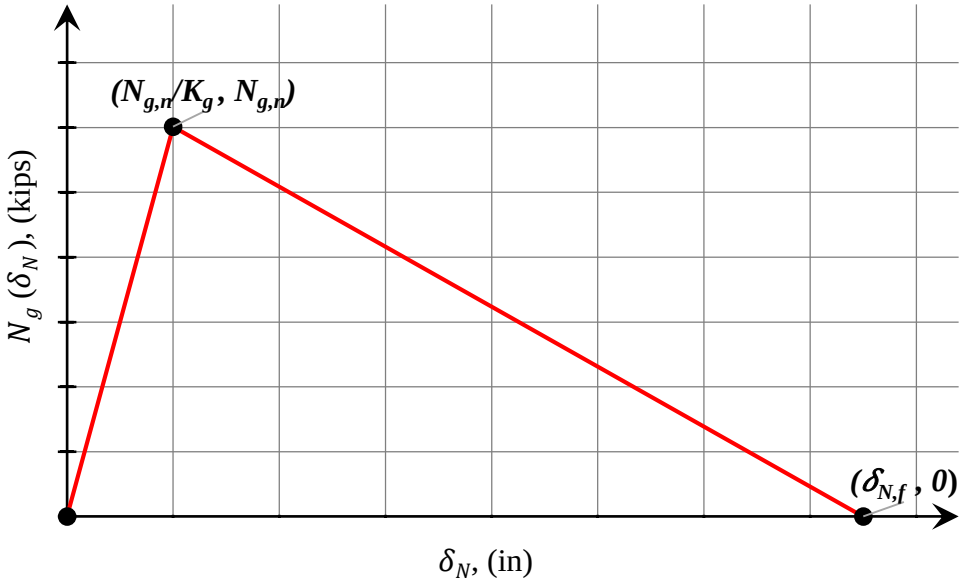

Figure 56 Concrete break-out and pullout failure behavior of stud group

4.2.6 Results of FEA parametric study and proposed method to estimate strength, stiffness, and ductility

A comprehensive FEA parametric study was conducted in order to improve existing provisions used to calculate the tensile stiffness, strength, and ductility of transversely grouped shear studs. The study is limited to the concrete break-out failure mode since it was found during the study that it will be the governing failure mode in the majority of shear stud configurations employed in typical composite steel bridges. The results of the parametric used were used to develop modification to the CCD methodology Fuchs et al. (1995) [32], which are included in Section 4.2.5. The scope of the study is limited to single shear studs (Section 4.2.6.1), two transversely grouped shear studs (Section 4.2.6.2), and three transversely grouped shear studs (Section 4.2.6.3). Although it is possible to encounter configurations with more than three transversely grouped shear studs, the configurations considered in the current study cover a large portion of the composite bridge inventory. It should be noted that the results and conclusion of the current parametric study may not be directly applicable to other shear stud assembly configuration

Furthermore, the developed methodology with flexural cracking were compared with Mouras et al. (2008) [12] in Table 10. It can be noted that the developed methodology is able to estimate the tensile capacity of the shear studs conservatively for 6 ft. span length especially for 9 in. high shear studs; since the methodology was purposed to be used for infinitely long spans.

Table 10 The comparisons between Mouras et al. 2008 [12] experiments and the developed methodology

Shear Stud Group Properties			**Strength**		
Height (in)	**Number**	**Spacing**	**Exp. (kips)**	**Simplified (kips)**	**5% Fractile (kips)**
5 (5.9 ksi)	1	-	22.3	20.3	15.2
	2	Transverse (4 in)	19.2	18.5	13.9
	3	Transverse (4 in)	17.3	16.6	12.5
7.25 (5.1 ksi)	1	-	26.2	21.0	15.8
	2	Transverse (4 in)	25.1	19.6	14.7
	3	Transverse (4 in)	20.3	18.2	13.7
	2	Longitudinal (12 in)	27.2	24.4	18.3
	3	Longitudinal (8 in)	28.3	22.7	17.0
9.25 (5.1 ksi)	1	-	28.4	20.5	15.4
	2	Transverse (4 in)	27.7	19.4	14.6
	3	Transverse (4 in)	31.4	18.3	13.7
	2	Longitudinal (12 in)	29.5	20.5	15.4
	3	Longitudinal (8 in)	30.0	19.5	14.6

4.2.6.1 ***Single shear stud configuration***

The first part of the parametric study was performed to obtain strength and ductility data for a single shear stud. To determine the concrete stiffness constant L_u, a two-step process was followed. First, the calculated steel stiffness (K_{s1}) was subtracted from the total FE stiffness (K_g) to obtain the concrete stiffness under the head of a single stud (K_{c1}). Next, concrete stiffness obtain to determine the constant in Section 4.5.2.1 as shown in Table 11.

From here on, rather than focusing on the nominal concrete break-out strength, N_{cb}, which is based on 5% fractile of the used test data, the focus will be on the average concrete break-out strength, $N_{cb,avg}$. From Section 4.2.5.2, it can be recalled that, in the calculation of the single shear stud concrete break-out capacity, a constant k was utilized. According to Fuchs et al. (1995) [32], the value of that constant is 24 for a 5% fractile strength calculation, and 40 for an average strength calculation. Since the FEA methodology was developed with the objective of capturing the behavior observed in experiments, the results from FEA are compared against average strength calculated values.

The average concrete break-out strength, initial stiffness and displacement at failure calculated by the FEA are shown in Table 12. These are compared against initial stiffness calculated per Section 4.2.5.1, and concrete break-out strength calculated per Section 4.2.5.2 with k equal to 40. The mean and standard deviation of the difference in stiffness are -2.19% and 3.06%, respectively, the mean and standard deviation of the difference in strength are -2.50% and 8.27%, respectively. Given the very good correlation between the FEA stiffness and strength results with the simplified calculations, the following equation for the displacement at failure, $\delta_{N,f}$, was developed:

$$\delta_{N,f} = 16.0\frac{N_{cb,avg.}}{K_g}$$

which resulted in a mean and standard deviation of the difference in displacement at failure of -14.22% and 11.84%, respectively. Note, in the equation above, a constant of 16.0 was used rather than 20.0 as is shown in Section 4.2.5.3 since the mean value ($N_{cb,avg.}$) is being considered rather than 5% fracture strength and to ensure the target total displacement is the same regardless of what fractile is used in the strength calculation.

Table 11 Determination of concrete stiffness constant L_u

f'_c (ksi)	h_{ef} (in)	l_s (in)	w_h (in)	FEA Results K_g (kip/in)	Simplified Method K_{s1} (kip/in)	Concrete Stiffness K_{c1} (kip/in)	Concrete Stiffness $4L_u$
4	5	10	9	1562	3770	2667	4.78
7	5	10	9	1804	3770	3459	4.87
4	7	10	9	1343	2632	2742	4.65
7	7	10	9	1518	2632	3586	4.70
4	5	18	9	1494	3770	2474	5.15
7	5	18	9	1817	3770	3507	4.81
4	7	18	9	1354	2632	2788	4.57
7	7	18	9	1505	2632	3514	4.80
4	5	10	12	1606	3770	2798	4.55
7	5	10	12	1842	3770	3601	4.68
4	7	10	12	1379	2632	2896	4.40
7	7	10	12	1517	2632	3581	4.71
4	5	18	12	1439	3770	2327	5.47
7	5	18	12	1750	3770	3266	5.16
4	7	18	12	1374	2632	2874	4.43
7	7	18	12	1520	2632	3597	4.69
						Average	4.78 ≈ 5.0

Notes:

- f'_c = Concrete compressive strength.
- h_{ef} = Effective stud height.
- l_s = Longitudinal stud spacing.
- w_h = Haunch width.
- K_g = Initial stiffness.
- K_{s1} = Calculated single stud steel stiffness according to Section 4.2.5.1.
- K_{c1} = Single stud concrete stiffness [$K_{c1} = (\frac{1}{K_g} - \frac{1}{K_{s1}})^{-1}$].
- $4L_u$ = a constant equal to ($4L_u = \pi E_c \left({d_h}^2 - {d_s}^2\right) / K_{c1}$).

Table 12 Single Shear Stud FEA vs Simplified Methodology Results

f'_c (ksi)	h_{ef} (in)	l_s (in)	w_h (in)	FEA Results			Simplified Method			Difference		
				K_g (kip/in)	$N_{cb,avg}$ (kip)	$\delta_{N,f}$ (in)	K_g (kip/in)	$N_{cb,avg}$ (kip)	$\delta_{N,f}$ (in)	K_g (%)	$N_{cb,avg}$ (%)	$\delta_{N,f}$ (%)
4	5	10	9	1562	10.86	0.12	1521	10.52	0.11	-2.62	-3.13	-7.78
7	5	10	9	1804	15.44	0.12	1780	13.92	0.13	-1.33	-9.84	4.27
4	7	10	9	1343	12.21	0.16	1295	10.26	0.13	-3.57	-15.97	-20.77
7	7	10	9	1518	15.26	0.16	1478	13.58	0.15	-2.64	-11.01	-8.12
4	5	18	9	1494	15.06	0.2	1521	14.6	0.15	1.81	-3.05	-23.21
7	5	18	9	1817	20.59	0.2	1780	19.32	0.17	-2.04	-6.17	-13.17
4	7	18	9	1354	17.89	0.28	1295	18.47	0.23	-4.36	3.24	-18.5
7	7	18	9	1505	24.84	0.28	1478	24.44	0.26	-1.79	-1.61	-5.51
4	5	10	12	1606	13.54	0.2	1521	15.05	0.16	-5.29	11.15	-20.84
7	5	10	12	1842	18.6	0.2	1780	19.91	0.18	-3.37	7.04	-10.52
4	7	10	12	1379	12.6	0.24	1295	11.55	0.14	-6.09	-8.33	-40.54
7	7	10	12	1517	17.47	0.24	1478	15.28	0.17	-2.57	-12.54	-31.08
4	5	18	12	1439	19.13	0.24	1521	20.88	0.22	5.7	9.15	-8.48
7	5	18	12	1750	25.59	0.24	1780	27.62	0.25	1.71	7.93	3.45
4	7	18	12	1374	22.08	0.32	1295	20.78	0.26	-5.75	-5.89	-19.77
7	7	18	12	1520	27.79	0.32	1478	27.5	0.3	-2.76	-1.04	-6.97

Notes:

- f'_c = Concrete compressive strength.
- h_{ef} = Effective stud height.
- l_s = Longitudinal stud spacing.
- w_h = Haunch width.
- K_g = Initial stiffness.
- $N_{cb,avg}$ = Average concrete break-out strength.
- $\delta_{N,f}$= Displacement at failure.

4.2.6.2 ***Two shear stud configuration***

The second part of the parametric study was performed to obtain strength and ductility data for two transversely grouped shear studs. As above, rather than focusing on the nominal concrete break-out strength, N_{cb}, which is based on 5% fractile of the used test data, the focus will be on the average concrete break-out strength, $N_{cb,avg}$. From Section 4.2.5.2, it can be recalled that, in the calculation of the single shear stud concrete break-out capacity, a constant k was utilized. According to Fuchs et al. (1995) [32], the value of that constant is 24 for a 5% fractile strength calculation, and 40 for an average strength calculation. Since the FEA methodology was developed with the objective of capturing the behavior observed in experiments, the results from FEA are compared against average strength calculated values.

The average concrete break-out strength, initial stiffness and displacement at failure calculated by the FEA are shown in Table 13. These are compared against initial stiffness calculated per Section 4.2.5.1, and concrete break-out strength calculated per Section 4.2.5.2 with k equal to 40. The mean and standard deviation of the difference in stiffness are -1.25% and 9.17%, respectively, the mean and standard deviation of the difference in strength are 1.73% and 10.78%, respectively. Given the very good correlation between the FEA stiffness and strength results with the simplified calculations, the following equation for the displacement at failure, $\delta_{N,f}$, was developed:

$$\delta_{N,f} = 6.0 \frac{N_{cb,avg.}}{K_g}$$

which resulted in a mean and standard deviation of the difference in displacement at failure of -1.70% and 32.95%, respectively. Note, in the equation above, a constant of 6.0 was used rather than 7.5 as in Section 4.2.5.3 since the mean value ($N_{cb,avg.}$) is being considered rather than 5% fracture strength and to ensure the target total displacement is the same regardless of what fractile is used in the strength calculation.

Table 13 Two Transversely Grouped Shear Stud FAE vs Simplified Methodology Results

f'_c (ksi)	h_{ef} (in)	l_s (in)	t_f (in)	w_h (in)	FEA Results			Simplified Method			Difference		
					K_g (kip/in)	$N_{cb,avg}$ (kip)	$\delta_{N,f}$ (in)	K_g (kip/in)	$N_{cb,avg}$ (kip)	$\delta_{N,f}$ (in)	K_g (%)	$N_{cb,avg}$ (%)	$\delta_{N,f}$ (%)
4	5	10	1	12	1931	14.74	0.04	1942	13.01	0.04	0.55	-11.74	0.49
7	5	10	1	12	2129	19.91	0.06	2141	17.22	0.05	0.55	-13.51	-19.57
4	7	10	1	12	1795	17.37	0.04	1747	15.93	0.05	-2.67	-8.29	36.78
7	7	10	1	12	1960	22.86	0.06	1907	21.07	0.07	-2.72	-7.83	10.49
4	5	18	1	12	2116	21.67	0.06	2313	18.06	0.05	9.33	-16.66	-21.92
7	5	18	1	12	2351	29.39	0.07	2602	23.89	0.06	10.66	-18.71	-21.3
4	7	18	1	12	1822	28.7	0.06	2042	28.67	0.08	12.1	-0.1	40.4
7	7	18	1	12	2025	36.86	0.07	2264	37.92	0.1	11.79	2.88	43.56
4	5	10	3	12	2857	15.4	0.03	2979	13.01	0.03	4.26	-15.52	-12.66
7	5	10	3	12	3314	21.13	0.03	3474	17.22	0.03	4.84	-18.5	-0.86
4	7	10	3	12	2513	17.63	0.04	2544	15.93	0.04	1.24	-9.64	-6.07
7	7	10	3	12	2805	22.82	0.06	2897	21.07	0.04	3.28	-7.67	-27.27
4	5	18	3	12	3017	20.79	0.04	3006	18.06	0.04	-0.36	-13.13	-9.88
7	5	18	3	12	3566	26.99	0.04	3512	23.89	0.04	-1.52	-11.49	2.04
4	7	18	3	12	2360	29.63	0.06	2564	28.67	0.07	8.65	-3.24	11.82
7	7	18	3	12	2672	38.54	0.07	2923	37.92	0.08	9.39	-1.61	11.2

Table 13 continued

f'_c (ksi)	h_{ef} (in)	l_s (in)	t_f (in)	w_h (in)	FEA Results			Simplified Method			Difference		
					K_g (kip/in)	$N_{cb,avg}$ (kip)	$\delta_{N,f}$ (in)	K_g (kip/in)	$N_{cb,avg}$ (kip)	$\delta_{N,f}$ (in)	K_g (%)	$N_{cb,avg}$ (%)	$\delta_{N,f}$ (%)
4	5	10	1	20	1047	20.08	0.11	840	23.95	0.17	-19.8	19.27	55.52
7	5	10	1	20	1093	27.21	0.14	875	31.68	0.22	-19.96	16.43	55.17
4	7	10	1	20	1011	20.32	0.13	801	19.7	0.15	-20.76	-3.05	13.51
7	7	10	1	20	1054	25.91	0.15	833	26.06	0.19	-20.96	0.58	25.14
4	5	18	1	20	1210	32.07	0.13	1238	33.23	0.16	2.31	3.62	23.88
7	5	18	1	20	1307	41.68	0.15	1316	43.96	0.2	0.69	5.47	33.62
4	7	18	1	20	1127	34.44	0.15	1156	35.46	0.18	2.57	2.96	22.7
7	7	18	1	20	1256	44.28	0.18	1224	46.91	0.23	-2.57	5.94	27.75
4	5	10	3	20	3073	20.23	0.11	2772	23.95	0.05	-9.8	18.39	-52.87
7	5	10	3	20	3376	26.49	0.14	3196	31.68	0.06	-5.32	19.59	-57.52
4	7	10	3	20	2587	20.6	0.1	2392	19.7	0.05	-7.55	-4.37	-50.59
7	7	10	3	20	2864	26.51	0.13	2701	26.06	0.06	-5.69	-1.7	-55.47
4	5	18	3	20	3017	32.61	0.1	2885	33.23	0.07	-4.36	1.9	-30.89
7	5	18	3	20	3341	41.42	0.13	3348	43.96	0.08	0.21	6.13	-39.4
4	7	18	3	20	2378	34.4	0.13	2476	35.46	0.09	4.11	3.08	-33.9
7	7	18	3	20	2885	44.54	0.14	2809	46.91	0.1	-2.64	5.32	-28.43

Notes:

- f'_c = Concrete compressive strength.
- h_{ef} = Effective stud height.
- l_s = Longitudinal stud spacing.
- t_f = Flange thickness.
- K_g = Initial stiffness.
- $N_{cb,avg}$ = Average concrete break-out strength.
- $\delta_{N,f}$= Displacement at failure.
- w_h = Haunch width.

4.2.6.3 ***Three shear stud configuration***

The final part of the parametric study was performed to obtain strength and ductility data for three transversely grouped shear studs. Again, the focus will be paid on the average concrete break-out strength, $N_{cb,avg}$. From Section 4.2.5.2, it can be recalled that, in the calculation of the single shear stud concrete break-out capacity, a constant k was utilized. According to Fuchs et al. (1995) [32], the value of that constant is 24 for a 5% fractile strength calculation, and 40 for an average strength calculation. Since the FEA methodology was developed with the objective of capturing the behavior observed in experiments, the results from FEA are compared against average calculated strength values.

The average concrete break-out strength, initial stiffness and displacement at failure calculated by the FEA are shown in Table 14. These are compared against initial stiffness calculated per Section 4.2.5.1, and concrete break-out strength calculated per Section 4.2.5.2 with k equal to 40. The mean and standard deviation of the difference in stiffness are -0.59% and 5.36%, respectively, the mean and standard deviation of the difference in strength are 3.25% and 10.07%., respectively. Given the very good correlation between the FEA stiffness and strength results with the simplified calculations, the following equation for the displacement at failure, $\delta_{N,f}$, was developed:

$$\delta_{N,f} = 5.1\frac{N_{cb,avg.}}{K_g}$$

which resulted in a mean and standard deviation of the difference in displacement at failure of -8.70% and 40.73%, respectively. Note, in the equation above, a constant of 5.1 was used rather than 6.4 as in Section 4.2.5.3 since the mean value ($N_{cb,avg.}$) is being considered rather than 5% fracture strength and to ensure the target total displacement is the same regardless of what fractile is used in the strength calculation.

Table 14 Three Transversely Grouped Shear Stud FAE vs Simplified Methodology Results

f'_c (ksi)	h_{ef} (in)	l_s (in)	t_f (in)	w_h (in)	FEA Results			Simplified Method			Difference		
					K_g (kip/in)	$N_{cb,avg}$ (kip)	$\delta_{N,f}$ (in)	K_g (kip/in)	$N_{cb,avg}$ (kip)	$\delta_{N,f}$ (in)	K_g (%)	$N_{cb,avg}$ (%)	$\delta_{N,f}$ (%)
4	5	10	1	12	2932	15.09	0.02	2819	13.55	0.02	-3.86	-10.21	19.32
7	5	10	1	12	3243	19.84	0.02	3164	17.93	0.03	-2.43	-9.63	29.81
4	7	10	1	12	2739	17.48	0.03	2503	17.81	0.04	-8.61	1.89	16.12
7	7	10	1	12	2914	22.37	0.03	2761	23.56	0.04	-5.26	5.32	28.45
4	5	18	1	12	3143	22.15	0.03	3263	18.81	0.03	3.81	-15.08	6.73
7	5	18	1	12	3518	29.99	0.03	3680	24.88	0.04	4.62	-17.04	19.32
4	7	18	1	12	2746	28.81	0.04	2879	32.06	0.06	4.83	11.28	34.81
7	7	18	1	12	3042	37.77	0.05	3192	42.42	0.07	4.93	12.31	30.62
4	5	10	3	12	4293	15.36	0.02	4418	13.55	0.02	2.9	-11.78	-18.6
7	5	10	3	12	4842	21.01	0.02	5144	17.93	0.02	6.23	-14.66	-6.04
4	7	10	3	12	3834	17.54	0.02	3779	17.81	0.03	-1.43	1.54	20.12
7	7	10	3	12	4236	22.69	0.03	4298	23.56	0.03	1.46	3.83	-5.24
4	5	18	3	12	4576	21.2	0.03	4480	18.81	0.02	-2.1	-11.27	-35.61
7	5	18	3	12	5215	27.45	0.03	5228	24.88	0.02	0.25	-9.36	-20
4	7	18	3	12	3827	28.07	0.03	3825	32.06	0.04	-0.06	14.21	33.05
7	7	18	3	12	4203	36.66	0.04	4357	42.42	0.05	3.66	15.71	22.98

Table 14 continued

f'_c (ksi)	h_{ef} (in)	l_s (in)	t_f (in)	w_h (in)	FEA Results			Simplified Method			Difference		
					K_g (kip/in)	$N_{cb,avg}$ (kip)	$\delta_{N,f}$ (in)	K_g (kip/in)	$N_{cb,avg}$ (kip)	$\delta_{N,f}$ (in)	K_g (%)	$N_{cb,avg}$ (%)	$\delta_{N,f}$ (%)
4	5	10	1	20	1913	20.74	0.06	1780	21.98	0.06	-6.97	5.98	-1.99
7	5	10	1	20	2196	28	0.07	2042	29.07	0.07	-7.01	3.82	-2.54
4	7	10	1	20	1760	23.55	0.07	1550	25.36	0.08	-11.93	7.69	10.8
7	7	10	1	20	1926	30.85	0.09	1737	33.55	0.09	-9.84	8.75	2.89
4	5	18	1	20	1870	28.86	0.07	1957	30.49	0.08	4.66	5.65	8.07
7	5	18	1	20	2250	36.39	0.09	2226	40.34	0.09	-1.08	10.85	-0.46
4	7	18	1	20	1830	40.24	0.09	1721	45.65	0.13	-5.97	13.44	31.41
7	7	18	1	20	2018	53.52	0.1	1913	60.39	0.16	-5.21	12.84	35.9
4	5	10	3	20	3673	20.17	0.06	3696	21.98	0.03	0.64	8.97	-85.73
7	5	10	3	20	4261	27.43	0.07	4209	29.07	0.04	-1.23	5.98	-95.33
4	7	10	3	20	3352	22.64	0.07	3229	25.36	0.04	-3.66	12.01	-70.9
7	7	10	3	20	3773	29.89	0.09	3610	33.55	0.05	-4.32	12.24	-93.44
4	5	18	3	20	3702	30.47	0.07	4011	30.49	0.04	8.36	0.07	-60.95
7	5	18	3	20	4260	39	0.09	4608	40.34	0.05	8.17	3.44	-85.99
4	7	18	3	20	3305	40.16	0.09	3474	45.65	0.07	5.12	13.67	-24.2
7	7	18	3	20	3819	54.22	0.1	3912	60.39	0.08	2.42	11.38	-21.82

Notes:

- f'_c = Concrete compressive strength.
- h_{ef} = Effective stud height.
- l_s = Longitudinal stud spacing.
- t_f = Flange thickness.
- K_g = Initial stiffness.
- $N_{cb,avg}$ = Average concrete break-out strength.
- $\delta_{N,f}$= Displacement at failure.
- w_h = Haunch width.

4.3 Combined Shear and Tension Behavior

The interaction of tensile and shear coupled behavior can be estimated according to the approach by Bode and Roik (1987) [35]. This interaction approach is also recommended in ACI 318-14 (2014) "Section 17.6" [11] and in LRFD Design Equation 6.16.4.3-1 (AASHTO LRFD BDS [13]). In this study, the load-displacement methodology was studied to provide guidance on how to address coupled behavior in system analysis. The resistance of shear studs subjected to combined shear and axial tension shall be evaluated according to the following tension-shear interaction equation, adapted from Section 6.16.4.3 in the AASHTO LRFD BDS [13]:

$$\left[\frac{N_g(\delta_N)}{N_{g,n}}\right]^{5/3} + \left[\frac{Q_g(\delta_Q)}{Q_{g,n}}\right]^{5/3} \leq 1.0$$

It shall be noted that the above equation is only valid within the ascending branch of the tensile load-displacement relation. In the case where the governing failure mode is stud rupture $\delta_N \leq 0.05h_{ef}$, and in the case where the governing failure mode is concrete break-out or pullout $\delta_N \leq N_{g,n}/K_g$.

While the equation above is well established, because it is a coupled non-linear load-displacement relationship, it is not easily implementable in the formulation of a connector element. Unfortunately, no such approach has been developed or fully validated that is reported in the literature. Therefore, a simplified alternative procedure intended to approximate the equation above was developed and presented below. It must be pointed out, that while the methodology below is recommended in this study, it has not been fully validated or benchmarked with experimental data.

Proposed Simplified Approach to Address Combined Shear/Tensile Interaction

According to ACI 318 (2014) [11] if $Q_g(\delta_Q)/Q_{g,n} \leq 0.2$ or $N_g(\delta_N)/N_{g,n} \leq 0.2$, the interaction effects between shear and tension in transversely grouped shear studs are negligible, and therefore, need not be considered, and the shear and tensile behavior of the studs can be evaluated separately. When interaction must be considered, the tension force is a function of both axial displacement and the shear displacement for a shear stud group embedded in concrete: $N_{cg}(\delta_N, \delta_Q)$). Similarly,

the combined shear is a function of both axial and shear displacement: $Q_{cg}(\delta_N, \delta_Q)$. These two relations may be as follows:

$$N_{cg}(\delta_N, \delta_Q) = [\min(R_{N1}, R_{N2})]^{3/5} \; N_{g,n}$$

$$Q_{cg}(\delta_N, \delta_Q) = [\min(R_{Q1}, R_{Q2})]^{3/5} \; Q_{g,n}$$

where:

$$R_{N1} = (N_g(\delta_N) \,/\, N_{g,n})^{5/3}$$

$$R_{N2} = R_{N1}/(R_{N1} + R_{Q1})$$

$$R_{Q1} = (Q_g(\delta_Q) \,/\, Q_{g,n})^{5/3}$$

$$R_{Q2} = R_{Q1}/(R_{N1} + R_{Q1})$$

The above approach was developed based on the assumption that the magnitude of the displacement in the ascending branch when damage begins to initiate is a constant (*i.e., the specific point when the descending portion of the curve shown in Figure 56 begins*) that is a function of the parameters influencing strength and stiffness. When interaction must be considered, it is also noted that the above approach utilized the accepted ACI approach which results in the corresponding strength being calculated using the non-linear power relationship (see the calculation of the ratios R_{N1} *and* R_{Q1}). These above relations can be employed to construct tabular data that defines the combined actions of tension and shear on shear stud groups.

4.4 Application to System Analysis

A simplified modeling approach was developed in this study in order to save significant amount of computational time. Connector elements were used to define the axial and interfacial shear interaction between the shear studs and concrete slab. Connector elements are special purpose elements used to model discrete physical connections between deformable or rigid bodies, and are able to model linear or nonlinear force-displacement behavior in their unconstrained relative motion components. In general, the Engineer needs to construct tabular data in which the tensile

force, shear force, tensile displacement, and shear displacement are included, calculated in accordance with Section 4.1, Section 4.2, and Section 4.3. When introducing the appropriate constraint between the connector element and the concrete slab and/or the steel flange, the Engineer shall check that the forces are distributed so that additional unrealistic forces are not developed in the connector element, the concrete slab, or the steel flange.

4.5 Application Example

An example has been developed to illustrate how to utilize the aforementioned modeling recommendations is presented next. In this case, the shear stud assembly has the following characteristics:

- Ultimate tensile strength of the stud, f_{uta} : 60 ksi.
- Yield tensile strength of the stud, f_{ya}: 50 ksi.
- Concrete compressive strength, f_c': 4 ksi.
- Shear stud height: 6 inches.
- Shear stud effective height, h_{ef}: 5.625 inches.
- Shear stud diameter, d_s: 7/8 inch.
- Shear stud head diameter, d_h: 1-3/8 inch.
- Number of transversely spaced shear studs, N_s: 3 (s_o, spaced at 6 inches).
- Longitudinal spacing of shear studs, l_s: 12 inches.
- Haunch width, w_h: 16 inches.
- Net haunch thickness, t_h: 3 inches (measured from top of top flange to underside of slab).
- Top flange thickness, t_f: 1.5 inches.
- Assume that cracking is expected at service levels.
- Assume that concrete break-out cracking does not interact with other cracking due to flexure of the slab.

4.5.1 Shear behavior (From Section 4.1)

To calculate the shear capacity of the shear stud assembly, the calculations in AASHTO LRFD BDS [13] “Section - 6.10.10.4.3” and in Ollgaard et al. (1971) [30] needs to be followed. This

results in the nominal shear resistance of one shear stud, Q_n, of 36.08 kips, nominal shear resistance of the group of shear studs, $Q_{g,n}$, of 108.24 kips. The shear load-slip relation is per the following equation:

$$Q_g(\delta_Q) = 108.24\left(1 - e^{-18\delta_Q}\right)^{\frac{2}{5}} for\ \delta_Q \leq 0.2\ in$$

Failure of the shear stud shall be introduced at a shear displacement, δ_Q, equal to 0.2 inches.

4.5.2 Tensile behavior (From Section 4.2.5)

To calculate the initial tensile stiffness, the nominal tensile, the tensile displacement at failure, and the governing failure mode of the shear stud assembly, the calculations in the Section A.2.5 need to be followed.

4.5.2.1 *Initial tensile stiffness (From Section 4.2.5.1)*

Single stud steel stiffness, K_{s1}:

$$K_{s1} = \frac{\pi E_s {d_s}^2}{4h_{ef}} = \frac{\pi\ 29000\ (0.875)^2}{4\ (5.625)} = 3100\ kip/in$$

Single stud concrete stiffness, K_{c1}:

$$K_{c1} = \frac{\pi E_c\ ({d_h}^2 - {d_s}^2)}{5} = \frac{\pi\ 3605\ (1.375^2 - 0.875^2)}{5} = 2548\ kip/in$$

Flange bending stiffness, K_{p1}:

$$K_{p1} = \frac{E_s\ l_s {t_f}^3}{4{s_o}^3} = \frac{29000\ (12)\ (1.5)^3}{4\ (6)^3} = 1359\ kip/in$$

Single stud cumulative stiffness neglecting effect of flange flexibility, K_1:

$$K_1 = \frac{1}{\frac{1}{K_{c1}} + \frac{1}{K_{s1}}} = \frac{1}{\frac{1}{2548} + \frac{1}{3100}} = 1399\ kip/in$$

Load distribution ratio, R:

$$R = \frac{K_1 + K_{p1}}{K_{p1}} = \frac{1399 + 1359}{1359} = 2.03$$

The axial stiffness of the shear stud group, K_g:

$$K_g = K_1 \frac{R+2}{R} = 1399 \left(\frac{2.03+2}{2.03}\right) = 2784\ kip/in$$

4.5.2.2 ***Tensile strength (From Section 4.2.5.2)***

Tensile rupture strength of transversely grouped shear stud, N_{sa}:

$$N_{sa} = N_s\, A_{se,N} f_{ya} + S_N\left(f_{uta} - f_{ya}\right) A_{se,N} = 3\frac{\pi\, 0.875^2}{4}\, 50 + 1.99(60-50)\frac{\pi\, 0.875^2}{4}$$
$$= 102.2\ kip$$

Pullout strength of transversely grouped shear studs, N_{pn}:

$$N_{pn} = \frac{R+2}{R}\psi_{c,P}\left(8A_{brg}f_c'\right) = \left(\frac{2.03+2}{2.03}\right)1.0\left(\frac{8\pi(1.375^2 - 0.875^2)4}{4}\right) = 56.27\ kip$$

To calculate the concrete break-out strength of transversely grouped shear studs, N_{cb}, the following are needed:

- Effective edge distance, c_1:
  - $c_1 = max\left(1.5\left(h_{ef} - t_h\right), 0.5w_h - s_o\right) = max(3.94, 2.00) = 3.94\ inches \leq 1.5h_{ef}$
- Cracking modification factor for calculation of break-out strength, $\psi_{c,N}$:
  - $\psi_{c,N} = 1$
- Edge modification factor for calculation of concrete break-out strength, $\psi_{ed,N}$:

- $\psi_{ed,N} = 0.7 + 0.3\frac{c_1}{1.5h_{ef}} = 0.84$

- Non-modified concrete break-out strength of a single shear stud, N_b:
  - $N_b = \frac{k}{1000}(1000f_c')^{0.5}{h_{ef}}^{1.5} = 0.024\ (4000)^{0.5}\ 5.625^{1.5} = 20.25\ kip$
- Projected area of the failure surface for a single shear stud, A_{No}:
  - $A_{No} = 9{h_{ef}}^2 = 9(5.625)^2 = 284.8\ in^2$
- Combined projected area of the failure surface for a group of shear studs, A_N:
  - $A_N = \left[2l_s(c_1 + s_0) \le 6h_{ef}(c_1 + s_0)\right] = [2(12)(3.94 + 6) \le 6(5.625)(3.94 + 6)] = 238.6\ in^2$

Using the previous quantities, concrete break-out strength of transversely grouped shear studs, N_{cb}:

$$N_{cb} = \frac{A_N}{A_{No}}\psi_{ed,N}\psi_{c,N}N_b = \frac{238.6}{284.8}(0.84)(1)(20.25) = 14.25\ kip$$

The nominal tensile strength of the shear stud group, $N_{g,n}$:

$$\boldsymbol{N_{g,n} = \min\left(N_{sa}, N_{pn}, N_{cb}\right) = 14.25\ kip}$$

The governing failure mode is concrete break-out failure.

4.5.2.3 ***Load-displacement relationships (From Section 4.5.2.3)***

To calculate the load-displacement relation for concrete break-out failure mode the following are used:

- Axial stiffness of the shear stud group, K_g:
  - $K_g = 2784\ kip/in$
- Nominal tensile strength of the shear stud group, $N_{g,n}$:
  - $N_{g,n} = 14.25\ kip$
- Tensile displacement of a shear stud group at failure, $\delta_{N,f}$:
  - $\delta_{N,f} = 6.4\frac{N_{g,n}}{K_g} = 0.033\ inches$

The tensile load-displacement relation is as follows:

$$N_g(\delta_N) = \begin{cases} K_g\ \delta_N & for\ \ \delta_N \le \dfrac{N_{g,n}}{K_g} \\ K_g\ N_{g,n}\dfrac{\delta_{N,f} - \delta_N}{K_g\delta_{N,f} - N_{g,n}} & for\ \ \dfrac{N_{g,n}}{K_g} < \delta_N \le \delta_{N,f} \end{cases}$$

$$\boldsymbol{N_g(\delta_N)} = \begin{cases} 2784\ \delta_N & for\ \ \delta_N \le\ 0.0051\ in \\ 511(0.033 - \delta_N) & for\ \ 0.0051\ in < \delta_N \le 0.033\ in \end{cases}$$

The load-displacement relation is shown in Figure 57.

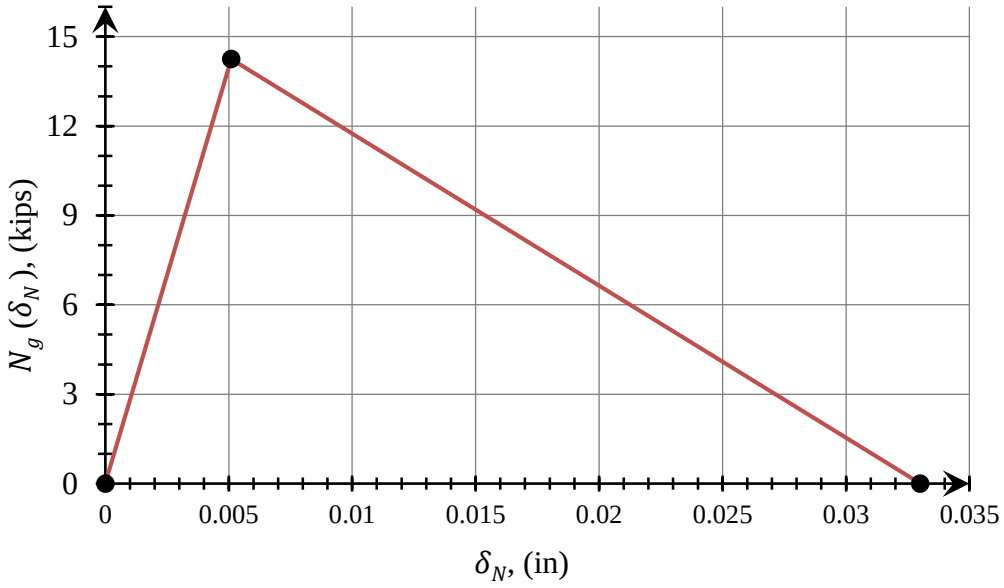

Figure 57 Concrete failure behavior of stud group

4.5.3 Combined shear/tensile interaction (From Section 4.3)

To assign both axial displacement and the shear force-displacement for a shear stud group embedded in concrete ($N_{cg}(\delta_N\ , \delta_Q)$) and the shear force-displacement relation of the shear stud assembly, the calculations in the Section 4.3 need to be followed:

$$N_{cg}(\delta_N, \delta_Q) = [\min(R_{N1}, R_{N2})]^{\,3/5}\ 14.25$$

$$Q_{cg}(\delta_N, \delta_Q) = [\min(R_{Q1}, R_{Q2})]^{3/5}\ 108.24$$

where:

$$R_{N1} = (N_g(\delta_N) / 14.25)^{5/3}$$

$$R_{N2} = R_{N1}/(R_{N1} + R_{Q1})$$

$$R_{Q1} = (Q_g(\delta_Q) / 108.24)^{5/3}$$

$$R_{Q2} = R_{Q1}/(R_{N1} + R_{Q1})$$

An illustration of the application in three dimensions is shown in Table 15.

Table 15 Three dimensional examples for combined shear/tensile interaction

δ_N (in) (X-Axis)	δ_{QT} (in) (Y-Axis)	δ_{QL} (in) (Z-Axis)	δ_Q (in) (on the YZ Plane)	$min(R_{N1}, R_{N2})$	$min(R_{Q1}, R_{Q2})$	$N_{cg}(\delta_N, \delta_Q)$	$Q_{cg}(\delta_N, \delta_Q)$
0.0000	0.003	0.004	0.005	0.000	0.195	0.00	40.58
0.0010	0.003	0.004	0.005	0.066	0.195	2.78	40.58
0.0020	0.003	0.004	0.005	0.209	0.195	5.57	40.58
0.0030	0.003	0.004	0.005	0.410	0.195	8.35	40.58
0.0040	0.003	0.004	0.005	0.663	0.195	11.14	40.58
0.0050	0.003	0.004	0.005	0.831	0.169	12.76	37.19
0.0051	0.003	0.004	0.005	0.837	0.163	12.81	36.46
0.0000	0.030	0.040	0.050	0.000	0.706	0.00	87.85
0.0010	0.030	0.040	0.050	0.066	0.706	2.78	87.85
0.0020	0.030	0.040	0.050	0.209	0.706	5.57	87.85
0.0030	0.030	0.040	0.050	0.368	0.632	7.82	82.22
0.0040	0.030	0.040	0.050	0.484	0.516	9.22	72.75
0.0050	0.030	0.040	0.050	0.577	0.423	10.24	64.63
0.0051	0.030	0.040	0.050	0.586	0.414	10.34	63.75

Notes:

- δ_{QT} = shear displacement in transverse direction (in)
- δ_{QL} = shear displacement in longitudinal direction (in)

CHAPTER 5 BENCHMARK MODELING AND ANALYSIS

In this chapter, the 3-D non-linear FE model (Figure 58) was benchmarked to the three full-scale experimental tests by Neuman (2009) [3] performed at the University of Texas, Austin. The effects of material nonlinearity, dynamic amplification factor, nonlinear geometries, shear stud damage behavior, and bolted connection details were considered. As shown in Figure 59, the model includes the reinforced concrete deck, reinforced concrete parapet, shear studs, and all other steel components (which are girders, diaphragms, stiffeners and braces). In the analysis, what are referred to as the "south" supports were modeled as rollers whereas the "north" supports were modeled as pin supports.

Neuman (2009) [3] noted that the full-scale specimen was originally in-service at the interchange between IH-10 and Loop 610 in Houston. Due to the road expansion at this interchange, the girder was removed. After the reconstruction process of the bridge, these full-scale destructive tests were performed by Neuman (2009) [3]. The test specimen was a simple-span curved bridge (Figure 60). The length of the bridge was 120 ft. and the width of the composite deck was 23.3 ft. The radius of the curvature was equal to 1365.4 ft. The bridge was classified as having Fracture Critical Members (FCMs).

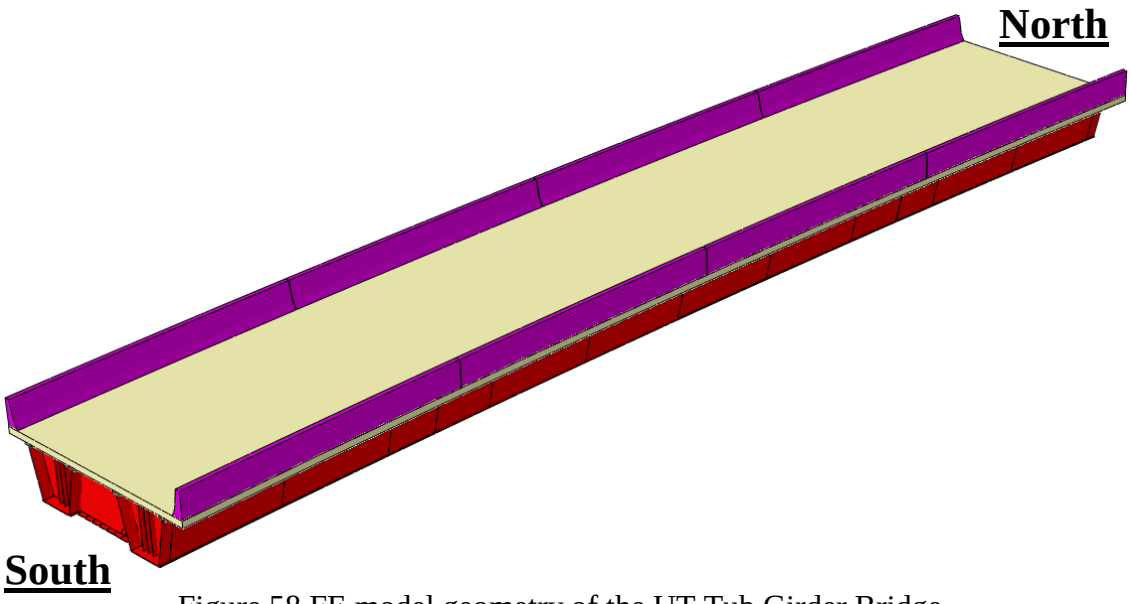

Figure 58 FE model geometry of the UT Tub Girder Bridge

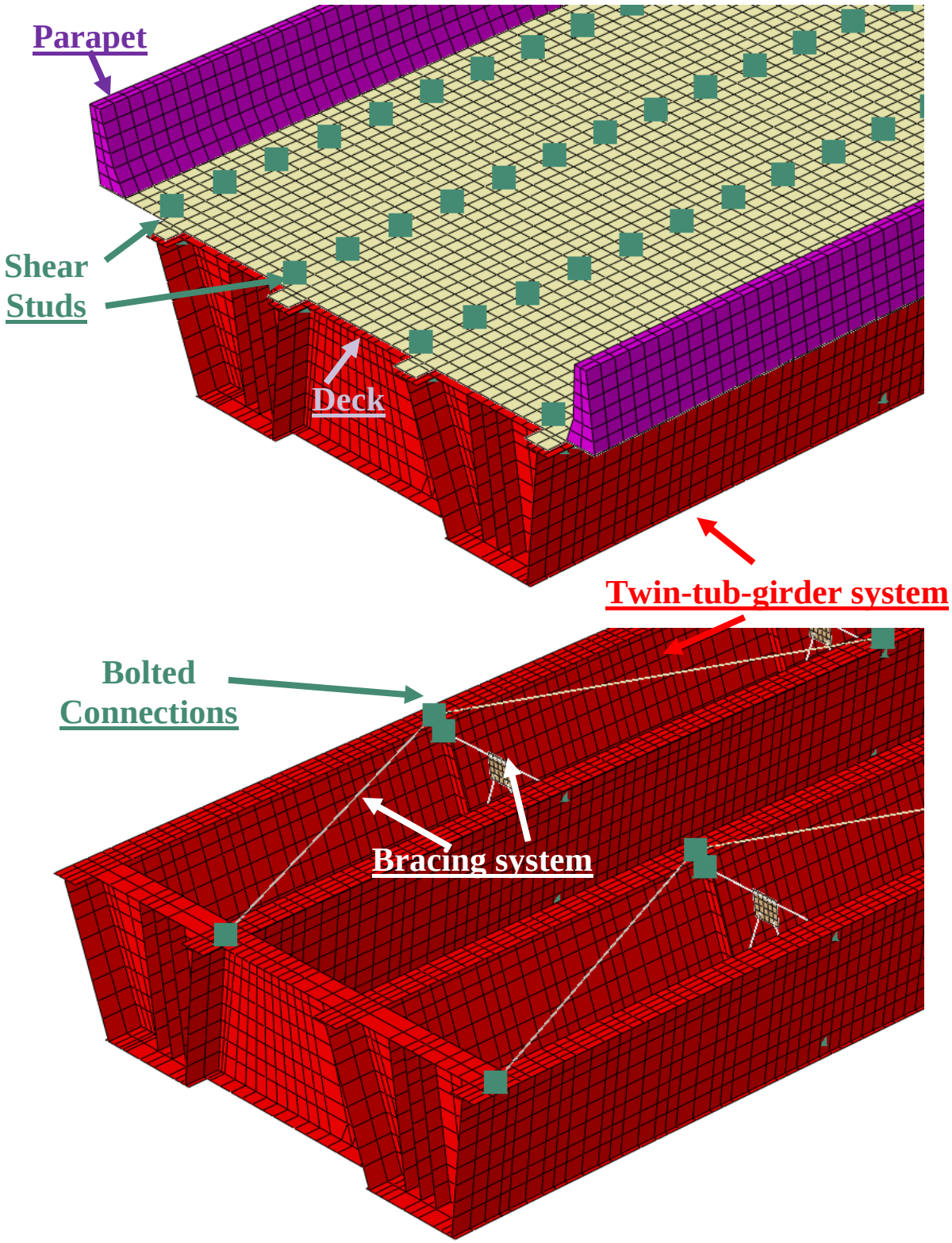

Figure 59 FE model details of the UT Tub Girder Bridge

Figure 60 Photograph of the UT Tub Girder Bridge from Neuman (2009) [3]

A summary of the tests with the outcome of the results are explained below.

5.1 Full-scale Test 1

5.1.1 Experiment detail

The purpose of the first experiment was to observe the behavior of the bridge after the bottom tension flange at the exterior girder was fractured instantaneously. Only the bottom flange at the mid-span was fractured (i.e., the webs remained intact). The concrete strength on the test day was 5.37 ksi. Before this fracture process, concrete blocks were placed close to the mid span and near the exterior parapet. The concrete block (76 kips) was used to simulate the HS-20 truck. Wooden blocks were placed under the concrete blocks. The simulated truck was centered 3.67 ft. away from the midspan.

As a result of the Test-1, no major plasticity and no damage was observed. There was no crack initiation into the web. The deflection change on the fractured girder was only 0.08 in. noted in Barnard et al. (2010) [19]. A significant amount of redundancy was observed.

5.1.2 FE model steps

Implicit and explicit solvers were used to perform the finite element analysis. First, in the implicit solver, the construction sequence was performed. Second, in the explicit solver, the concrete weights over wooden block (shown in Figure 61) were placed on the deck. Finally, instantaneous fracture on the bottom flange was implemented. The outcomes of FE results, after the dynamic effect was fully dissipated, were used to compare to experiment results. The static transversely grouped headed stud strength was "32 kips".

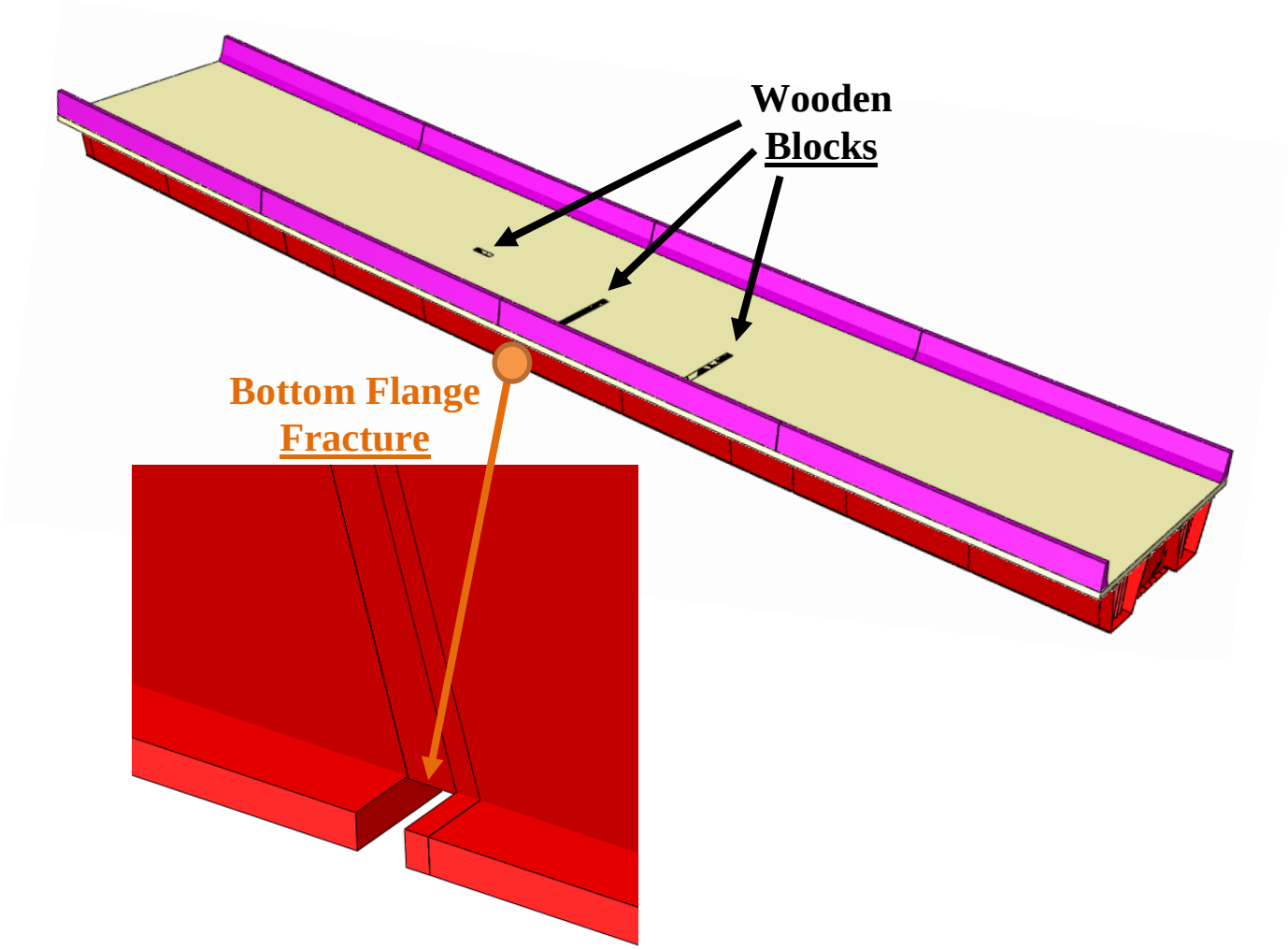

Figure 61 FE model details of the Test 1

5.1.3 Comparison between FE model and experimental results

The only reported outcomes from the Test-1 results were displacement readings. The load-displacement curves were obtained from Barnard et al. (2010) [19]. After fracture occurred, the displacements of the bridge are shown in Figure 62. These displacement curves were derived by subtracting the before-fracture displacements from the self-weight of the steel box girders from after-fracture total displacements.

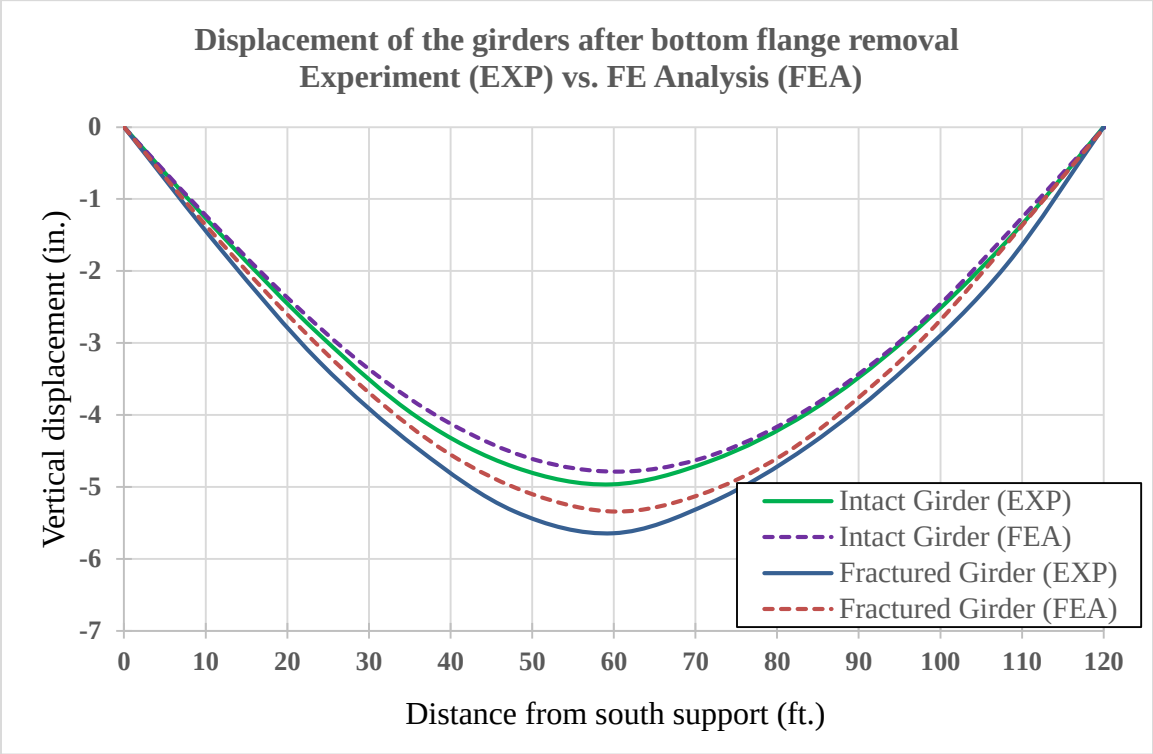

Figure 62 Total displacement after fracture at the girder bottom flanges

From FEA, the maximum predicted displacement of the fractured girder of the bottom flange at the location the simulated fracture was introduced was 5.35 in after the fracture occurred. This was slightly less than the experimentally measured displacement, 5.64 in. The experimentally measured displacement change after the simulated fracture was introduced was recorded as 0.08 in. This was very close to the displacement change predicted by the FEA, which was 0.11 in. The FEA numerical results for Test 1 were close to experiment's outcomes; hence, FEM was successfully benchmarked to Test-1.

5.2 Full-scale Test 2

5.2.1 Experiment detail

In Test 2, the performance of the bridge with the web fractured was investigated. Initially, the girder was supported with scissor jacks and the web was cut using a torch to a depth 10” below the top flange surface (shown in Figure 63). Once all cutting was completed, concrete blocks weighing a total of 76 kips were placed on the mid-span of the deck. The test was implemented, when the scissor jacks were quickly removed (exploded instantaneously). Thus, the complete bottom flange and partial web fracture were simulated. The concrete strength on the test day was 6.26 ksi.

As a result of the test (noted in Bernard et al. (2010) [19]), a considerable amount of concrete break-out damage on the interior top flange of the fractured girder and some concrete cracking on the exterior top flange of the fractured girder were observed. The damage zone was thirty feet away from the mid-span in each direction. Maximum 3.5 in. shear stud separation was noticed. The dynamic amplification factor was measured, and the average reported number was 1.30. In addition, 1 in. crack growth into the web was observed. Exterior parapet expansion joints contacted to each other at the mid span.

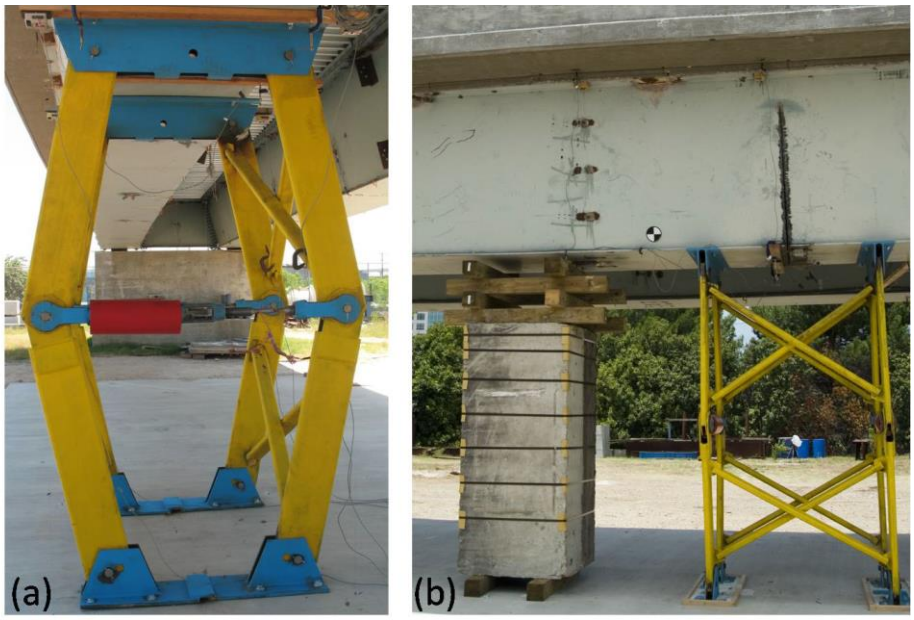

Figure 63 Test-2 details of the UT Tub Girder Bridge from Neuman (2009) [3]

5.2.2 FE model steps

Implicit and explicit solvers were used to perform the finite element analysis. In the implicit solver (the first step), the construction sequence was performed. In the explicit solver (the second step), scissor jacks were placed under the flange fractured section as boundary condition, and then torch cutting simulated by deleting element over the web up to 9 in below the top surface (shown in Figure 64). The concrete weights over wooden block were placed on the deck. Finally, instantaneous boundary condition removal was performed. The outputs of FE analysis were recorded throughout the analysis to calculate dynamic amplification factor. When the dynamic effect was fully dissipated, shear stud separation displacements were measured.

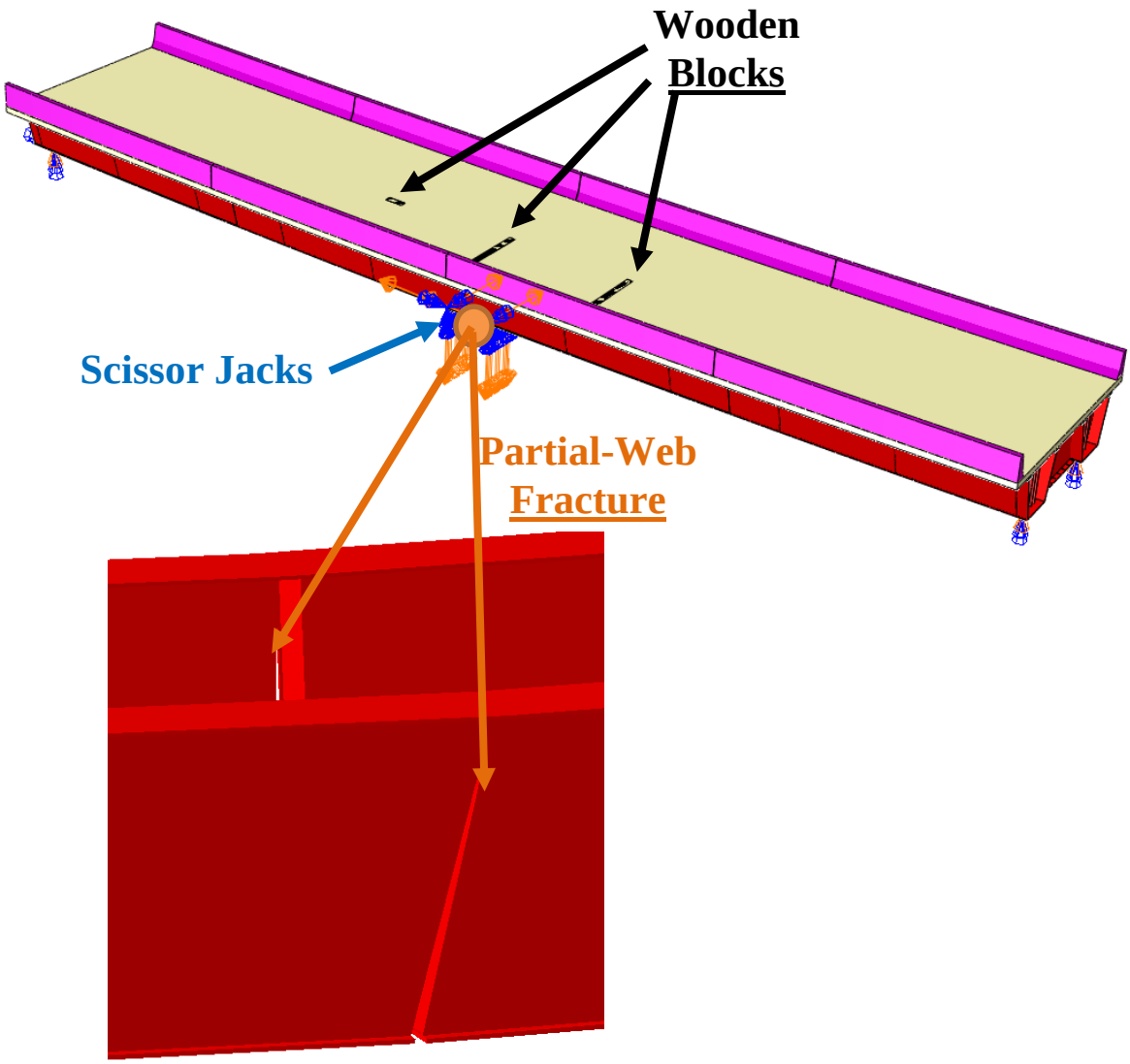

Figure 64 FE Model Details of the Test 2

5.2.3 Comparison between FE model and experimental results

In this section, experimentally and numerically measured dynamic amplification factor, the period of the fractured bridge, shear stud opening displacement, and parapet contacts were compared for the data from Test 2.

The average dynamic amplification factor was reported as 1.30 from the experiment. From the FE model, the longitudinal normal stress at bottom flange of the intact girder after sudden fracture is shown in Figure 65, the peak and final stresses are 47.1 and 36.2 ksi. Thus, the calculated dynamic amplification factor (DA_R) is 0.3 which is same as the experimental result.

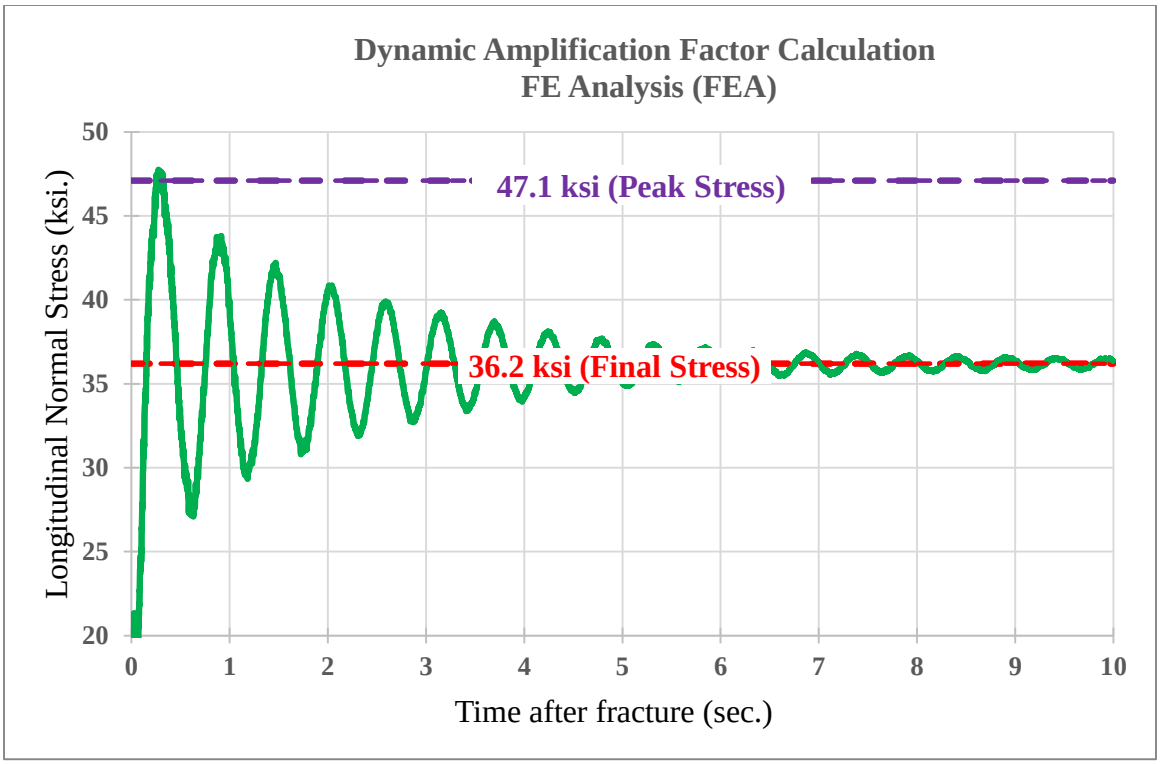

Figure 65 Longitudinal stress at bottom flange of the intact girder after sudden fracture

After the sudden cutting of the girder, experimental and numerical longitudinal normal strain at bottom flange of the intact girder 6 ft away from the midspan was compared. The periods of the fractured bridge for both experiment and FE model were approximately 0.6 second. As shown in Figure 66, there is a good agreement in both longitudinal strains and periods of the experiment and FE model.

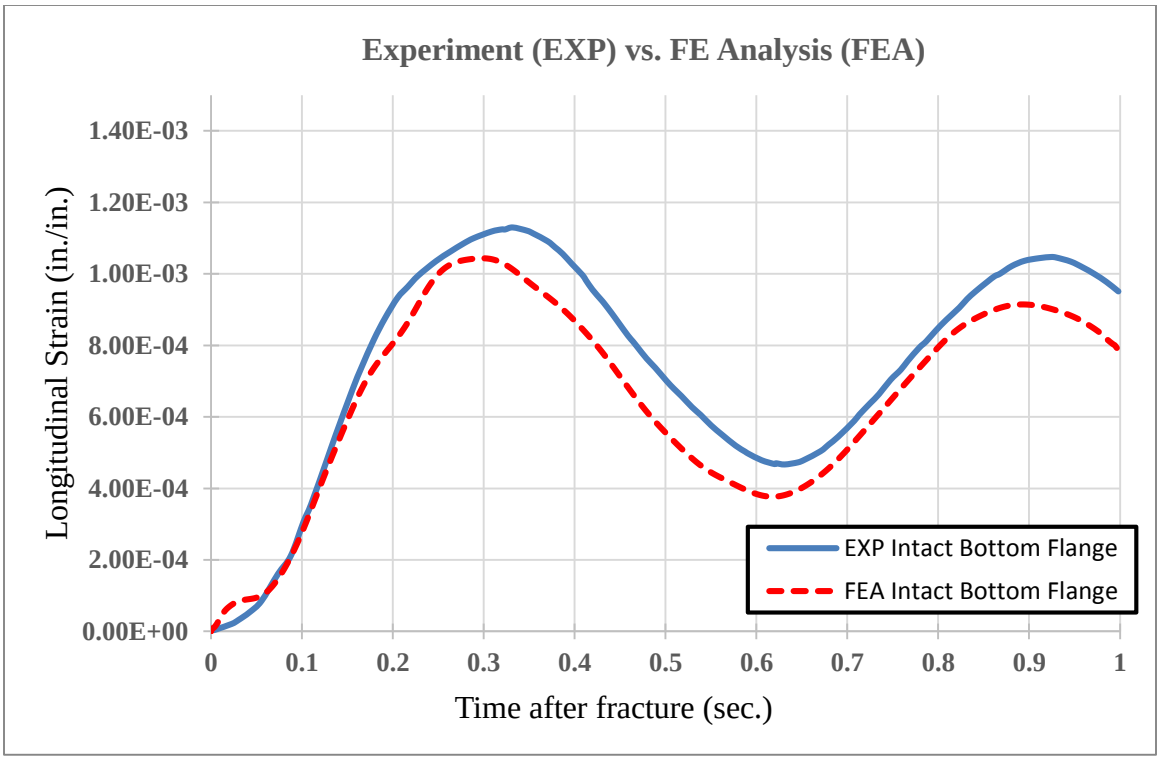

Figure 66 Longitudinal strain at bottom flange of the intact girder after sudden fracture.

The shear stud separation curves obtained from the experiment and the FE model were presented in Figure 47, and were discussed in Section 4.2.1.

As shown in the figure, the exterior parapet surfaces contacted to each other at the mid span both in the experiment (Figure 67) and FE model (Figure 68).

Figure 67 Parapet contact at the mid-span from Neuman (2009) [3]

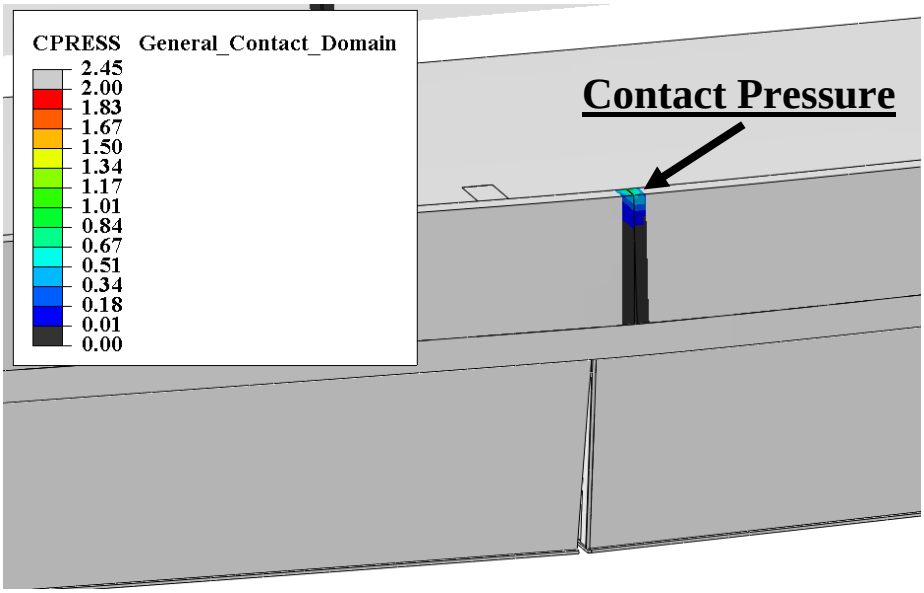

Figure 68 Parapet contact at the mid-span from FEM

The model was capable of predicting complex behavior of fractured girder which includes concrete break-out failure, dynamic response and damaged behavior; hence, FEM was successfully benchmarked to Test 2.

5.2.4 Test 2 with full depth fracture

Neuman 2009 [3] showed that the UT test bridge had a significant amount of reserve capacity, carrying loads far in excess of the original design loads even in the faulted state. However, according to the redundancy analyses based on the failure criteria developed in NCHRP 12-87a. [5], the UT Tub Girder Bridge would not meet the proposed performance requirements for system analysis. The main reason for this difference in evaluation results could be that any of the UT tests did not consist of the fracture of the bottom flange, both webs, and both top flanges, whereas in the damage scenario according to NCHRP 12-87a. [5], complete full-depth fracture of one of the tub girders was assigned for redundancy evaluation.

The reason why full depth fracture was applied throughout this dissertation is based on the Hoan Bridge Investigation [14] and was explained in Section 2.2.1. Further, the FHWA 2012 Memo explicitly states that the entire FCM must be assumed to have failed, including the compression portions. If full depth fracture had been performed during the UT test, the author believes that the outcome of the experiment would likely have been much different. The continuity provided by remaining web and top flanges (which now are acting as tension elements), has been shown analytically to carry significant load through catenary action. For example, each top flange is 12 inches wide and 0.625 inch thick and can each transfer 375 kips through catenary action before the plates start yielding, whereas the total weight of fractured girder is approximately only 50 kips. The top flanges of the faulted girder were in pure axial tension in the FEA and observed to be acting as catenaries, acting as a "sling" so to speak. Further this prevented additional shear stud failure as compared to the case when entire girder as assumed fractured as it prevents the girder from dropping.

In this section, the second UT Test which had partial web fracture (a depth 10" below the top flange surface) was simulated as if it had full-depth fracture. In the following FE model, the following were observed:

1- The bridge exhibited almost all shear stud failures on the fractured girder (see Figure 69),
2- This was followed by deck reinforcement yielding (see Figure 70) and parapet crushing.
3- High level of plasticity on the end diaphragms was observed.

If full depth fracture had been performed during the UT test, the bridge would have collapsed according to the FEA models.

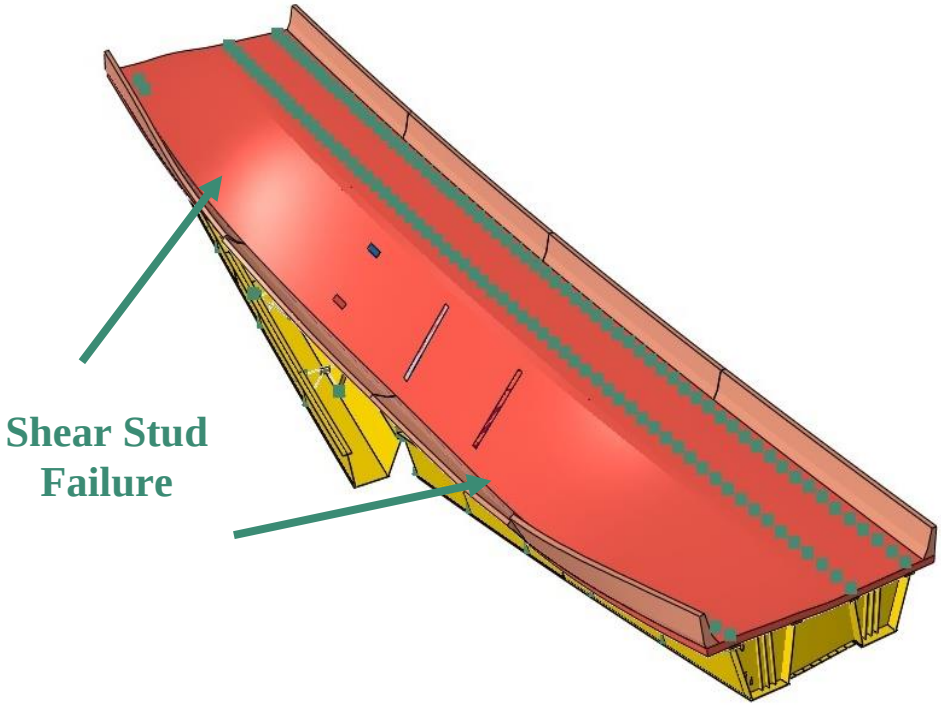

Figure 69 Stud failure after live load placement

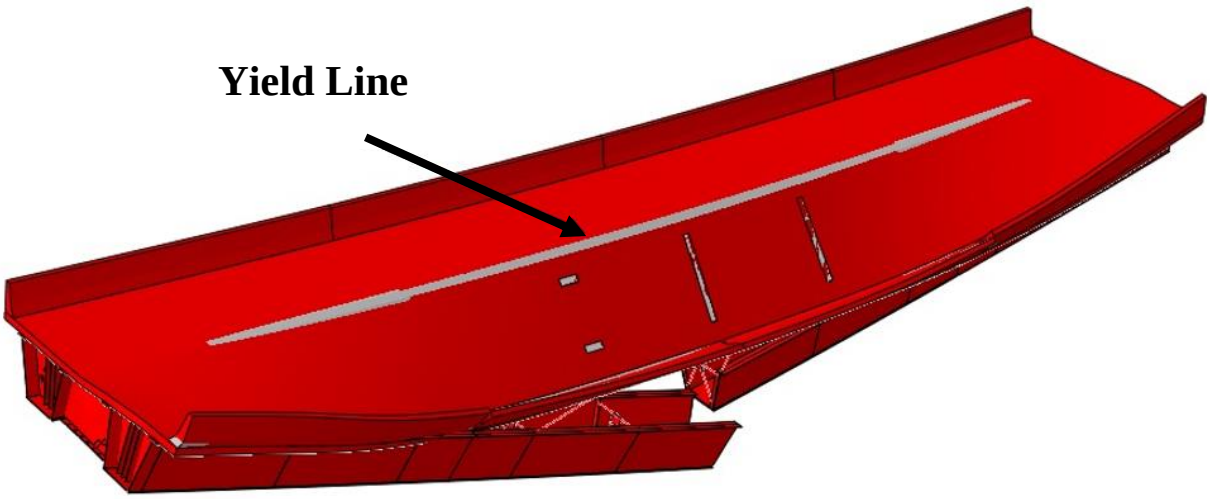

Figure 70 Deck reinforcement yielding

5.3 Full-scale Test 3

5.3.1 Experiment detail

The object of the final test (i.e., Test 3) was to investigate the maximum loading capacity following Test 2 and to observe what failure mode governed. Concrete blocks with a total weight of 82.1 kips were placed on the damaged bridge. In addition to the concrete blocks, a sand load was applied and incrementally increased up to failure (shown in Figure 71 and Figure 72).

When the concrete blocks were placed on the deck, the crack which was initially up to 9 in below the top surface from Test-2 propagated up to the bottom surfaces of the top flanges in the experiment. As the load reached 161.5 kips, the concrete break-out failure was noticed at the outside top flange of the fractured girder. After the load was equal to 234.5 kips, the shear stud failure at the interior top flange of the fractured girder extended throughout the span. As additional load was applied, the following conditions were observed: plastic hinge behavior at the deck contact between the railing surfaces, railing concrete crushing, continued deformation and continued shear stud failures. The bridge started to collapse when the load was 363.75 kips. At that loading, all of the shear stud connections of the damaged girder failed; hence, there was slip between the girder and the deck. The concrete strength on the test day was 6.26 ksi.

5.3.2 FE model steps

Implicit and explicit solvers were used to conduct the finite element analysis. In the implicit solver (the first step), the construction sequence was performed. In the explicit solver (the second step), quasi-static web and bottom fractures were applied by deleting element over bottom flange and the web up to top flange. The concrete weights over wooden block were placed on the deck. The concrete block weights were placed on the deck as surface traction. Finally, the sand load was increased incrementally up to the failure observed.

Figure 71 Test-3 details of the UT Tub Girder Bridge from Neuman (2009) [3]

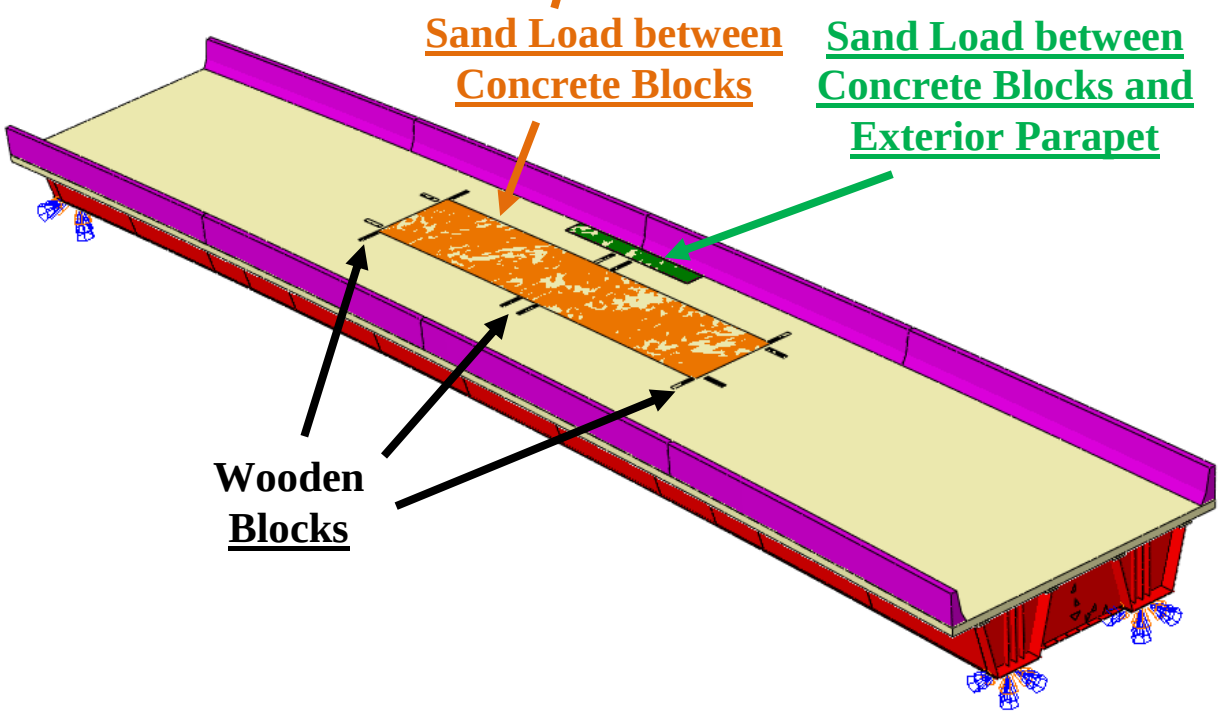

Figure 72 FE Model Details of the Test 3

5.3.3 Comparison between FE model and experimental results

In this section, experimentally and numerically obtained load displacement curves, governing failure mode, and deformed geometries were compared. The shape of the load displacement curves (Figure 73) varies based on the length of crack at the time the load is applied. In the experiment, the web was not fractured fully before applying load. The crack propagated through the web and up to the top flange after the concrete blocks were placed. When the load reached 161.5 kips, concrete break-out failure was noticed at the outside of the top flange. Because of complexities associated with modeling crack growth during FE analysis, the numerical simulation assumed an initial crack through the web up to top flange before load is applied. Despite the difference in load pattern, the final crack configuration and the total bridge capacities are the same in the numerical and experimental simulations.

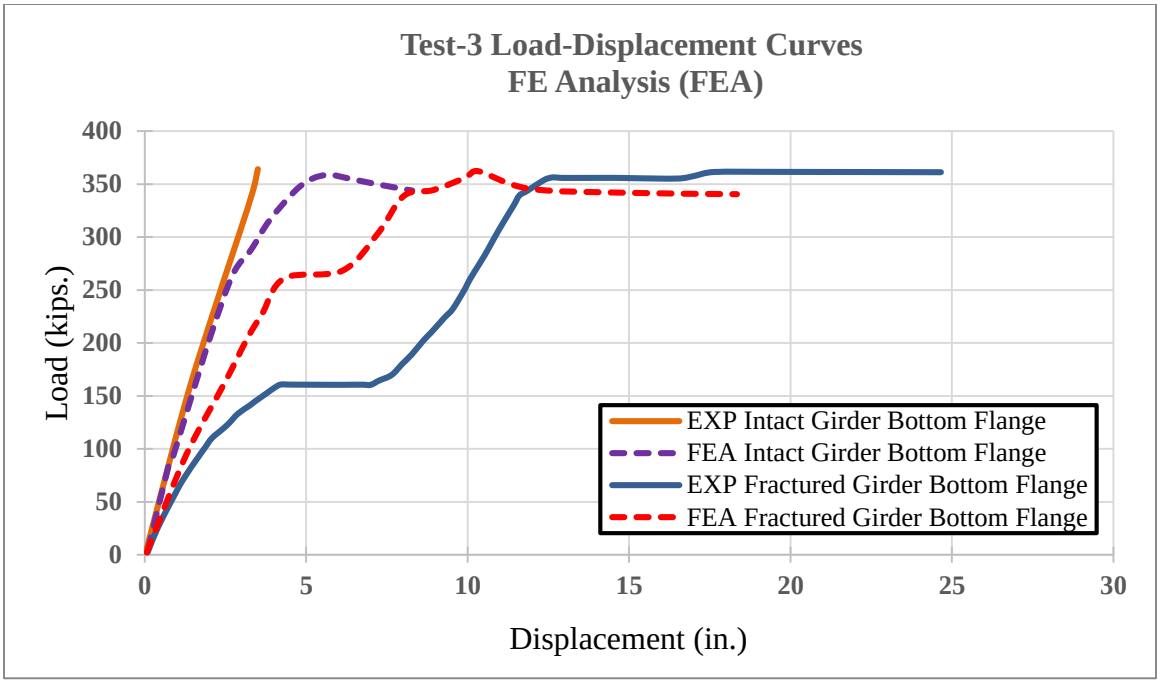

Figure 73 Experimental and numerical load-displacement curves

The model was capable of predicting the complex behavior of the fractured girder which includes deck reinforcement yielding (yield line), parapet crushing and complex shear stud damage behavior; hence, the FEM was successfully benchmarked to Test 3. Similar to the FEA model, in Test-3, Neuman (2009) [3] noted that shear stud failures occurred first (as shown in Figure 74).

The stud failures are followed by parapet crushing (as shown in Figure 75), and deck reinforcement yielding (as shown in Figure 76).

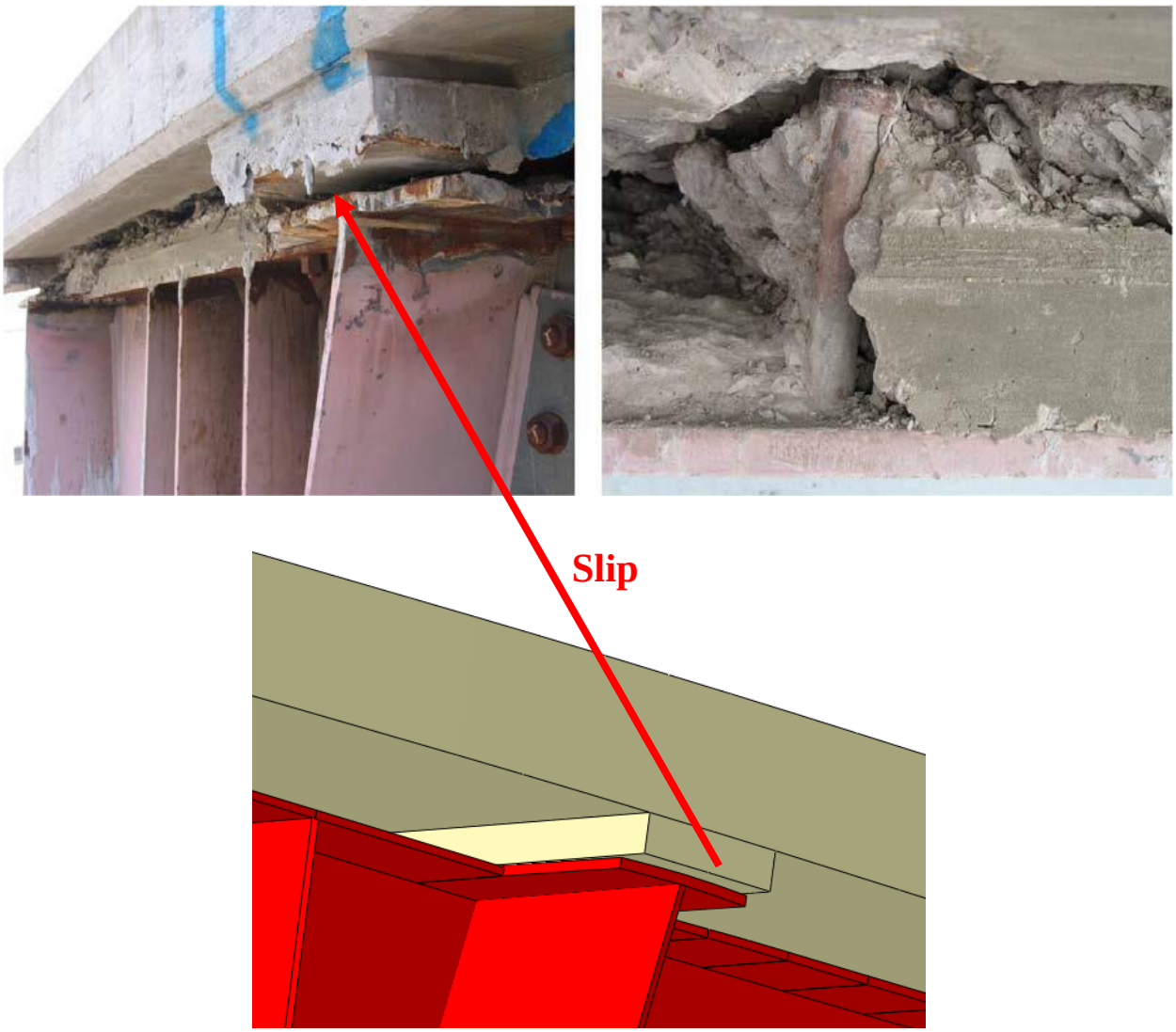

Figure 74 Slip between the fractured girder and the concrete deck at the support in both the experiment of Neuman (2009) [3] and FEA

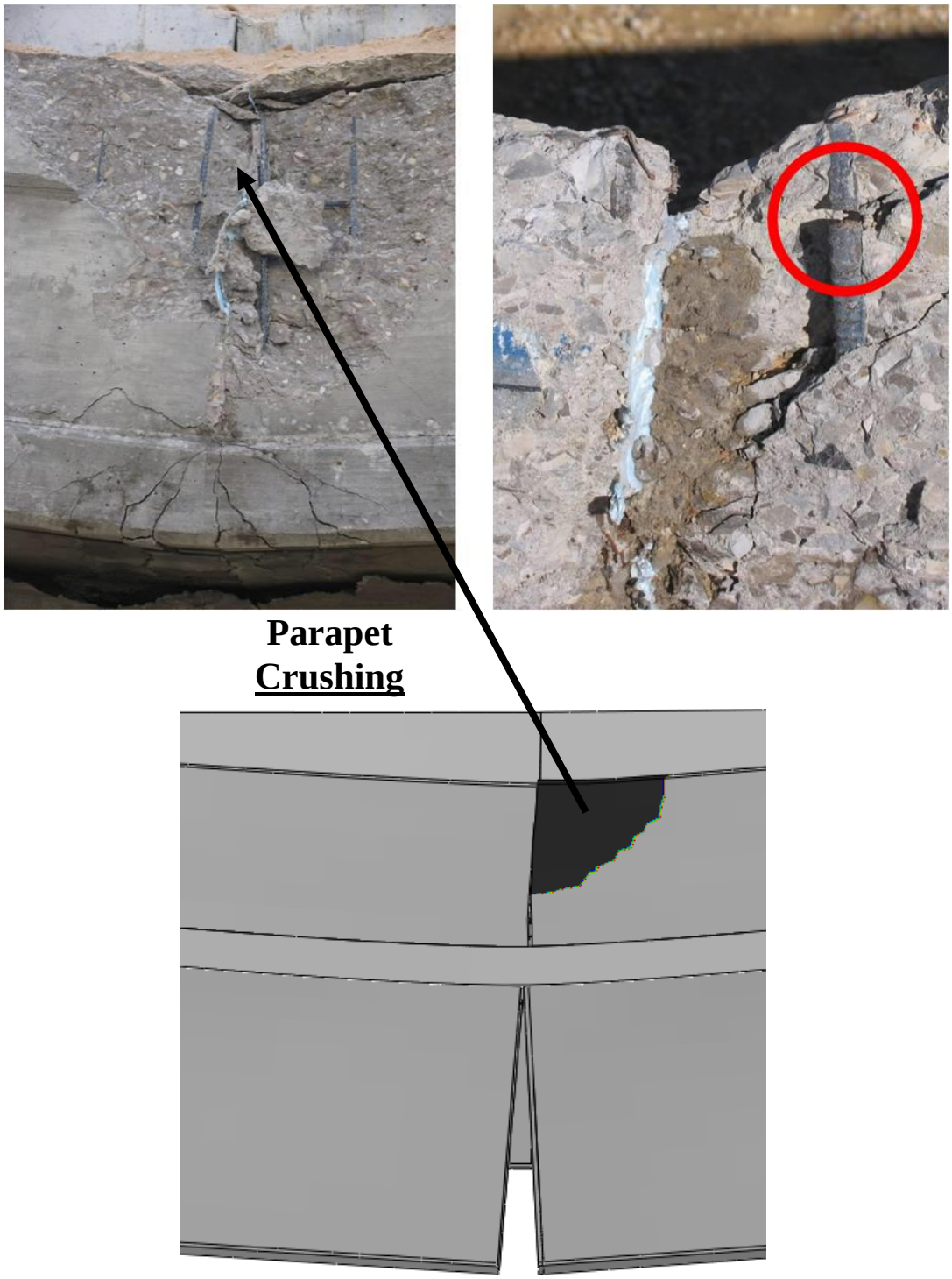

Figure 75 Parapet crushing in both the experiment of Neuman (2009) [3] and FEA

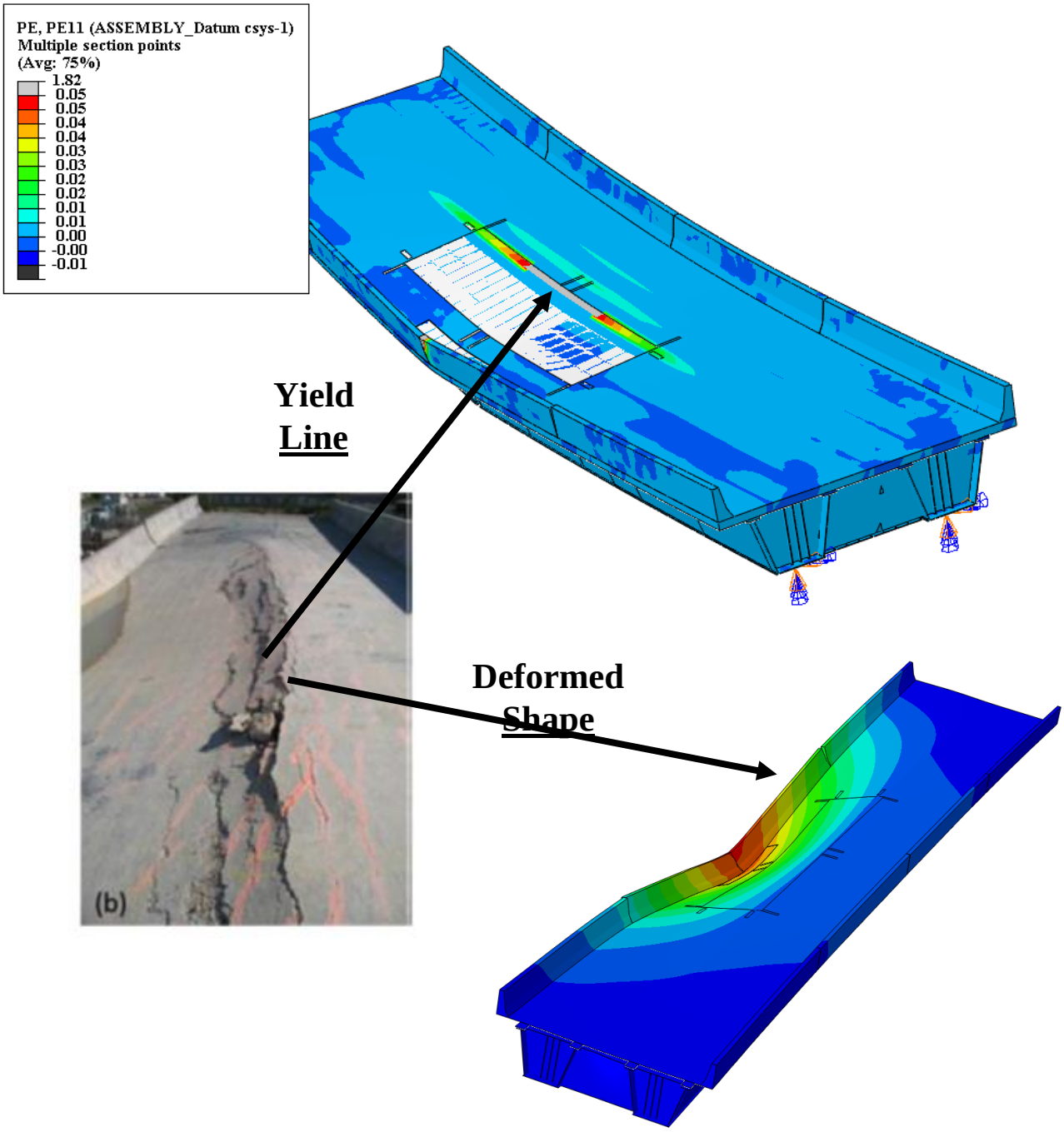

Figure 76 Deck reinforcement yielding in both the experiment of Neuman (2009) [3] and FEA

CHAPTER 6 RELIABILITY AND REDUNDANCY EVALUATION

The bridges were evaluated using the system analysis procedures developed at Purdue University under NCHRP Project 12-87a [5]. The overall evaluation is a reliability-based approach that ensures a target reliability index (i.e., beta) of 1.5 in the faulted state for all load combinations considered. Using strength and serviceability-based failure criteria, the member in which has a simulated fracture can be classified as a FCM or not. In other words, the failure criteria ensures that the structure has adequate strength and stability to avoid partial or total collapse and to allow traffic to continue safely in the presence of a totally fractured FCM.

6.1 Load Combinations

A load model was developed using a reliability-based approach as part of NCHRP 12-87a [5]. The approach used to develop the load factors is consistent with that used in the development of the existing AASHTO LRFD Bridge Design Specification [13]. The reliability analysis utilized the statistical parameters.

6.1.1 Basic information related to the development of the load factors is as follows:

The approach in NCHRP Project 12-87a [5] was to use finite element analysis to most accurately estimate the resistance of a damaged structure to factored loads. The load factors used herein were developed to achieve a specific target reliability index, including the statistical parameters of both load and resistance. In that case, the basic design equation becomes:

$$R_n \geq \Gamma Q_n$$

Where R_n is the nominal resistance, Q_n is the nominal load and Γ is the reliability based load factor. In other words, the target reliability is reached by only factoring the loads with no adjustment to the resistance of a material or component strength.

Using established reliability theory, two load combinations, referred to as Redundancy I and II, have been developed for evaluation of this existing bridge in the faulted condition. They are applied to evaluate whether or not the bridge has adequate strength after the fracture.

The Redundancy I load combination is intended to conservatively describe the loading condition of the structure at the instant the failure of the member occurred. This load case only evaluates the ability of the bridge to immediately survive a sudden brittle fracture. The load factors developed for Redundancy I correspond to a target reliability factor of 1.5 in the faulted state. Note, this load combination is not intended to produce the fracture but to represent the average maximum load (in particular live load) that may be on the bridge at the time of the fracture. This level of reliability ensures with high confidences that the bridge will survive the initial fracture.

The second case is referred to as the Redundancy II load combination. The Redundancy II load combination is intended to evaluate the structure at a level of live load that could be expected between the instant the failure occurs and the time the damage is discovered. This interval is assumed to be between 5 and 50 years. The target reliability factor is 1.5 for Redundancy II.

The resulting load combinations for the evaluations of existing structures is as follows:

$$Redundancy\ I : (1 + DA_R)[1.05(DC) + 1.05(DW) + 0.85(\mathrm{LL})]$$

$$Redundancy\ II : 1.05(DC) + 1.05(DW) + 1.30(1{+}\mathrm{IM})(\mathrm{LL})$$

In the above equations, DC is the dead load, DW is the future wearing surface/utilities, LL is the live load, and IM is the impact modifier. The density of the concrete deck was increased by 10% in order to include the weight of the stay-in-place forms, extra concrete above the forms, and additional thickness of concrete at the overhang. This 10% was determined by comparing the design calculations of the Zoo Interchange Reconstruction State Projects. For example, in the design calculations [36] for the B40-868 Bridge, the additional dead load from the elements mentioned above was assumed to be 0.343 kip/ft per girder. This is approximately 10% of the deck weight per girder (3.3 kips/ft).

6.1.2 Dynamic amplification

In the above equations, DA_R is the dynamic amplification factor due to the sudden fracture. This dynamic amplification is calculated as the ratio of the peak stress in a given member in free vibration following the sudden fracture to the stress in that member after the structure comes to rest. More explanations about DA_R was noted in Section 3.4. To avoid the need for complex

dynamic analyses to be required for future evaluations, one simply multiplies the static response of the bridge in the faulted condition by DA_R when subjected to the Redundancy I load combination. Thus, the dynamic amplification is applied using the Redundancy I load combination in which both dead and live loads are applied. In these models, the dynamic amplification factor was conservatively assumed to be 0.35 for simple span and 0.2 for continuous span bridges. These values are based on analysis of multiple simple span and continuous twin-tub-girder bridges performed in this study as shown in Table 16 and Table 17 respectively. The values of 0.35 for simple span and 0.2 for continuous have been shown to be conservative for the twin-tub configurations analyzed.

Table 16 Dynamic amplification factors for simple span twin-tub-girder bridges

Bridge	**DA_R**
UT-Texas-Test-Bridge	0.30
Simple-Span-1Lane-128ft	0.32
Simple-Span-2Lanes-204ft	0.35

Table 17 Dynamic amplification factors for continuous twin-tub-girder bridges

Bridge	**DA_R**
B40-868	0.20
B05-661	0.19
B40-776	0.16
B40-834	0.15
B40-783	0.17
B40-854-Unit3	0.18
B05-660-Unit2	0.16
B05-658-Unit2	0.15
B40-868 w/o intermediate diaphragms	0.21
B05-661 w/o intermediate diaphragms	0.20
B40-854-Unit3 w/o intermediate diaphragms	0.19

For the Redundancy II load combination, the impact factor for live load is assumed to be 0.15 since only a nominal impact is assumed during normal daily traffic.

6.1.3 Longitudinal and transverse position of live load

To maximize the load effects on the remaining intact components in the faulted state, the centroid of the HS-20 component of the HL-93 was positioned longitudinally coincident with the location of the faulted member. This is consistent with typical current approaches to positioning live load longitudinally. A fixed axle spacing of 14 feet was also conservatively used. Multiple presence factors were applied according to AASHTO LRFD Bridge Design Specification [13] (shown in Table 18). The transverse position of the live loads is discussed below.

Table 18 Multiple Presence Factor (m) (AASHTO LRFD [13] "Table 3.6.1.1.2-1")

Number of Loaded Lanes	Multiple Presence Factor, m
1	1.20
2	1.00
3	0.85
>3	0.65

Redundancy I load combination:

While vehicles may occasionally be positioned outside of the normal travel lanes, it was deemed to be unrealistic to position vehicles outside of the striped lane for the Redundancy I load case, regardless of the number of normal travel lanes carried by the bridge, as reported in NCHRP 12-87a [5]. The number of lanes used in this analysis thus correspond to the number of striped lanes. The number of loaded lanes for this load combination should be no greater than two lanes for the cases where the bridge is striped for two or more lanes. Thus, if only one lane is shown on the design plans, only one lane should be used regardless of the width of the bridge. The Redundancy I load combination is intended to be representative of the mean maximum live load, it would only be reasonable to use a single lane of HL-93 for Redundancy I when the bridge is intended to carry only one lane (i.e., striped for one lane). The live load was positioned in the center of the striped lane(s). If a bridge has two lanes of traffic, two lane load combinations were separately used for the redundancy analysis. The first considered loading in only the exterior lane load with a higher multiple presence factor and the second considered loading in both lanes. For example, B40-868 has two lanes of traffic in the design plan, therefore in the first analysis (Figure 77), a single lane load was used with only one truck. In the second analysis (Figure 78), the bridge was intended to

carry two lane traffic in the model. In these figures, the area in cyan corresponds to the lane loading and "red dots" correspond to the position of the truck wheel footprints.

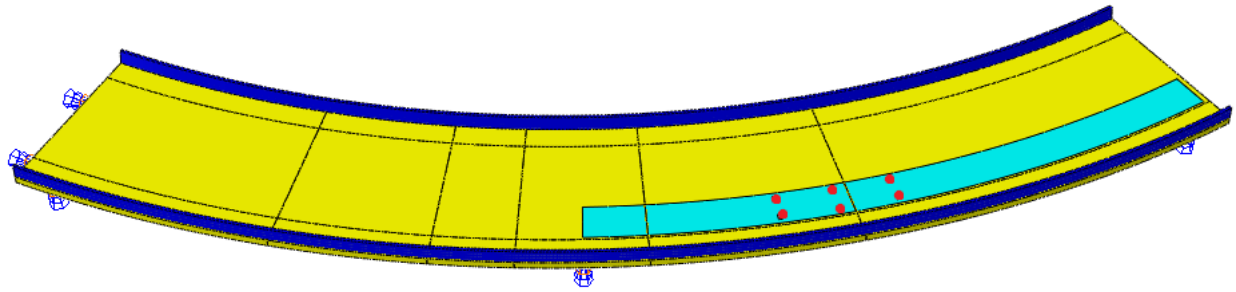

Figure 77 Redundancy I – Analysis I (single lane analysis) of B40-868

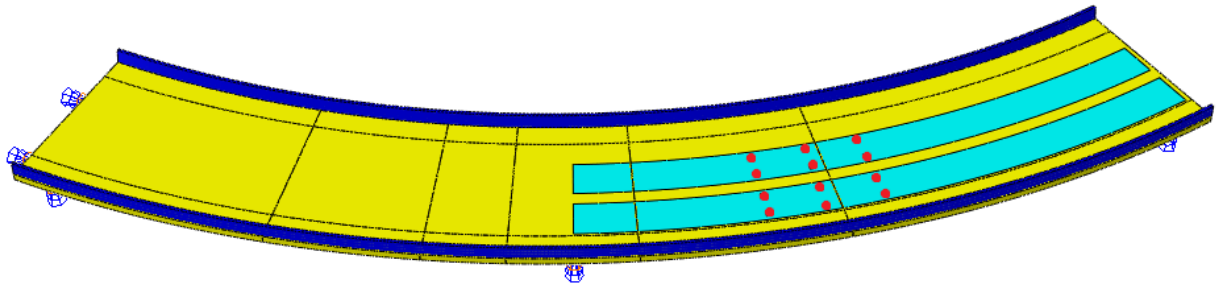

Figure 78 Redundancy I – Analysis II (two lane analysis) of B40-868

Redundancy II load combination:

The Redundancy II load combination must also represent an event that could reasonably occur during the interval between when the fault occurs and the time it is discovered. For the Redundancy II load combination, the HL-93 load(s) was positioned transversely such that the load effects are maximized in the faulted state. It may be possible to fit two full lanes of HL-93 on a one lane bridge, or it is reasonable to fit three full lanes of HL-93 on a two full lanes bridge for the longer interval between when the fracture occurs and when it is discovered. For Redundancy II, loading up to maximum number of lanes that fit on the bridge was used. The approach is based on AASHTO LRFD [13] lane configuration for bridges. Additional analyses with less than the maximum number of lanes with higher multiple presence factors were also performed. For example, B40-868 has two lanes of traffic in the design plan; however, it is possible to fit three lanes. In the first analysis (Figure 79), a single lane load was used with only one truck, in the second analysis (Figure 80), the bridge was intended to carry two lane traffic in the model. The

third analysis (Figure 81) includes the maximum amount of traffic lanes which can fit on the bridge. The same color scheme applies for Redundancy II figures.

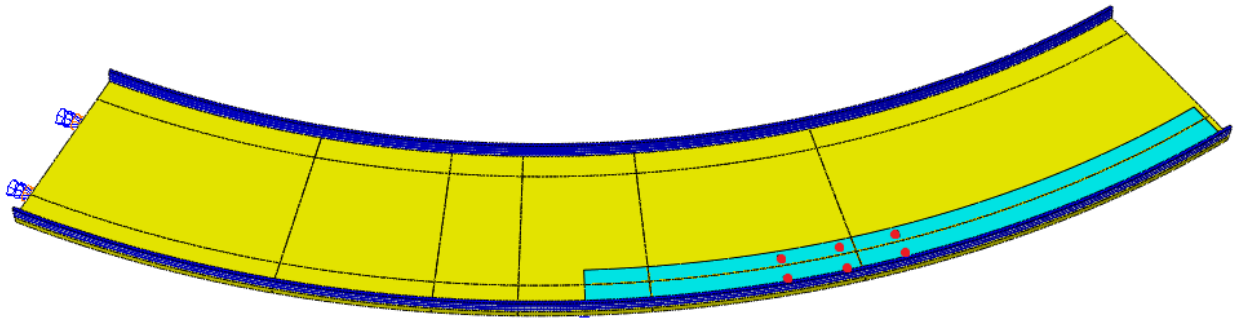

Figure 79 Redundancy II – Analysis I (single lane analysis) of B40-868

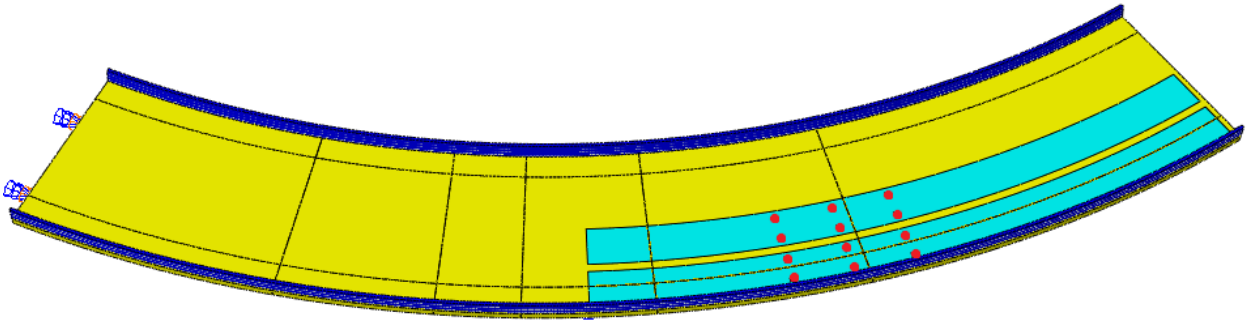

Figure 80 Redundancy II – Analysis II (two lane analysis) of B40-868

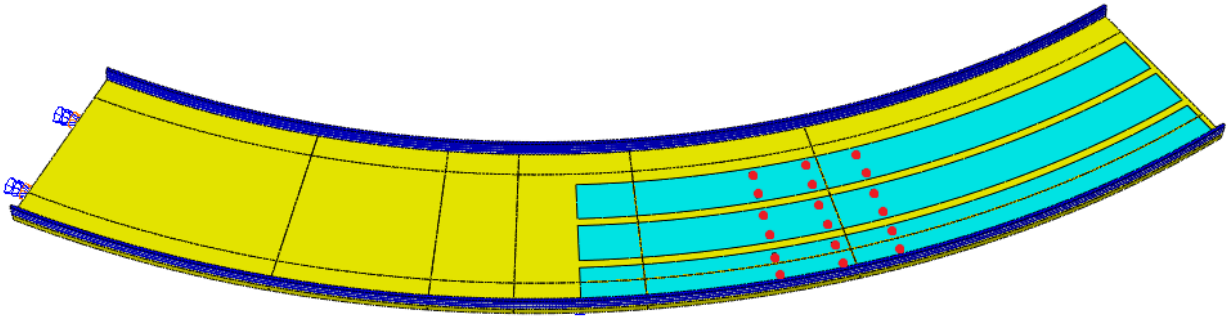

Figure 81 Redundancy II – Analysis III (three lane analysis) of B40-868

6.2 Damage Scenarios to be Considered

The damage scenario that was considered included complete full-depth fracture (including the top flanges) of one of the tub girders. It was observed that fracture in the end-span was more critical than mid-span fracture. The analyses for mid-span fracture were also performed for two bridges which are "B05-678-Unit 5 in Section 7.9" and "B40-854-Unit 3 in Section 7.19", and it was observed that the effect of mid-span fracture is insignificant and does not need to be considered for other bridges. At a minimum, fracture of the exterior girder before the first intermediate diaphragm and fracture near the center of the end span were evaluated for the Redundancy I and Redundancy II load combinations. Multiple fracture scenarios were used to identify the most critical location. In addition, for some bridges, interior girder section details were different than the exterior girders; therefore, interior girder fracture was also modelled for the bridges "B40-776 in Section 7.11", "B40-783 in Section 7.12", and "B40-834 in Section 7.15".

6.3 Model Steps

The finite element analysis was divided into two parts. The first portion was performed using implicit static analysis for the construction sequence. In this step, only the factored self-weight of the steel girders and wet concrete was applied to the steel tub girders. The wet concrete was modeled by assigning very low stiffness for the concrete and rebar. The deck was then "hardened" in the FE model by increasing the stiffness of the concrete and rebar. Explicit dynamic analysis was then used for the second portion which includes importing the results from Step 1, simulating the fracture, and evaluating the performance of the bridge after fracture under the two load combinations discussed above. Two different models were used since the Redundancy I and Redundancy II load combinations were treated separately. A quasi-static analysis was used so that inertial effects are neglected. Note that the dynamic effects due to free vibration after the fracture were included with DA_R. In the models, minimum specified time increment to stabilize the explicit analyses was determined according to the mass and element sizes, and it was set to 5 E-6. The lower time increments significantly reduce the oscillations (the noise effect) in the result outputs. In order to validate whether quasi-static analysis successfully was progressed in the explicit model, kinetic energy was checked and it was always less than 1% of the whole model strain energy.

6.4 Minimum Performance Requirements in the Faulted State

Once the analysis has been completed, it is necessary to establish whether the structure has adequate capacity (i.e., redundancy) in the faulted state. Thus, minimum strength and serviceability performance requirements have been developed as described below.

6.4.1 Minimum strength requirements

Steel components

Four basic strength criteria for primary steel components must be met when the bridge is subjected to the Redundancy I and II load combinations according to NCHRP Project 12-87a [5].

These failure criteria used herein are as follows:

- The average strain across a component of a cross section (e.g., a flange) must be below 5 times the yield strain, or 1% strain, whichever is smaller. The objective of this criterion is to limit the amount of redistribution of forces to other components while the structure remains in service. This criterion is intended to be conservative and to prevent the placement of excessive demands on the intact components that may be difficult to accommodate.
- The maximum strain anywhere in a primary component shall not exceed ultimate strain, which is conservatively limited to 5% strain.
- The compression stress must remain below the critical buckling stress of the component in cases where the FEA does not account for the buckling mode. It is noted that the analysis conducted in this study is capable of capturing local and global buckling and hence, this limit does not explicitly need to be checked.
- The system shall demonstrate a reserve margin of at least 15% of the applied live load in the Redundancy I and II load combinations. Effectively, this requirement ensures the slope of the load vs displacement curve (still on the ascending branch) for the system structure remains positive. It is noted that although this requirement is not specific to the steel components alone, but rather the entire bridge as a system.

Reinforced concrete

The nominal compressive strength of concrete may be exceeded in the analysis as well. This is acceptable if the regions where this has taken place are in the barriers or haunches and the system is able to sustain the factored loads. Concrete crushing in the aforementioned regions is not expected to result in reduction of strength based on the results of the analysis and in-situ performance of bridges where tension members have failed. However, if concrete crushing or deck reinforcement yielding (up to the fracture of the reinforcement) takes place over a maximum 50% span length of the slab, or if concrete crushing results in a flat or negative slope of the load-deflection curve, the structure should not be considered redundant as passage of traffic and environmental conditions will rapidly deteriorate the slab to a point where capacity may further be reduced. In other words, if the portion of the slab where a compressive strain of 0.003 (based on ACI 318-14 [11] analysis procedures for flexural members) has been exceeded is large enough to compromise the overall load carrying capacity of the system or if significant hinging occurs, the structure should not be considered as sufficiently redundant.

Substructure

In addition to checking the strength of the superstructure, the substructure must also be analyzed. Although the substructure may not be explicitly included in the finite element model in all load combinations, the displacements and reaction forces at support locations are checked in the analysis. In this evaluation, the capacity of the bearings as provided in the design plans was compared to that obtained from the FEA of the faulted bridge. Conservatively, only one support per bridge was assigned as hinge and all other boundary conditions were set to roller; therefore, the horizontal displacements at the bearing maximized after fracture occurred.

6.4.2 Minimum serviceability requirements

There are several minimum serviceability requirements for the bridge in the faulted state. It is also noted that the structure will not have any overall stability problems if the results of the analysis comply with these requirements. According to NCHRP Project 12-87a [5], the minimum serviceability criteria for the Redundancy I and II load combinations is explained as follows:

The change in the maximum vertical deflections of the superstructure should not exceed *L*/50. The deflection change is defined as a displacement difference between before fracture and

after fracture cases, but only under Redundancy II factored dead loads. As a load factor of 1.05 is applied, the limit is taken as L/50. The value was developed based on that traffic can safely crossed the bridge with the roadway in a severely distorted condition.

Uplift at supports beneath a joint in the deck due to Redundancy II factored dead loads should not exceed 3.5 inches. The load case used is Redundancy II, but only with dead load applied.

Horizontal translation at supports shall not result in the bridge falling off a support. Transverse and longitudinal displacements at support locations should be considered as a member may lose support, particularly at supports that allow for expansion. Hence, it should be verified that these horizontal displacements can be accommodated by the support. The criteria simply require that the structure does not fall off of a support, whether that be a bearing tipping over or a girder coming completely off of a pier or abutment.

CHAPTER 7 TWIN-TUB-GIRDER PARAMETRIC STUDY

In this chapter, twenty-one (21) continuous span twin-tub-girder bridge units from the existing inventory of the Wisconsin Department of Transportation (WisDOT) and three (3) simple span twin-tub-girder bridge units from the existing inventory of other states were evaluated for the case where one of the two tub girders fails due to brittle fracture. The bridges were evaluated using the system analysis procedures developed at Purdue University under NCHRP Project 12-87a [5]. The current parametric study includes the following bridges:

- Section 6.1 includes the bridge “B05-658-Unit1”.
- Section 6.2 includes the bridge “B05-658-Unit2”.
- Section 6.3 includes the bridge “B05-660-Unit1”.
- Section 6.4 includes the bridge “B05-660-Unit2”.
- Section 6.5 includes the bridge “B05-660-Unit3”.
- Section 6.6 includes the bridge “B05-661”.
- Section 6.7 includes the bridge “B05-678-Unit3”.
- Section 6.8 includes the bridge “B05-678-Unit4”.
- Section 6.9 includes the bridge “B05-678-Unit5”.
- Section 6.10 includes the bridge “B05-679-Unit1&2”.
- Section 6.11 includes the bridge “B40-776”.
- Section 6.12 includes the bridge “B40-783”.
- Section 6.13 includes the bridge “B40-786-Unit1”.
- Section 6.14 includes the bridge “B40-786-Unit2”.
- Section 6.15 includes the bridge “B40-834”.
- Section 6.16 includes the bridge “B40-837”.
- Section 6.17 includes the bridge “B40-854-Unit1”.
- Section 6.18 includes the bridge “B40-854-Unit2”.
- Section 6.19 includes the bridge “B40-854-Unit3”.
- Section 6.20 includes the bridge “B40-856-Unit2”.
- Section 6.21 includes the bridge “B40-868”.
- Section 6.22 includes the bridge “UT-Test Bridge”.

- Section 6.23 includes the bridge “Simple-Span-1Lane-128ft”.
- Section 6.24 includes the bridge “Simple-Span-2Lanes-204ft”.

All the analyzed bridges were assumed to be flat in the horizontal plane. In other words, geometry changes due to cross slope were not included in the models. All the bridges have a system of K-frames, struts and braces within each girder to provide stability. The bearings are multi-rotational unidirectional bearings at the abutments, and multi-rotational fixed bearing over the piers. The structures were designed according to AASHTO LRFD Specifications 4th, 5th or 6th Editions.

7.1 B05-658-Unit1 (4 Spans)

7.1.1 Background, geometry, and loading

The structural redundancy of Ramp FEN over STH 29 EB TO USH 41NB (Structure ID B05-658-Unit1 in Figure 82) was evaluated for the case where one of the two twin-tub-girders fails due to an assumed sudden full-depth failure. In the analysis, the outside girder was assumed to have fractured. The bridge is symmetric about the center of the middle pier. As discussed in Section 3.3 only first two and half span needs to be modeled as shown in Figure 82.

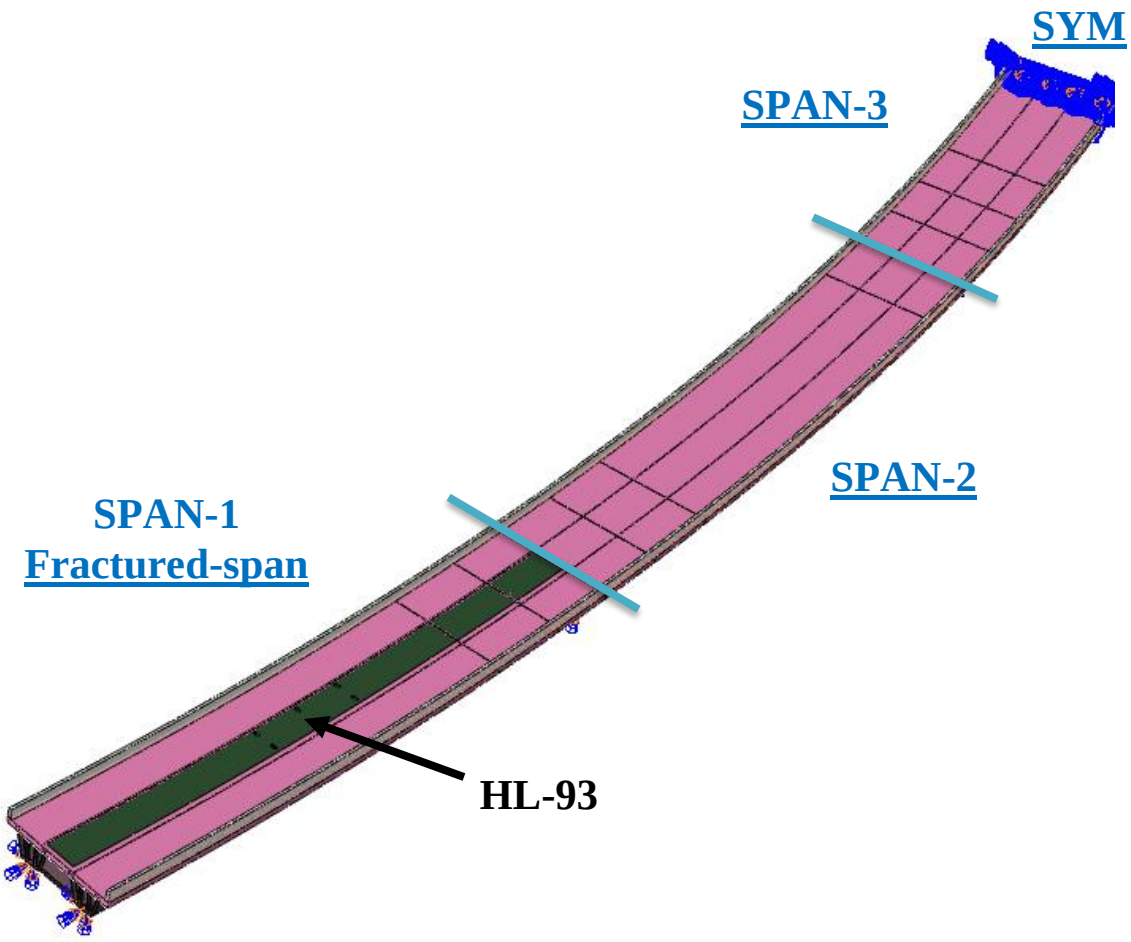

Figure 82 General Isometric View of B05-658-Unit1-LF (Span 1 to Half of Span 3)

Table 19 provides details related to the geometry and material properties associated with the structure.

Table 19 The bridge geometry and material properties

Bridge Details	
Bridge Name	B05-658-Unit1
Radius of Curvature	1363.5 ft. (measured from bridge centerline)
Span Lengths	LF: 170.0 - 210.0 - 105.0 ft. Span 3 = 210.0/2 = 105.0
Girder Details	
Girder Steel	ASTM A709 HPS 50WF
Box Girder Width (from the centers of interior top-flange to the center of exterior top-flange)	9.5 ft.
Girders Spacing (from the centers of the girders' bottom flanges)	19.0 ft.
Top Flange	20.0 in. wide Varies, 1.0 in. to 1.75 in. thick
Web	86 in. high Varies, 0.75 in. to 0.875 in. thick
Bottom Flange	75 in. wide Varies, 0.875 in. to 1.375 in. thick
Diaphragms	Three full depth diaphragms for end spans
Internal Cross Frames	L6x6x9/16 (Top), L6x6x9/16 (Inclined)
Strut Braces	-
Lateral Braces	WT7x34
Longitudinal Stiffeners on Bottom Flanges	-
Deck Details	
Concrete Material Strength	4 ksi (HPC)
Composite Deck	35.896 ft. wide, 10.0 in. thick 4 in. haunch thick
Transverse Reinforcement	No. 5 rebars with 6.5 in. spacing
Longitudinal Reinforcement	No. 4 & No. 5 rebars with 5 in. spacing
Overhang Reinforcement	No. 4 rebars with 5 in. spacing
Shear Studs	6 in. height. Longitudinal spacings are 18-19-22 in. Three shear studs spaced equally in the transverse direction
Parapet Type	LF (Interior) – HF (Exterior)
Load Details	
Number of Lane	Single lane traffic
Future Wearing Surface	-
Maximum Dead Load Displacement (before fracture)	L/630

Three different full-depth fractures were applied separately in each after-fracture performance analysis. Specifically, the tension flange, both webs, and both upper compression flanges were assumed to have failed in one of the girders for each scenario. The locations where the three fractures were assumed to have occurred is shown in Figure 83.

The locations are as follows:

- Crack 1 (C1) just before 1st (D1) intermediate diaphragm after 1st (S1A) exterior support,
- Crack 2 (C2) between 1st (D1) and 2nd (D2) intermediate diaphragms,
- Crack 3 (C3) just before 2nd (D2) intermediate diaphragm.

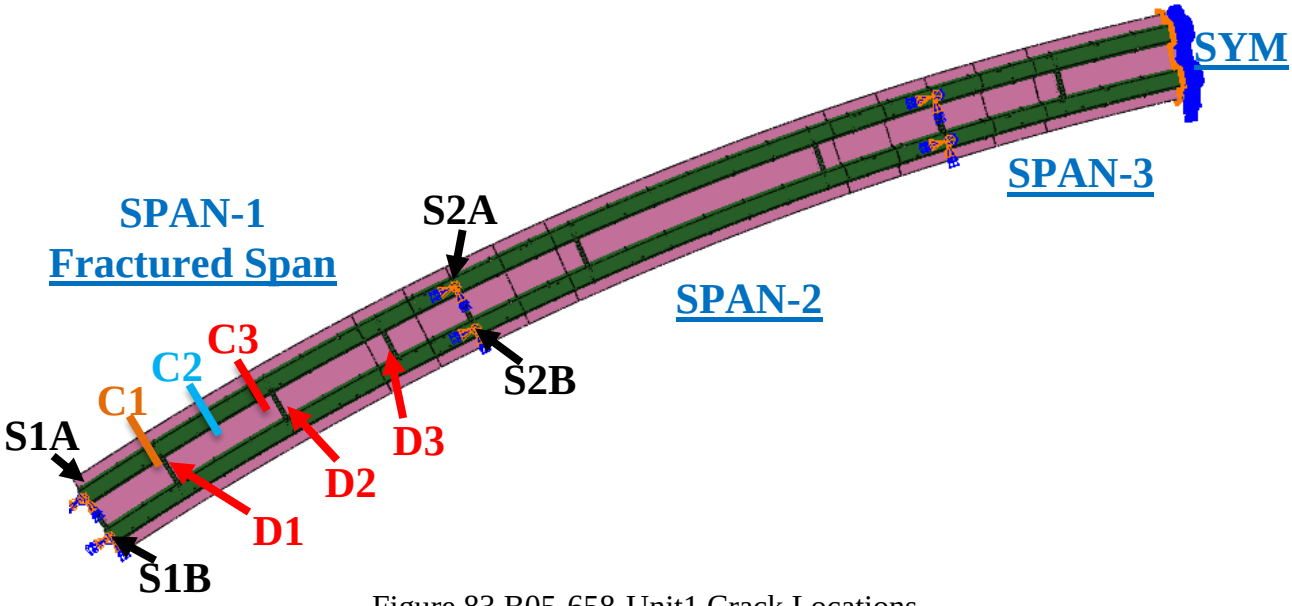

Figure 83 B05-658-Unit1 Crack Locations

The Redundancy I and Redundancy II load combinations require different positioning of traffic live loads. For analyses where only a single lane of live load is applied for the Redundancy I load combination, the HL-93 live load was positioned in the center of the design (i.e., striped) traffic lane. For the Redundancy II load combination, up to two HL-93 vehicular live loads were placed according to the procedure explained in Section 6.1.3. Full non-linear dynamic analysis was performed to determine the level of dynamic amplification that could be expected upon sudden failure of the tub girder. Based on this analysis, the dynamic amplification factor can conservatively be taken as 0.2 (i.e., 20%). Table 20 demonstrates the amount of total load applied in the Redundancy I (R1) and II (R2) load combinations.

Table 20 Total load applied on the fractured bridge

Type of Loading	Dead Load (1.05 * DA_R)	Future Wearing Surface (1.05 * DA_R)	Live Load (0.85 * m * DA_R)	Total Load (DA_R)
R1 **1 HL-93**	5251.20 (1.05 * 1.2)	- (1.05 * 1.2)	221.30 (0.85 * 1.2 * 1.2) 253.84 (15% More LL)	5472.50 5505.04 (15% More LL)

Type of Loading	Dead Load (1.05)	Future Wearing Surface (1.05)	Live Load (1.3 * m)	Total Load
R2 **1 HL-93**	4376.00 (1.05)	- (1.05)	298.90 (1.3 * 1.2) * (15% more per HS-20 impact) 327.64 (15% More LL)	4674.90 4703.64 (15% More LL)
R2 **2 HL-93**	4376.00 (1.05)	- (1.05)	498.16 (1.3 * 1.0) * (15% more per HS-20 impact) 555.64 (15% More LL)	4874.16 4931.64 (15% More LL)

7.1.2 Results for B05-658-Unit1

The analysis has shown that Ramp FEN over STH 29 EB TO USH 41NB (Structure ID B05-658-Unit1) possesses considerable reserve strength in the faulted state and that the steel twin-tub-girders do not meet the definition of a fracture critical member when evaluated using the prescribed loading and failure criteria developed in NCHRP 12-87a [5]. Table 21 summarizes the results obtained from the redundancy analysis of the structure in faulted state. The fracture case C2 was found to result in the most critical crack location, and hence the numerical values are presented in Table 21. The evaluation presents the results for the Redundancy I and II load combinations and compares the results to the minimum performance criteria discussed in CHAPTER 6.

Table 21 Results obtained for redundancy evaluation

Fracture Locations		C1, C2, C3	
Load Combination		Redundancy I	Redundancy II
Max. Equivalent Plastic Strain in the Main Girder	**Value**	No plastic strain	No plastic strain
	Location	-	-
Concrete Crushing	**Extent**	No concrete crushing	No concrete crushing
	Location	-	-
Stud Failing	**Value**	No stud failure	No stud failure
	Location	-	-
Max. Vert. Reaction Force	**Value**	1271 kips	1276 kips
	Location	S2A (C2 - 1HL-93)	S2A (C2 - 2HL-93)
Uplift at Supports	**Value**	No Uplift	
	Location		
Max. Hor. Displacement at Supports	**Value**	2.44 in.	3.45 in.
	Location	S1A (C2 - 1HL-93)	S1A (C2 - 2HL-93)
Max. Vertical Deflection Change	**Value**	Not Applicable	3.25 in. (C2)

Notes:
- Service bearing capacities for strength is 1372 kips.
- Shear capacity of the deck is checked.

For both Redundancy I and Redundancy II, the structure has adequate redundancy after the fracture of an exterior girder using the criteria for the strength and displacement requirements discussed above. The following were observed:

- Plastic strain is not reached in the steel tub girders (as shown in Figure 84).
- Crushing does not occur in the concrete deck and the parapet, Figure 85 shows in transverse, and Figure 86 shows in longitudinal directions.
- No haunch separation or shear stud failure is observed in Figure 87.
- The maximum vertical deflection change (difference between before fracture and after fracture stages) is 3.25 inches (as shown in Figure 88) which is lower than L/50 (40.80 inches) and the maximum change in cross-slope is below 5%.

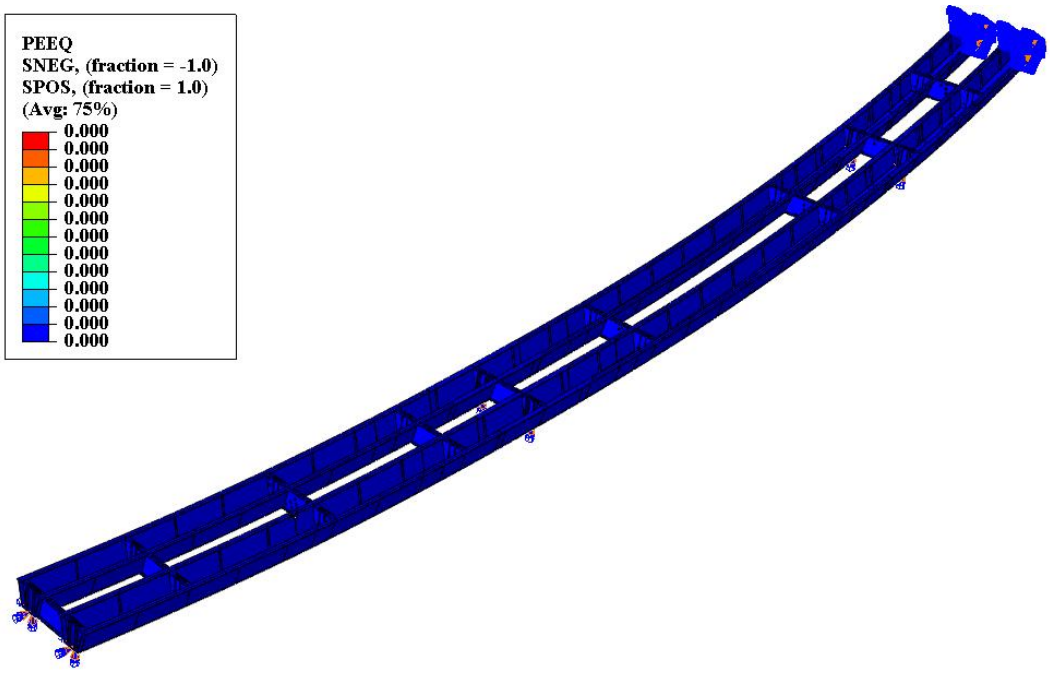

Figure 84 Absence of plastic equivalent strain in primary steel members when crack at C1, C2 or C3 applied in Redundancy I or Redundancy II

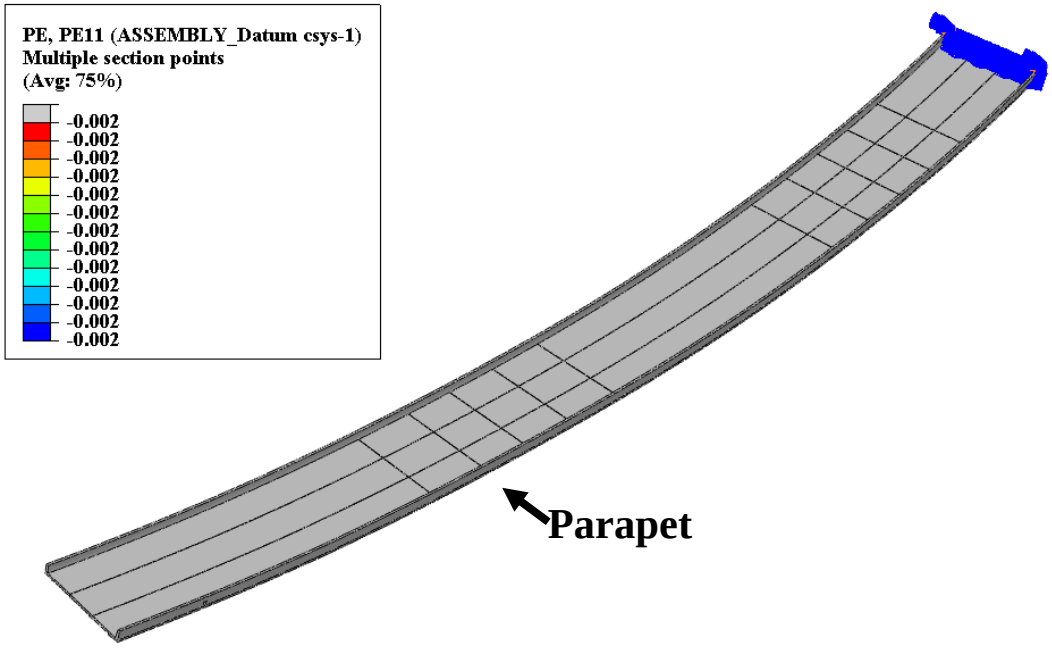

Figure 85 Absence of concrete crushing in deck and parapet in transverse direction when crack at C1, C2 or C3 applied in Redundancy I or Redundancy II

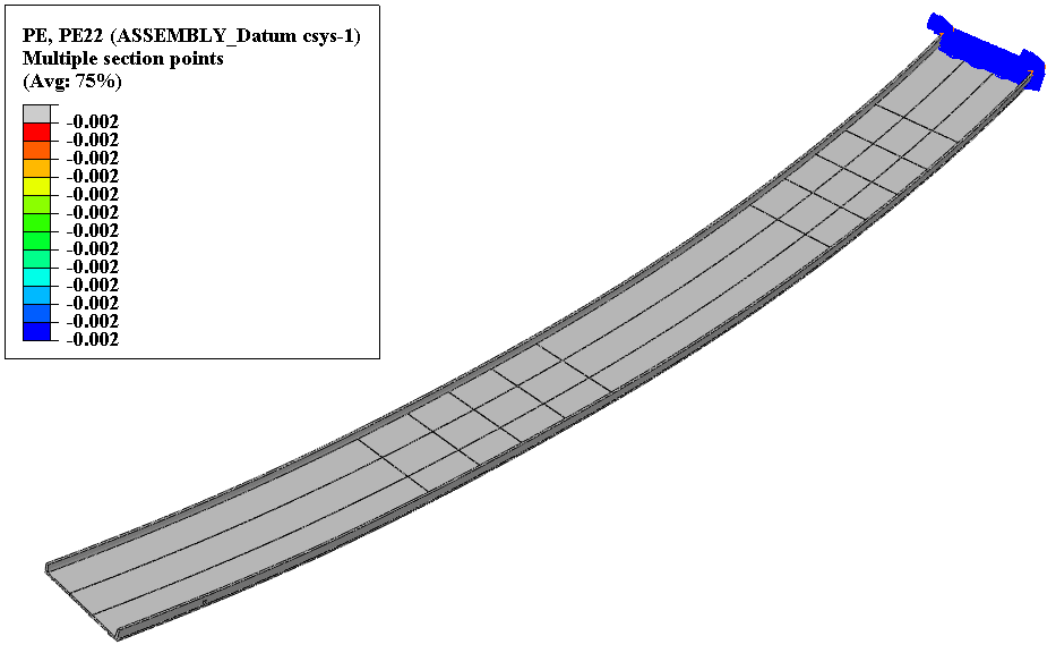

Figure 86 Absence of concrete crushing in deck and parapet in longitudinal direction when crack at C1, C2 or C3 applied in Redundancy I or Redundancy II

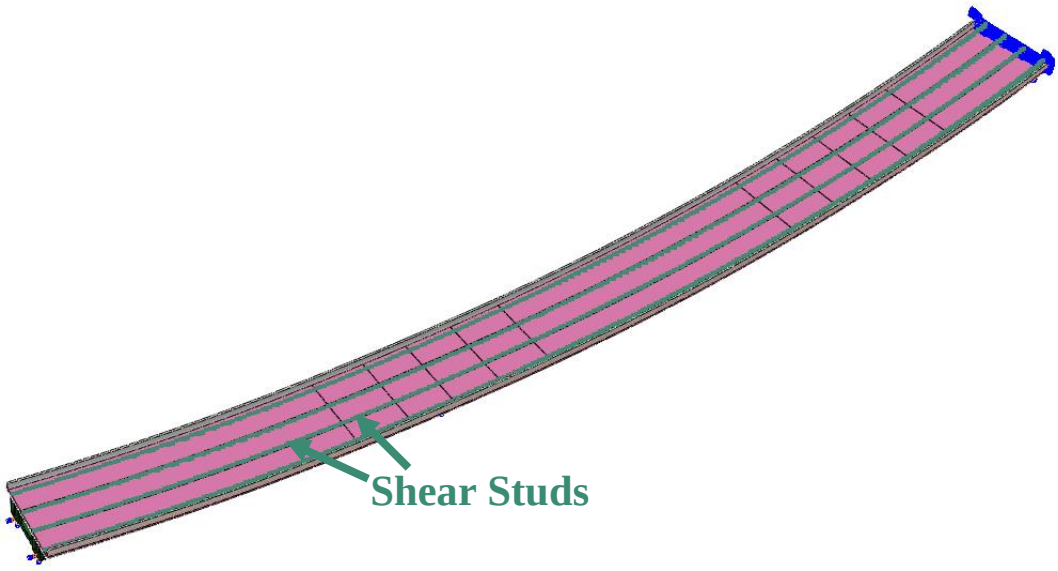

Figure 87 Absence of shear stud failure when crack at C1, C2 or C3 applied in Redundancy I or Redundancy II

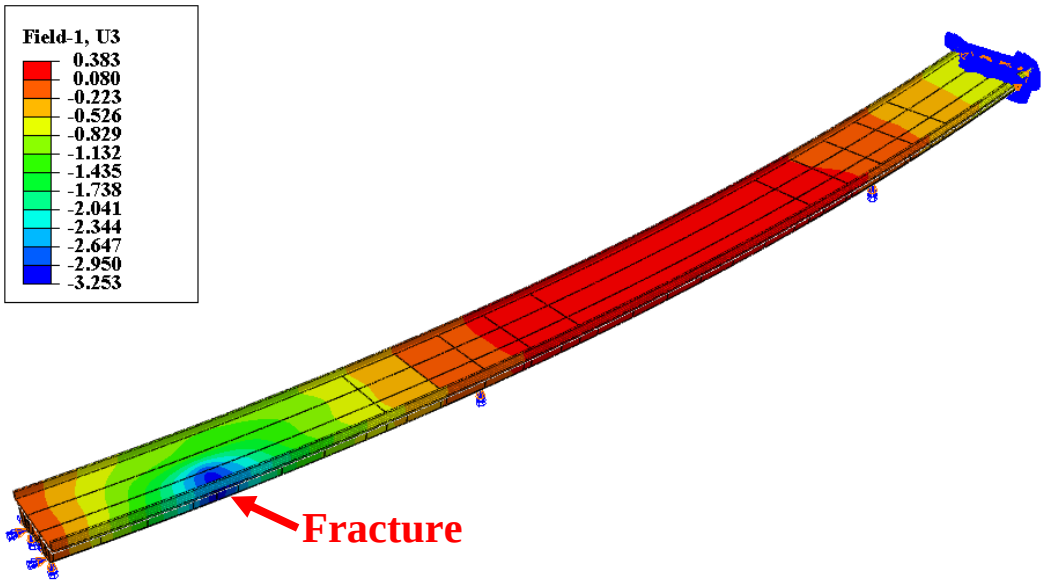

Figure 88 Deflection after failure of primary steel tension member when crack at C2 applied

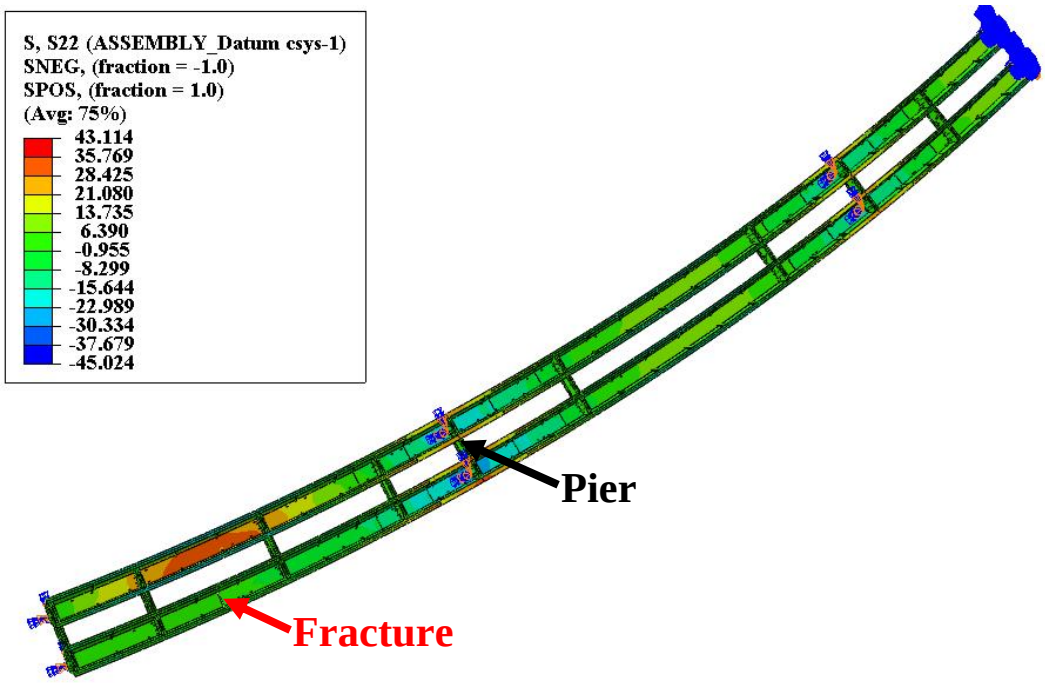

Figure 89 Longitudinal stress after failure of primary steel tension member when crack at C2 applied with 2-lanes load in Redundancy II

When the C2 crack location and two HL93 traffic loads were applied in the Redundancy II load combination, the maximum nominal longitudinal stresses at the center of the bottom flange of the fractured girder at the pier equal to 28.3 (as shown in Figure 89). This is the most critical

combination of loading and fracture location. This stress is lower than the bottom flange buckling capacity at the same location which is equal to 40.9 in the design calculations from Highway Structures Information System (HSI) [37]. Summary of the redundancy evaluation is shown in Table 22.

Table 22 Summary of Redundancy failure criteria evaluation

Performance Requirement		**Most Critical Analysis Case**	**Result**	**Acceptable?**
Strength Requirements	Steel Primary Members	-	No component has strain larger than $5\varepsilon_y$ or 1%. Failure strain was not reached anywhere.	**YES**
	Concrete Crushing	-	No concrete crushing	**YES**
Serviceability Requirements	Vertical Deflection Change	C2. (Only Redundancy II DL considered).	Maximum deflection change is 3.3 in, which is lower than L/50 (40.8in)	**YES**
	Cross-Slope Change	C2. (Only Redundancy II considered).	Maximum additional cross-slope is less than 5%.	**YES**
	Uplift	None.	No uplift.	**YES**

Notes:
- The analysis showed that the structure is capable of resisting an additional 15% of the applied factored live load.
- The horizontal displacement changes at support locations were lower than 6 in.

7.1.3 Summary

Analytical models have been developed to evaluate the structural redundancy of Ramp FEN over STH 29 EB TO USH 41NB (Structure ID B05-658-Unit1) in the state of Wisconsin. The girders are presently classified as Fracture Critical Members. A full depth fracture, including both webs and the top and bottom flange was simulated at three different locations in the exterior girder. The analysis confirms that the bridge satisfies the performance requirements for both Redundancy I and Redundancy II load combinations based on the failure criteria developed in NCHRP 12-87a [5]. Hence, the girders need not be classified as Fracture Critical Members (FCMs).

7.2 B05-658-Unit2 (6 Spans)

7.2.1 Background, geometry, and loading

The structural redundancy of Ramp FEN over STH 29 EB TO USH 41NB (Structure ID B05-658-Unit2 in Figure 90) was evaluated for the case where one of the two twin-tub-girders fails due to an assumed sudden full-depth failure. In the analysis, the outside girder was assumed to have fractured. The bridge is symmetric about the center of the middle pier. As discussed in Section 3.3 only first two and half span needs to be modeled as shown in Figure 90.

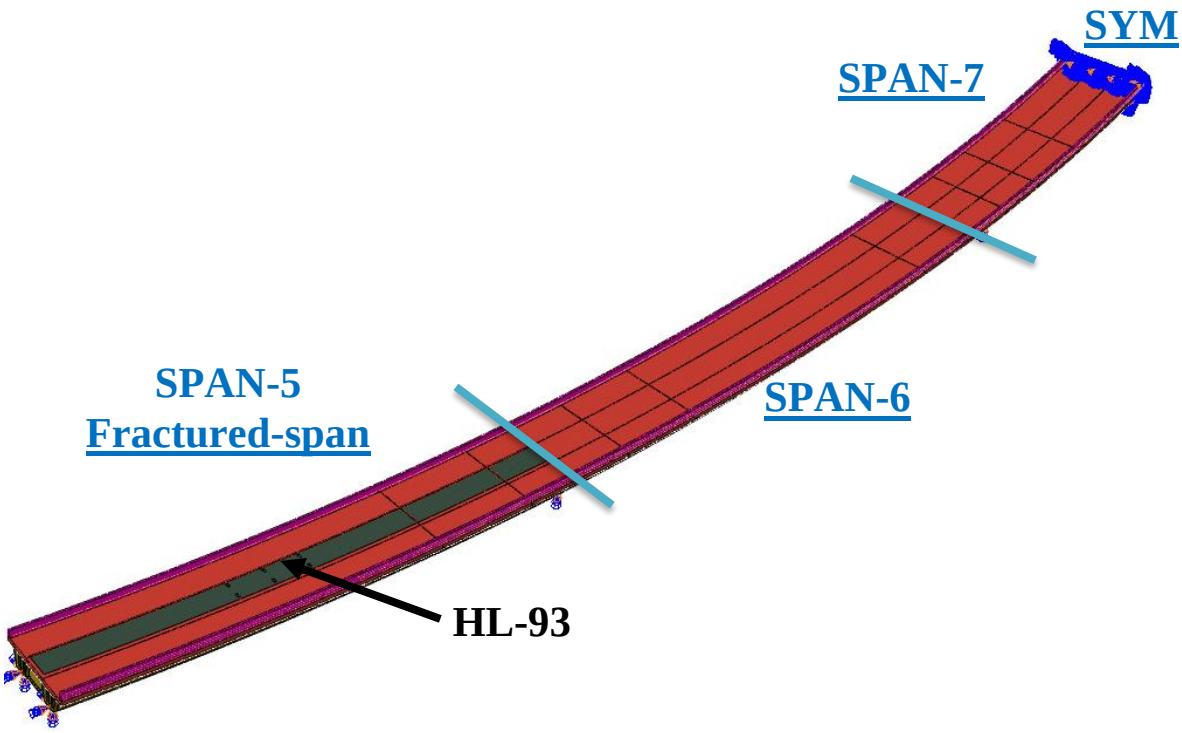

Figure 90 General Isometric View of B05-658-Unit2-LF (Span 5 to Half of Span 7)

Table 23 provides details related to the geometry and material properties associated with the structure.

Table 23 The bridge geometry and material properties

Bridge Details	
Bridge Name	B05-658-Unit2
Radius of Curvature	1363.5 ft. (measured from bridge centerline)
Span Lengths	LF: 199.2 - 250.0 - 125.0 ft. Span 7 = 250.0/2 = 125.0
Girder Details	
Girder Steel	ASTM A709 HPS 50WF
Box Girder Width (from the centers of interior top-flange to the center of exterior top-flange)	9.5 ft.
Girders Spacing (from the centers of the girders' bottom flanges)	19.0 ft.
Top Flange	20.0 in. wide Varies, 1.0 in. to 1.75 in. thick
Web	86 in. high Varies, 0.75 in. to 0.875 in. thick
Bottom Flange	75 in. wide Varies, 0.875 in. to 1.375 in. thick
Diaphragms	Three full depth diaphragms for end spans
Internal Cross Frames	L6x6x9/16 (Top), L6x6x9/16 (Inclined)
Strut Braces	-
Lateral Braces	WT7x34
Longitudinal Stiffeners on Bottom Flanges	-
Deck Details	
Concrete Material Strength	4 ksi (HPC)
Composite Deck	35.896 ft. wide, 10.0 in. thick 4.0 in. haunch thick
Transverse Reinforcement	No. 5 rebars with 6.5 in. spacing
Longitudinal Reinforcement	No. 4 & No. 5 rebars with 5 in. spacing
Overhang Reinforcement	No. 4 rebars with 5 in. spacing
Shear Studs	6 in. height. Longitudinal spacings are 18-19-22 in. Three shear studs spaced equally in the transverse direction
Parapet Type	LF (Interior) – HF (Exterior)
Load Details	
Number of Lane	Single lane traffic
Future Wearing Surface	-
Maximum Dead Load Displacement (before fracture)	L/415

Two different full-depth fractures were applied separately in each after-fracture performance analysis. Specifically, the tension flange, both webs, and both upper compression flanges were assumed to have failed in one of the girders for each scenario. The locations where the two fractures were assumed to have occurred is shown in Figure 91. The locations are as follows:

- Crack 1 (C1) just before 1st (D1) intermediate diaphragm after 1st (S1A) exterior support,
- Crack 2 (C2) between 1st (D1) and 2nd (D2) intermediate diaphragms.

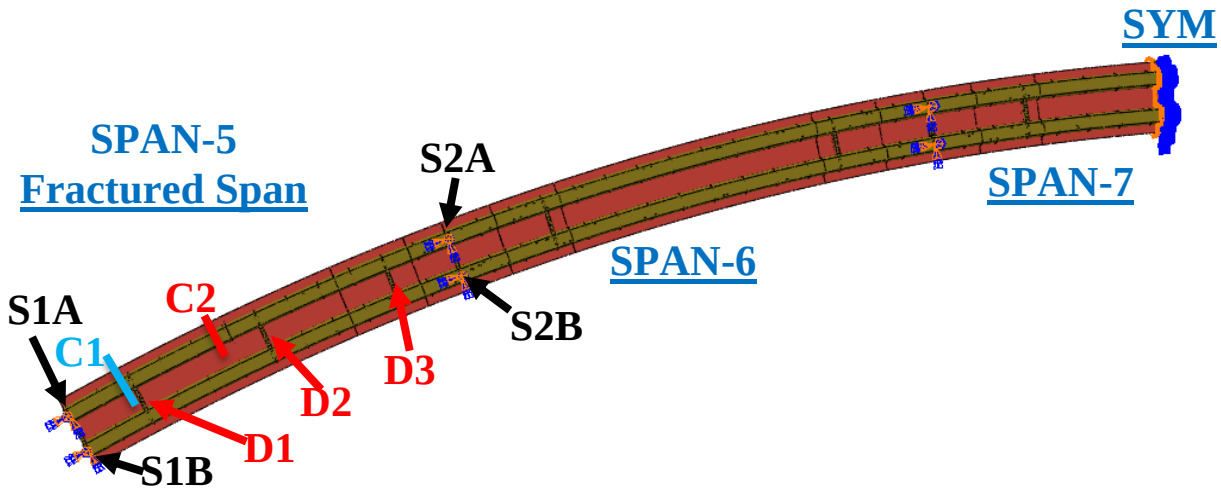

Figure 91 B05-679-Unit2 Crack Locations

The Redundancy I and Redundancy II load combinations require different positioning of traffic live loads. For analyses where only a single lane of live load is applied for the Redundancy I load combination, the HL-93 live load was positioned in the center of the design (i.e., striped) traffic lane. For the Redundancy II load combination, up to two HL-93 vehicular live loads were placed according to the procedure explained in Section 6.1.3. Full non-linear dynamic analysis was performed to determine the level of dynamic amplification that could be expected upon sudden failure of the tub girder. Based on this analysis, the dynamic amplification factor can conservatively be taken as 0.2 (i.e., 20%). Table 24 demonstrates the amount of total load applied in the Redundancy I (R1) and II (R2) load combinations.

Table 24 Total load applied on the fractured bridge

Type of Loading	Dead Load ($1.05 * DA_R$)	Future Wearing Surface ($1.05 * DA_R$)	Live Load ($0.85 * m * DA_R$)	Total Load (DA_R)
Redundancy-1 1 HL-93	6400.80 (1.05 * 1.2)	- (1.05 * 1.2)	244.02 (0.85 * 1.2 * 1.2) 279.90 (15% More LL)	6644.82 6680.70 (15% More LL)

Type of Loading	Dead Load (1.05)	Future Wearing Surface (1.05)	Live Load (1.3 * m)	Total Load
Redundancy-2 1 HL-93	5334.00 (1.05)	- (1.05)	327.85 (1.3 * 1.2) * (15% more per HS-20 impact) 359.37 (15% More LL)	5661.85 5693.37 (15% More LL)
Redundancy-2 2 HL-93	5334.00 (1.05)	- (1.05)	546.42 (1.3 * 1.0) * (15% more per HS-20 impact) 609.46 (15% More LL)	5880.42 5943.46 (15% More LL)

7.2.2 Results for B05-658-Unit2

The analysis has shown that Ramp FEN over STH 29 EB TO USH 41NB (Structure ID B05-658-Unit2) possesses considerable reserve strength in the faulted state and that the steel twin-tub-girders do not meet the definition of a fracture critical member when evaluated using the prescribed loading and failure criteria developed in NCHRP 12-87a [5]. Table 25 summarizes the results obtained from the redundancy analysis of the structure in faulted stage. The fracture case C2 was found to result in the most critical crack location, and hence the numerical values are presented in Table 25. The evaluation presents the results for the Redundancy I and II load combinations and compares the results to the minimum performance criteria discussed in CHAPTER 6.

Table 25 Results obtained for redundancy evaluation

Fracture Locations		**C1, C2**	
Load Combination		**Redundancy I**	**Redundancy II**
Max. Equivalent Plastic Strain in the Main Girder	**Value**	No plastic strain	0.003 (C1)
	Location	-	Very localized yielding Intermediate Diag. "D1" flanges & Intact girder bottom flanges next to D1
Concrete Crushing	**Extent**	No concrete crushing	Localized Crushing (C2)
	Location	-	Only over fracture
Stud Failing	**Value**	No stud failure	No stud failure
	Location	-	-
Max. Vert. Reaction Force	**Value**	1693 kips	1559 kips
	Location	S2B (C2 - 2HL-93)	S2A (C2 - 3HL-93)
Uplift at Supports	**Value**	No Uplift	
	Location		
Max. Hor. Displacement at Supports	**Value**	2.57 in.	5.41 in.
	Location	S1A (C2 - 2HL-93)	S1A (C2 - 3HL-93)
Max. Vertical Deflection Change	**Value**	Not Applicable	4.14 in. (C2)

Notes:
- Strength bearing capacities for strength is 1604 kips.
- Shear capacity of the deck is checked.

For both Redundancy I and Redundancy II, the structure has adequate redundancy after the fracture of an exterior girder using the criteria for the strength and displacement requirements discussed above. The following were observed:

- Insignificant plastic strain is not higher than 0.003 in Redundancy II analysis.
- Only localized insignificant crushing occurs in the concrete deck.
- No haunch separation or shear stud failure is observed.
- The maximum vertical deflection change (difference between before fracture and after fracture stages) is 4.14 inches which is lower than L/50 (47.76 inches) and the maximum change in cross-slope is below 5%.

Summary of the redundancy evaluation is shown in Table 26.

Table 26 Summary of Redundancy failure criteria evaluation

Performance Requirement		Most Critical Analysis Case	Result	Acceptable?
Strength Requirements	**Steel Primary Members**	C1. Redundancy II.	No component has strain larger than $5\varepsilon_y$ or 1%. Failure strain was not reached anywhere.	**YES**
	Concrete Crushing	C2. Redundancy II.	No concrete crushing	**YES**
Serviceability Requirements	**Vertical Deflection Change**	C2. (Only Redundancy II DL considered).	Maximum deflection change is 4.1 in, which is lower than L/50 (47.8in)	**YES**
	Cross-Slope Change	C2. (Only Redundancy II considered).	Maximum additional cross-slope is less than 5%.	**YES**
	Uplift	None.	No uplift.	**YES**

Notes:

- The analysis showed that the structure is capable of resisting an additional 15% of the applied factored live load.
- The horizontal displacement changes at support locations were lower than 6 in.

When the C2 crack location and two HL93 traffic loads were applied in the Redundancy II load combination, the maximum nominal longitudinal stresses at the center of the bottom flange of the fractured girder at the pier equal to 33.4. This is the most critical combination of loading and fracture location. The bottom flange buckling capacity at the same locations are equal to 47.2 in the design calculations from Highway Structures Information System (HSI) [37].

7.2.3 Summary

Analytical models have been developed to evaluate the structural redundancy of Ramp FEN over STH 29 EB TO USH 41NB (Structure ID B05-658-Unit2) in the state of Wisconsin. The girders are presently classified as Fracture Critical Members. A full depth fracture, including both webs and the top and bottom flange was simulated at two different locations in the exterior girder. The analysis confirms that the bridge satisfies the performance requirements for both Redundancy I and Redundancy II load combinations based on the failure criteria developed in NCHRP 12-87a [5]. Hence, the girders need not be classified as Fracture Critical Members (FCMs).

7.3 B05-660-Unit1 (3 Spans)

7.3.1 Background, geometry, and loading

The structural redundancy of Ramp FNW over NB USH 41 to WB STH 29 (Structure ID B05-660-Unit1 in Figure 92 and Figure 93) was evaluated for the case where one of the two twin-tub-girders fails due to an assumed sudden full-depth failure. In the analysis, the outside girder was assumed to have fractured.

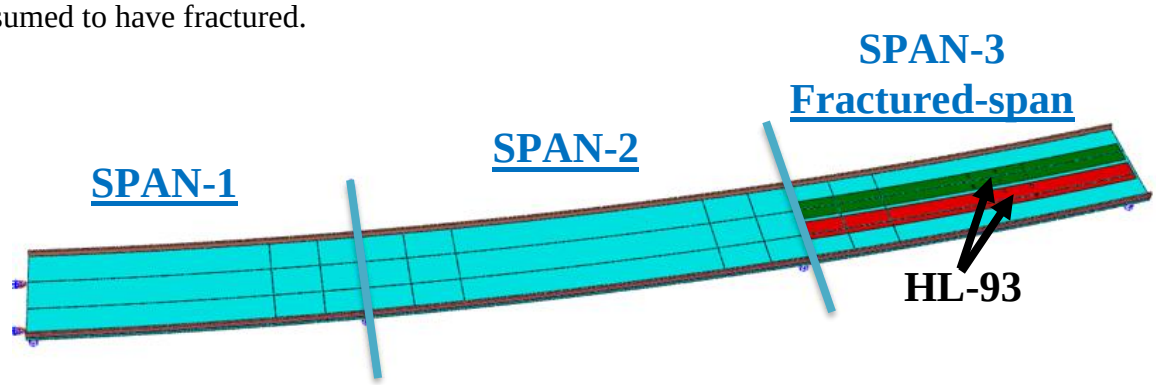

Figure 92 General Isometric View of B05-660-Unit1 (Span 1 to Span 3)

Figure 93 Google Map View of B05-660-Unit1

Table 27 provides details related to the geometry and material properties associated with the structure.

Table 27 The bridge geometry and material properties

Bridge Details	
Bridge Name	B05-660-Unit1
Radius of Curvature	Straight
Span Lengths	145.0-205.0-168.2 ft.
Girder Details	
Girder Steel	ASTM A709 HPS 50WF
Box Girder Width (from the centers of interior top-flange to the center of exterior top-flange)	12.5 ft.
Girders Spacing (from the centers of the girders' bottom flanges)	25.0 ft.
Top Flange	22.0 in. wide Varies, 1.0 in. to 2.0 in. thick
Web	86 in. high 0.75 in. thick
Bottom Flange	111 in. wide Varies, 0.75 in. to 1.25 in. thick
Diaphragms	Three full depth diaphragms per span
Internal Cross Frames	L6x6x9/16 (Top), L6x6x9/16 (Inclined)
Strut Braces	-
Lateral Braces	WT7x34
Longitudinal Stiffeners on Bottom Flanges	WT10.5x24
Deck Details	
Concrete Material Strength	4 ksi (HPC)
Composite Deck	44.896 ft. wide 11.0 in. thick 4 in. haunch thick
Transverse Reinforcement	No. 6 rebar with 7 in. spacing
Longitudinal Reinforcement	No. 4 & No. 5 rebar with 5. in. spacing
Overhang Reinforcement	-
Shear Studs	8 in. height. Longitudinal spacings are 13-15-18 in. Three shear studs spaced equally in the transverse direction
Parapet Type	LF (Interior) – HF (Exterior)
Load Details	
Number of Lane	Two lanes traffic
Future Wearing Surface	-
Maximum Dead Load Displacement (before fracture)	L/560

Two different full-depth fractures were applied separately in each after-fracture performance analysis. Specifically, the tension flange, both webs, and both upper compression flanges were assumed to have failed in one of the girders for each scenario. The locations where the two fractures were assumed to have occurred is shown in Figure 94. The locations are as follows:

- Crack 1 (C1) just before 1st (D1) intermediate diaphragm after 1st (S1A) exterior support,
- Crack 2 (C2) between 1st (D1) and 2nd (D2) intermediate diaphragms.

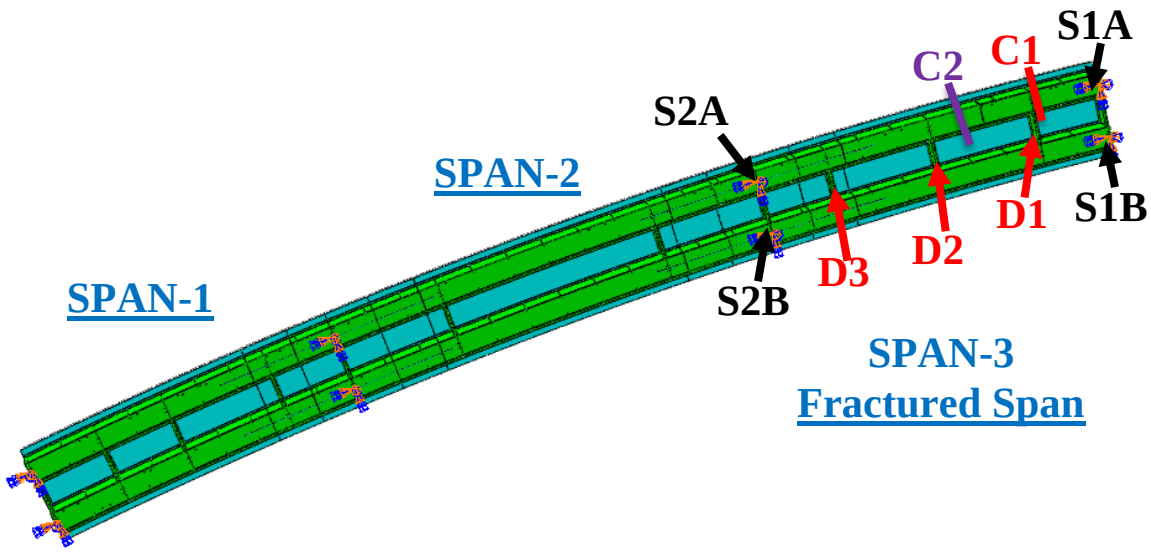

Figure 94 B05-660-Unit1 Crack Locations

The Redundancy I and Redundancy II load combinations require different positioning of traffic live loads. For analyses where only a single lane of live load is applied for the Redundancy I load combination, the HL-93 live load was positioned in the center of the exterior design (i.e., striped) traffic lane. In cases where two lanes of live load were considered, the HL-93 live loads were centered in the both design travel lanes. For the Redundancy II load combination, up to three HL-93 vehicular live loads were placed according to the procedure explained in Section 6.1.3. Full non-linear dynamic analysis was performed to determine the level of dynamic amplification that could be expected upon sudden failure of the tub girder. Based on this analysis, the dynamic amplification factor can conservatively be taken as 0.2 (i.e., 20%). Table 28 demonstrates the amount of total load applied in the Redundancy I (R1) and II (R2) load combinations.

Table 28 Total load applied on the fractured bridge

Type of Loading	Dead Load (1.05 * DA_R)	Future Wearing Surface (1.05 * DA_R)	Live Load (0.85 * m * DA_R)	Total Load (DA_R)
R1 1 HL-93	6931.20 (1.05 * 1.2)	- (1.05 * 1.2)	219.89 (0.85 * 1.2 * 1.2) 252.23 (15% More LL)	7151.09 7183.43 (15% More LL)
R1 2 HL-93	6931.20 (1.05 * 1.2)	- (1.05 * 1.2)	366.48 (0.85 * 1.0 * 1.2) 431.16 (15% More LL)	7297.68 7362.36 (15% More LL)

Type of Loading	Dead Load (1.05)	Future Wearing Surface (1.05)	Live Load (1.3 * m)	Total Load
R2 1 HL-93	5776.00 (1.05)	- (1.05)	297.10 (1.3 * 1.2 * (15% more per HS-20 impact) 325.67 (15% More LL)	6073.10 6101.67 (15% More LL)
R2 2 HL-93	5776.00 (1.05)	- (1.05)	495.16 (1.3 * 1.0) * (15% more per HS-20 impact) 552.30 (15% More LL)	6271.16 6328.30 (15% More LL)
R2 3 HL-93	5776.00 (1.05)	- (1.05)	631.34 (1.3 * 0.85) * (15% more per HS-20 impact) 717.04 (15% More LL)	6407.34 6493.04 (15% More LL)

7.3.2 Results for B05-660-Unit1

The analysis has shown that Ramp FNW over NB USH 41 to WB STH 29 (Structure ID B05-660-Unit1) possesses considerable reserve strength in the faulted state and that the steel twin-tub-girders do not meet the definition of a fracture critical member when evaluated using the prescribed loading and failure criteria developed in NCHRP 12-87a [5]. Table 29 summarizes the results obtained from the redundancy analysis of the structure in faulted stage. The fracture case C2 was found to result in the most critical crack location, and hence the numerical values are presented in Table 29. The evaluation presents the results for the Redundancy I and II load combinations and compares the results to the minimum performance criteria discussed in CHAPTER 6.

Table 29 Results obtained for redundancy evaluation

Fracture Locations		**C1, C2**	
Load Combination		**Redundancy I**	**Redundancy II**
Max. Equivalent Plastic Strain in the Main Girder	**Value**	No plastic strain	No plastic strain
	Location	-	-
Concrete Crushing	**Extent**	No concrete crushing	No concrete crushing
	Location	-	-
Stud Failing	**Value**	No stud failure	No stud failure
	Location	-	-
Max. Vert. Reaction Force	**Value**	1607 kips	1579 kips
	Location	S2A (C2 - 2HL-93)	S2A (C2 - 3HL-93)
Uplift at Supports	**Value**	No Uplift	
	Location		
Max. Hor. Displacement at Supports	**Value**	1.21 in.	3.19 in.
	Location	S1A (C2 - 2HL-93)	S1A (C2 - 3HL-93)
Max. Vertical Deflection Change	**Value**	Not Applicable	3.66 in. (C2)

Notes:
- Service bearing capacities for strength is 1661 kips.
- Shear capacity of the deck is checked.

For both Redundancy I and Redundancy II, the structure has adequate redundancy after the fracture of an exterior girder using the criteria for the strength and displacement requirements discussed above. The following were observed:

- Plastic strain is not reached in the steel tub girders.
- Crushing does not occur in the concrete deck.
- No haunch separation or shear stud failure is observed.
- The maximum vertical deflection change (difference between before fracture and after fracture stages) is 3.66 inches which is lower than L/50 (40.32 inches) and the maximum change in cross-slope is below 5%.

Summary of the redundancy evaluation is shown in Table 30.

Table 30 Summary of Redundancy failure criteria evaluation

Performance Requirement		Most Critical Analysis Case	Result	Acceptable?
Strength Requirements	**Steel Primary Members**	-	No component has strain larger than $5\varepsilon_y$ or 1%. Failure strain was not reached anywhere.	**YES**
	Concrete Crushing	-	No concrete crushing	**YES**
Serviceability Requirements	**Vertical Deflection Change**	C2. (Only Redundancy II DL considered).	Maximum deflection change is 3.7 in, which is lower than L/50 (40.3 in)	**YES**
	Cross-Slope Change	C2. (Only Redundancy II considered).	Maximum additional cross-slope is less than 5%.	**YES**
	Uplift	None.	No uplift.	**YES**

Notes

- The analysis showed that the structure is capable of resisting an additional 15% of the applied factored live load.
- The horizontal displacement changes at support locations were lower than 6 in.

7.3.3 Summary

Analytical models have been developed to evaluate the structural redundancy of Ramp FNW over NB USH 41 to WB STH 29 (Structure ID B05-660-Unit1) in the state of Wisconsin. The girders are presently classified as Fracture Critical Members. A full depth fracture, including both webs and the top and bottom flange was simulated at two different locations in the exterior girder. The analysis confirms that the bridge satisfies the performance requirements for both Redundancy I and Redundancy II load combinations based on the failure criteria developed in NCHRP 12-87a [5]. Hence, the girders need not be classified as Fracture Critical Members (FCMs).

7.4 B05-660-Unit2 (5 Spans)

7.4.1 Background, geometry, and loading

Th structural redundancy of Ramp FNW over NB USH 41 to WB STH 29 (Structure ID B05-660-Unit2) was evaluated for the case where one of the two tub girders fails due to an assumed sudden full-depth failure. In the analysis, the outside girder was assumed to have fractured. Th bridge is not symmetric; therefore, two analyses were performed to investigate fracture behavior. The first analysis considered Span 4 to the centerline of Span 6 "LF" (Figure 95) and the second analysis considered the centerline of Span 6 through Span 8 "RG" (Figure 96). As discussed in Section 3.3 only first two and half span needs to be modeled.

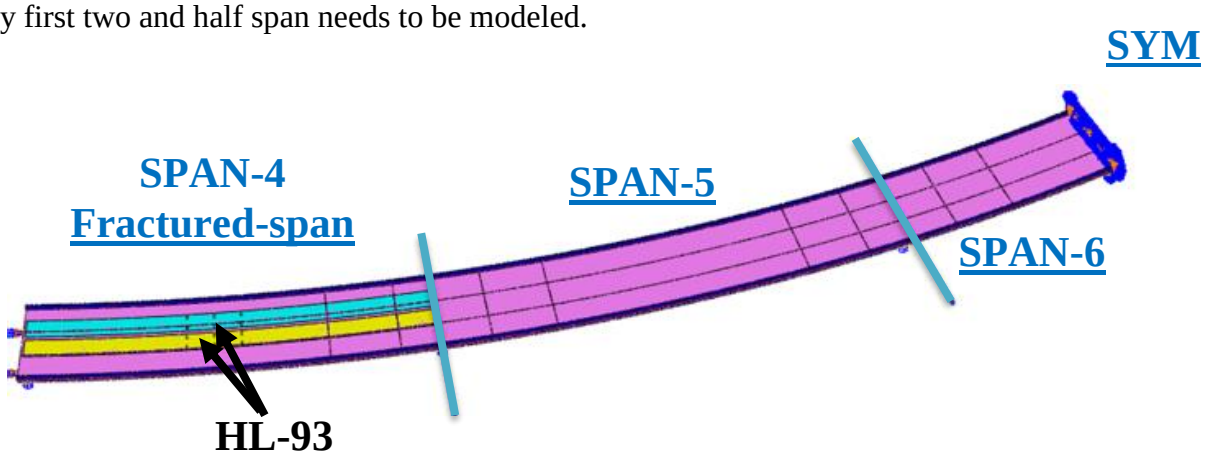

Figure 95 General Isometric View of B05-660-Unit2-LF (Span 4 to Half of Span 6)

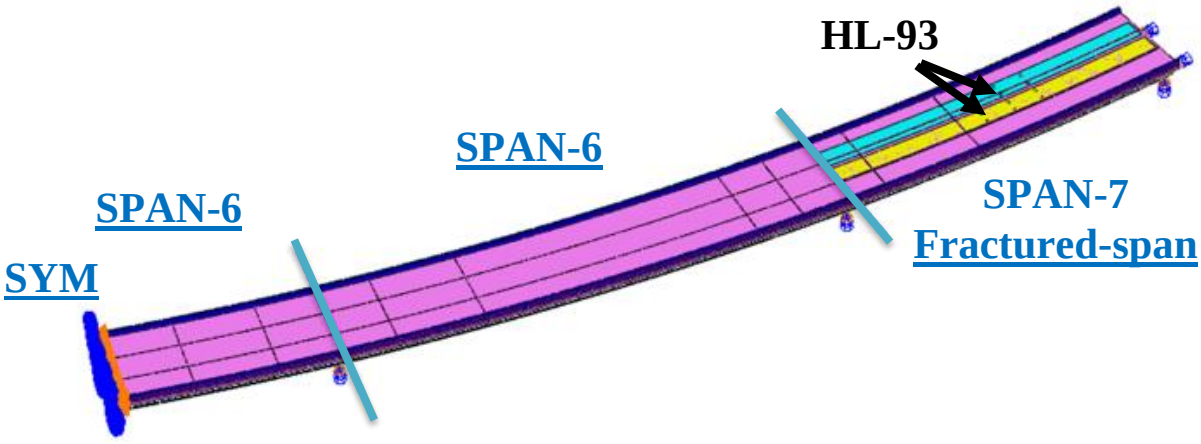

Figure 96 General Isometric View of B05-660-Unit2-RG (Half of Span 6 to Span 8)

Table 31 provides details related to the geometry and material properties associated with the structure.

Table 31 The bridge geometry and material properties

Bridge Details	
Bridge Name	B05-660-Unit2
Radius of Curvature	1358.0 ft. (measured from bridge centerline)
Span Lengths	LF: 211.0 - 255.0 - 127.5 ft. RG: 127.5 - 215.2 - 148.2 ft. Span 6 = 255.0/2 = 127.5
Girder Details	
Girder Steel	ASTM A709 HPS 50WF
Box Girder Width (from the centers of interior top-flange to the center of exterior top-flange)	12.5 ft.
Girders Spacing (from the centers of the girders' bottom flanges)	25.0 ft.
Top Flange	Varies, 22.0 in. to 26.0 in. wide Varies, 1.0 in. to 2.75 in. thick
Web	86 in. high Varies, 0.75 in. to 0.875 in. thick
Bottom Flange	111 in. wide Varies, 0.875 in. to 1.75 in. thick
Diaphragms	Three full depth diaphragms per span
Internal Cross Frames	L6x6x9/16 (Top), L6x6x9/16 (Inclined)
Strut Braces	-
Lateral Braces	WT7x34, WT8x50
Longitudinal Stiffeners on Bottom Flanges	WT10.5x24
Deck Details	
Concrete Material Strength	4 ksi (HPC)
Composite Deck	44.896 ft. wide, 11.0 in. thick 4 in. haunch thick
Transverse Reinforcement	No. 6 rebar with 7 in. spacing
Longitudinal Reinforcement	No. 4 & No. 5 rebar with 5. in. spacing
Overhang Reinforcement	-
Shear Studs	8 in. height. Longitudinal spacings are 13-15-18 in. Three shear studs spaced equally in the transverse direction
Parapet Type	LF (Interior) – HF (Exterior)
Load Details	
Number of Lane	Two lanes traffic
Future Wearing Surface	-
Maximum Dead Load Displacement	LF: L/325 – RG: L/925

Six different full-depth fractures were applied separately in each after-fracture performance analysis. Specifically, the tension flange, both webs, and both upper compression flanges were assumed to have failed in one of the girders for each scenario. The locations where the six fractures were assumed to have occurred is shown in both Figure 97 and Figure 98. The locations are as follows:

- Crack 1 (C1) just before 1st (D1) intermediate diaphragm after 1st (S1A) exterior support,
- Crack 2 (C2) between 1st (D1) and 2nd (D2) intermediate diaphragms,
- Crack 3 (C3) just after 2nd (D2) intermediate diaphragm,
- Crack 4 (C4) just before 5th (D5) intermediate diaphragms,
- Crack 5 (C5) between 5th (D5) and 6th (D6) intermediate diaphragms,
- Crack 6 (C6) just after 6th (D6) intermediate diaphragm before 4th (S4A) exterior support.

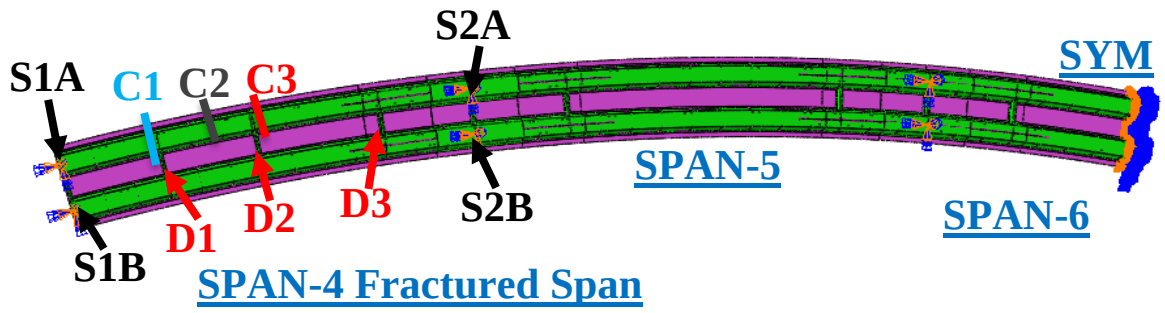

Figure 97 B05-660-Unit2-LF Crack Locations

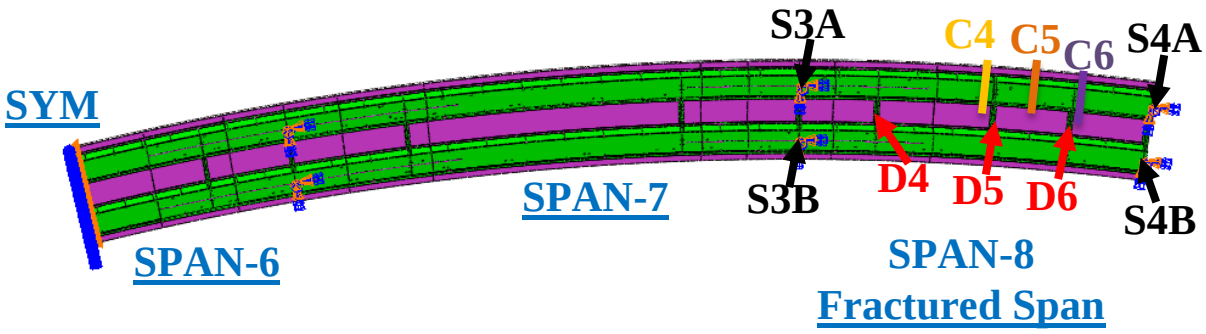

Figure 98 B05-660-Unit2-RG Crack Locations

The Redundancy I and Redundancy II load combinations require different positioning of traffic live loads. For analyses where only a single lane of live load is applied for the Redundancy I load combination, the HL-93 live load was positioned in the center of the exterior design (i.e., striped)

traffic lane. In cases where two lanes of live load were considered, the HL-93 live loads were centered in the both design travel lanes. For the Redundancy II load combination, up to three HL-93 vehicular live loads were placed according to the procedure explained in Section 6.1.3. Full non-linear dynamic analysis was performed to determine the level of dynamic amplification that could be expected upon sudden failure of the tub girder. Based on this analysis, the dynamic amplification factor can conservatively be taken as 0.2 (i.e., 20%). Table 32 demonstrates the amount of total load applied in the Redundancy I (R1) and II (R2) load combinations.

Table 32 Total load applied on the fractured bridge

Type of Loading	**Dead Load (1.05 * DA_R)**	**Future Wearing Surface (1.05 * DA_R)**	**Live Load (0.85 * m * DA_R)**	**Total Load (DA_R)**
R1 **1 HL-93**	8332.80 (LF) 6852.00 (RG) (1.05 * 1.2)	- (1.05 * 1.2)	253.42 (LF) 204.22 (RG) (0.85 * 1.2 * 1.2) 290.68 (LF) (15% More LL) 234.25 (RG) (15% More LL)	8586.22 (LF) 8623.48 (15% More LL) - 7056.22 (RG) 7086.25 (15% More LL)
R1 **2 HL-93**	8332.80 (LF) 6852.00 (RG) (1.05 * 1.2)	- (1.05 * 1.2)	422.36 (LF) 340.37 (RG) (0.85 * 1.0 * 1.2) 496.90 (LF) (15% More LL) 400.44 (RG) (15% More LL)	8755.16 (LF) 8829.70 (15% More LL) - 7192.37 (RG) 7252.44 (15% More LL)

Table 32 continued

Type of Loading	Dead Load (1.05)	Future Wearing Surface (1.05)	Live Load (1.3 * m)	Total Load
R2 1 HL-93	6944.00 (LF) 5710.00 (RG) (1.05)	- (1.05)	339.83 (LF) 277.13 (RG) (1.3 * 1.2) * (15% more per HS-20 impact) 372.51 (LF) (15% More LL) 303.78 (RG) (15% More LL)	7283.83 (LF) 7316.51 (15% More LL) - 5987.13 (RG) 6013.78 (15% More LL)
R2 2 HL-93	6944.00 (LF) 5710.00 (RG) (1.05)	- (1.05)	566.38 (LF) 461.88 (RG) (1.3 * 1.0) * (15% more per HS-20 impact) 631.74 (LF) (15% More LL) 515.18 (RG) (15% More LL)	7510.38 (LF) 7575.74 (15% More LL) - 6171.88 (RG) 6225.18 (15% More LL)
R2 3 HL-93	6944.00 (LF) 5710.00 (RG) (1.05)	- (1.05)	722.14 (LF) 588.90 (RG) (1.3 * 0.85) * (15% more per HS-20 impact) 820.17 (LF) (15% More LL) 668.84 (RG) (15% More LL)	7666.14 (LF) 7764.17 (15% More LL) - 6298.90 (RG) 6378.84 (15% More LL)

7.4.2 Results for B05-660-Unit2

The analysis has shown that Ramp FNW over NB USH 41 to WB STH 29 (Structure ID B05-660-Unit2) possesses considerable reserve strength in the faulted state and that the steel twin-tub-girders do not meet the definition of a fracture critical member when evaluated using the prescribed loading and failure criteria developed in NCHRP 12-87a [5]. Table 33 summarizes the results obtained from the redundancy analysis of the structure in faulted stage. The fracture case C2 was found to result in the most critical crack location, and hence the numerical values are presented in Table 33. The evaluation presents the results for the Redundancy I and II load combinations and compares the results to the minimum performance criteria discussed in CHAPTER 6.

Table 33 Results obtained for redundancy evaluation

Fracture Locations		**C1, C2, C3, C4, C5, C6**	
Load Combination		**Redundancy I**	**Redundancy II**
Max. Equivalent Plastic Strain in the Main Girder	**Value**	0.004 (C1, C2, C3)	0.009 (C1, C2, C3)
	Location	Very localized yielding Intermediate Diag. "D1-D2" Bottom Flange	Very localized yielding Intermediate diaphragm "D1-D2" flange
Concrete Crushing	**Extent**	No concrete crushing	Localized Crushing (C2)
	Location	-	Only over fracture
Stud Failing	**Value**	No stud failure	No stud failure
	Location	-	-
Max. Vert. Reaction Force	**Value**	2055 kips (LF) 1693 kips (RG)	2057 kips (LF) 1714 kips (RG)
	Location	S2B (C2 - 2HL-93) S3B (C5 - 2HL-93)	S2A (C2 - 3HL-93) S3A (C5 - 3HL-93)
Uplift at Supports	**Value**	No Uplift	
	Location		
Max. Hor. Displacement at Supports	**Value**	3.96 in.	6.10 in.
	Location	S1A (C2 - 2HL-93)	S1A (C2 - 3HL-93)
Max. Vertical Deflection Change	**Value**	Not Applicable	7.49 in. (C2) (LF) 1.60 in. (C5) (RG)

Notes:
- Service bearing capacities for strength are 2011 kips (LF) and 1576 kips (RG)
- Shear capacity of the deck is checked.

For both Redundancy I and Redundancy II, the structure has adequate redundancy after the fracture of an exterior girder using the criteria for the strength and displacement requirements discussed above. The following were observed:

- Insignificant localized plastic strain is not higher than 0.008 in D1-D2's flanges.
- Only localized insignificant crushing occurs in the concrete deck.
- No haunch separation or shear stud failure is observed.
- The maximum vertical deflection change (difference between before fracture and after fracture stages) is 7.5 inches which is lower than L/50 (50.64 inches) and the maximum change in cross-slope is below 5%.

Summary of the redundancy evaluation is shown in Table 34.

Table 34 Summary of Redundancy failure criteria evaluation

Performance Requirement		Most Critical Analysis Case	Result	Acceptable?
Strength Requirements	**Steel Primary Members**	C1 & C2. Redundancy I and II.	No component has strain larger than $5\varepsilon_y$ or 1%. Failure strain was not reached anywhere.	**YES**
	Concrete Crushing	C2. Redundancy II.	Localized insignificant crushing	**YES**
Serviceability Requirements	**Vertical Deflection Change**	C2. (Only Redundancy II DL considered).	Maximum deflection change is 7.5 in, which is lower than L/50 (50.7 in)	**YES**
	Cross-Slope Change	C2. (Only Redundancy II considered).	Maximum additional cross-slope is less than 5%.	**YES**
	Uplift	None.	No uplift.	**YES**

Notes:

- The analysis showed that the structure is capable of resisting an additional 15% of the applied factored live load.
- The horizontal displacement changes at support locations were lower than 6 in.

7.4.3 Summary

Analytical models have been developed to evaluate the structural redundancy of Ramp FNW over NB USH 41 to WB STH 29 (Structure ID B05-660-Unit2) in the state of Wisconsin. The girders are presently classified as Fracture Critical Members. A full depth fracture, including both webs and the top and bottom flange was simulated at six different locations in the exterior girder. The analysis confirms that the bridge satisfies the performance requirements for both Redundancy I and Redundancy II load combinations based on the failure criteria developed in NCHRP 12-87a [5]. Hence, the girders need not be classified as Fracture Critical Members (FCMs).

7.5 B05-660-Unit3 (7 Spans)

7.5.1 Background, geometry, and loading

The structural redundancy of Ramp FNW over NB USH 41 to WB STH 29 (Structure ID B05-660-Unit3) was evaluated for the case where one of the two twin-tub-girders fails due to an assumed sudden full-depth failure. In the analysis, the outside girder was assumed to have fractured. The bridge is not symmetric; two analyses were performed to investigate fracture behavior. The first analysis considered Span 9 to the centerline of Span 11 "LF" (Figure 99) and the second analysis considered the centerline of Span 13 through Span 15 "RG" (Figure 100). As discussed in Section 3.3 only first two and half span needs to be modeled.

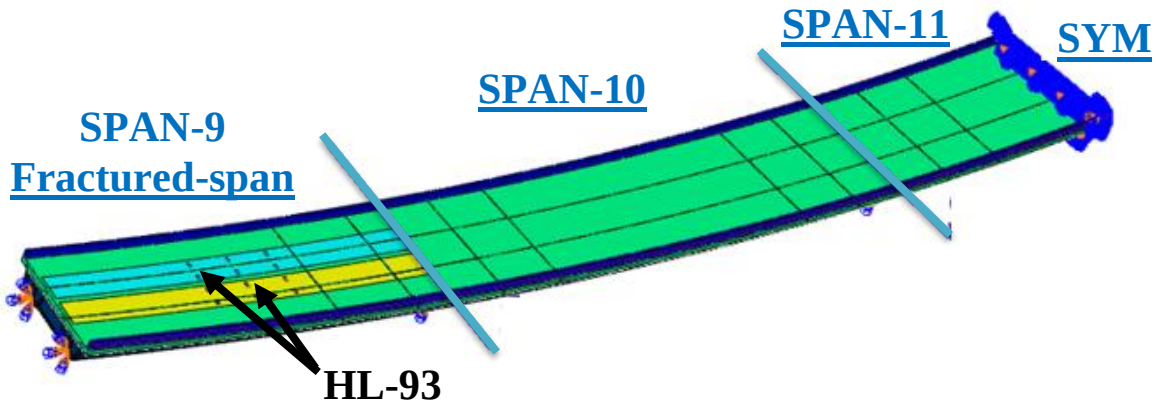

Figure 99 General Isometric View of B05-660-Unit3-LF (Span 9 to Half of Span 11)

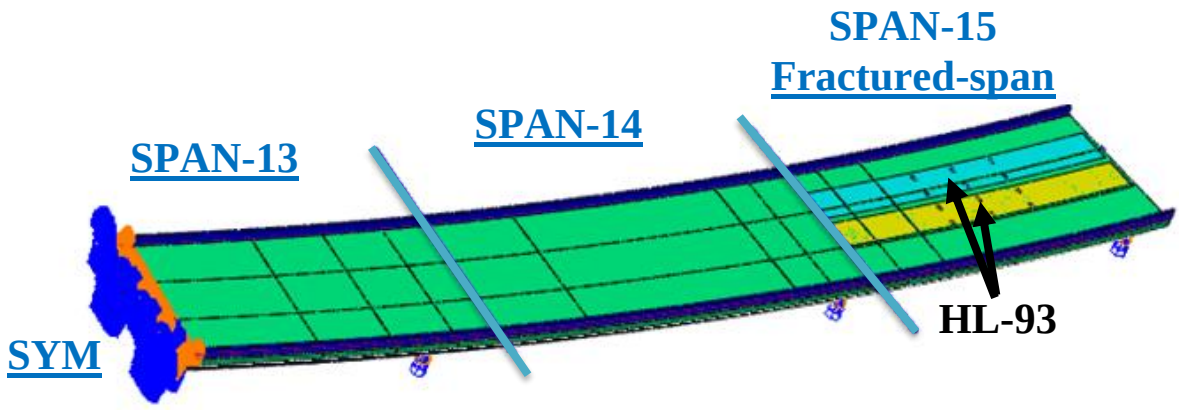

Figure 100 General Isometric View of B05-660-Unit3-RG (Half of Span 13 to Span 15)

Table 35 provides details related to the geometry and material properties associated with the structure.

Table 35 The bridge geometry and material properties

Bridge Details	
Bridge Name	B05-660-Unit3
Radius of Curvature	1358.0 ft. (measured from bridge centerline)
Span Lengths	LF: 128.2 - 175.0 - 87.5 ft. RG: 82.5 - 135.0 - 100.0 ft. Span 11 = 175.0/2 = 87.5 Span 13 = 165.0/2 = 82.5
Girder Details	
Girder Steel	ASTM A709 HPS 50WF
Box Girder Width (from the centers of interior top-flange to the center of exterior top-flange)	12.5 ft.
Girders Spacing (from the centers of the girders' bottom flanges)	25.0 ft.
Top Flange	22.0 in. wide Varies, 1.0 in. to 1.25 in. thick
Web	86 in. high, 0.75 in. thick
Bottom Flange	111 in. wide, 0.875 in. thick
Diaphragms	Span 9: Three full depth diaphragms Span 15: Two full depth diaphragms
Internal Cross Frames	L6x6x9/16 (Top), L6x6x9/16 (Inclined)
Strut Braces	-
Lateral Braces	WT7x34
Longitudinal Stiffeners on Bottom Flanges	WT10.5x24
Deck Details	
Concrete Material Strength	4 ksi (HPC)
Composite Deck	44.896 ft. wide, 11.0 in. thick 4 in. haunch thick
Transverse Reinforcement	No. 6 rebar with 7 in. spacing
Longitudinal Reinforcement	No. 4 & No. 5 rebar with 5. in. spacing
Overhang Reinforcement	-
Shear Studs	8 in. height. Longitudinal spacings are 12-14 in. Three shear studs spaced equally in the transverse direction
Parapet Type	LF (Interior) – HF (Exterior)
Load Details	
Number of Lane	Two lanes traffic
Future Wearing Surface	-
Maximum Dead Load Displacement	LF: L/1420 – RG: L/2500

Five different full-depth fractures were applied separately in each after-fracture performance analysis. Specifically, the tension flange, both webs, and both upper compression flanges were assumed to have failed in one of the girders for each scenario. The locations where the five fractures were assumed to have occurred is shown in both Figure 101 and Figure 102. The locations are as follows:

- Crack 1 (C1) just before 1st (D1) intermediate diaphragm after 1st (S1A) exterior support,
- Crack 2 (C2) between 1st (D1) and 2nd (D2) intermediate diaphragms,
- Crack 3 (C3) just after 2nd (D2),
- Crack 4 (C4) between 4th (D4) and 5th (D5) intermediate diaphragms,
- Crack 5 (C5) just after 5th (D5) intermediate diaphragm before 4th (S4A) exterior support.

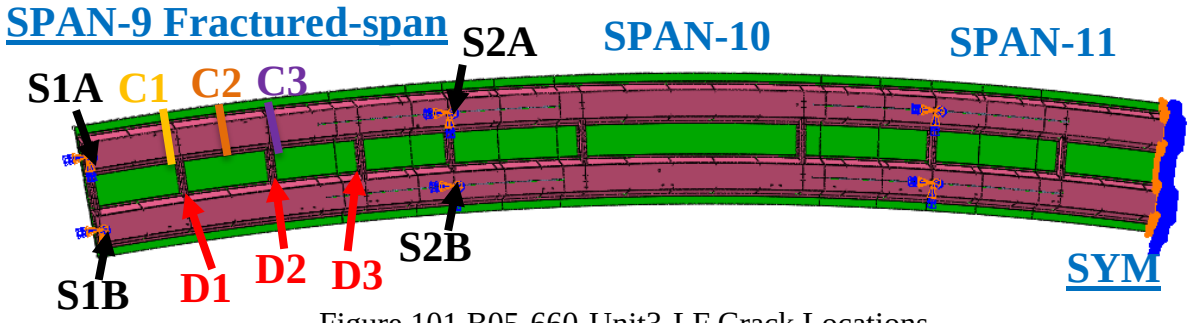

Figure 101 B05-660-Unit3-LF Crack Locations

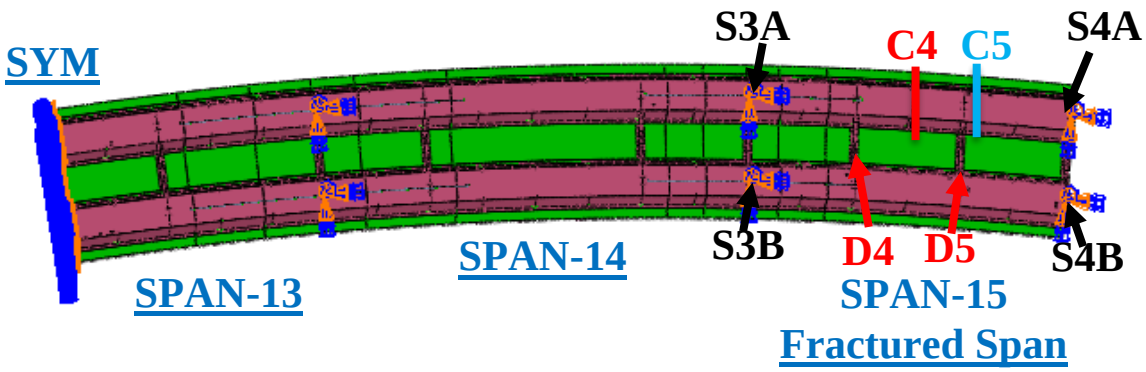

Figure 102 B05-660-Unit3-RG Crack Locations

The Redundancy I and Redundancy II load combinations require different positioning of traffic live loads. For analyses where only a single lane of live load is applied for the Redundancy I load combination, the HL-93 live load was positioned in the center of the exterior design (i.e., striped) traffic lane. In cases where two lanes of live load were considered, the HL-93 live loads were

centered in the both design travel lanes. For the Redundancy II load combination, up to three HL-93 vehicular live loads were placed according to the procedure explained in Section 6.1.3. Full non-linear dynamic analysis was performed to determine the level of dynamic amplification that could be expected upon sudden failure of the tub girder. Based on this analysis, the dynamic amplification factor can conservatively be taken as 0.2 (i.e., 20%). Table 36 demonstrates the amount of total load applied in the Redundancy I (R1) and II (R2) load combinations.

Table 36 Total load applied on the fractured bridge

Type of Loading	**Dead Load (1.05 * DA_R)**	**Future Wearing Surface (1.05 * DA_R)**	**Live Load (0.85 * m * DA_R)**	**Total Load (DA_R)**
R1 **1 HL-93**	5322.00 (LF) 4383.60 (RG) (1.05 * 1.2)	- (1.05 * 1.2)	188.55 (LF) 166.46 (RG) (0.85 * 1.2 * 1.2) 216.28 (LF) (15% More LL) 190.94 (RG) (15% More LL)	5510.55 (LF) 5538.28 (15% More LL) - 4550.06 (RG) 4574.54 (15% More LL)
R1 **2 HL-93**	5322.00 (LF) 4383.60 (RG) (1.05 * 1.2)	- (1.05 * 1.2)	314.26 (LF) 277.44 (RG) (0.85 * 1.0 * 1.2) 369.72 (LF) (15% More LL) 326.40 (RG) (15% More LL)	5636.26 (LF) 5691.72 (15% More LL) - 4661.04 (RG) 4710.00 (15% More LL)

Table 36 continued

Type of Loading	Dead Load (1.05)	Future Wearing Surface (1.05)	Live Load (1.3 * m)	Total Load
R2 1 HL-93	4435.00 (LF) 3653.00 (RG) (1.05)	- (1.05)	257.16 (LF) 229.01 (RG) (1.3 * 1.2) * (15% more per HS-20 impact) 281.89 (LF) (15% More LL) 251.03 (RG) (15% More LL)	4692.16 (LF) 4716.89 (15% More LL) - 3882.01 (RG) 3904.03 (15% More LL)
R2 2 HL-93	4435.00 (LF) 3653.00 (RG) (1.05)	- (1.05)	428.60 (LF) 381.68 (RG) (1.3 * 1.0) * (15% more per HS-20 impact) 478.06 (LF) (15% More LL) 425.72 (RG) (15% More LL)	4863.60 (LF) 4913.06 (15% More LL) - 4034.68 (RG) 4078.72 (15% More LL)
R2 3 HL-93	4435.00 (LF) 3653.00 (RG) (1.05)	- (1.05)	546.47 (LF) 486.64 (RG) (1.3 * 0.85) * (15% more per HS-20 impact) 620.65 (LF) (15% More LL) 552.70 (RG) (15% More LL)	4981.47 (LF) 5055.65 (15% More LL) - 4139.64 (RG) 4205.70 (15% More LL)

7.5.2 Results for B05-660-Unit3

The analysis has shown that Ramp FNW over NB USH 41 to WB STH 29 (Structure ID B05-660-Unit3) possesses considerable reserve strength in the faulted state and that the steel twin-tub-girders do not meet the definition of a fracture critical member when evaluated using the prescribed loading and failure criteria developed in NCHRP 12-87a [5]. Table 37 summarizes the results obtained from the redundancy analysis of the structure in faulted stage. The evaluation presents the results for the Redundancy I and II load combinations and compares the results to the minimum performance criteria discussed in CHAPTER 6.

Table 37 Results obtained for redundancy evaluation

Fracture Locations		**C1, C2, C3, C4, C5**	
Load Combination		**Redundancy I**	**Redundancy II**
Max. Equivalent Plastic Strain in the Main Girder	**Value**	No plastic strain	No plastic strain
	Location	-	-
Concrete Crushing	**Extent**	No concrete crushing	No concrete crushing
	Location	-	-
Stud Failing	**Value**	No stud failure	No stud failure
	Location	-	-
Max. Vert. Reaction Force	**Value**	1291 kips (LF) 952 kips (RG)	1315 kips (LF) 984 kips (RG)
	Location	S2B (C2 - 2HL-93) S3A (C5 - 2HL-93)	S2A (C2 - 3HL-93) S3A (C5 - 3HL-93)
Uplift at Supports	**Value**	No Uplift	
	Location		
Max. Hor. Displacement at Supports	**Value**	0.67 in.	0.97 in.
	Location	S1A (C2 - 2HL-93)	S1A (C2 - 3HL-93)
Max. Vertical Deflection Change	**Value**	Not Applicable	1.46 in. (C2) (LF) 0.84 in. (C5) (RG)

Notes:
- Service bearing capacities for strength are 1369 kips (LF) and 1083 kips (RG)
- Shear capacity of the deck is checked.

For both Redundancy I and Redundancy II, the structure has adequate redundancy after the fracture of an exterior girder using the criteria for the strength and displacement requirements discussed above. The following were observed:

- Plastic strain is not reached in the steel tub girders.
- Crushing does not occur in the concrete deck.
- No haunch separation or shear stud failure is observed.
- The maximum vertical deflection change (difference between before fracture and after fracture stages) is 1.46 inches which is lower than L/50 (30.77 inches) and the maximum change in cross-slope is below 5%.

Summary of the redundancy evaluation is shown in Table 38.

Table 38 Summary of Redundancy failure criteria evaluation

Performance Requirement		Most Critical Analysis Case	Result	Acceptable?
Strength Requirements	**Steel Primary Members**	-	No component has strain larger than $5\varepsilon_y$ or 1%. Failure strain was not reached anywhere.	**YES**
	Concrete Crushing	-	No concrete crushing	**YES**
Serviceability Requirements	**Vertical Deflection Change**	C2. (Only Redundancy II DL considered).	Maximum deflection change is 1.5 in, which is lower than L/50 (30.8 in)	**YES**
	Cross-Slope Change	C2. (Only Redundancy II considered).	Maximum additional cross-slope is less than 5%.	**YES**
	Uplift	None.	No uplift.	**YES**

Notes:

- The analysis showed that the structure is capable of resisting an additional 15% of the applied factored live load.
- The horizontal displacement changes at support locations were lower than 6 in.

7.5.3 Summary

Analytical models have been developed to evaluate the structural redundancy of Ramp FNW over NB USH 41 to WB STH 29 (Structure ID B05-660-Unit3) in the state of Wisconsin. The girders are presently classified as Fracture Critical Members. A full depth fracture, including both webs and the top and bottom flange was simulated at five different locations in the exterior girder. The analysis confirms that the bridge satisfies the performance requirements for both Redundancy I and Redundancy II load combinations based on the failure criteria developed in NCHRP 12-87a [5]. Hence, the girders need not be classified as Fracture Critical Members (FCMs).

7.6 B05-661 (2 Spans)

7.6.1 Background, geometry, and loading

The structural redundancy of Ramp FSW from SB USH 41 to WB STH 29 (Structure ID B05-661 in Figure 103) was evaluated for the case where one of the two twin-tub-girders fails due to an assumed sudden full-depth failure. In the analysis, the outside girder was assumed to have fractured. The bridge is symmetric about the center of the middle pier.

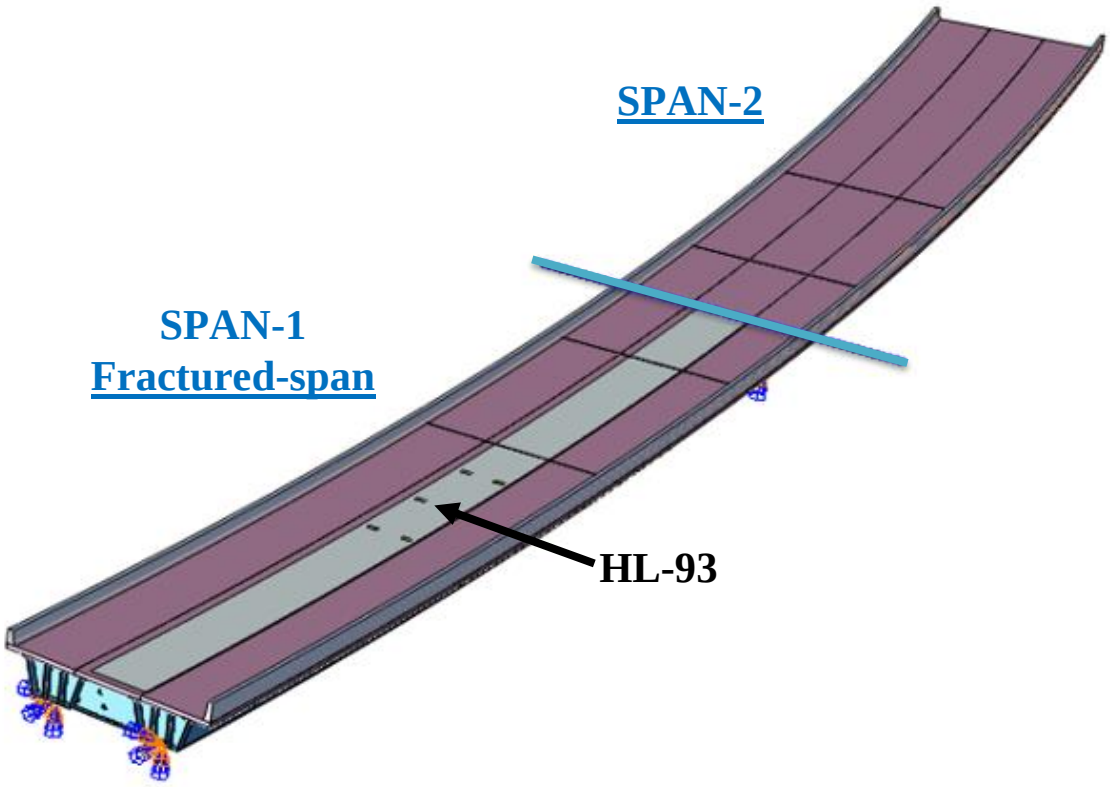

Figure 103 General Isometric View of B05-661

Table 39 provides details related to the geometry and material properties associated with the structure.

Table 39 The bridge geometry and material properties

Bridge Details	
Bridge Name	B05-661
Radius of Curvature	1346.5 ft. (measured from bridge centerline)
Span Lengths	187.0 – 187.0 ft.
Girder Details	
Girder Steel	ASTM A709 HPS 50WF
Box Girder Width (from the centers of interior top-flange to the center of exterior top-flange)	9.5 ft.
Girders Spacing (from the centers of the girders' bottom flanges)	19.0 ft.
Top Flange	Varies, 22 in. to 24 in. wide Varies, 1.0 in. to 2.25 in. thick
Web	72 in. high 0.75 in. thick
Bottom Flange	82 in. wide From 0.875 in. to 1.75 in. thick
Diaphragms	Three full depth diaphragms per span (3 bays)
Internal Cross Frames	L6x6x5/8 (Top), L6x6x5/8 (Inclined)
Strut Braces	-
Lateral Braces	WT7x41
Longitudinal Stiffeners on Bottom Flanges	-
Deck Details	
Concrete Material Strength	4 ksi (HPC)
Composite Deck	35.896 ft. wide 10 in. thick 4 in. thick haunch
Transverse Reinforcement	No. 5 rebar with 7 in. spacing
Longitudinal Reinforcement	No. 4 & No. 6 rebar with 7.5 in. spacing
Overhang Reinforcement	No. 4 rebar with 14 in. spacing
Shear Studs	7 in. height. Longitudinal spacings are 17 to 19 in. Three shear studs spaced equally in the transverse direction
Parapet Type	LF (Interior) – HF (Exterior)
Load Details	
Number of Lane	Single lane traffic
Future Wearing Surface	-
Maximum Dead Load Displacement (before fracture)	L/375

Two different full-depth fractures were applied separately in each after-fracture performance analysis. Specifically, the tension flange, both webs, and both upper compression flanges were assumed to have failed in one of the girders for each scenario. The locations where the two fractures were assumed to have occurred is shown in Figure 104. The locations are as follows:

- Crack 1 (C1) just before 1st (D1) intermediate diaphragm after 1st (S1A) exterior support,
- Crack 2 (C2) between 1st (D1) and 2nd (D2) intermediate diaphragms.

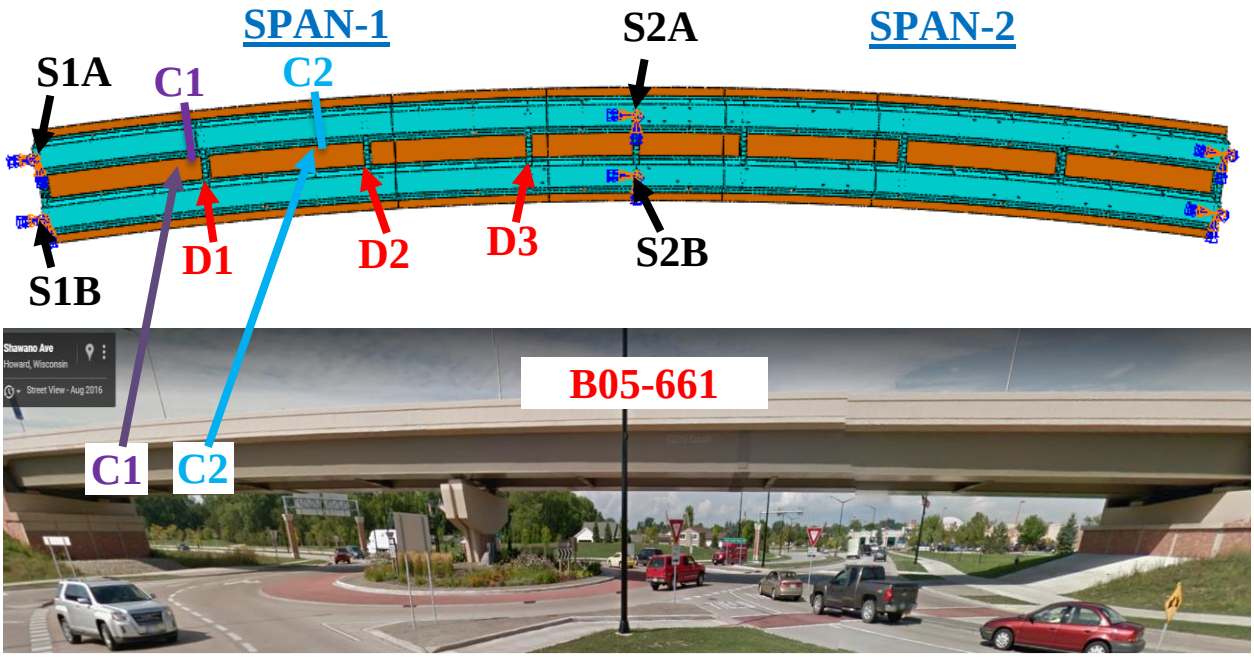

Figure 104 B05-661 Crack Locations

The Redundancy I and Redundancy II load combinations require different positioning of traffic live loads. For analyses where only a single lane of live load is applied for the Redundancy I load combination, the HL-93 live load was positioned in the center of the design (i.e., striped) traffic lane. For the Redundancy II load combination, up to two HL-93 vehicular live loads were placed according to the procedure explained in Section 6.1.3. Full non-linear dynamic analysis was performed to determine the level of dynamic amplification that could be expected upon sudden failure of the tub girder. Based on this analysis, the dynamic amplification factor can conservatively be taken as 0.2 (i.e., 20%). Table 40 demonstrates the amount of total load applied in the Redundancy I (R1) and II (R2) load combinations.

Table 40 Total load applied on the fractured bridge

Type of Loading	Dead Load (1.05 * DA_R)	Future Wearing Surface (1.05 * DA_R)	Live Load (0.85 * m * DA_R)	Total Load (DA_R)
R1 **1 HL-93**	4140.00 (1.05 * 1.2)	- (1.05 * 1.2)	234.62 (0.85 * 1.2 * 1.2) 269.12 (15% More LL)	4374.62 4409.12 (15% More LL)

Type of Loading	Dead Load (1.05)	Future Wearing Surface (1.05)	Live Load (1.3 * m)	Total Load
R2 **1 HL-93**	3450.00 (1.05)	- (1.05)	315.87 (1.3 * 1.2) * (15% more per HS-20 impact) 346.24 (15% More LL)	3765.87 3796.24 (15% More LL)
R2 **2 HL-93**	3450.00 (1.05)	- (1.05)	526.45 (1.3 * 1.0) * (15% more per HS-20 impact) 587.19 (15% More LL)	3976.45 4067.19 (15% More LL)

7.6.2 Results for B05-661

The analysis has shown that Ramp FSW over SB USH 41 to WB STH 29 (Structure ID B05-661) possesses considerable reserve strength in the faulted state and that the steel twin-tub-girders do not meet the definition of a fracture critical member when evaluated using the prescribed loading and failure criteria developed in NCHRP 12-87a [5]. Table 41 summarizes the results obtained from the redundancy analysis of the structure in faulted stage. The fracture case C2 was found to result in the most critical crack location, and hence the numerical values are presented in Table 41. The evaluation presents the results for the Redundancy I and II load combinations and compares the results to the minimum performance criteria discussed in CHAPTER 6.

Table 41 Results obtained for redundancy evaluation

Fracture Locations		**C1, C2**	
Load Combination		**Redundancy I**	**Redundancy II**
Max. Equivalent Plastic Strain in the Main Girder	**Value**	No plastic strain	0.007 (C1)
	Location	-	Very localized yielding Intermediate diaphragm "D1" flange & Intact girder bottom flange next to D1
Concrete Crushing	**Extent**	No concrete crushing	Localized Crushing (C2)
	Location	-	Over fracture zone
Stud Failing	**Value**	No stud failure	Few stud failure (C1)
	Location	-	Over exterior girder - interior top flange - next to fracture
Max. Vert. Reaction Force	**Value**	1369 kips	1410 kips
	Location	S2A (C1 - 1HL-93)	S2A (C2 - 2HL-93)
Uplift at Supports	**Value**	No Uplift	
	Location		
Max. Hor. Displacement at Supports	**Value**	2.74 in.	5.01 in.
	Location	S1A (C2 - 1HL-93)	S1A (C2 - 2HL-93)
Max. Vertical Deflection Change	**Value**	Not Applicable	3.30 in. (C2)

Notes:
- Design bearing capacity for strength is 1467 kips.
- Shear capacity of the deck is checked.

For both Redundancy I and Redundancy II, the structure has adequate redundancy after the fracture of an exterior girder using the criteria for the strength and displacement requirements discussed above. The following were observed:

- Insignificant plastic strain is not higher than 0.007 in Redundancy II analysis.
- Only localized insignificant crushing occurs in the concrete deck in Redundancy II analysis. While failure of a few shear studs was observed in Redundancy II analysis, the number was insignificant and did not result in the bridge becoming unstable.
- The maximum vertical deflection change (difference between before fracture and after fracture stages) is 3.30 inches which is lower than L/50 (44.8 inches) and the maximum change in cross-slope is below 5%.

Summary of the redundancy evaluation is shown in Table 42.

Table 42 Results obtained for redundancy evaluation

Performance Requirement		Most Critical Analysis Case	Result	Acceptable?
Strength Requirements	**Steel Primary Members**	C1. Redundancy II.	No component has strain larger than $5\varepsilon_y$ or 1%. Failure strain was not reached anywhere.	**YES**
	Concrete Crushing	C2. Redundancy II.	Localized concrete crushing	**YES**
Serviceability Requirements	**Vertical Deflection Change**	C2. (Only Redundancy II DL considered).	Maximum deflection change is 3.3 in, which is lower than L/50 (44.8 in)	**YES**
	Cross-Slope Change	C2. (Only Redundancy II considered).	Maximum additional cross-slope is less than 5%.	**YES**
	Uplift	None.	No uplift.	**YES**

Notes:

- The analysis showed that the structure is capable of resisting an additional 15% of the applied factored live load.
- The horizontal displacement changes at support locations were lower than 6 in.

When the C2 crack location and two HL93 traffic loads were applied in the Redundancy II load combination, the maximum nominal longitudinal stresses at the center of the bottom flange of the fractured girder at the pier I equal to 33.5. This is the most critical combination of loading and fracture location. The bottom flange buckling capacity at the same location is equal to 45.2 ksi in the design calculations from Highway Structures Information System (HSI) [38].

7.6.3 Summary

Analytical models have been developed to evaluate the structural redundancy of Ramp FSW over SB USH 41 to WB STH 29 (Structure ID B05-661) in the state of Wisconsin. The girders are presently classified as Fracture Critical Members. A full depth fracture, including both webs and the top and bottom flange was simulated at two different locations in the exterior girder. The analysis confirms that the bridge satisfies the performance requirements for both Redundancy I and Redundancy II load combinations based on the failure criteria developed in NCHRP 12-87a [5]. Hence, the girders need not be classified as Fracture Critical Members (FCMs).

7.7 B05-678-Unit3 (4 Spans)

7.7.1 Background, geometry, and loading

The structural redundancy of Ramp IHB over IH 43 NB to USH 41 SB (Structure ID B05-678-Unit3) was evaluated for the case where one of the two twin-tub-girders fails due to an assumed sudden full-depth failure. In the analysis, the outside girder was assumed to have fractured. The bridge is not symmetric; therefore, two analyses were performed to investigate fracture behavior. The first analysis considered Span 11 to the centerline of Span 13 "LF" (Figure 105) and the second analysis considered the centerline of Span 12 through Span 14 "RG" (Figure 106). As discussed in Section 3.3 only first two and half span needs to be modeled.

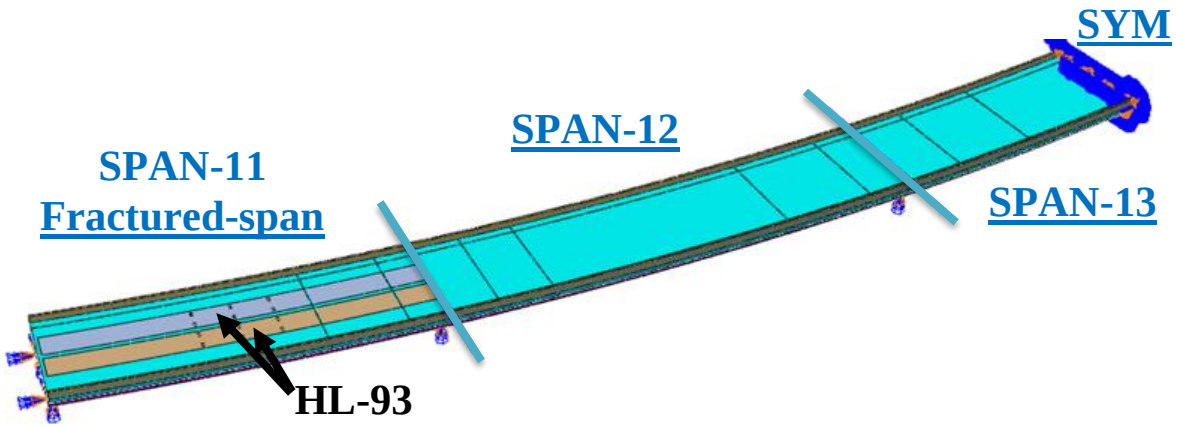

Figure 105 General Isometric View of B05-678-Unit3-LF (Span 11 to Half of Span 13)

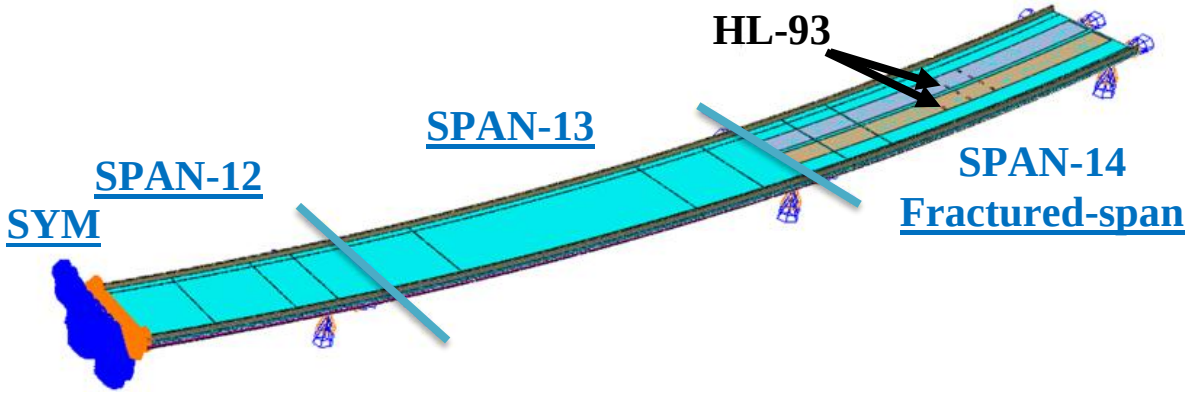

Figure 106 General Isometric View of B05-678-Unit3-RG (Half of Span 12 to Span 14)

Table 43 provides details related to the geometry and material properties associated with the structure.

Table 43 The bridge geometry and material properties

Bridge Details	
Bridge Name	B05-678-Unit3
Radius of Curvature	1409.0 ft. (measured from bridge centerline)
Span Lengths	LF: 137.2 - 192.0 - 114.6 ft. RG: 96.0 - 229.3 - 180.3 ft. Span 12 = 192.0/2 = 96.0 Span 13 = 229.3/2 = 114.6
Girder Details	
Girder Steel	ASTM A709 HPS 50WF
Box Girder Width (from the centers of interior top-flange to the center of exterior top-flange)	12.5 ft.
Girders Spacing (from the centers of the girders' bottom flanges)	25.0 ft.
Top Flange	Varies, 22.0 in. to 24.0 in. wide Varies, 1.0 in. to 2.5 in. thick
Web	86 in. high Varies, 0.75 in. to 0.875 in. thick
Bottom Flange	111 in. wide Varies, 0.875 in. to 1.25 in. thick
Diaphragms	Three full depth diaphragms
Internal Cross Frames	L6x6x5/8 (Top), L6x6x5/8 (Inclined)
Strut Braces	-
Lateral Braces	WT7x34
Longitudinal Stiffeners on Bottom Flanges	WT10.5x25
Deck Details	
Concrete Material Strength	4 ksi (HPC)
Composite Deck	44.896 ft. wide, 10.0 in. thick 4 in. haunch thick
Transverse Reinforcement	No. 6 rebar with 7 in. spacing
Longitudinal Reinforcement	No. 4 & No. 6 rebar with 6. in. spacing
Overhang Reinforcement	-
Shear Studs	7 in. height. Longitudinal spacing is 13 in. Three shear studs spaced equally in the transverse direction
Parapet Type	32SS (Interior) – 42SS (Exterior)
Load Details	
Number of Lane	Two lanes traffic
Future Wearing Surface	3 lb/ft^2
Maximum Dead Load Displacement	LF: L/1140 – RG: L/545

Five different full-depth fractures were applied separately in each after-fracture performance analysis. Specifically, the tension flange, both webs, and both upper compression flanges were assumed to have failed in one of the girders for each scenario. The locations where the five fractures were assumed to have occurred is shown in both Figure 107 and Figure 108. The locations are as follows:

- Crack 1 (C1) just before 1st (D1) intermediate diaphragm after 1st (S1A) exterior support,
- Crack 2 (C2) just before 2nd (D2) intermediate diaphragm,
- Crack 3 (C3) just after 5th (D5),
- Crack 4 (C4) between 5th (D5) and 6th (D6) intermediate diaphragms,
- Crack 5 (C5) just after 6th (D6) intermediate diaphragm before 4th (S4A) exterior support.

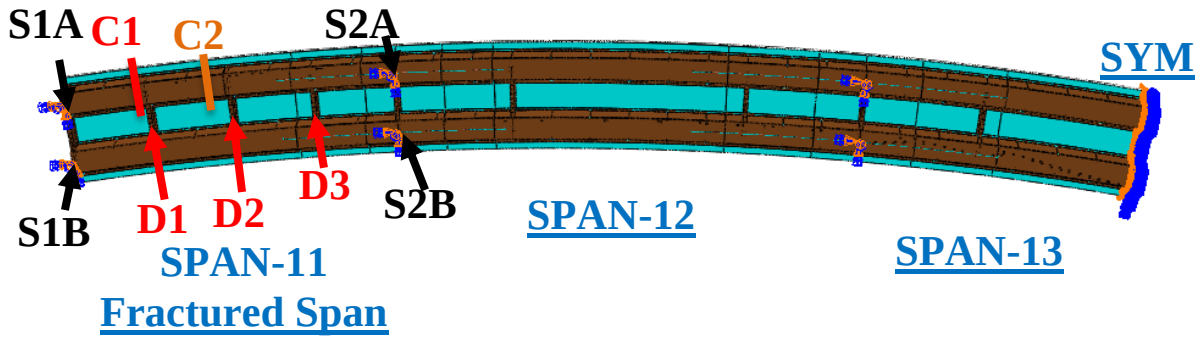

Figure 107 B05-678-Unit3-LF Crack Locations

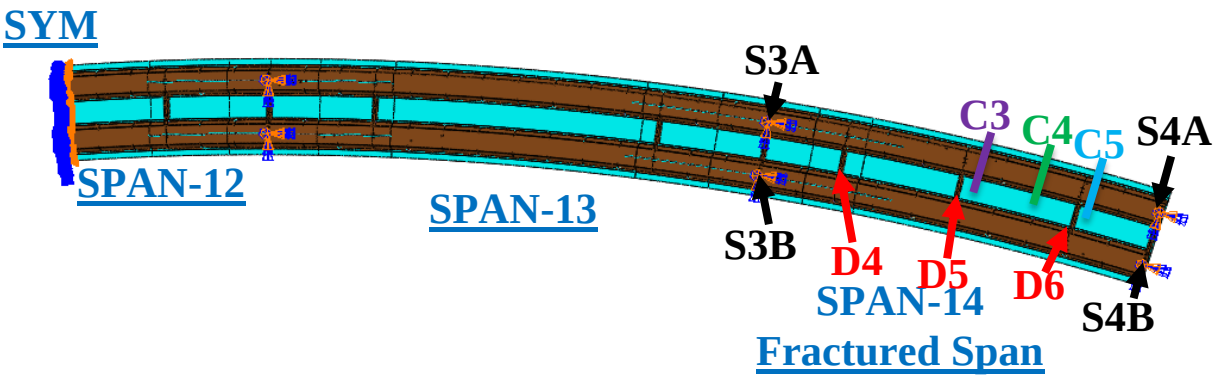

Figure 108 B05-678-Unit3-RG Crack Locations

The Redundancy I and Redundancy II load combinations require different positioning of traffic live loads. For analyses where only a single lane of live load is applied for the Redundancy I load combination, the HL-93 live load was positioned in the center of the exterior design (i.e., striped) traffic lane. In cases where two lanes of live load were considered, the HL-93 live loads were centered in the both design travel lanes. For the Redundancy II load combination, up to three HL-93 vehicular live loads were placed according to the procedure explained in Section 6.1.3. Full non-linear dynamic analysis was performed to determine the level of dynamic amplification that could be expected upon sudden failure of the tub girder. Based on this analysis, the dynamic amplification factor can conservatively be taken as 0.2 (i.e., 20%). Table 44 demonstrates the amount of total load applied in the Redundancy I (R1) and II (R2) load combinations.

Table 44 Total load applied on the fractured bridge

Type of Loading	**Dead Load (1.05 * DA_R)**	**Future Wearing Surface (1.05 * DA_R)**	**Live Load (0.85 * m * DA_R)**	**Total Load (DA_R)**
R1 1 HL-93	5844.00 (LF) 6561.60 (RG) (1.05 * 1.2)	70.43 (LF) 80.27 (RG) (1.05 * 1.2)	195.45 (LF) 229.37 (RG) (0.85 * 1.2 * 1.2) 224.19 (LF) (15% More LL) 263.10 (RG) (15% More LL)	6109.87 (LF) 6138.62 (15% More LL) - 6871.24 (RG) 6904.97 (15% More LL)
R1 2 HL-93	5844.00 (LF) 6561.60 (RG) (1.05 * 1.2)	70.43 (LF) 80.27 (RG) (1.05 * 1.2)	325.75 (LF) 382.28 (RG) (0.85 * 1.0 * 1.2) 383.23 (LF) (15% More LL) 449.74 (RG) (15% More LL)	6240.17 (LF) 6297.66 (15% More LL) - 7024.15 (RG) 7091.61 (15% More LL)

Table 44 continued

Type of Loading	Dead Load (1.05)	Future Wearing Surface (1.05)	Live Load (1.3 * m)	Total Load
R2 1 HL-93	4870.00 (LF) 5468.00 (RG) (1.05)	58.69 (LF) 66.89 (RG) (1.05)	265.95 (LF) 309.18 (RG) (1.3 * 1.2) * (15% more per HS-20 impact) 291.52 (LF) (15% More LL) 338.91 (RG) (15% More LL)	5194.64 (LF) 5220.21 (15% More LL) - 5844.07 (RG) 5873.80 (15% More LL)
R2 2 HL-93	4870.00 (LF) 5468.00 (RG) (1.05)	58.69 (LF) 66.89 (RG) (1.05)	443.25 (LF) 515.30 (RG) (1.3 * 1.0) * (15% more per HS-20 impact) 494.39 (LF) (15% More LL) 574.76 (RG) (15% More LL)	5371.94 (LF) 5423.08 (15% More LL) - 6050.19 (RG) 6109.65 (15% More LL)
R2 3 HL-93	4870.00 (LF) 5468.00 (RG) (1.05)	58.69 (LF) 66.89 (RG) (1.05)	565.14 (LF) 657.01 (RG) (1.3 * 0.85) * (15% more per HS-20 impact) 641.86 (LF) (15% More LL) 746.19 (RG) (15% More LL)	5493.83 (LF) 5570.55 (15% More LL) - 6191.90 (RG) 6281.08 (15% More LL)

7.7.2 Results for B05-678-Unit3

The analysis has shown that Ramp IHB over IH 43 NB to USH 41 SB (Structure ID B05-678-Unit3) possesses considerable reserve strength in the faulted state and that the steel twin-tub-girders do not meet the definition of a fracture critical member when evaluated using the prescribed loading and failure criteria developed in NCHRP 12-87a [5]. Table 45 summarizes the results obtained from the redundancy analysis of the structure in faulted stage. The fracture case C4 was found to result in the most critical crack location, and hence the numerical values are presented in

Table 45. The evaluation presents the results for the Redundancy I and II load combinations and compares the results to the minimum performance criteria discussed in CHAPTER 6.

Table 45 Results obtained for redundancy evaluation

Fracture Locations		**C1, C2, C3, C4, C5**	
Load Combination		**Redundancy I**	**Redundancy II**
Max. Equivalent Plastic Strain in the Main Girder	**Value**	No plastic strain	No plastic strain
	Location	-	-
Concrete Crushing	**Extent**	No concrete crushing	No concrete crushing
	Location	-	-
Stud Failing	**Value**	No stud failure	No stud failure
	Location	-	-
Max. Vert. Reaction Force	**Value**	1300 kips (LF) 1692 kips (RG)	1294 kips (LF) 1710 kips (RG)
	Location	S2B (C2 - 2HL-93) S3B (C4 - 2HL-93)	S2A (C2 - 3HL-93) S3A (C4 - 3HL-93)
Uplift at Supports	**Value**	No Uplift	
	Location		
Max. Hor. Displacement at Supports	**Value**	2.30 in.	4.58 in.
	Location	S4A (C3 - 2HL-93)	S4A (C3 - 3HL-93)
Max. Vertical Deflection Change	**Value**	Not Applicable	1.01 in. (C2) (LF) 4.48 in. (C4) (RG)

Notes:
- Strength bearing capacities for strength are 1657 kips (LF) and 1762 kips (RG)
- Shear capacity of the deck is checked.

For both Redundancy I and Redundancy II, the structure has adequate redundancy after the fracture of an exterior girder using the criteria for the strength and displacement requirements discussed above. The following were observed:

- Plastic strain is not reached in the steel tub girders.
- Crushing does not occur in the concrete deck.
- No haunch separation or shear stud failure is observed.
- The maximum vertical deflection change (difference between before fracture and after fracture stages) is 4.48 inches which is lower than L/50 (43.27 inches) and the maximum change in cross-slope is below 5%.

Summary of the redundancy evaluation is shown in Table 46.

Table 46 Summary of Redundancy failure criteria evaluation

Performance Requirement		Most Critical Analysis Case	Result	Acceptable?
Strength Requirements	**Steel Primary Members**	-	No component has strain larger than $5\varepsilon_y$ or 1%. Failure strain was not reached anywhere.	**YES**
	Concrete Crushing	-	No concrete crushing	**YES**
Serviceability Requirements	**Vertical Deflection Change**	C3. (Only Redundancy II DL considered).	Maximum deflection change is 4.5 in, which is lower than L/50 (43.3 in)	**YES**
	Cross-Slope Change	C3. (Only Redundancy II considered).	Maximum additional cross-slope is less than 5%.	**YES**
	Uplift	None.	No uplift.	**YES**

Notes:
- The analysis showed that the structure is capable of resisting an additional 15% of the applied factored live load.
- The horizontal displacement changes at support locations were lower than 6 in.

For LF, when the C2 crack location and three HL93 traffic loads were applied in the Redundancy II load combination, the maximum nominal longitudinal stresses at the bottom flange of the fractured girder at the pier is equal to 22.5. This is the most critical combination of loading and fracture location. This stress is lower than the bottom flange buckling capacity at the same location which are equal to 41.9 ksi in the design calculations from Highway Structures Information System (HSI) [39].

For RG, when the C4 crack location and three HL93 traffic loads were applied in the Redundancy II load combination, the maximum nominal longitudinal stresses at the bottom flange of the fractured girder at the pier and at the bottom flange section change closest to the pier are equal to 34.9 and 34.2 ksi respectively. This is the most critical combination of loading and fracture location. This stress is lower than the bottom flange buckling capacity at the same locations which

are equal to 45.1 and 41.9 ksi in the design calculations from Highway Structures Information System (HSI) [39].

7.7.3 Summary

Analytical models have been developed to evaluate the structural redundancy of Ramp IHB over IH 43 NB to USH 41 SB (Structure ID B05-678-Unit3) in the state of Wisconsin. The girders are presently classified as Fracture Critical Members. A full depth fracture, including both webs and the top and bottom flange was simulated at five different locations in the exterior girder. The analysis confirms that the bridge satisfies the performance requirements for both Redundancy I and Redundancy II load combinations based on the failure criteria developed in NCHRP 12-87a [5]. Hence, the girders need not be classified as Fracture Critical Members (FCMs).

7.8 B05-678-Unit4 (4 Spans)

7.8.1 Background, geometry, and loading

The structural redundancy of Ramp IHB over IH 43 NB to USH 41 SB (Structure ID B05-678-Unit4 in Figure 109 and Figure 110) was evaluated for the case where one of the two twin-tub-girders fails due to an assumed sudden full-depth failure. In the analysis, the outside girder was assumed to have fractured. The bridge is symmetric about the center of the middle pier. As discussed in Section 3.3 only first two and half span needs to be modeled as shown in Figure 109.

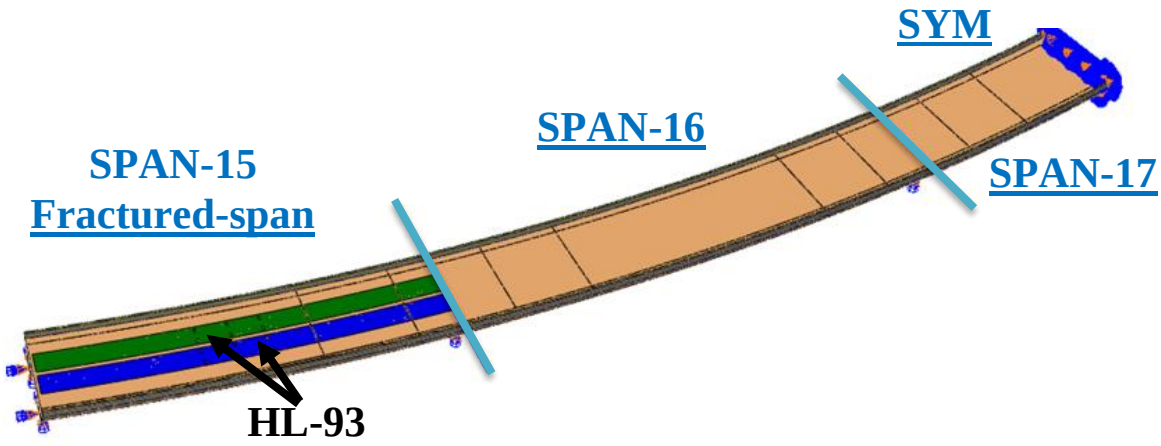

Figure 109 General Isometric View of B05-678-Unit4-LF (Span 15 to Half of Span 17)

Figure 110 Google Map View of B05-678-Unit4-LF

Table 47 provides details related to the geometry and material properties associated with the structure.

Table 47 The bridge geometry and material properties

Bridge Details	
Bridge Name	B05-678-Unit4
Radius of Curvature	1409.0 ft. (measured from bridge centerline)
Span Lengths	LF: 176.0 - 241.6 - 120.8 ft. Span 16 = 241.6/2 = 120.8 Span 17 = 241.6/2 = 120.8
Girder Details	
Girder Steel	ASTM A709 HPS 50WF
Box Girder Width (from the centers of interior top-flange to the center of exterior top-flange)	12.5 ft.
Girders Spacing (from the centers of the girders' bottom flanges)	25.0 ft.
Top Flange	Varies, 22.0 in. to 26.0 in. wide Varies, 1.0 in. to 2.75 in. thick
Web	86 in. high Varies, 0.75 in. to 0.875 in. thick
Bottom Flange	111 in. wide Varies, 0.875 in. to 1.625 in. thick
Diaphragms	Three full depth diaphragms
Internal Cross Frames	L6x6x5/8 (Top), L6x6x5/8 (Inclined)
Strut Braces	-
Lateral Braces	WT7x34
Longitudinal Stiffeners on Bottom Flanges	WT10.5x25
Deck Details	
Concrete Material Strength	4 ksi (HPC)
Composite Deck	44.896 ft. wide, 10.0 in. thick 4 in. haunch thick
Transverse Reinforcement	No. 6 rebar with 7 in. spacing
Longitudinal Reinforcement	No. 4 & No. 6 rebar with 6. in. spacing
Overhang Reinforcement	-
Shear Studs	7 in. height. Longitudinal spacing is 12 in. Three shear studs spaced equally in the transverse direction
Parapet Type	32SS (Interior) – 42SS (Exterior)
Load Details	
Number of Lane	Two lanes traffic
Future Wearing Surface	3 lb/ft2
Maximum Dead Load Displacement	L/610

Three different full-depth fractures were applied separately in each after-fracture performance analysis. Specifically, the tension flange, both webs, and both upper compression flanges were assumed to have failed in one of the girders for each scenario. The locations where the three fractures were assumed to have occurred is shown in Figure 111. The locations are as follows:

- Crack 1 (C1) just before 1st (D1) intermediate diaphragm after 1st (S1A) exterior support,
- Crack 2 (C2) between 1st (D1) and 2nd (D2) intermediate diaphragms,
- Crack 3 (C3) just before 2nd (D2) intermediate diaphragm.

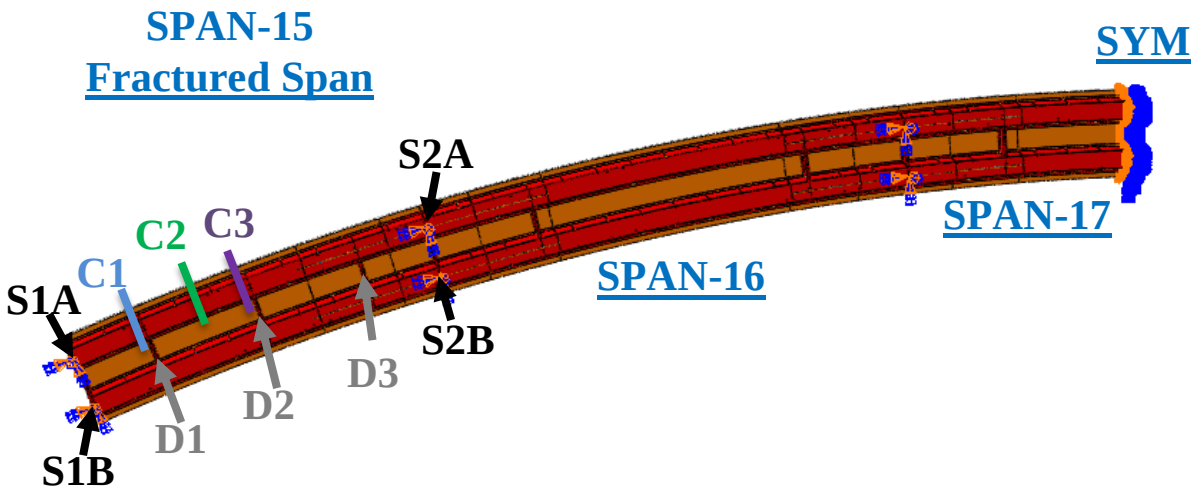

Figure 111 B05-678-Unit4 Crack Locations

The Redundancy I and Redundancy II load combinations require different positioning of traffic live loads. For analysis where only a single lane of live load is applied for the Redundancy I load combination, the HL-93 live load was positioned in the center of the exterior design (i.e., striped) traffic lane. In cases where two lanes of live load were considered, the HL-93 live loads were centered in the both design travel lanes. For the Redundancy II load combination, up to three HL-93 vehicular live loads were placed according to procedure explained in Section 6.1.3. Full non-linear dynamic analysis was performed to determine the level of dynamic amplification that could be expected upon sudden failure of the tub girder. Based on this analysis, the dynamic amplification factor can conservative taken as 0.2 (i.e., 20%). Table 48 demonstrates the amount of total load applied in the Redundancy I (R1) and II (R2) load combinations.

Table 48 Total load applied on the fractured bridge

Type of Loading	Dead Load (1.05 * DA_R)	Future Wearing Surface (1.05 * DA_R)	Live Load (0.85 * m * DA_R)	Total Load (DA_R)
R1 1 HL-93	7033.20 (1.05 * 1.2)	85.48 (1.05 * 1.2)	226.00 (0.85 * 1.2 * 1.2) 259.23 (15% More LL)	7344.68 7377.91 (15% More LL)
R1 2 HL-93	7033.20 (1.05 * 1.2)	85.48 (1.05 * 1.2)	376.67 (0.85 * 1.0 * 1.2) 443.14 (15% More LL)	7495.34 7561.81 (15% More LL)

Type of Loading	Dead Load (1.05)	Future Wearing Surface (1.05)	Live Load (1.3 * m)	Total Load
R2 1 HL-93	5861.00 (1.05)	71.23 (1.05)	304.89 (1.3 * 1.2) * (15% more per HS-20 impact) 334.20 (15% More LL)	6237.12 6266.43 (15% More LL)
R2 2 HL-93	5861.00 (1.05)	71.23 (1.05)	508.14 (1.3 * 1.0) * (15% more per HS-20 impact) 566.78 (15% More LL)	6440.37 6499.01 (15% More LL)
R2 3 HL-93	5861.00 (1.05)	71.23 (1.05)	647.88 (1.3 * 0.85) * (15% more per HS-20 impact) 735.83 (15% More LL)	6580.11 6668.06 (15% More LL)

7.8.2 Results for B05-678-Unit4

The analysis has shown that Ramp IHB over IH 43 NB to USH 41 SB (Structure ID B05-678-Unit4) possesses considerable reserve strength in the faulted state and that the steel twin-tub-girders do not meet the definition of a fracture critical member when evaluated using the prescribed loading and failure criteria developed in NCHRP 12-87a [5]. Table 49 summarizes the results obtained from the redundancy analysis of the structure in faulted stage. The fracture case C2 was found to result in the most critical crack location, and hence the numerical values are presented in Table 49. The evaluation presents the results for the Redundancy I and II load combinations and compares the results to the minimum performance criteria discussed in CHAPTER 6.

Table 49 Results obtained for redundancy evaluation

Fracture Locations		**C1, C2, C3**	
Load Combination		**Redundancy I**	**Redundancy II**
Max. Equivalent Plastic Strain in the Main Girder	**Value**	No plastic strain	No plastic strain
	Location	-	-
Concrete Crushing	**Extent**	No concrete crushing	No concrete crushing
	Location	-	-
Stud Failing	**Value**	No stud failure	No stud failure
	Location	-	-
Max. Vert. Reaction Force	**Value**	1693 kips	1608 kips
	Location	S2B (C2 - 2HL-93)	S2A (C2 - 3HL-93)
Uplift at Supports	**Value**	No Uplift	
	Location		
Max. Hor. Displacement at Supports	**Value**	2.19 in.	4.03 in.
	Location	S1A (C2 - 2HL-93)	S1A (C2 - 3HL-93)
Max. Vertical Deflection Change	**Value**	Not Applicable	3.22 in. (C2)

Notes:
- Strength bearing capacities for strength is 1779 kips.
- Shear capacity of the deck is checked.

For both Redundancy I and Redundancy II, the structure has adequate redundancy after the fracture of an exterior girder using the criteria for the strength and displacement requirements discussed above. The following were observed:

- Plastic strain is not reached in the steel tub girders.
- Crushing does not occur in the concrete deck.
- No haunch separation or shear stud failure is observed.
- The maximum vertical deflection change (difference between before fracture and after fracture stages) is 3.22 inches which is lower than L/50 (57.98 inches) and the maximum change in cross-slope is below 5%.

Summary of the redundancy evaluation is shown in Table 50.

Table 50 Summary of Redundancy failure criteria evaluation

Performance Requirement		Most Critical Analysis Case	Result	Acceptable?
Strength Requirements	**Steel Primary Members**	-	No component has strain larger than $5\varepsilon_y$ or 1%. Failure strain was not reached anywhere.	**YES**
	Concrete Crushing	-	No concrete crushing	**YES**
Serviceability Requirements	**Vertical Deflection Change**	C2. (Only Redundancy II DL considered).	Maximum deflection change is 3.2 in, which is lower than L/50 (58.0 in)	**YES**
	Cross-Slope Change	C2. (Only Redundancy II considered).	Maximum additional cross-slope is less than 5%.	**YES**
	Uplift	None.	No uplift.	**YES**

Notes:

- The analysis showed that the structure is capable of resisting an additional 15% of the applied factored live load.
- The horizontal displacement changes at support locations were lower than 6 in.

When the C2 crack location and three HL93 traffic loads were applied in the Redundancy II load combination, the maximum nominal longitudinal stresses at the bottom flange of the fractured girder at the pier and at the bottom flange section change closest to the pier are equal to 31.8 and 36.9 ksi, respectively. This is the most critical combination of loading and fracture location. This stress is lower than the bottom flange buckling capacity at the same locations which are equal to 47.0 and 41.9 ksi in the design calculations from Highway Structures Information System (HSI) [39].

7.8.3 Summary

Analytical models have been developed to evaluate the structural redundancy of Ramp IHB over IH 43 NB to USH 41 SB (Structure ID B05-678-Unit4) in the state of Wisconsin. A full depth fracture, including both webs and the top and bottom flange was simulated at three different locations in the exterior girder. The analysis confirms that the bridge satisfies the performance requirements for both Redundancy I and Redundancy II load combinations based on the failure criteria developed in NCHRP 12-87a [5].

7.9 B05-678-Unit5 (5 Spans)

7.9.1 Background, geometry, and loading

The structural redundancy of Ramp IHB over IH 43 NB to USH 41 SB (Structure ID B05-678-Unit5 in Figure 112 and Figure 113) was evaluated for the case where one of the two twin-tub-girders fails due to an assumed sudden full-depth failure. In the analysis, the outside girder was assumed to have fractured. The bridge is symmetric about the center of its midspan. As discussed in Section 3.3 only first two and half span needs to be modeled as shown in Figure 112.

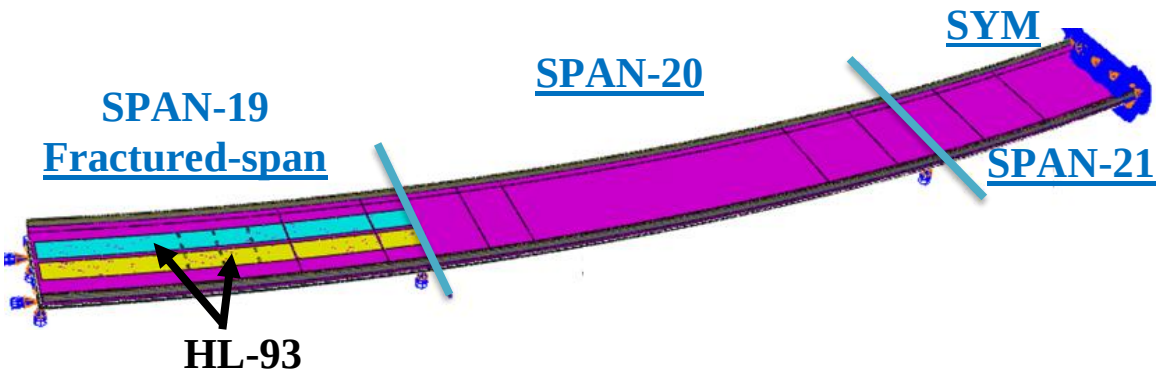

Figure 112 General Isometric View of B05-678-Unit5 (Span 19 to Half of Span 21)

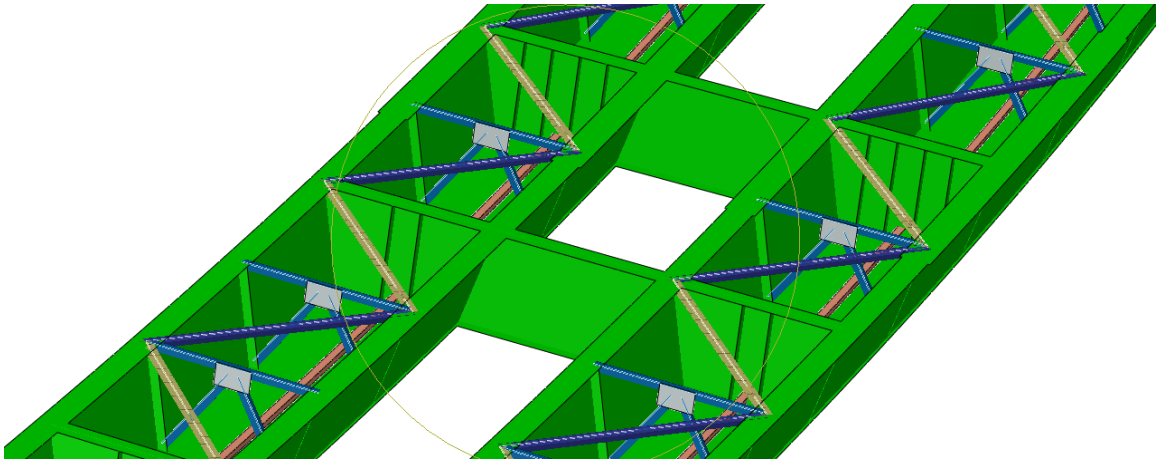

Figure 113 Interior View of B05-678-Unit5

Table 51 provides details related to the geometry and material properties associated with the structure.

Table 51 The bridge geometry and material properties

Bridge Details	
Bridge Name	B05-678-Unit5
Radius of Curvature	1409.0 ft. (measured from bridge centerline)
Span Lengths	LF: 151.2 - 247.0 - 123.5 ft. Span 21 = 247.0/2 = 123.5
Girder Details	
Girder Steel	ASTM A709 HPS 50WF
Box Girder Width (from the centers of interior top-flange to the center of exterior top-flange)	12.5 ft.
Girders Spacing (from the centers of the girders' bottom flanges)	25.0 ft.
Top Flange	Varies, 22.0 in. to 28.0 in. wide Varies, 1.0 in. to 2.75 in. thick
Web	86 in. high Varies, 0.75 in. to 0.875 in. thick
Bottom Flange	111 in. wide Varies, 0.875 in. to 1.625 in. thick
Diaphragms	Three full depth diaphragms
Internal Cross Frames	L6x6x5/8 (Top), L6x6x5/8 (Inclined)
Strut Braces	-
Lateral Braces	WT7x34
Longitudinal Stiffeners on Bottom Flanges	WT10.5x25
Deck Details	
Concrete Material Strength	4 ksi (HPC)
Composite Deck	44.896 ft. wide, 10.0 in. thick 4 in. haunch thick
Transverse Reinforcement	No. 6 rebar with 7 in. spacing
Longitudinal Reinforcement	No. 4 & No. 6 rebar with 6. in. spacing
Overhang Reinforcement	-
Shear Studs	7 in. height. Longitudinal spacing is 12 in. Three shear studs spaced equally in the transverse direction
Parapet Type	32SS (Interior) – 42SS (Exterior)
Load Details	
Number of Lane	Two lanes traffic
Future Wearing Surface	3 lb/ft2
Maximum Dead Load Displacement (before fracture)	L/2160

Three different full-depth fractures were applied separately in each after-fracture performance analysis. Specifically, the tension flange, both webs, and both upper compression flanges were assumed to have failed in one of the girders for each scenario. The locations where the three fractures were assumed to have occurred is shown in Figure 114. The locations are as follows:

- Crack 1 (C1) just before 1st (D1) intermediate diaphragm after 1st (S1A) exterior support,
- Crack 2 (C2) between 1st (D1) and 2nd (D2) intermediate diaphragms,
- Crack 3 (C2) just before 2nd (D2) intermediate diaphragm.

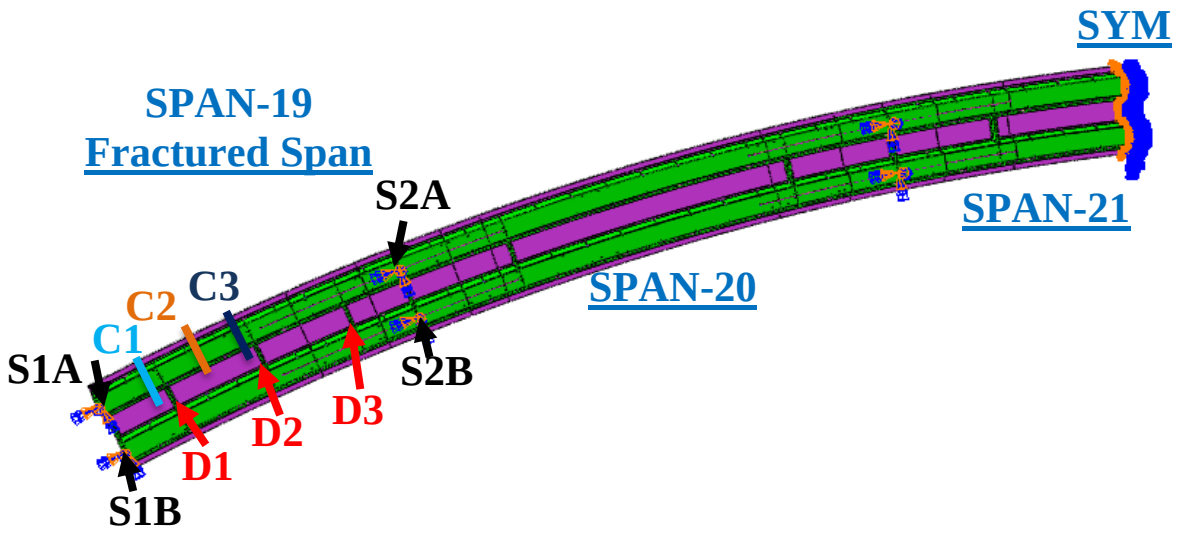

Figure 114 B05-678-Unit5 Crack Locations

The Redundancy I and Redundancy II load combinations require different positioning of traffic live loads. For analyses where only a single lane of live load is applied for the Redundancy I load combination, the HL-93 live load was positioned in the center of the exterior design (i.e., striped) traffic lane. In cases where two lanes of live load were considered, the HL-93 live loads were centered in the both design travel lanes. For the Redundancy II load combination, up to three HL-93 vehicular live loads were placed according to the procedure explained in Section 6.1.3. Full non-linear dynamic analysis was performed to determine the level of dynamic amplification that could be expected upon sudden failure of the tub girder. Based on this analysis, the dynamic amplification factor can conservatively be taken as 0.2 (i.e., 20%). Table 52 demonstrates the amount of total load applied in the Redundancy I (R1) and II (R2) load combinations.

Table 52 Total load applied on the fractured bridge

Type of Loading	Dead Load (1.05 * DA_R)	Future Wearing Surface (1.05 * DA_R)	Live Load (0.85 * m * DA_R)	Total Load (DA_R)
R1 1 HL-93	6841.20 (1.05 * 1.2)	82.83 (1.05 * 1.2)	206.42 (0.85 * 1.2 * 1.2) 236.77 (15% More LL)	7130.44 7160.80 (15% More LL)
R1 2 HL-93	6841.20 (1.05 * 1.2)	82.83 (1.05 * 1.2)	344.03 (0.85 * 1.0 * 1.2) 404.74 (15% More LL)	7268.05 7328.76 (15% More LL)

Type of Loading	Dead Load (1.05)	Future Wearing Surface (1.05)	Live Load (1.3 * m)	Total Load
R2 1 HL-93	5701.00 (1.05)	69.02 (1.05)	279.93 (1.3 * 1.2) * (15% more per HS-20 impact) 306.84 (15% More LL)	6049.95 6076.86 (15% More LL)
R2 2 HL-93	5701.00 (1.05)	69.02 (1.05)	466.54 (1.3 * 1.0) * (15% more per HS-20 impact) 520.39 (15% More LL)	6236.56 6290.40 (15% More LL)
R2 3 HL-93	5701.00 (1.05)	69.02 (1.05)	594.84 (1.3 * 0.85) * (15% more per HS-20 impact) 675.59 (15% More LL)	6364.86 6445.61 (15% More LL)

7.9.2 Results for B05-678-Unit5

The analysis has shown that Ramp IHB over IH 43 NB to USH 41 SB (Structure ID B05-678-Unit5) possesses considerable reserve strength in the faulted state and that the steel twin-tub-girders do not meet the definition of a fracture critical member when evaluated using the prescribed loading and failure criteria developed in NCHRP 12-87a [5]. Table 53 summarizes the results obtained from the redundancy analysis of the structure in faulted stage. The fracture case C2 was found to result in the most critical crack location, and hence the numerical values are presented in Table 53. The evaluation presents the results for the Redundancy I and II load combinations and compares the results to the minimum performance criteria discussed in CHAPTER 6.

Table 53 Results obtained for redundancy evaluation

Fracture Locations		**C1, C2, C3**	
Load Combination		**Redundancy I**	**Redundancy II**
Max. Equivalent Plastic Strain in the Main Girder	**Value**	No plastic strain	No plastic strain
	Location	-	-
Concrete Crushing	**Extent**	No concrete crushing	No concrete crushing
	Location	-	-
Stud Failing	**Value**	No stud failure	No stud failure
	Location	-	-
Max. Vert. Reaction Force	**Value**	1633 kips	1510 kips
	Location	S2A (C2 - 2HL-93)	S2A (C2 - 3HL-93)
Uplift at Supports	**Value**	No Uplift	
	Location		
Max. Hor. Displacement at Supports	**Value**	0.81 in.	1.53 in.
	Location	S1A (C2 - 2HL-93)	S1A (C2 - 3HL-93)
Max. Vertical Deflection Change	**Value**	Not Applicable	1.51 in. (C2)

Notes
- Strength bearing capacities for strength is 1779 kips.
- Shear capacity of the deck is checked.

For both Redundancy I and Redundancy II, the structure has adequate redundancy after the fracture of an exterior girder using the criteria for the strength and displacement requirements discussed above. The following were observed:

- Plastic strain is not reached in the steel tub girders.
- Crushing does not occur in the concrete deck.
- No haunch separation or shear stud failure is observed.
- The maximum vertical deflection change (difference between before fracture and after fracture stages) is 1.51 inches which is lower than L/50 (36.24 inches) and the maximum change in cross-slope is below 5%.

Summary of the redundancy evaluation is shown in Table 54.

Table 54 Summary of Redundancy failure criteria evaluation

Performance Requirement		Most Critical Analysis Case	Result	Acceptable?
Strength Requirements	**Steel Primary Members**	-	No component has strain larger than $5\varepsilon_y$ or 1%. Failure strain was not reached anywhere.	**YES**
	Concrete Crushing	-	No concrete crushing	**YES**
Serviceability Requirements	**Vertical Deflection Change**	C2. (Only Redundancy II DL considered).	Maximum deflection change is 1.5 in, which is lower than L/50 (36.2 in)	**YES**
	Cross-Slope Change	C2. (Only Redundancy II considered).	Maximum additional cross-slope is less than 5%.	**YES**
	Uplift	None.	No uplift.	**YES**

Notes:

- The analysis showed that the structure is capable of resisting an additional 15% of the applied factored live load.
- The horizontal displacement changes at support locations were lower than 6 in.

When the C2 crack location and three HL93 traffic loads were applied in the Redundancy II load combination, the maximum nominal longitudinal stresses at the bottom flange of the fractured girder at the pier and at the bottom flange section change closest to the pier are equal to 27.4 and 25.7 ksi, respectively. This is the most critical combination of loading. This stress is lower than the bottom flange buckling capacity at the same locations which are equal to 45.1 and 41.9 ksi in the design calculations from Highway Structures Information System (HSI) [39].

7.9.3 Summary

Analytical models have been developed to evaluate the structural redundancy of Ramp IHB over IH 43 NB to USH 41 SB (Structure ID B05-678-Unit5) in the state of Wisconsin. The girders are presently classified as Fracture Critical Members. A full depth fracture, including both webs and the top and bottom flange was simulated at three different locations in the exterior girder. The analysis confirms that the bridge satisfies the performance requirements for both Redundancy I and Redundancy II load combinations based on the failure criteria developed in NCHRP 12-87a [5]. Hence, the girders need not be classified as Fracture Critical Members (FCMs).

7.10 B05-679-Unit1&2 (5 Spans)

7.10.1 Background, geometry, and loading

The structural redundancy of Ramp NIH over IH 43 NB to USH 41 SB (Structure ID B05-679-Unit1&2 in Figure 115 and Figure 116) was evaluated for the case where one of the two twin-tub-girders fails due to an assumed sudden full-depth failure. In the analysis, the outside girder was assumed to have fractured. The bridge is symmetric about the center of its midspan. As discussed in Section 3.3 only first two and half span needs to be modeled as shown in Figure 115.

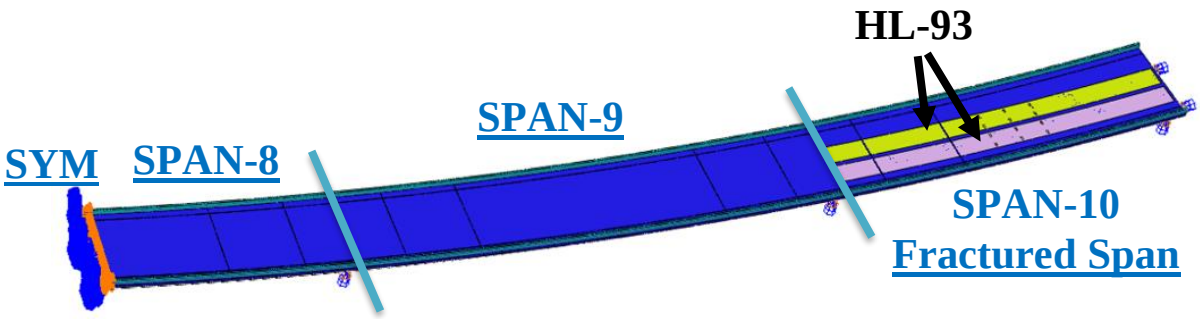

Figure 115 General Isometric View of B05-679-Unit2-RG (Half of Span 8 to Span 10)

Figure 116 Google Map View of B05-679-Unit2-RG

Table 55 provides details related to the geometry and material properties associated with the structure.

Table 55 The bridge geometry and material properties

Bridge Details	
Bridge Name	B05-679-Unit2
Radius of Curvature	1409.0 ft. (measured from bridge centerline)
Span Lengths	RG: 124.0 - 248.0 - 180.9 ft. Span 8 = 248.0/2 = 124.0
Girder Details	
Girder Steel	ASTM A709 HPS 50WF
Box Girder Width (from the centers of interior top-flange to the center of exterior top-flange)	12.5 ft.
Girders Spacing (from the centers of the girders' bottom flanges)	25.0 ft.
Top Flange	Varies, 22.0 in. to 26.0 in. wide Varies, 1.0 in. to 2.625 in. thick
Web	86 in. high Varies, 0.75 in. to 0.875 in. thick
Bottom Flange	111 in. wide Varies, 0.875 in. to 1.625 in. thick
Diaphragms	Three full depth diaphragms
Internal Cross Frames	L6x6x5/8 (Top), L6x6x5/8 (Inclined)
Strut Braces	-
Lateral Braces	WT7x34
Longitudinal Stiffeners on Bottom Flanges	WT10.5x25
Deck Details	
Concrete Material Strength	4 ksi (HPC)
Composite Deck	44.896 ft. wide, 10.0 in. thick 4 in. haunch thick
Transverse Reinforcement	No. 5 rebar with 6.5 in. spacing
Longitudinal Reinforcement	No. 4 & No. 6 rebar with 6.5 in. spacing
Overhang Reinforcement	-
Shear Studs	7 in. height. Longitudinal spacing is 13 in. Three shear studs spaced equally in the transverse direction
Parapet Type	42SS (Interior) – 42SS (Exterior)
Load Details	
Number of Lane	Two lanes traffic
Future Wearing Surface	3 lb/ft2
Maximum Dead Load Displacement (before fracture)	L/650

Three different full-depth fractures were applied separately in each after-fracture performance analysis. Specifically, the tension flange, both webs, and both upper compression flanges were assumed to have failed in one of the girders for each scenario. The locations where the three fractures were assumed to have occurred is shown in Figure 117. The locations are as follows:

- Crack 1 (C1) just before 1st (D1) intermediate diaphragm after 1st (S1A) exterior support,
- Crack 2 (C2) between 1st (D1) and 2nd (D2) intermediate diaphragms,
- Crack 3 (C3) just before 2nd (D2) intermediate diaphragm.

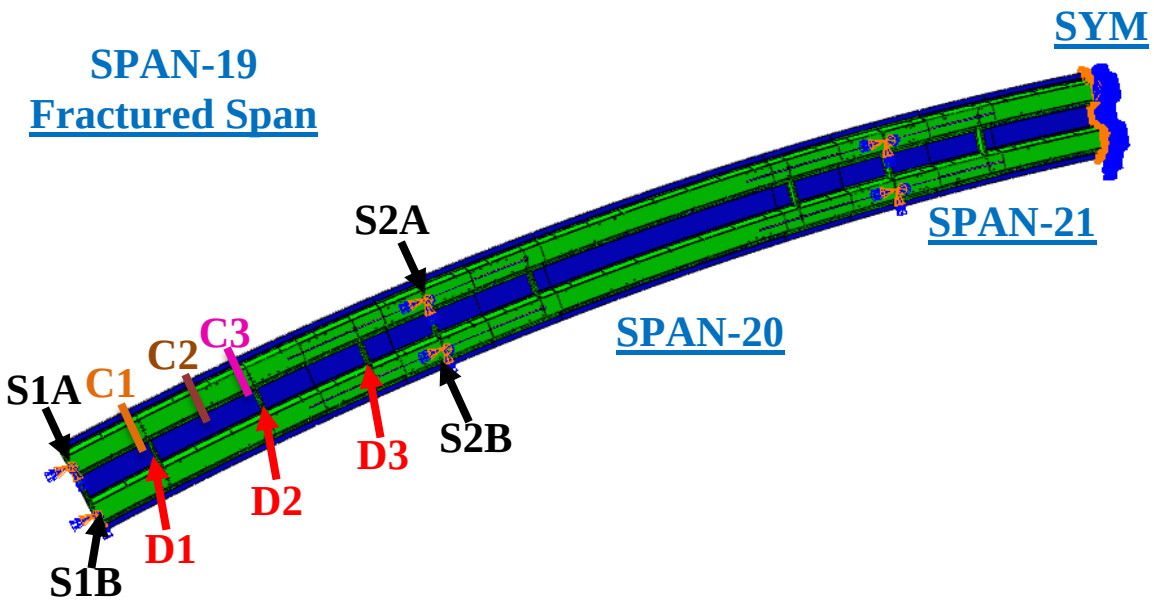

Figure 117 B05-679-Unit2 Crack Locations

The Redundancy I and Redundancy II load combinations require different positioning of traffic live loads. For analysis where only a single lane of live load is applied for the Redundancy I load combination, the HL-93 live load was positioned in the center of the exterior design (i.e., striped) traffic lane. In cases where two lanes of live load were considered, the HL-93 live loads were centered in the both design travel lanes. For the Redundancy II load combination, up to three HL-93 vehicular live loads were placed according to procedure explained in Section 6.1.3. Full non-linear dynamic analysis was performed to determine the level of dynamic amplification that could be expected upon sudden failure of the tub girder. Based on this analysis, the dynamic amplification factor can conservative taken as 0.2 (i.e., 20%). Table 56 demonstrates the amount of total load applied in the Redundancy I (R1) and II (R2) load combinations.

Table 56 Total load applied on the fractured bridge

Type of Loading	Dead Load (1.05 * DA_R)	Future Wearing Surface (1.05 * DA_R)	Live Load (0.85 * m * DA_R)	Total Load (DA_R)
R1 1 HL-93	7290.00 (1.05 * 1.2)	87.78 (1.05 * 1.2)	229.92 (0.85 * 1.2 * 1.2) 263.73 (15% More LL)	7607.69 7641.51 (15% More LL)
R1 2 HL-93	7290.00 (1.05 * 1.2)	87.78 (1.05 * 1.2)	383.19 (0.85 * 1.0 * 1.2) 450.82 (15% More LL)	7760.97 7828.59 (15% More LL)

Type of Loading	Dead Load (1.05)	Future Wearing Surface (1.05)	Live Load (1.3 * m)	Total Load
R2 1 HL-93	5701.00 (1.05)	69.02 (1.05)	309.88 (1.3 * 1.2) * (15% more per HS-20 impact) 339.67 (15% More LL)	6458.03 6487.82 (15% More LL)
R2 2 HL-93	5701.00 (1.05)	69.02 (1.05)	516.46 (1.3 * 1.0) * (15% more per HS-20 impact) 576.06 (15% More LL)	6664.61 6724.20 (15% More LL)
R2 3 HL-93	5701.00 (1.05)	69.02 (1.05)	658.49 (1.3 * 0.85) * (15% more per HS-20 impact) 747.88 (15% More LL)	6806.64 6896.03 (15% More LL)

7.10.2 Results for B05-679-Unit1&2

The analysis has shown that Ramp NIH over IH 43 NB to USH 41 SB (Structure ID B05-679-Unit1&2) possesses considerable reserve strength in the faulted state and that the steel twin-tub-girders do not meet the definition of a fracture critical member when evaluated using the prescribed loading and failure criteria developed in NCHRP 12-87a [5]. The fracture case C2 was found to result in the most critical crack location, and hence the numerical values are presented in Table 57 which summarizes the results obtained from the redundancy analysis of the structure in faulted stage. The evaluation presents the results for the Redundancy I and II load combinations and compares the results to the minimum performance criteria discussed in CHAPTER 6.

Table 57 Results obtained for redundancy evaluation

Fracture Locations		**C1, C2, C3**	
Load Combination		**Redundancy I**	**Redundancy II**
Max. Equivalent Plastic Strain in the Main Girder	**Value**	No plastic strain	No plastic strain
	Location	-	-
Concrete Crushing	**Extent**	No concrete crushing	No concrete crushing
	Location	-	-
Stud Failing	**Value**	No stud failure	No stud failure
	Location	-	-
Max. Vert. Reaction Force	**Value**	1666 kips	1499 kips
	Location	S2A (C2 - 2HL-93)	S2A (C2 - 3HL-93)
Uplift at Supports	**Value**	No Uplift	
	Location		
Max. Hor. Displacement at Supports	**Value**	2.57 in.	4.29 in.
	Location	S1A (C2 - 2HL-93)	S1A (C2 - 3HL-93)
Max. Vertical Deflection Change	**Value**	Not Applicable	3.36 in. (C2)

Notes:
- Strength bearing capacities for strength is 1896 kips.
- Shear capacity of the deck is checked.

For both Redundancy I and Redundancy II, the structure has adequate redundancy after the fracture of an exterior girder using the criteria for the strength and displacement requirements discussed above. The following were observed:

- Plastic strain is not reached in the steel tub girders.
- Crushing does not occur in the concrete deck.
- No haunch separation or shear stud failure is observed.
- The maximum vertical deflection change (difference between before fracture and after fracture stages) is 3.36 inches which is lower than L/50 (43.20 inches) and the maximum change in cross-slope is below 5%.

Summary of the redundancy evaluation is shown in Table 58.

Table 58 Summary of Redundancy failure criteria evaluation

Performance Requirement		Most Critical Analysis Case	Result	Acceptable?
Strength Requirements	**Steel Primary Members**	-	No component has strain larger than $5\varepsilon_y$ or 1%. Failure strain was not reached anywhere.	**YES**
	Concrete Crushing	-	No concrete crushing	**YES**
Serviceability Requirements	**Vertical Deflection Change**	C2. (Only Redundancy II DL considered).	Maximum deflection change is 3.4 in, which is lower than L/50 (43.2 in)	**YES**
	Cross-Slope Change	C2. (Only Redundancy II considered).	Maximum additional cross-slope is less than 5%.	**YES**
	Uplift	None.	No uplift.	**YES**

Notes:
- The analysis showed that the structure is capable of resisting an additional 15% of the applied factored live load.
- The horizontal displacement changes at support locations were lower than 6 in.

When the C2 crack location and three HL93 traffic loads were applied in the Redundancy II load combination, the maximum nominal longitudinal stresses at the bottom flange of the fractured girder at the pier and at the bottom flange section change closest to the pier are 31.5 and 39.5 ksi, respectively. This is the most critical combination of loading and fracture location. This stress is lower than the bottom flange buckling capacity at the same locations which are equal to 47.7 and 41.9 ksi in the design calculations from Highway Structures Information System (HSI) [40].

7.10.3 Summary

Analytical models have been developed to evaluate the structural redundancy of Ramp NIH over IH 43 NB to USH 41 SB (Structure ID B05-679-Unit1&2) in the state of Wisconsin. The girders are presently classified as Fracture Critical Members. A full depth fracture, including both webs and the top and bottom flange was simulated at three different locations in the exterior girder. The analysis confirms that the bridge satisfies the performance requirements for both Redundancy I and Redundancy II load combinations based on the failure criteria developed in NCHRP 12-87a [5]. Hence, the girders need not be classified as Fracture Critical Members (FCMs).

7.11 B40-776 (3 Spans)

7.11.1 Background, geometry, and loading

The structural redundancy of Watertown Plank Road Ramp WH over USH (Structure ID B40-776 in Figure 118) was evaluated for the case where one of the two twin-tub-girders fails due to an assumed sudden full-depth failure. In the analysis, the outside girder was assumed to have fractured. The bridge is symmetric about the center of its midspan.

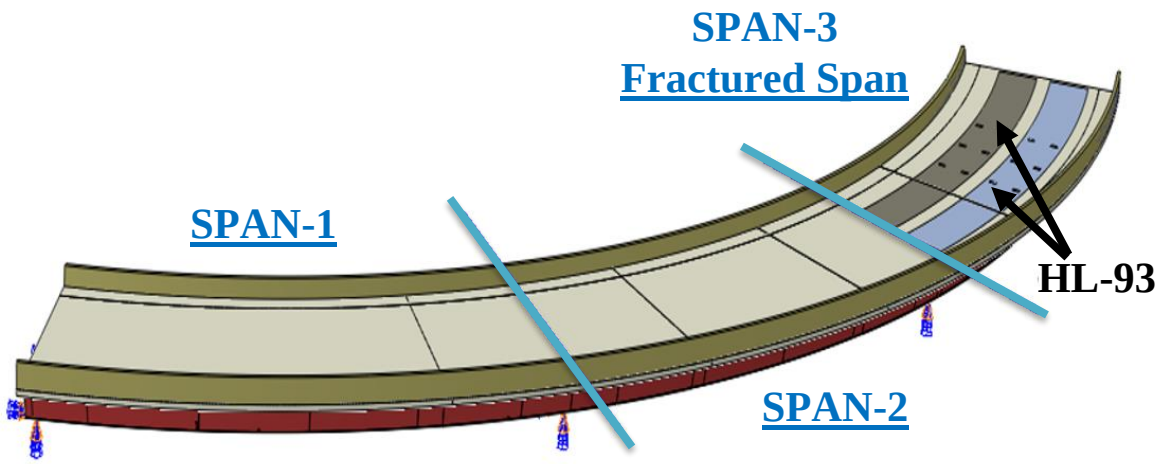

Figure 118 General Isometric View of B40-776

Table 59 provides details related to the geometry and material properties associated with the structure.

Table 59 The bridge geometry and material properties

Bridge Details	
Bridge Name	B40-776
Radius of Curvature	227.5 ft. (measured from bridge centerline)
Span Lengths	105.75 – 102.0 - 105.75 ft.
Girder Details	
Girder Steel	ASTM A709 HPS 50WF
Box Girder Width (from the centers of interior top-flange to the center of exterior top-flange)	9.0 ft.
Girders Spacing (from the centers of the girders' bottom flanges)	21.0 ft
Top Flange	18.0 in. wide Varies, 0.75 in. to 1.25 in. thick
Web	60 in. high 0.625 in. thick
Bottom Flange	81 in. wide Varies, 0.75 in. to 1.375 in. thick
Diaphragms	Two full depth diaphragms per span (3 bays)
Internal Cross Frames	2L6x4x1/2 (Top), 2L6x3-1/2x3/8 (Inclined)
Strut Braces	2L6x4x1/2
Lateral Braces	WT7x30.5, WT8x33.5, WT8x38.5
Longitudinal Stiffeners on Bottom Flanges	-
Deck Details	
Concrete Material Strength	4 ksi (HPC)
Composite Deck	41.896 ft. wide, 10 in. thick 3 in. haunch thick
Transverse Reinforcement	No. 6 rebar with 7 in. spacing
Longitudinal Reinforcement	No. 4 & No. 6 rebar with 6. in. spacing
Overhang Reinforcement	No. 4 rebar with 7 in. spacing
Shear Studs	7 in. height. Longitudinal spacing is 8 in. Three shear studs spaced equally in the transverse direction
Parapet Type	32SS (Interior) – 42SS (Exterior)
Load Details	
Number of Lane	Two lanes traffic
Future Wearing Surface	20 lb/ft^2
Maximum Dead Load Displacement (before fracture)	L/365

Two different full-depth fractures were applied separately in each after-fracture performance analysis. Specifically, the tension flange, both webs, and both upper compression flanges were assumed to have failed in one of the girders for each scenario. The locations where the two fractures were assumed to have occurred is shown in Figure 119. The locations are as follows:

- Crack 1 (C1) just after 2nd (D2) intermediate diaphragm before 4th (S4A) exterior support,
- Crack 2 (C2) between 1st (D1) and 2nd (D2) intermediate diaphragms,
- Crack 3 (C3) between 1st (D1) and 2nd (D2) intermediate diaphragms on the interior girder.

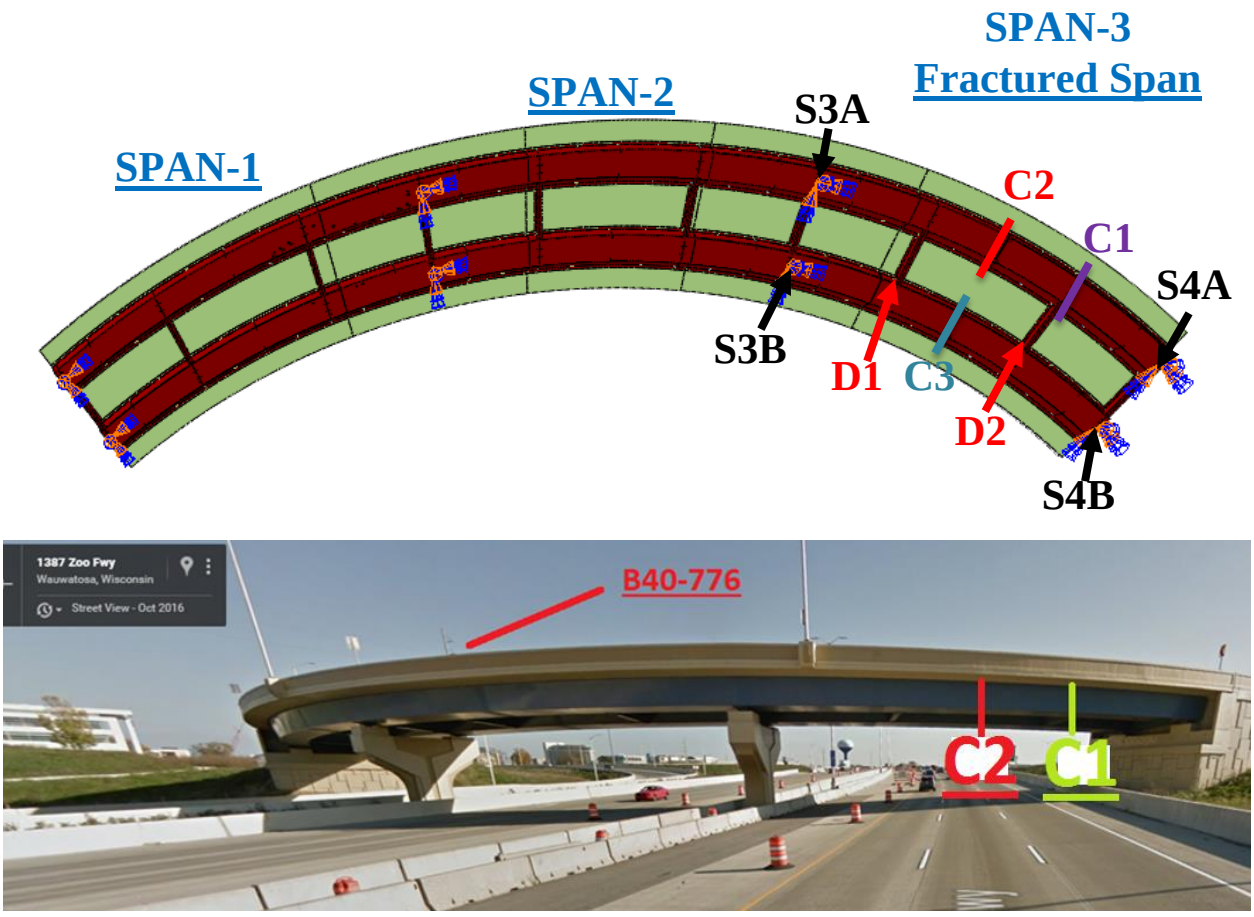

Figure 119 B40-776 Crack Locations

The Redundancy I and Redundancy II load combinations require different positioning of traffic live loads. For analyses where only a single lane of live load is applied for the Redundancy I load combination, the HL-93 live load was positioned in the center of the exterior design (i.e., striped)

traffic lane. In cases where two lanes of live load were considered, the HL-93 live loads were centered in the both design travel lanes. For the Redundancy II load combination, up to three HL-93 vehicular live loads were placed according to the procedure explained in Section 6.1.3. Full non-linear dynamic analysis was performed to determine the level of dynamic amplification that could be expected upon sudden failure of the tub girder. Based on this analysis, the dynamic amplification factor can conservatively be taken as 0.2 (i.e., 20%). Table 60 demonstrates the total load applied in the Redundancy I and II load combinations.

Table 60 Total load applied on the fractured bridge

Type of Loading	**Dead Load (1.05 * DA_R)**	**Future Wearing Surface (1.05 * DA_R)**	**Live Load (0.85 * m * DA_R)**	**Total Load (DA_R)**
R1 1 HL-93	3432.00 (1.05 * 1.2)	294.84 (1.05 * 1.2)	166.46 (0.85 * 1.2 * 1.2) 190.94 (15% More LL)	3893.30 3917.78 (15% More LL)
R1 2 HL-93	3432.00 (1.05 * 1.2)	294.84 (1.05 * 1.2)	277.44 (0.85 * 1.0 * 1.2) 326.40 (15% More LL)	4004.28 4053.24 (15% More LL)

Type of Loading	**Dead Load (1.05)**	**Future Wearing Surface (1.05)**	**Live Load (1.3 * m)**	**Total Load**
R2 1 HL-93	2860.00 (1.05)	245.70 (1.05)	229.01 (1.3 * 1.2) * (15% more per HS-20 impact) 251.03 (15% More LL)	3334.71 3356.73 (15% More LL)
R2 2 HL-93	2860.00 (1.05)	245.70 (1.05)	381.68 (1.3 * 1.0) * (15% more per HS-20 impact) 425.72 (15% More LL)	3487.38 3531.42 (15% More LL)
R2 3 HL-93	2860.00 (1.05)	245.70 (1.05)	486.64 (1.3 * 0.85) * (15% more per HS-20 impact) 552.70 (15% More LL)	3592.34 3658.40 (15% More LL)

7.11.2 Results for B40-776

The analysis has shown that Watertown Plank Road Ramp WH over USH (Structure ID B40-776) possesses considerable reserve strength in the faulted state and that the steel twin-tub-girders do not meet the definition of a fracture critical member when evaluated using the prescribed loading and failure criteria developed in NCHRP 12-87a [5]. Table 61 summarizes the results obtained from the redundancy analysis of the structure in faulted stage. The fracture case C2 was found to result in the most critical crack location, and hence the numerical values are presented in Table 61. The evaluation presents the results for the Redundancy I and II load combinations and compares the results to the minimum performance criteria discussed in CHAPTER 6.

Table 61 Results obtained for redundancy evaluation

Fracture Locations		**C1, C2**	
Load Combination		**Redundancy I**	**Redundancy II**
Max. Equivalent Plastic Strain in the Main Girder	**Value**	No plastic strain	0.002 (C1)
	Location	-	Very localized yielding Intermediate diaphragm "D2" flange
Concrete Crushing	**Extent**	No concrete crushing	No concrete crushing
	Location	-	-
Stud Failing	**Value**	No stud failure	No stud failure
	Location	-	-
Max. Vert. Reaction Force	**Value**	885 kips	932 kips
	Location	S3A (C2 - 2HL-93)	S3A (C2 - 3HL-93)
Uplift at Supports	**Value**	No Uplift	
	Location		
Max. Hor. Displacement at Supports	**Value**	0.87 in.	1.7 in. (C2 - 3HL-93)
	Location	S4A (C2 - 2HL-93)	S4A (C2 - 3HL-93)
Max. Vertical Deflection Change	**Value**	Not Applicable	1.5 in. (C2)
• Design bearing capacity for strength is 960 kips. • Shear capacity of the deck is checked.			

For both Redundancy I and Redundancy II, the structure has adequate redundancy after the fracture of an exterior girder using the criteria for the strength and displacement requirements discussed above. The following were observed:

- Insignificant plastic strain is not higher than 0.002 in D2's flange.
- Crushing does not occur in the concrete deck.
- No haunch separation or shear stud failure is observed.
- The maximum vertical deflection change (difference between before fracture and after fracture stages) is 1.5 inches which is lower than L/50 (25.4 inches) and the maximum change in cross-slope is below 5%.

Summary of the redundancy evaluation is shown in Table 62.

Table 62 Summary of Redundancy failure criteria evaluation

Performance Requirement		**Most Critical Analysis Case**	**Result**	**Acceptable?**
Strength Requirements	**Steel Primary Members**	C1. Redundancy II.	No component has strain larger than $5\varepsilon_y$ or 1%. Failure strain was not reached anywhere.	**YES**
	Concrete Crushing	-	No concrete crushing	**YES**
Serviceability Requirements	**Vertical Deflection Change**	C2. (Only Redundancy II DL considered).	Maximum deflection change is 1.5 in, which is lower than L/50 (25.4 in)	**YES**
	Cross-Slope Change	C2. (Only Redundancy II considered).	Maximum additional cross-slope is less than 5%.	**YES**
	Uplift	None.	No uplift.	**YES**
Notes: • The analysis showed that the structure is capable of resisting an additional 15% of the applied factored live load. • The horizontal displacement changes at support locations were lower than 6 in.				

When the C2 crack location and three HL93 traffic loads were applied in the Redundancy II load combination, the maximum nominal longitudinal stresses at the bottom flange of the fractured girder at the pier is equal to 24.2 ksi. This is the most critical combination of loading and fracture location. This stress is lower than the bottom flange buckling capacity at the same location which is equal to 33.5 in the design calculations from Highway Structures Information System (HSI) [41]. For this bridge, the interior girder fracture was applied, and the maximum vertical

displacement was equal to 0.84 in. This displacement was much lower than the case the exterior girder fracture (1.5 in).

7.11.3 Summary

Analytical models have been developed to evaluate the structural redundancy of Watertown Plank Road Ramp WH over USH (Structure ID B40-776) in the state of Wisconsin. The girders are presently classified as Fracture Critical Members. A full depth fracture, including both webs and the top and bottom flange was simulated at two different locations in the exterior girder. The analysis confirms that the bridge satisfies the performance requirements for both Redundancy I and Redundancy II load combinations based on the failure criteria developed in NCHRP 12-87a [5]. Hence, the girders need not be classified as Fracture Critical Members (FCMs).

7.12 B40-783 (3 Spans)

7.12.1 Background, geometry, and loading

The structural redundancy of Watertown Plank Road Ramp WF over USH 45 (Structure ID B40-783 in Figure 120) was evaluated for the case where one of the two twin-tub-girders fails due to an assumed sudden full-depth failure. In the analysis, the outside girder was assumed to have fractured.

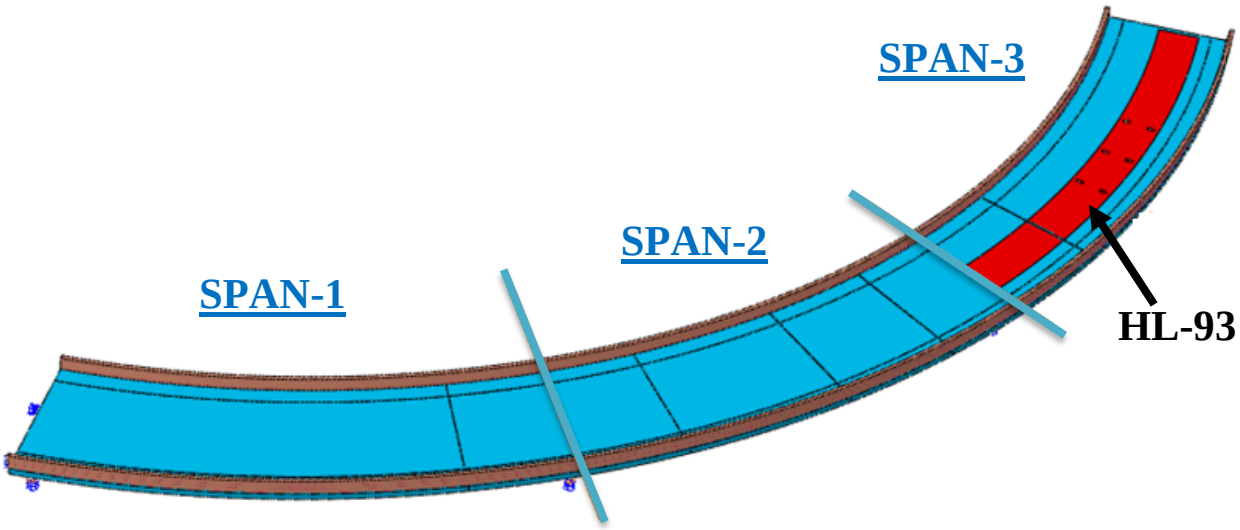

Figure 120 General Isometric View of B40-783

Table 63 provides details related to the geometry and material properties associated with the structure.

Table 63 The bridge geometry and material properties

Bridge Details	
Bridge Name	B40-783
Radius of Curvature	220.5 ft. (measured from bridge centerline)
Span Lengths	111.5 – 111.0 - 119.0 ft.
Girder Details	
Girder Steel	ASTM A709 HPS 50WF
Box Girder Width (from the centers of interior top-flange to the center of exterior top-flange)	7.5 ft.
Girders Spacing (from the centers of the girders' bottom flanges)	16.0 ft
Top Flange	18.0 in. wide Varies, 0.75 in. to 1.125 in. thick
Web	60 in. high 0.625 in. thick
Bottom Flange	63 in. wide Varies, 0.75 in. to 1.25 in. thick
Diaphragms	Two full depth diaphragms per span (4 bays)
Internal Cross Frames	2L6x4x1/2 (Top), 2L6x3-1/2x3/8 (Inclined)
Strut Braces	2L6x4x1/2
Lateral Braces	WT7x30.5, WT8x33.5, WT8x38.5
Longitudinal Stiffeners on Bottom Flanges	-
Deck Details	
Concrete Material Strength	4 ksi (HPC)
Composite Deck	31.896 ft. wide, 8.5 in. thick 3 in. haunch thick
Transverse Reinforcement	No. 5 rebar with 6 in. spacing
Longitudinal Reinforcement	No. 4 & No. 6 rebar with 7. in. spacing
Overhang Reinforcement	No. 5 rebar with 6 in. spacing
Shear Studs	6 in. height. Longitudinal spacing is 12 in. Three shear studs spaced equally in the transverse direction
Parapet Type	32SS (Interior) – 42SS (Exterior)
Load Details	
Number of Lane	Single lane traffic
Future Wearing Surface	20 lb/ft^2
Maximum Dead Load Displacement (before fracture)	L/410

Four different full-depth fractures were applied separately in each after-fracture performance analysis. Specifically, the tension flange, both webs, and both upper compression flanges were assumed to have failed in one of the girders for each scenario. The locations where the four fractures were assumed to have occurred is shown in Figure 121. The locations are as follows:

- Crack 1 (C1) just before 1st (D1) intermediate diaphragm after 1st (S1A) exterior support,
- Crack 2 (C2) between 1st (D1) and 2nd (D2) intermediate diaphragms,
- Crack 3 (C3) between 3rd (D3) and 4th (D4) intermediate diaphragms,
- Crack 4 (C4) just after 4th (D4) intermediate diaphragm before 4th (S4A) exterior support,
- Crack 5 (C5) between 3rd (D3) and 4th (D4) intermediate diaphragms on the interior girder.

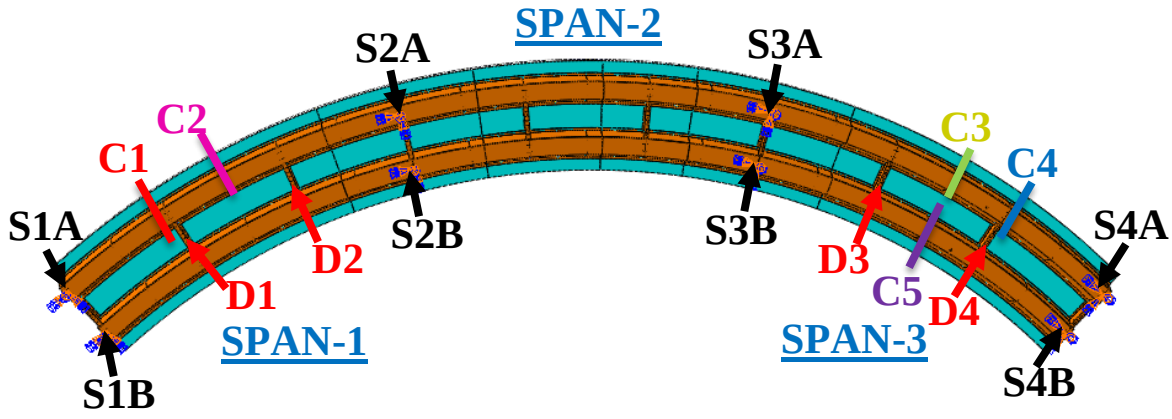

Figure 121 B40-783 Crack Locations

The Redundancy I and Redundancy II load combinations require different positioning of traffic live loads. For analyses where only a single lane of live load is applied for the Redundancy I load combination, the HL-93 live load was positioned in the center of the design (i.e., striped) traffic lane. For the Redundancy II load combination, up to two HL-93 vehicular live loads were placed according to the procedure explained in Section 6.1.3. Full non-linear dynamic analysis was performed to determine the level of dynamic amplification that could be expected upon sudden failure of the tub girder. Based on this analysis, the dynamic amplification factor can

conservatively be taken as 0.2 (i.e., 20%). Table 64 demonstrates the amount of total load applied in the Redundancy I (R1) and II (R2) load combinations.

Table 64 Total load applied on the fractured bridge

Type of Loading	Dead Load ($1.05 * DA_R$)	Future Wearing Surface ($1.05 * DA_R$)	Live Load ($0.85 * m * DA_R$)	Total Load (DA_R)
R1 **1 HL-93**	2716.80 (1.05 * 1.2)	247.74 (1.05 * 1.2)	181.35 (0.85 * 1.2 * 1.2) 208.02 (15% More LL)	3145.89 3172.56 (15% More LL)

Type of Loading	Dead Load (1.05)	Future Wearing Surface (1.05)	Live Load (1.3 * m)	Total Load
R2 **1 HL-93**	2264.00 (1.05)	247.74 (1.05)	247.98 (1.3 * 1.2) * (15% more per HS-20 impact) 271.82 (15% More LL)	2718.43 2742.27 (15% More LL)
R2 **2 HL-93**	2264.00 (1.05)	247.74 (1.05)	413.30 (1.3 * 1.0) * (15% more per HS-20 impact) 460.98 (15% More LL)	2883.75 2931.44 (15% More LL)

7.12.2 Results for B05-783

The analysis has shown that Watertown Plank Road Ramp WF over USH 45 (Structure ID B40-783) possesses considerable reserve strength in the faulted state and that the steel twin-tub-girders do not meet the definition of a fracture critical member when evaluated using the prescribed loading and failure criteria developed in NCHRP 12-87a [5]. Table 65 summarizes the results obtained from the redundancy analysis of the structure in faulted stage. The fracture case C3 was found to result in the most critical crack location, and hence the numerical values are presented in Table 65. The evaluation presents the results for the Redundancy I and II load combinations and compares the results to the minimum performance criteria discussed in CHAPTER 6.

Table 65 Results obtained for redundancy evaluation

Fracture Locations		**C1, C2, C3, C4**	
Load Combination		**Redundancy I**	**Redundancy II**
Max. Equivalent Plastic Strain in the Main Girder	**Value**	No plastic strain	< 0.001 (C1, C4)
	Location	-	Very localized yielding Intermediate diaphragm "D1-D4" flange
Concrete Crushing	**Extent**	No concrete crushing	No concrete crushing
	Location	-	-
Stud Failing	**Value**	No stud failure	No stud failure
	Location	-	-
Max. Vert. Reaction Force	**Value**	701 kips	725 kips
	Location	S3B (C3 - 1HL-93)	S3A (C3 - 2HL-93)
Uplift at Supports	**Value**	No Uplift	
	Location		
Max. Hor. Displacement at Supports	**Value**	1.29 in.	2.39 in.
	Location	S4A (C3 - 1HL-93)	S4A (C3 - 2HL-93)
Max. Vertical Deflection Change	**Value**	Not Applicable	1.54 in. (C3)

Notes:
- Design bearing capacity for strength is 1110 kips.
- Shear capacity of the deck is checked.

For both Redundancy I and Redundancy II, the structure has adequate redundancy after the fracture of an exterior girder using the criteria for the strength and displacement requirements discussed above. The following were observed:

- Insignificant localized plastic strain is not higher than 0.001 in D1-D4's flange.
- Crushing does not occur in the concrete deck.
- No haunch separation or shear stud failure is observed.
- The maximum vertical deflection change (difference between before fracture and after fracture stages) is 1.5 inches which is lower than L/50 (28.6 inches) and the maximum change in cross-slope is below 5%.

Summary of the redundancy evaluation is shown in Table 66.

Table 66 Summary of Redundancy failure criteria evaluation

Performance Requirement		Most Critical Analysis Case	Result	Acceptable?
Strength Requirements	**Steel Primary Members**	C1 & C4. Redundancy II.	No component has strain larger than $5\varepsilon_y$ or 1%. Failure strain was not reached anywhere.	**YES**
	Concrete Crushing	-	No concrete crushing	**YES**
Serviceability Requirements	**Vertical Deflection Change**	C3. (Only Redundancy II DL considered).	Maximum deflection change is 1.5 in, which is lower than L/50 (28.6 in)	**YES**
	Cross-Slope Change	C3. (Only Redundancy II considered).	Maximum additional cross-slope is less than 5%.	**YES**
	Uplift	None.	No uplift.	**YES**

Notes:

- The analysis showed that the structure is capable of resisting an additional 15% of the applied factored live load.
- The horizontal displacement changes at support locations were lower than 6 in.

When the C2 crack location and two HL93 traffic loads were applied in the Redundancy II load combination, the maximum nominal longitudinal stresses at the bottom flange of the fractured girder at the pier and at the bottom flange section change closest to the pier are equal to 25.5 and 14.7 ksi, respectively. This is the most critical combination of loading and fracture location. This stress is lower than the bottom flange buckling capacity at the same locations which are equal to 36.3 and 16.5 ksi in the design calculations from Highway Structures Information System (HSI) [42].

When the C3 crack location and two HL93 traffic loads were applied in the Redundancy II load combination, the maximum nominal longitudinal stresses at the bottom flange of the fractured girder at the pier and at the bottom flange section change closest to the pier are equal to 28.3 and 14.1 ksi, respectively. This is the most critical combination of loading and fracture location. This stress is lower than the bottom flange buckling capacity at the same locations which are equal to 39.2 and 17.0 ksi in the design calculations from Highway Structures Information System (HSI)

[42]. For this bridge, the interior girder fracture was applied, and the maximum vertical displacement was equal to 0.78 in. This displacement was much lower than the case when the exterior girder fracture was applied (1.54 in).

7.12.3 Summary

Analytical models have been developed to evaluate the structural redundancy of Watertown Plank Road Ramp WF over USH 45 (Structure ID B40-783) in the state of Wisconsin. The girders are presently classified as Fracture Critical Members. A full depth fracture, including both webs and the top and bottom flange was simulated at four different locations in the exterior girder. The analysis confirms that the bridge satisfies the performance requirements for both Redundancy I and Redundancy II load combinations based on the failure criteria developed in NCHRP 12-87a [5]. Hence, the girders need not be classified as Fracture Critical Members (FCMs).

7.13 B40-786-Unit1 (4 Spans)

7.13.1 Background, geometry, and loading

The structural redundancy of Ramp WS over Zoo Interchange (Structure ID B40-786-Unit1 in Figure 122) was evaluated for the case where one of the two twin-tub-girders fails due to an assumed sudden full-depth failure. In the analysis, the outside girder was assumed to have fractured. The bridge is symmetric about the center of the middle pier. As discussed in Section 3.3 only first two and half span needs to be modeled as shown in Figure 122. It is assumed all the bridge under curve.

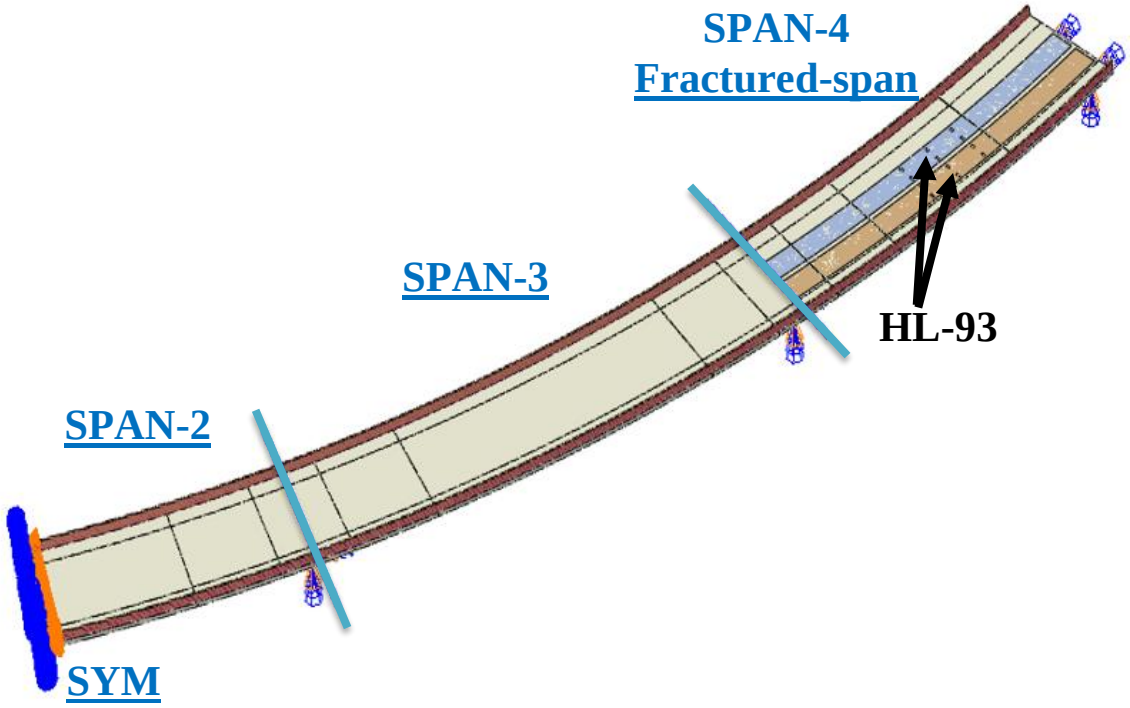

Figure 122 General Isometric View of B40-786-Unit1-RG (Half of Span 2 to Span 4)

Table 67 provides details related to the geometry and material properties associated with the structure.

Table 67 The bridge geometry and material properties

Bridge Details	
Bridge Name	B40-786-Unit1
Radius of Curvature	842.0 ft. (measured from bridge centerline) Assume all spans are horizontally curved.
Span Lengths	RG: 107.5 - 215.0 - 160.0 ft. Span 2 = 215.0/2 = 107.5
Girder Details	
Girder Steel	ASTM A709 HPS 50WF
Box Girder Width (from the centers of interior top-flange to the center of exterior top-flange)	9.5 ft.
Girders Spacing (from the centers of the girders' bottom flanges)	23.0 ft.
Top Flange	Varies, 20.0 in. to 28.0 in. wide Varies, 1.0 in. to 2.5 in. thick
Web	84 in. high Varies, 0.625 in. to 0.6875 in. thick
Bottom Flange	75 in. wide Varies, 0.75 in. to 2.25 in. thick
Diaphragms	Two full depth diaphragms for end spans
Internal Cross Frames	L6x6x1/2 (Top), L6x6x1/2 (Inclined)
Strut Braces	L6x6x1/2
Lateral Braces	WT7x30.5
Longitudinal Stiffeners on Bottom Flanges	-
Deck Details	
Concrete Material Strength	4 ksi (HPC)
Composite Deck	44.896 ft. wide, 10.5 in. thick 4 in. haunch thick
Transverse Reinforcement	No. 6 rebars with 7 in. spacing
Longitudinal Reinforcement	No. 4 & No. 6 rebars with 6in. spacing
Overhang Reinforcement	No. 4 rebars with 7 in. spacing
Shear Studs	6 in. height. Longitudinal spacing is 12 in. Three shear studs spaced equally in the transverse direction
Parapet Type	42SS (Interior) – 42SS (Exterior)
Load Details	
Number of Lane	Two lanes traffic
Future Wearing Surface	20 lb/ft2
Maximum Dead Load Displacement	L/570

Two different full-depth fractures were applied separately in each after-fracture performance analysis. Specifically, the tension flange, both webs, and both upper compression flanges were assumed to have failed in one of the girders for each scenario. The locations where the two fractures were assumed to have occurred is shown in Figure 123. The locations are as follows:

- Crack 1 (C1) just before 2nd (D2) intermediate diaphragm after 4th (S4A) exterior support,
- Crack 2 (C2) between 1st (D1) and 2nd (D2) intermediate diaphragms.

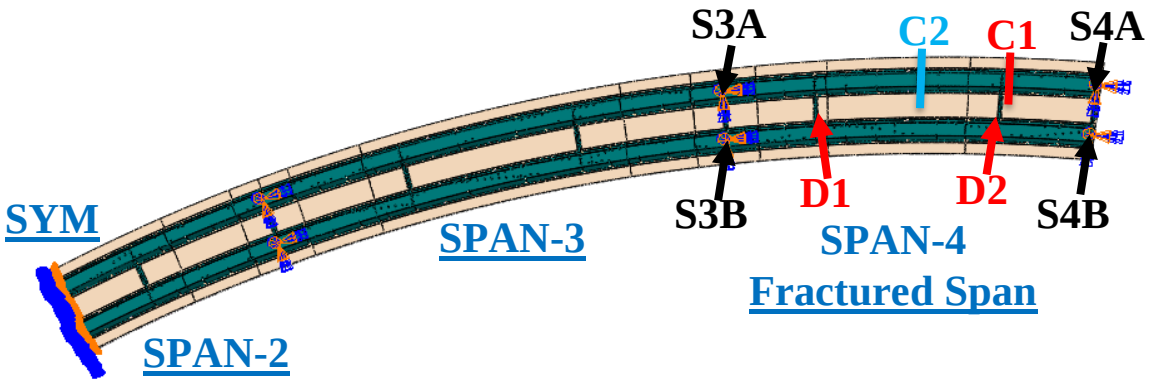

Figure 123 B40-786-Unit1 Crack Locations

The Redundancy I and Redundancy II load combinations require different positioning of traffic live loads. For analysis where only a single lane of live load is applied for the Redundancy I load combination, the HL-93 live load was positioned in the center of the exterior design (i.e., striped) traffic lane. In cases where two lanes of live load were considered, the HL-93 live loads were centered in the both design travel lanes. For the Redundancy II load combination, up to three HL-93 vehicular live loads were placed according to procedure explained in Section 6.1.3. Full non-linear dynamic analysis was performed to determine the level of dynamic amplification that could be expected upon sudden failure of the tub girder. Based on this analysis, the dynamic amplification factor can conservative taken as 0.2 (i.e., 20%). Table 68 demonstrates the amount of total load applied in the Redundancy I (R1) and II (R2) load combinations.

Table 68 Total load applied on the fractured bridge

Type of Loading	Dead Load (1.05 * DA_R)	Future Wearing Surface (1.05 * DA_R)	Live Load (0.85 * m * DA_R)	Total Load (DA_R)
R1 1 HL-93	6442.80 (1.05 * 1.2)	510.68 (1.05 * 1.2)	213.47 (0.85 * 1.2 * 1.2) 244.86 (15% More LL)	7166.94 7198.34 (15% More LL)
R1 2 HL-93	6442.80 (1.05 * 1.2)	510.68 (1.05 * 1.2)	355.78 (0.85 * 1.0 * 1.2) 418.56 (15% More LL)	7309.25 7372.04 (15% More LL)

Type of Loading	Dead Load (1.05)	Future Wearing Surface (1.05)	Live Load (1.3 * m)	Total Load
R2 1 HL-93	5369.00 (1.05)	425.57 (1.05)	288.91 (1.3 * 1.2) * (15% more per HS-20 impact) 316.69 (15% More LL)	6083.48 6111.26 (15% More LL)
R2 2 HL-93	5369.00 (1.05)	425.57 (1.05)	481.52 (1.3 * 1.0) * (15% more per HS-20 impact) 537.08 (15% More LL)	6276.09 6331.65 (15% More LL)
R2 3 HL-93	5369.00 (1.05)	425.57 (1.05)	613.94 (1.3 * 0.85) * (15% more per HS-20 impact) 697.28 (15% More LL)	6408.50 6491.84 (15% More LL)

7.13.2 Results for B40-786-Unit1

The analysis has shown that Ramp WS over Zoo Interchange (Structure ID B40-786-Unit1) possesses considerable reserve strength in the faulted state and that the steel twin-tub-girders do not meet the definition of a fracture critical member when evaluated using the prescribed loading and failure criteria developed in NCHRP 12-87a [5]. Table 69 summarizes the results obtained from the redundancy analysis of the structure in faulted stage. The fracture case C2 was found to result in the most critical crack location, and hence the numerical values are presented in Table 69. The fracture case C2 was found to result in the most critical crack location, and hence the numerical values are presented in Table 69. The evaluation presents the results for the Redundancy I and II

load combinations and compares the results to the minimum performance criteria discussed in CHAPTER 6.

Table 69 Results obtained for redundancy evaluation

Fracture Locations		**C1, C2**	
Load Combination		**Redundancy I**	**Redundancy II**
Max. Equivalent Plastic Strain in the Main Girder	**Value**	No plastic strain	No plastic strain
	Location	-	-
Concrete Crushing	**Extent**	No concrete crushing	No concrete crushing
	Location	-	-
Stud Failing	**Value**	No stud failure	No stud failure
	Location	-	-
Max. Vert. Reaction Force	**Value**	1693 kips	1570 kips
	Location	S3B (C2 - 2HL-93)	S3A (C2 - 3HL-93)
Uplift at Supports	**Value**	No Uplift	
	Location		
Max. Hor. Displacement at Supports	**Value**	2.45 in.	3.47 in.
	Location	S4A (C2 - 2HL-93)	S4A (C2 - 3HL-93)
Max. Vertical Deflection Change	**Value**	Not Applicable	2.79 in. (C2)

Notes:
- Strength bearing capacities for strength is 2430 kips.
- Shear capacity of the deck is checked.

For both Redundancy I and Redundancy II, the structure has adequate redundancy after the fracture of an exterior girder using the criteria for the strength and displacement requirements discussed above. The following were observed:

- Plastic strain is not reached in the steel tub girders.
- Crushing does not occur in the concrete deck.
- No haunch separation or shear stud failure is observed.
- The maximum vertical deflection change (difference between before fracture and after fracture stages) is 2.79 inches which is lower than L/50 (38.40 inches) and the maximum change in cross-slope is below 5%.

Summary of the redundancy evaluation is shown in Table 70.

Table 70 Summary of Redundancy failure criteria evaluation

Performance Requirement		Most Critical Analysis Case	Result	Acceptable?
Strength Requirements	**Steel Primary Members**	-	No component has strain larger than $5\varepsilon_y$ or 1%. Failure strain was not reached anywhere.	**YES**
	Concrete Crushing	-	No concrete crushing	**YES**
Serviceability Requirements	**Vertical Deflection Change**	C2. (Only Redundancy II DL considered).	Maximum deflection change is 2.8 in, which is lower than L/50 (38.4in)	**YES**
	Cross-Slope Change	C2. (Only Redundancy II considered).	Maximum additional cross-slope is less than 5%.	**YES**
	Uplift	None.	No uplift.	**YES**

Notes:

- The analysis showed that the structure is capable of resisting an additional 15% of the applied factored live load.
- The horizontal displacement changes at support locations were lower than 6 in.

When the C2 crack location and three HL93 traffic loads were applied in the Redundancy II load combination, the maximum nominal longitudinal stresses at the bottom flange of the fractured girder at the pier and at the bottom flange section change closest to the pier are 33.7 and 34.8 ksi, respectively. This is the most critical combination of loading and fracture location. This stress is lower than the bottom flange buckling capacity at the same locations which are equal to 47.8 and 42.9 ksi in the design calculations from Highway Structures Information System (HSI) [43].

7.13.3 Summary

Analytical models have been developed to evaluate the structural redundancy of Ramp WS over Zoo Interchange (Structure ID B40-786-Unit1) in the state of Wisconsin. The girders are presently classified as Fracture Critical Members. A full depth fracture, including both webs and the top and bottom flange was simulated at two different locations in the exterior girder. The analysis confirms that the bridge satisfies the performance requirements for both Redundancy I and Redundancy II load combinations based on the failure criteria developed in NCHRP 12-87a [5]. Hence, the girders need not be classified as Fracture Critical Members (FCMs).

7.14 B40-786-Unit2 (4 Spans)

7.14.1 Background, geometry, and loading

The structural redundancy of Ramp WS over Zoo Interchange (Structure ID B40-786-Unit2 in Figure 124) was evaluated for the case where one of the two twin-tub-girders fails due to an assumed sudden full-depth failure. In the analysis, the outside girder was assumed to have fractured. The bridge is symmetric about the center of the middle pier. As discussed in Section 3.3 only first two and half span needs to be modeled as shown in Figure 124.

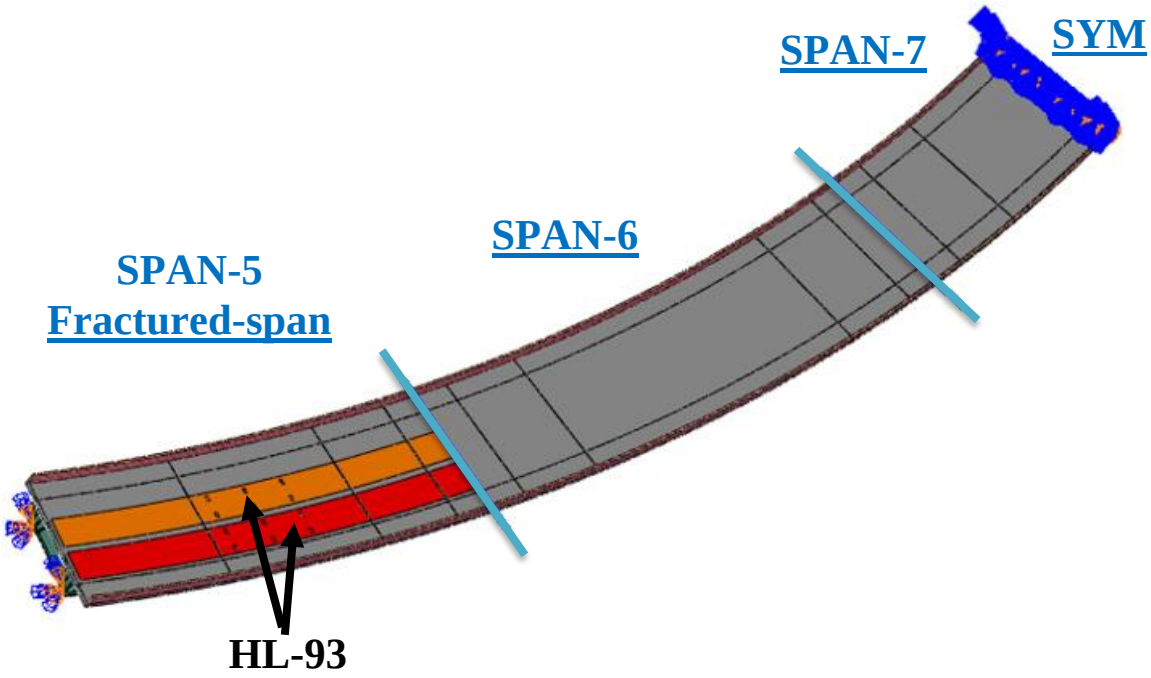

Figure 124 General Isometric View of B40-786-Unit2-LF (Span 5 to Half of Span 7)

Table 71 provides details related to the geometry and material properties associated with the structure.

Table 71 The bridge geometry and material properties

Bridge Details	
Bridge Name	B40-786-Unit2
Radius of Curvature	842.0 ft. (measured from bridge centerline)
Span Lengths	LF: 146.0 - 196.0 - 98.0 ft. Span 7 = 196.0/2 = 98.0
Girder Details	
Girder Steel	ASTM A709 HPS 50WF
Box Girder Width (from the centers of interior top-flange to the center of exterior top-flange)	9.5 ft.
Girders Spacing (from the centers of the girders' bottom flanges)	23.0 ft.
Top Flange	Varies, 20.0 in. to 26.0 in. wide Varies, 1.0 in. to 2.5 in. thick
Web	84 in. high Varies, 0.625 in. to 0.6875 in. thick
Bottom Flange	75 in. wide Varies, 0.75 in. to 2.25 in. thick
Diaphragms	Two full depth diaphragms for end spans
Internal Cross Frames	L6x6x1/2 (Top), L6x6x1/2 (Inclined)
Strut Braces	L6x6x1/2
Lateral Braces	WT7x30.5
Longitudinal Stiffeners on Bottom Flanges	-
Deck Details	
Concrete Material Strength	4 ksi (HPC)
Composite Deck	44.896 ft. wide, 10.5 in. thick 4 in. haunch thick
Transverse Reinforcement	No. 6 rebars with 7 in. spacing
Longitudinal Reinforcement	No. 4 & No. 6 rebars with 6in. spacing
Overhang Reinforcement	No. 4 rebars with 7 in. spacing
Shear Studs	6 in. height. Longitudinal spacing is 12 in. Three shear studs spaced equally in the transverse direction
Parapet Type	42SS (Interior) – 42SS (Exterior)
Load Details	
Number of Lane	Two lanes traffic
Future Wearing Surface	20 lb/ft2
Maximum Dead Load Displacement (before fracture)	L/770

Two different full-depth fractures were applied separately in each after-fracture performance analysis. Specifically, the tension flange, both webs, and both upper compression flanges were assumed to have failed in one of the girders for each scenario. The locations where the two fractures were assumed to have occurred is shown in Figure 125. The locations are as follows:

- Crack 1 (C1) just before 1st (D1) intermediate diaphragm after 1st (S1A) exterior support,
- Crack 2 (C2) between 1st (D1) and 2nd (D2) intermediate diaphragms.

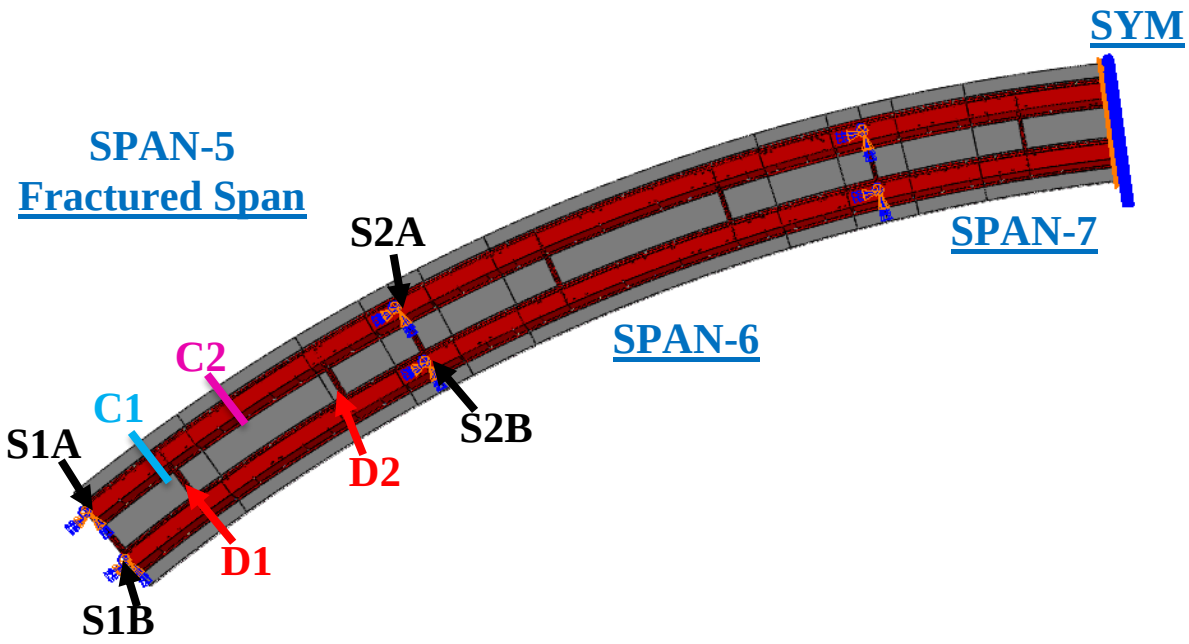

Figure 125 B40-786-Unit2 Crack Locations

The Redundancy I and Redundancy II load combinations require different positioning of traffic live loads. For analyses where only a single lane of live load is applied for the Redundancy I load combination, the HL-93 live load was positioned in the center of the exterior design (i.e., striped) traffic lane. In cases where two lanes of live load were considered, the HL-93 live loads were centered in the both design travel lanes. For the Redundancy II load combination, up to three HL-93 vehicular live loads were placed according to the procedure explained in Section 6.1.3. Full non-linear dynamic analysis was performed to determine the level of dynamic amplification that could be expected upon sudden failure of the tub girder. Based on this analysis, the dynamic amplification factor can conservatively be taken as 0.2 (i.e., 20%). Table 72 demonstrates the amount of total load applied in the Redundancy I (R1) and II (R2) load combinations.

Table 72 Total load applied on the fractured bridge

Type of Loading	Dead Load (1.05 * DA_R)	Future Wearing Surface (1.05 * DA_R)	Live Load (0.85 * m * DA_R)	Total Load (DA_R)
R1 1 HL-93	5794.80 (1.05 * 1.2)	465.70 (1.05 * 1.2)	213.47 (0.85 * 1.2 * 1.2) 244.86 (15% More LL)	6462.99 6492.77 (15% More LL)
R1 2 HL-93	5794.80 (1.05 * 1.2)	465.70 (1.05 * 1.2)	355.78 (0.85 * 1.0 * 1.2) 418.56 (15% More LL)	6597.99 6657.55 (15% More LL)

Type of Loading	Dead Load (1.05)	Future Wearing Surface (1.05)	Live Load (1.3 * m)	Total Load
R2 1 HL-93	4829.00 (1.05)	388.08 (1.05)	288.91 (1.3 * 1.2) * (15% more per HS-20 impact) 316.69 (15% More LL)	5492.01 5518.45 (15% More LL)
R2 2 HL-93	4829.00 (1.05)	388.08 (1.05)	481.52 (1.3 * 1.0) * (15% more per HS-20 impact) 537.08 (15% More LL)	5675.30 5728.18 (15% More LL)
R2 3 HL-93	4829.00 (1.05)	388.08 (1.05)	613.94 (1.3 * 0.85) * (15% more per HS-20 impact) 697.28 (15% More LL)	5801.32 5880.62 (15% More LL)

7.14.2 Results for B40-786-Unit2

The analysis has shown that Ramp WS over Zoo Interchange (Structure ID B40-786-Unit2) possesses considerable reserve strength in the faulted state and that the steel twin-tub-girders do not meet the definition of a fracture critical member when evaluated using the prescribed loading and failure criteria developed in NCHRP 12-87a [5]. Table 73 summarizes the results obtained from the redundancy analysis of the structure in faulted stage. The fracture case C2 was found to result in the most critical crack location, and hence the numerical values are presented in Table 73. The evaluation presents the results for the Redundancy I and II load combinations and compares the results to the minimum performance criteria discussed in CHAPTER 6.

Table 73 Results obtained for redundancy evaluation

Fracture Locations		**C1, C2**	
Load Combination		**Redundancy I**	**Redundancy II**
Max. Equivalent Plastic Strain in the Main Girder	**Value**	No plastic strain	No plastic strain
	Location	-	-
Concrete Crushing	**Extent**	No concrete crushing	No concrete crushing
	Location	-	-
Stud Failing	**Value**	No stud failure	No stud failure
	Location	-	-
Max. Vert. Reaction Force	**Value**	1526 kips	1397 kips
	Location	S2B (C2 - 2HL-93)	S2A (C2 - 3HL-93)
Uplift at Supports	**Value**	No Uplift	
	Location		
Max. Hor. Displacement at Supports	**Value**	1.58 in.	2.18 in.
	Location	S1A (C2 - 2HL-93)	S1A (C2 - 3HL-93)
Max. Vertical Deflection Change	**Value**	Not Applicable	1.94 in. (C2)

Notes:
- Strength bearing capacities for strength is 1880 kips.
- Shear capacity of the deck is checked.

For both Redundancy I and Redundancy II, the structure has adequate redundancy after the fracture of an exterior girder using the criteria for the strength and displacement requirements discussed above. The following were observed:

- Plastic strain is not reached in the steel tub girders.
- Crushing does not occur in the concrete deck.
- No haunch separation or shear stud failure is observed.
- The maximum vertical deflection change (difference between before fracture and after fracture stages) is 1.94 inches which is lower than L/50 (35.04 inches) and the maximum change in cross-slope is below 5%.

Summary of the redundancy evaluation is shown in Table 74.

Table 74 Summary of Redundancy failure criteria evaluation

Performance Requirement		Most Critical Analysis Case	Result	Acceptable?
Strength Requirements	**Steel Primary Members**	-	No component has strain larger than $5\varepsilon_y$ or 1%. Failure strain was not reached anywhere.	**YES**
	Concrete Crushing	-	No concrete crushing	**YES**
Serviceability Requirements	**Vertical Deflection Change**	C2. (Only Redundancy II DL considered).	Maximum deflection change is 1.9 in, which is lower than L/50 (35.0in)	**YES**
	Cross-Slope Change	C2. (Only Redundancy II considered).	Maximum additional cross-slope is less than 5%.	**YES**
	Uplift	None.	No uplift.	**YES**

Notes:

- The analysis showed that the structure is capable of resisting an additional 15% of the applied factored live load.
- The horizontal displacement changes at support locations were lower than 6 in.

When the C2 crack location and three HL93 traffic loads were applied in the Redundancy II load combination, the maximum nominal longitudinal stresses at the bottom flange of the fractured girder at the pier and at the bottom flange section change closest to the pier are 32.0 and 29.0 ksi, respectively. This is the most critical combination of loading and fracture location. This stress is lower than the bottom flange buckling capacity at the same locations which are equal to 45.6 and 39.1 ksi in the design calculations from Highway Structures Information System (HSI) [43].

7.14.3 Summary

Analytical models have been developed to evaluate the structural redundancy of Ramp WS over Zoo Interchange (Structure ID B40-786-Unit2) in the state of Wisconsin. The girders are presently classified as Fracture Critical Members. A full depth fracture, including both webs and the top and bottom flange was simulated at two different locations in the exterior girder. The analysis confirms that the bridge satisfies the performance requirements for both Redundancy I and Redundancy II load combinations based on the failure criteria developed in NCHRP 12-87a [5]. Hence, the girders need not be classified as Fracture Critical Members (FCMs).

7.15 B40-834 (3 Spans)

7.15.1 Background, geometry, and loading

The structural redundancy of Ramp TF (S–W) over IH 43/894 (Structure ID B40-834 in Figure 126) was evaluated for the case where one of the two twin-tub-girders fails due to an assumed sudden full-depth failure. In the analysis, the outside girder was assumed to have fractured.

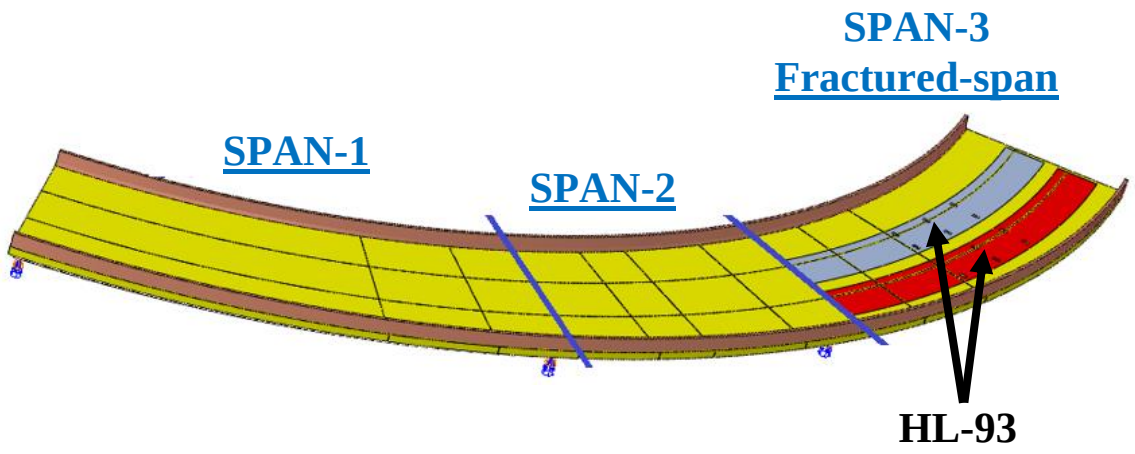

Figure 126 General Isometric View of B40-834

Table 75 provides details related to the geometry and material properties associated with the structure.

Table 75 The bridge geometry and material properties

Bridge Details	
Bridge Name	B40-834
Radius of Curvature	217.5 ft. (measured from bridge centerline)
Span Lengths	112.0 – 73.3 - 116.6 ft.
Girder Details	
Girder Steel	ASTM A709 HPS 50WF
Box Girder Width (from the centers of interior top-flange to the center of exterior top-flange)	9.0 ft.
Girders Spacing (from the centers of the girders' bottom flanges)	21.0 ft
Top Flange	18.0 in. wide Varies, 0.75 in. to 1.25 in. thick
Web	60 in. high 0.625 in. thick
Bottom Flange	81 in. wide Varies, 0.75 in. to 1.375 in. thick
Diaphragms	Two full depth diaphragms per span (3 bays)
Internal Cross Frames	2L6x4x1/2 (Top), 2L6x3-1/2x3/8 (Inclined)
Strut Braces	2L6x4x1/2
Lateral Braces	WT7x30.5, WT8x33.5, WT8x38.5, WT8x44.5, WT8x50
Longitudinal Stiffeners on Bottom Flanges	-
Deck Details	
Concrete Material Strength	4 ksi (HPC)
Composite Deck	41.896 ft. wide, 11 in. thick 3 in. haunch thick
Transverse Reinforcement	No. 6 rebar with 7 in. spacing
Longitudinal Reinforcement	No. 4 & No. 6 rebar with 6. in. spacing
Overhang Reinforcement	No. 4 rebar with 7 in. spacing
Shear Studs	8 in. height. Longitudinal spacing is 10 in. Three shear studs spaced equally in the transverse direction
Parapet Type	HF
Load Details	
Number of Lane	Two lanes traffic
Future Wearing Surface	-
Maximum Dead Load Displacement (before fracture)	L/350

Two different full-depth fractures were applied separately in each after-fracture performance analysis. Specifically, the tension flange, both webs, and both upper compression flanges were assumed to have failed in one of the girders for each scenario. The locations where the two fractures were assumed to have occurred is shown in Figure 127. The locations are as follows:

- Crack 1 (C1) just after 2nd (D2) intermediate diaphragm before 4th (S4A) exterior support,
- Crack 2 (C2) between 1st (D1) and 2nd (D2) intermediate diaphragms,
- Crack 3 (C3) between 1st (D1) and 2nd (D2) intermediate diaphragms on the interior girder.

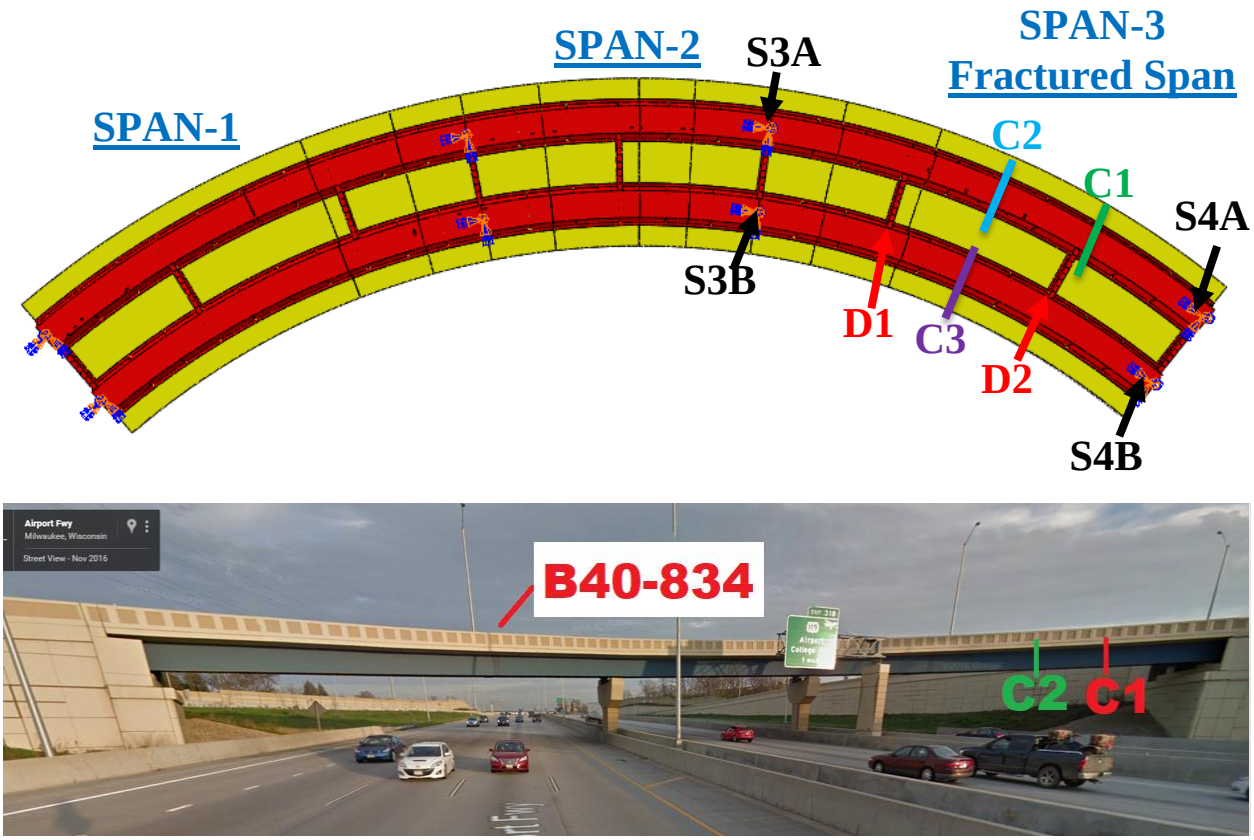

Figure 127 B40-834 Crack Locations

The Redundancy I and Redundancy II load combinations require different positioning of traffic live loads. For analyses where only a single lane of live load is applied for the Redundancy I load combination, the HL-93 live load was positioned in the center of the exterior design (i.e., striped) traffic lane. In cases where two lanes of live load were considered, the HL-93 live loads were

centered in the both design travel lanes. For the Redundancy II load combination, up to three HL-93 vehicular live loads were placed according to the procedure explained in Section 6.1.3. Full non-linear dynamic analysis was performed to determine the level of dynamic amplification that could be expected upon sudden failure of the tub girder. Based on this analysis, the dynamic amplification factor can conservatively be taken as 0.2 (i.e., 20%). Table 76 demonstrates the amount of total load applied in the Redundancy I (R1) and II (R2) load combinations.

Table 76 Total load applied on the fractured bridge

Type of Loading	**Dead Load (1.05 * DA_R)**	**Future Wearing Surface (1.05 * DA_R)**	**Live Load (0.85 * m * DA_R)**	**Total Load (DA_R)**
R1 1 HL-93	3720.00 (1.05 * 1.2)	- (1.05 * 1.2)	179.00 (0.85 * 1.2 * 1.2) 205.32 (15% More LL)	3900.00 3925.32 (15% More LL)
R1 2 HL-93	3720.00 (1.05 * 1.2)	- (1.05 * 1.2)	298.33 (0.85 * 1.0 * 1.2) 350.98 (15% More LL)	4018.33 4070.98 (15% More LL)

Type of Loading	**Dead Load (1.05)**	**Future Wearing Surface (1.05)**	**Live Load (1.3 * m)**	**Total Load**
R2 1 HL-93	3100.00 (1.05)	- (1.05)	244.98 (1.3 * 1.2) * (15% more per HS-20 impact) 268.54 (15% More LL)	3344.98 3368.54 (15% More LL)
R2 2 HL-93	3100.00 (1.05)	- (1.05)	408.30 (1.3 * 1.0) * (15% more per HS-20 impact) 455.42 (15% More LL)	3508.30 3555.42 (15% More LL)
R2 3 HL-93	3100.00 (1.05)	- (1.05)	520.59 (1.3 * 0.85) * (15% more per HS-20 impact) 591.26 (15% More LL)	3620.59 3691.26 (15% More LL)

7.15.2 Results for B40-834

The analysis has shown that Ramp TF (S–W) over IH 43/894 (Structure ID B40-834) possesses considerable reserve strength in the faulted state and that the steel twin-tub-girders do not meet the

definition of a fracture critical member when evaluated using the prescribed loading and failure criteria developed in NCHRP 12-87a [5]. Table 77 summarizes the results obtained from the redundancy analysis of the structure in faulted stage. The fracture case C2 was found to result in the most critical crack location, and hence the numerical values are presented in Table 77. The evaluation presents the results for the Redundancy I and II load combinations and compares the results to the minimum performance criteria discussed in CHAPTER 6.

Table 77 Results obtained for redundancy evaluation

Fracture Locations		**C1, C2**	
Load Combination		**Redundancy I**	**Redundancy II**
Max. Equivalent Plastic Strain in the Main Girder	**Value**	No plastic strain	0.001 (C1)
	Location	-	Very localized yielding Intermediate diaphragm "D2" flange
Concrete Crushing	**Extent**	No concrete crushing	No concrete crushing
	Location	-	-
Stud Failing	**Value**	No stud failure	No stud failure
	Location	-	-
Max. Vert. Reaction Force	**Value**	842 kips	913 kips
	Location	S3A (C2- 2HL-93)	S3A (C2 - 3HL-93)
Uplift at Supports	**Value**	No Uplift	
	Location		
Max. Hor. Displacement at Supports	**Value**	1.19 in.	1.81 in.
	Location	S4A (C2- 2HL-93)	S4A (C2 - 3HL-93)
Max. Vertical Deflection Change	**Value**	Not Applicable	2.2 in. (C2)

Notes:
- Design bearing capacity for strength is 1330 kips.
- Shear capacity of the deck is checked.

For both Redundancy I and Redundancy II, the structure has adequate redundancy after the fracture of an exterior girder using the criteria for the strength and displacement requirements discussed above. The following were observed:

- Insignificant plastic strain is not higher than 0.001 in D2's flange.
- Crushing does not occur in the concrete deck.
- No haunch separation or shear stud failure is observed.

- The maximum vertical deflection change (difference between before fracture and after fracture stages) is 2.2 inches which is lower than L/50 (28.1 inches) and the maximum change in cross-slope is below 5%.

Summary of the redundancy evaluation is shown in Table 78.

Table 78 Summary of Redundancy failure criteria evaluation

Performance Requirement		Most Critical Analysis Case	Result	Acceptable?
Strength Requirements	**Steel Primary Members**	C1. Redundancy II.	No component has strain larger than $5\varepsilon_y$ or 1%. Failure strain was not reached anywhere.	**YES**
	Concrete Crushing	-	No concrete crushing	**YES**
Serviceability Requirements	**Vertical Deflection Change**	C2. (Only Redundancy II DL considered).	Maximum deflection change is 2.2 in, which is lower than L/50 (28.1 in)	**YES**
	Cross-Slope Change	C2. (Only Redundancy II considered).	Maximum additional cross-slope is less than 5%.	**YES**
	Uplift	None.	No uplift.	**YES**

Notes:
- The analysis showed that the structure is capable of resisting an additional 15% of the applied factored live load.
- The horizontal displacement changes at support locations were lower than 6 in.

When the C2 crack location and three HL93 traffic loads were applied in the Redundancy II load combination, the maximum nominal longitudinal stresses at the bottom flange of the fractured girder at the pier and at the bottom flange section change closest to the pier are equal to 27.3 and 16.3 ksi, respectively. This is the most critical combination of loading and fracture location. This stress is lower than the bottom flange buckling capacity at the same locations which are equal to 37.2 and 17.3 ksi in the design calculations from Highway Structures Information System (HSI) [44]. For this bridge, the interior girder fracture was applied, and the maximum vertical displacement was equal to 1.0 in. This displacement was much lower than the case the exterior girder fracture (2.2 in).

7.15.3 Summary

Analytical models have been developed to evaluate the structural redundancy of Ramp TF (S–W) over IH 43/894 (Structure ID B40-834) in the state of Wisconsin. The girders are presently classified as Fracture Critical Members. A full depth fracture, including both webs and the top and bottom flange was simulated at two different locations in the exterior girder. The analysis confirms that the bridge satisfies the performance requirements for both Redundancy I and Redundancy II load combinations based on the failure criteria developed in NCHRP 12-87a [5]. Hence, the girders need not be classified as Fracture Critical Members (FCMs).

7.16 B40-837 (2 Spans)

7.16.1 Background, geometry, and loading

The structural redundancy of Ramp TH (S–W) over IH 43/894 (Structure ID B40-837 in Figure 128) was evaluated for the case where one of the two twin-tub-girders fails due to an assumed sudden full-depth failure. In the analysis, the outside girder was assumed to have fractured.

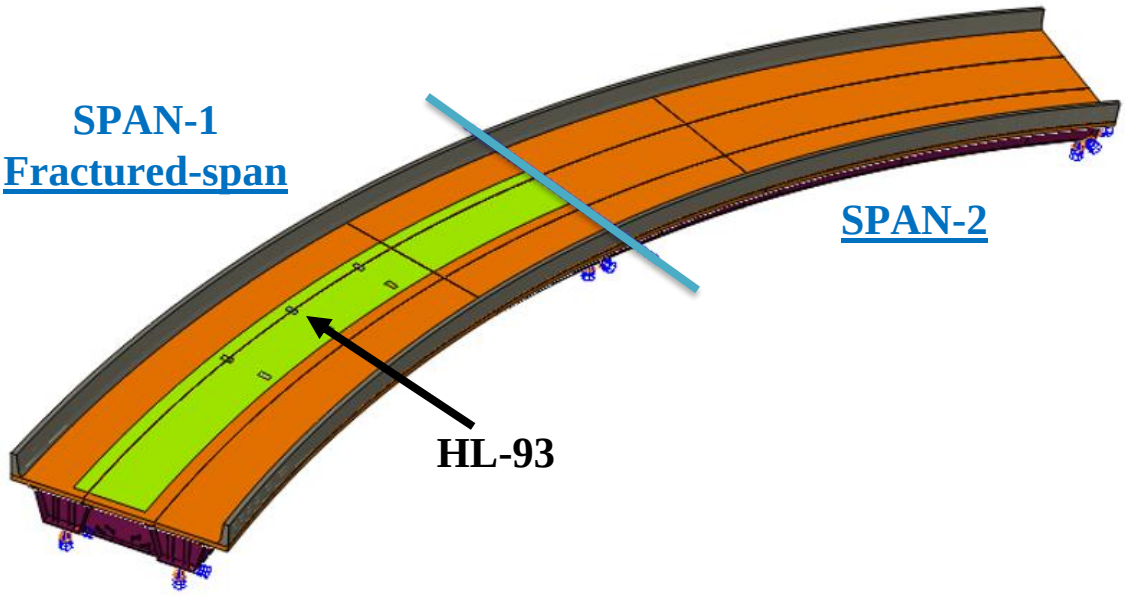

Figure 128 General Isometric View of B40-837

Table 79 provides details related to the geometry and material properties associated with the structure.

Table 79 The bridge geometry and material properties

Bridge Details	
Bridge Name	B40-837
Radius of Curvature	213.0 ft. (measured from bridge centerline)
Span Lengths	100.0 – 100.0 ft.
Girder Details	
Girder Steel	ASTM A709 HPS 50W
Box Girder Width (top flange center-to-center)	7.5 ft.
Girder Spacing (interior girder to exterior girder center)	16.0ft
Top Flange	16 in. wide 0.75 in. thick
Web	60 in. high 0.625 in. thick
Bottom Flange	63 in. wide Varies, 0.75 in. to 1.125 in. thick
Intermediate Diaphragms	Two full depth diaphragms
Internal Cross Frames	2L7x4x5/8 (Top), 2L6x3-1/2x1/2 (Inclined)
Strut Braces	2L7x4x5/8
Lateral Braces	WT7x30.5
Longitudinal Stiffeners on Bottom Flanges	-
Deck Details	
Concrete Material Strength	4 ksi (HPC)
Composite Deck	29.896 ft. wide, 9.5 in. thick 3 in. haunch thick
Transverse Reinforcement	No. 5 rebar with 7 in. spacing
Longitudinal Reinforcement	No. 4 & No. 6 rebar with 7 in. spacing
Overhang Reinforcement	No. 4 rebar with 7 in. spacing
Shear Studs	6 in. height. Longitudinal spacing is 9 in. Three shear studs spaced equally in the transverse direction
Parapet Type	HF
Load Details	
Number of Lane	Single lane of traffic
Future Wearing Surface	-
Maximum Dead Load Displacement (before fracture)	L/1250

Two different full-depth fractures were applied separately in each after-fracture performance analysis. Specifically, the tension flange, both webs, and both upper compression flanges were assumed to have failed in one of the girders for each scenario. The locations where the two fractures were assumed to have occurred is shown in Figure 146. The locations are as follows:

- Crack 1 (C1) just before 1st (D1) intermediate diaphragm after 1st (S1A) exterior support,
- Crack 2 (C2) between 1st (D1) and 2nd (D2) intermediate diaphragms.

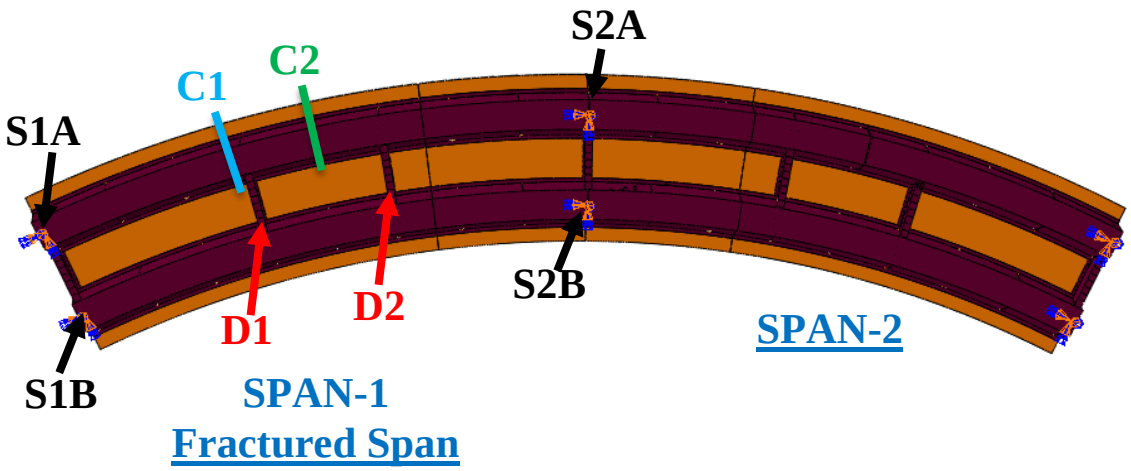

Figure 129 B40-837 Crack Locations

The Redundancy I and Redundancy II load combinations require different positioning of traffic live loads. For analyses where only a single lane of live load is applied for the Redundancy I load combination, the HL-93 live load was positioned in the center of the design (i.e., striped) traffic lane. For the Redundancy II load combination, up to two HL-93 vehicular live loads were placed according to the procedure explained in Section 6.1.3. Full non-linear dynamic analysis was performed to determine the level of dynamic amplification that could be expected upon sudden failure of the tub girder. Based on this analysis, the dynamic amplification factor can conservatively be taken as 0.2 (i.e., 20%). Table 80 demonstrates the amount of total load applied in the Redundancy I (R1) and II (R2) load combinations.

Table 80 Total load applied on the fractured bridge

Type of Loading	Dead Load (1.05 * DA_R)	Future Wearing Surface (1.05 * DA_R)	Live Load (0.85 * m * DA_R)	Total Load (DA_R)
R1 1 HL-93	1632.00 (1.05 * 1.2)	- (1.05 * 1.2)	166.46 (0.85 * 1.2 * 1.2) 190.94 (15% More LL)	1798.46 1822.94 (15% More LL)

Type of Loading	Dead Load (1.05)	Future Wearing Surface (1.05)	Live Load (1.3 * m)	Total Load
R2 1 HL-93	1360.00 (1.05)	- (1.05)	229.63 (1.3 * 1.2) * (15% more per HS-20 impact) 251.71 (15% More LL)	1589.63 1611.71 (15% More LL)
R2 2 HL-93	1360.00 (1.05)	- (1.05)	382.72 (1.3 * 1.0) * (15% more per HS-20 impact) 426.88 (15% More LL)	1742.72 1786.88 (15% More LL)

7.16.2 Results for B40-837

The analysis has shown that Ramp TH (S–W) over IH 43/894 (Structure ID B40-837) possesses considerable reserve strength in the faulted state and that the steel twin-tub-girders do not meet the definition of a fracture critical member when evaluated using the prescribed loading and failure criteria developed in NCHRP 12-87a [5]. Table 81 summarizes the results obtained from the redundancy analyses of the structure in faulted stages. The fracture case C2 was found to result in the most critical crack location, and hence the numerical values are presented in Table 81. The evaluation presents the results for the Redundancy I and II load combinations and compares the results to the minimum performance criteria discussed in CHAPTER 6.

Table 81 Results obtained for redundancy evaluation

Fracture Locations		**C1, C2**	
Load Combination		**Redundancy I**	**Redundancy II**
Max. Equivalent Plastic Strain in the Main Girder	**Value**	No plastic strain	No plastic strain
	Location	-	
Concrete Crushing	**Extent**	No concrete crushing	No concrete crushing
	Location	-	-
Stud Failing	**Value**	No stud failure	No stud failure
	Location	-	-
Max. Vert. Reaction Force	**Value**	596.7 kips	581.5 kips
	Location	S2B (C2 - 1HL-93)	S2B (C2 - 1HL-93)
Uplift at Supports	**Value**	No Uplift	
	Location		
Max. Hor. Displacement at Supports	**Value**	0.40 in.	0.48 in.
	Location	S1A (C2 - 1HL-93)	S1A (C2 - 2HL-93)
Max. Vertical Deflection Change	**Value**	Not Applicable	0.51 in. (C2)

Notes:
- Design bearing capacity for strength is 985 kips.
- Shear capacity of the deck is checked.

For both Redundancy I and Redundancy II, the structure has adequate redundancy after the fracture of an exterior girder using the criteria for the strength and displacement requirements discussed above. The following were observed:

- Plastic strain is not reached in the steel tub girder.
- Crushing does not occur in the concrete deck.
- No haunch separation or shear stud failure is observed.
- The maximum vertical deflection change (difference between before fracture and after fracture stages) is 0.51 inches which is lower than L/50 (24.0 inches) and the maximum change in cross-slope is below 5%.

A summary of the redundancy evaluation is shown in Table 82.

Table 82 Summary of Redundancy failure criteria evaluation

Performance Requirement		Most Critical Analysis Case	Result	Acceptable?
Strength Requirements	**Steel Primary Members**	-	No component has strain larger than $5\varepsilon_y$ or 1%. Failure strain was not reached anywhere.	**YES**
	Concrete Crushing	-	No concrete crushing	**YES**
Serviceability Requirements	**Vertical Deflection Change**	C2. (Only Redundancy II DL considered).	Maximum deflection change is 0.5 in, which is lower than L/50 (24.0 in)	**YES**
	Cross-Slope Change	C2. (Only Redundancy II considered).	Maximum additional cross-slope is less than 5%.	**YES**
	Uplift	None.	No uplift.	**YES**

Notes

- The analysis showed that the structure is capable of resisting an additional 15% of the applied factored live load.
- The horizontal displacement changes at support locations were lower than 6 in.

7.16.3 Summary

Analytical models have been developed to evaluate the structural redundancy of Ramp TH (S–W) over IH 43/894 (Structure ID B40-837) in the state of Wisconsin. The girders are presently classified as Fracture Critical Members. A full depth fracture, including both webs and the top and bottom flange was simulated at two different locations in the exterior girder. The analysis confirms that the bridge satisfies the performance requirements for both Redundancy I and Redundancy II load combinations based on the failure criteria developed in NCHRP 12-87a. [5] Hence, the girders need not be classified as Fracture Critical Members (FCMs).

7.17 B40-854-Unit1 (5 Spans)

7.17.1 Background, geometry, and loading

The structural redundancy of Ramp ES over Zoo Interchange (Structure ID B40-854-Unit1) was evaluated for the case where one of the two twin-tub-girders fails due to an assumed sudden full-depth failure. In the analysis, the outside girder was assumed to have fractured. The bridge is not symmetric; therefore, two analyses were performed to investigate fracture behavior. The first analysis considered Span 1 to the centerline of Span 3 "LF" (Figure 130) and the second analysis considered the centerline of Span 3 through Span 5 "RG" (Figure 131). As discussed in Section 3.3 only first two and half span needs to be modeled.

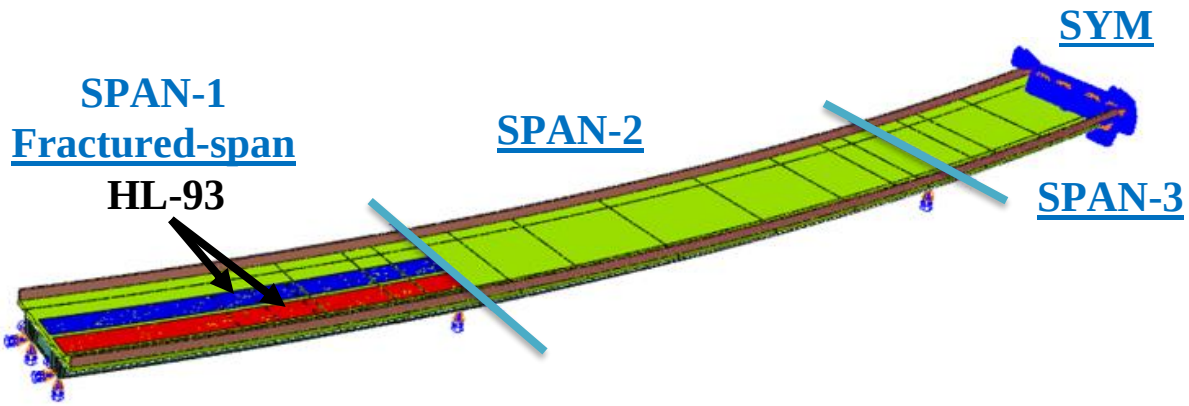

Figure 130 General Isometric View of B40-854-Unit1-LF (Span 1 to Half of Span 3)

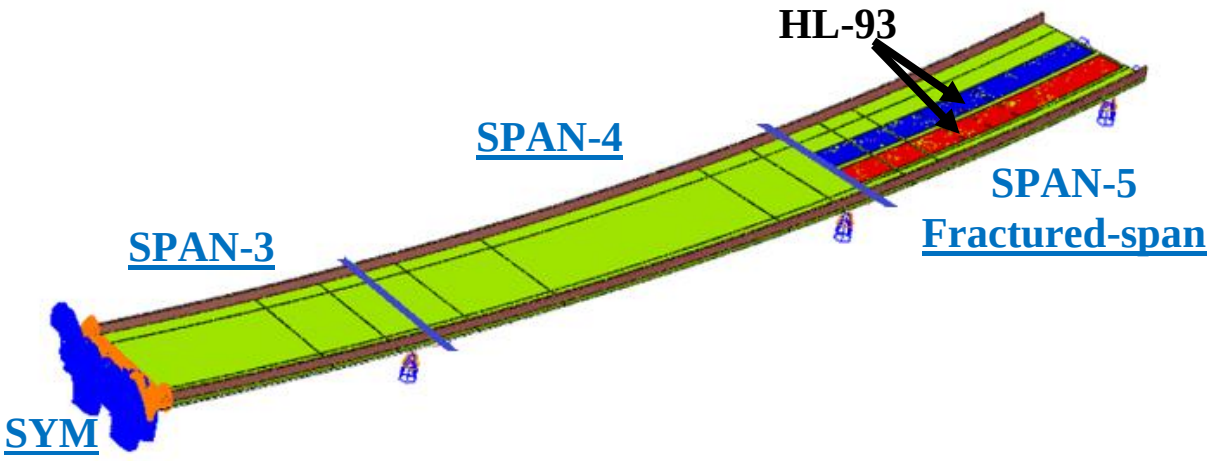

Figure 131 General Isometric View of B40-854-Unit1-RG (Half of Span 3 to Span 5)

Table 83 provides details related to the geometry and material properties associated with the structure.

Table 83 The bridge geometry and material properties

Bridge Details	
Bridge Name	B40-854-Unit1
Radius of Curvature	1493.75 ft. (measured from bridge centerline)
Span Lengths	LF: 146.0 - 225.0 - 112.5 ft. RG: 112.5 - 194.5 - 136.0 ft. Span 3 = 225.0/2 = 112.5
Girder Details	
Girder Steel	ASTM A709 HPS 50WF ASTM A709 HPS 70WF (Top Flanges)
Box Girder Width (from the centers of interior top-flange to the center of exterior top-flange)	9.5 ft.
Girders Spacing (from the centers of the girders' bottom flanges)	23.0 ft.
Top Flange	Varies, 20.0 in. to 28.0 in. wide Varies, 0.875 in. to 2.0 in. thick
Web	84 in. high, 0.6875 in. thick
Bottom Flange	75 in. wide Varies, 1.0 in. to 2.5 in. thick
Diaphragms	Two full depth diaphragms
Internal Cross Frames	L6x6x1/2 (Top), L6x6x1/2 (Inclined)
Strut Braces	L6x6x1/2
Lateral Braces	WT7x30.5, WT8x33.5
Longitudinal Stiffeners on Bottom Flanges	-
Deck Details	
Concrete Material Strength	4 ksi (HPC)
Composite Deck	44.896 ft. wide, 10.5 in. thick 4 in. haunch thick
Transverse Reinforcement	No. 6 rebar with 7 in. spacing
Longitudinal Reinforcement	No. 4 & No. 6 rebar with 6. in. spacing
Overhang Reinforcement	No. 4 rebar with 7 in. spacing
Shear Studs	8 in. height. Longitudinal spacing is 14 in. Three shear studs spaced equally in the transverse direction
Parapet Type	42SS (Interior) – 42SS (Exterior)
Load Details	
Number of Lane	Two lanes traffic
Future Wearing Surface	20 lb/ft^2
Maximum Dead Load Displacement	LF: L/1120 – RG: L/850

Four different full-depth fractures were applied separately in each after-fracture performance analysis. Specifically, the tension flange, both webs, and both upper compression flanges were assumed to have failed in one of the girders for each scenario. The locations where the four fractures were assumed to have occurred is shown in both Figure 132 and Figure 133. The locations are as follows:

- Crack 1 (C1) just before 1st (D1) intermediate diaphragm after 1st (S1A) exterior support,
- Crack 2 (C2) between 1st (D1) and 2nd (D2) intermediate diaphragms,
- Crack 3 (C3) between 3rd (D3) and 4th (D4) intermediate diaphragms,
- Crack 4 (C4) just after 4th (D4) intermediate diaphragm before 4th (S4A) exterior support.

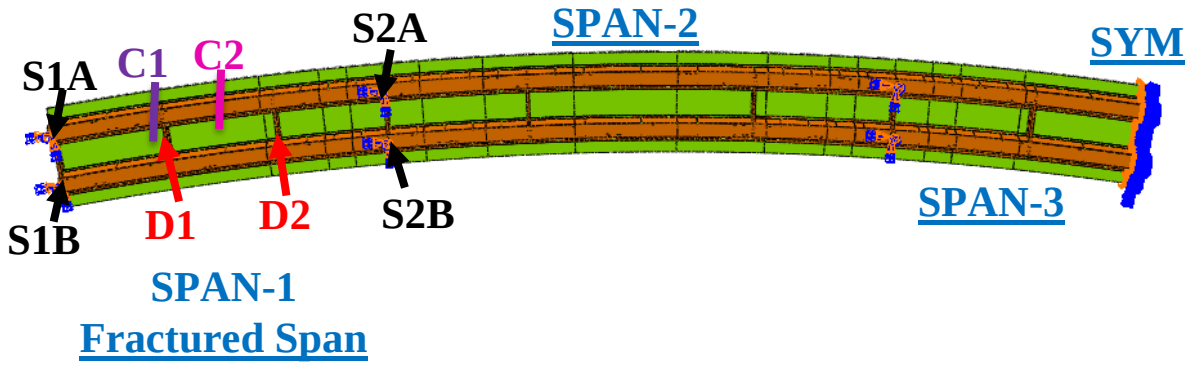

Figure 132 B40-854-Unit1-LF Crack Locations

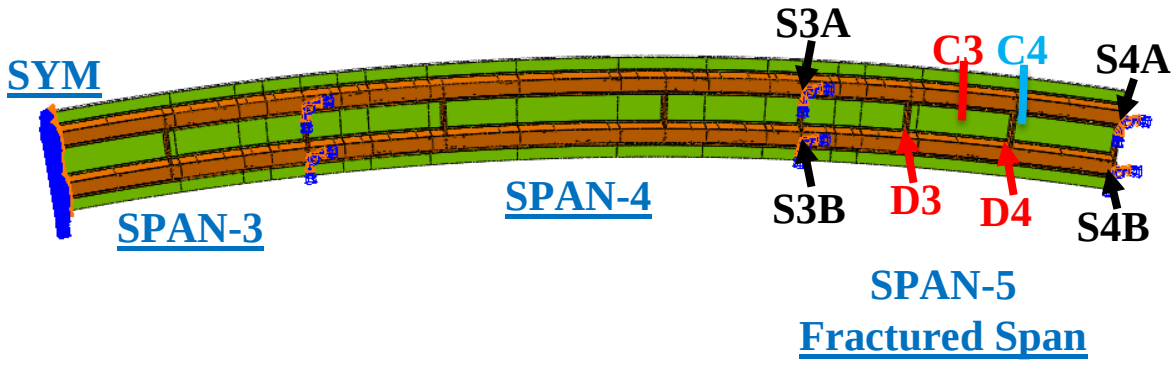

Figure 133 B40-854-Unit1-RG Crack Locations

The Redundancy I and Redundancy II load combinations require different positioning of traffic live loads. For analyses where only a single lane of live load is applied for the Redundancy I load

combination, the HL-93 live load was positioned in the center of the exterior design (i.e., striped) traffic lane. In cases where two lanes of live load were considered, the HL-93 live loads were centered in the both design travel lanes. For the Redundancy II load combination, up to three HL-93 vehicular live loads were placed according to the procedure explained in Section 6.1.3. Full non-linear dynamic analysis was performed to determine the level of dynamic amplification that could be expected upon sudden failure of the tub girder. Based on this analysis, the dynamic amplification factor can conservatively be taken as 0.2 (i.e., 20%). Table 84 demonstrates the amount of total load applied in the Redundancy I (R1) and II (R2) load combinations.

Table 84 Total load applied on the fractured bridge

Type of Loading	**Dead Load ($1.05 * DA_R$)**	**Future Wearing Surface ($1.05 * DA_R$)**	**Live Load ($0.85 * m * DA_R$)**	**Total Load (DA_R)**
R1 1 HL-93	6420.00 (LF) 5848.80 (RG) (1.05 * 1.2)	511.74 (LF) 468.87 (RG) (1.05 * 1.2)	202.50 (LF) 194.66 (RG) (0.85 * 1.2 * 1.2) 232.28 (LF) (15% More LL) 223.29 (RG) (15% More LL)	7134.23 (LF) 7164.01 (15% More LL) - 6512.34 (RG) 6540.96 (15% More LL)
R1 2 HL-93	6420.00 (LF) 5848.80 (RG) (1.05 * 1.2)	511.74 (LF) 468.87 (RG) (1.05 * 1.2)	337.50 (LF) 324.44 (RG) (0.85 * 1.0 * 1.2) 397.06 (LF) (15% More LL) 381.70 (RG) (15% More LL)	7269.23 (LF) 7328.79 (15% More LL) - 6642.11 (RG) 6699.37 (15% More LL)

Table 84 continued

Type of Loading	Dead Load (1.05)	Future Wearing Surface (1.05)	Live Load (1.3 * m)	Total Load
R2 1 HL-93	5350.00 (LF) 4874.00 (RG) (1.05)	426.45 (LF) 390.73 (RG) (1.05)	274.93 (LF) 264.95 (RG) (1.3 * 1.2) * (15% more per HS-20 impact) 301.37 (LF) (15% More LL) 290.43 (RG) (15% More LL)	6051.38 (LF) 6077.82 (15% More LL) - 5529.68 (RG) 5555.15 (15% More LL)
R2 2 HL-93	5350.00 (LF) 4874.00 (RG) (1.05)	426.45 (LF) 390.73 (RG) (1.05)	458.22 (LF) 441.58 (RG) (1.3 * 1.0) * (15% more per HS-20 impact) 511.10 (LF) (15% More LL) 492.54 (RG) (15% More LL)	6234.67 (LF) 6287.54 (15% More LL) - 5706.31 (RG) 5757.26 (15% More LL)
R2 3 HL-93	5350.00 (LF) 4874.00 (RG) (1.05)	426.45 (LF) 390.73 (RG) (1.05)	584.24 (LF) 563.02 (RG) (1.3 * 0.85) * (15% more per HS-20 impact) 663.54 (LF) (15% More LL) 639.45 (RG) (15% More LL)	6360.68 (LF) 6439.99 (15% More LL) - 5827.75 (RG) 5904.17 (15% More LL)

7.17.2 Results for B40-854-Unit1

The analysis has shown that Ramp ES over Zoo Interchange (Structure ID B40-854-Unit1) possesses considerable reserve strength in the faulted state and that the steel twin-tub-girders do not meet the definition of a fracture critical member when evaluated using the prescribed loading and failure criteria developed in NCHRP 12-87a [5]. Table 85 summarizes the results obtained from the redundancy analysis of the structure in faulted stage. The fracture case C3 was found to result in the most critical crack location, and hence the numerical values are presented in Table 85. The evaluation presents the results for the Redundancy I and II load combinations and compares the results to the minimum performance criteria discussed in CHAPTER 6.

Table 85 Results obtained for redundancy evaluation

Fracture Locations		**C1, C2, C3, C4**	
Load Combination		**Redundancy I**	**Redundancy II**
Max. Equivalent Plastic Strain in the Main Girder	**Value**	No plastic strain	No plastic strain
	Location	-	-
Concrete Crushing	**Extent**	No concrete crushing	No concrete crushing
	Location	-	-
Stud Failing	**Value**	No stud failure	No stud failure
	Location	-	-
Max. Vert. Reaction Force	**Value**	1570 kips (LF) 1420 kips (RG)	1529 kips (LF) 1359 kips (RG)
	Location	S2B (C2 - 2HL-93) S3A (C3 - 2HL-93)	S2A (C2 - 3HL-93) S3A (C3 - 3HL-93)
Uplift at Supports	**Value**	No Uplift	
	Location		
Max. Hor. Displacement at Supports	**Value**	0.92 in.	2.05 in.
	Location	S4A (C2 - 2HL-93)	S4A (C3 - 3HL-93)
Max. Vertical Deflection Change	**Value**	Not Applicable	0.70 in. (C2) (LF) 1.08 in. (C3) (RG)

Notes:
- Strength bearing capacities for strength are 2560 kips (LF) and 2290 kips (RG)
- Shear capacity of the deck is checked.

For both Redundancy I and Redundancy II, the structure has adequate redundancy after the fracture of an exterior girder using the criteria for the strength and displacement requirements discussed above. The following were observed:

- Plastic strain is not reached in the steel tub girders.
- Crushing does not occur in the concrete deck.
- No haunch separation or shear stud failure is observed.
- The maximum vertical deflection change (difference between before fracture and after fracture stages) is 1.08 inches which is lower than L/50 (32.64 inches) and the maximum change in cross-slope is below 5%.

Summary of the redundancy evaluation is shown in Table 86.

Table 86 Summary of Redundancy failure criteria evaluation

Performance Requirement		Most Critical Analysis Case	Result	Acceptable?
Strength Requirements	**Steel Primary Members**	-	No component has strain larger than $5\varepsilon_y$ or 1%. Failure strain was not reached anywhere.	**YES**
	Concrete Crushing	-	No concrete crushing	**YES**
Serviceability Requirements	**Vertical Deflection Change**	C3. (Only Redundancy II DL considered).	Maximum deflection change is 1.08 in, which is lower than L/50 (32.6 in)	**YES**
	Cross-Slope Change	C3. (Only Redundancy II considered).	Maximum additional cross-slope is less than 5%.	**YES**
	Uplift	None.	No uplift.	**YES**

Notes:

- The analysis showed that the structure is capable of resisting an additional 15% of the applied factored live load.
- The horizontal displacement changes at support locations were lower than 6 in.

7.17.3 Summary

Analytical models have been developed to evaluate the structural redundancy of Ramp ES over Zoo Interchange (Structure ID B40-854-Unit1) in the state of Wisconsin. The girders are presently classified as Fracture Critical Members. A full depth fracture, including both webs and the top and bottom flange was simulated at four different locations in the exterior girder. The analysis confirms that the bridge satisfies the performance requirements for both Redundancy I and Redundancy II load combinations based on the failure criteria developed in NCHRP 12-87a [5]. Hence, the girders need not be classified as Fracture Critical Members (FCMs).

7.18 B40-854-Unit2 (5 Spans)

7.18.1 Background, geometry, and loading

The structural redundancy of Ramp ES over Zoo Interchange (Structure ID B40-854-Unit2) was evaluated for the case where one of the two twin-tub-girders fails due to an assumed sudden full-depth failure. In the analysis, the outside girder was assumed to have fractured. The bridge is not symmetric; therefore, two analyses were performed to investigate fracture behavior. The first analysis considered Span 6 to the centerline of Span 8 "LF" (Figure 134) and the second analysis considered the centerline of Span 8 through Span 10 "RG" (Figure 135). As discussed in Section 3.3 only first two and half span needs to be modeled.

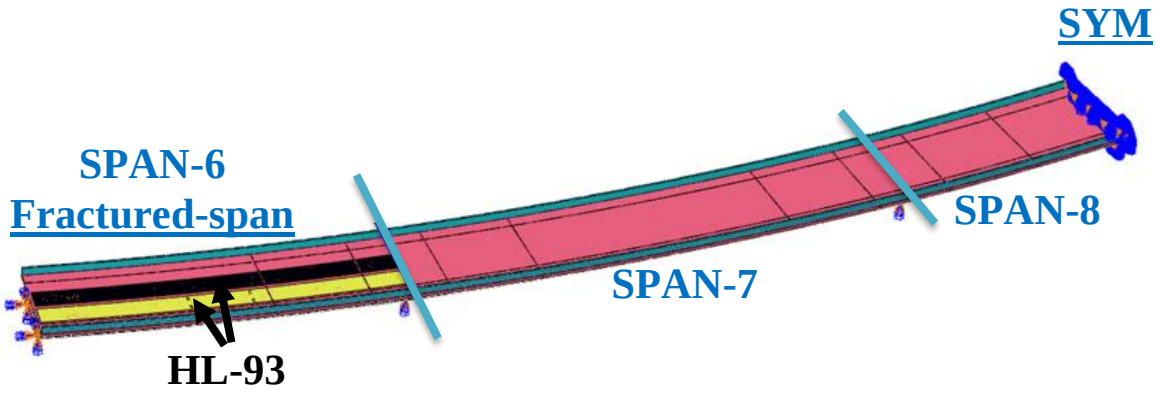

Figure 134 General Isometric View of B40-854-Unit2-LF (Span 6 to Half of Span 8)

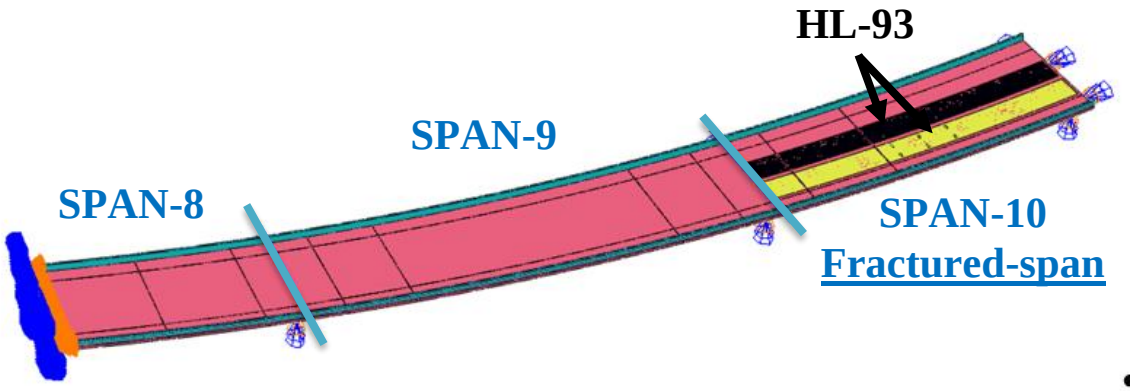

Figure 135 General Isometric View of B40-854-Unit2-RG (Half of Span 8 to Span 10)

Table 87 provides details related to the geometry and material properties associated with the structure.

Table 87 The bridge geometry and material properties

Bridge Details	
Bridge Name	B40-854-Unit2
Radius of Curvature	1493.75 ft. (measured from bridge centerline)
Span Lengths	LF: 164.5 - 235.0 - 109.0 ft. RG: 109.0 - 220.0 - 157.0 ft. Span 8 = 218.0/2 = 109.0
Girder Details	
Girder Steel	ASTM A709 HPS 50WF ASTM A709 HPS 70WF (Top Flanges)
Box Girder Width (from the centers of interior top-flange to the center of exterior top-flange)	9.5 ft.
Girders Spacing (from the centers of the girders' bottom flanges)	23.0 ft.
Top Flange	Varies, 20.0 in. to 28.0 in. wide Varies, 0.875 in. to 2.5 in. thick
Web	84 in. high, 0.6875 in. thick
Bottom Flange	75 in. wide Varies, 1.0 in. to 2.5 in. thick
Diaphragms	Two full depth diaphragms
Internal Cross Frames	L6x6x1/2 (Top), L6x6x1/2 (Inclined)
Strut Braces	L6x6x1/2
Lateral Braces	WT7x30.5
Longitudinal Stiffeners on Bottom Flanges	-
Deck Details	
Concrete Material Strength	4 ksi (HPC)
Composite Deck	44.896 ft. wide, 10.5 in. thick 4 in. haunch thick
Transverse Reinforcement	No. 6 rebar with 7 in. spacing
Longitudinal Reinforcement	No. 4 & No. 6 rebar with 6. in. spacing
Overhang Reinforcement	No. 4 rebar with 7 in. spacing
Shear Studs	8 in. height. Longitudinal spacing is 14 in. Three shear studs spaced equally in the transverse direction
Parapet Type	42SS (Interior) – 42SS (Exterior)
Load Details	
Number of Lane	Two lanes traffic
Future Wearing Surface	20 lb/ft^2
Maximum Dead Load Displacement	LF: L/685 – RG: L/680

Four different full-depth fractures were applied separately in each after-fracture performance analysis. Specifically, the tension flange, both webs, and both upper compression flanges were assumed to have failed in one of the girders for each scenario. The locations where the four fractures were assumed to have occurred is shown in both Figure 136 and Figure 137. The locations are as follows:

- Crack 1 (C1) just before 1st (D1) intermediate diaphragm after 1st (S1A) exterior support,
- Crack 2 (C2) between 1st (D1) and 2nd (D2) intermediate diaphragms,
- Crack 3 (C3) between 3rd (D3) and 4th (D4) intermediate diaphragms,
- Crack 4 (C4) just after 4th (D4) intermediate diaphragm before 4th (S4A) exterior support.

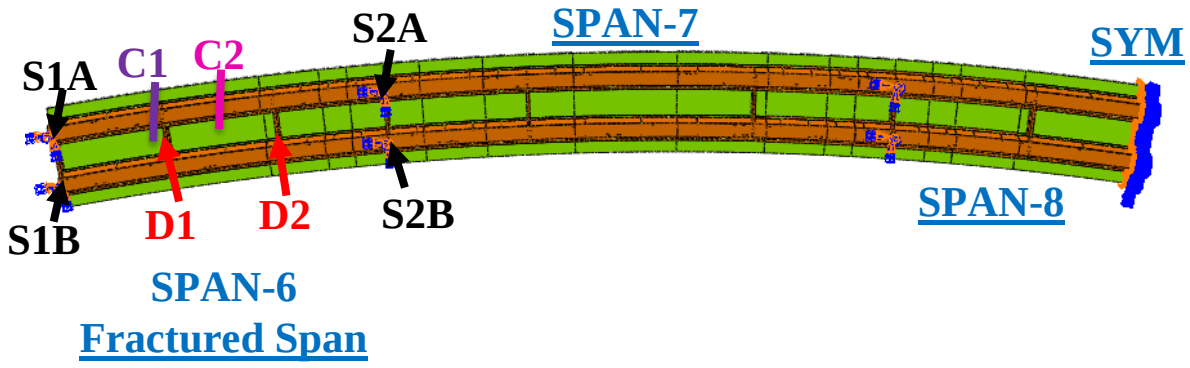

Figure 136 B40-854-Unit2-LF Crack Locations

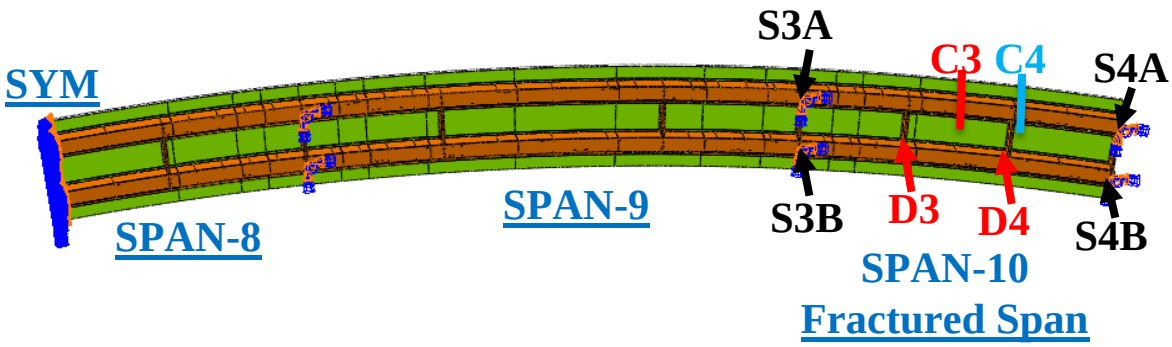

Figure 137 B40-854-Unit2-RG Crack Locations

The Redundancy I and Redundancy II load combinations require different positioning of traffic live loads. For analyses where only a single lane of live load is applied for the Redundancy I load combination, the HL-93 live load was positioned in the center of the exterior design (i.e., striped) traffic lane. In cases where two lanes of live load were considered, the HL-93 live loads were

centered in the both design travel lanes. For the Redundancy II load combination, up to three HL-93 vehicular live loads were placed according to the procedure explained in Section 6.1.3. Full non-linear dynamic analysis was performed to determine the level of dynamic amplification that could be expected upon sudden failure of the tub girder. Based on this analysis, the dynamic amplification factor can conservatively be taken as 0.2 (i.e., 20%). Table 88 demonstrates the amount of total load applied in the Redundancy I (R1) and II (R2) load combinations.

Table 88 Total load applied on the fractured bridge

Type of Loading	**Dead Load ($1.05 * DA_R$)**	**Future Wearing Surface ($1.05 * DA_R$)**	**Live Load ($0.85 * m * DA_R$)**	**Total Load (DA_R)**
R1 1 HL-93	6843.60 (LF) 6430.80 (RG) (1.05 * 1.2)	538.20 (LF) 514.38 (RG) (1.05 * 1.2)	216.99 (LF) 211.12 (RG) (0.85 * 1.2 * 1.2) 248.90 (LF) (15% More LL) 242.16 (RG) (15% More LL)	7598.79 (LF) 7630.70 (15% More LL) - 7156.30 (RG) 7187.34 (15% More LL)
R1 2 HL-93	6843.60 (LF) 6430.80 (RG) (1.05 * 1.2)	538.20 (LF) 514.38 (RG) (1.05 * 1.2)	361.65 (LF) 351.86 (RG) (0.85 * 1.0 * 1.2) 425.47 (LF) (15% More LL) 413.95 (RG) (15% More LL)	7743.45 (LF) 7807.27 (15% More LL) - 7297.04 (RG) 7359.13 (15% More LL)

Table 88 continued

Type of Loading	Dead Load (1.05)	Future Wearing Surface (1.05)	Live Load (1.3 * m)	Total Load
R2 1 HL-93	5703.00 (LF) 5359.00 (RG) (1.05)	448.50 (LF) 428.65 (RG) (1.05)	293.40 (LF) 285.92 (RG) (1.3 * 1.2) * (15% more per HS-20 impact) 321.62 (LF) (15% More LL) 313.41 (RG) (15% More LL)	6444.90 (LF) 6473.11 (15% More LL) - 6073.57 (RG) 6101.06 (15% More LL)
R2 2 HL-93	5703.00 (LF) 5359.00 (RG) (1.05)	448.50 (LF) 428.65 (RG) (1.05)	489.01 (LF) 476.53 (RG) (1.3 * 1.0) * (15% more per HS-20 impact) 545.43 (LF) (15% More LL) 531.51 (RG) (15% More LL)	6640.51 (LF) 6696.93 (15% More LL) - 6264.18 (RG) 6319.16 (15% More LL)
R2 3 HL-93	5703.00 (LF) 5359.00 (RG) (1.05)	448.50 (LF) 428.65 (RG) (1.05)	623.49 (LF) 607.57 (RG) (1.3 * 0.85) * (15% more per HS-20 impact) 708.12 (LF) (15% More LL) 690.05 (RG) (15% More LL)	6774.98 (LF) 6859.62 (15% More LL) - 6395.23 (RG) 6477.70 (15% More LL)

7.18.2 Results for B40-854-Unit2

The analysis has shown that Ramp ES over Zoo Interchange (Structure ID B40-854-Unit2) possesses considerable reserve strength in the faulted state and that the steel twin-tub-girders do not meet the definition of a fracture critical member when evaluated using the prescribed loading and failure criteria developed in NCHRP 12-87a [5]. Table 89 summarizes the results obtained from the redundancy analysis of the structure in faulted stage. The fracture case C3 was found to result in the most critical crack location, and hence the numerical values are presented in Table 89.

The evaluation presents the results for the Redundancy I and II load combinations and compares the results to the minimum performance criteria discussed in CHAPTER 6.

Table 89 Results obtained for redundancy evaluation

Fracture Locations		**C1, C2, C3, C4**	
Load Combination		**Redundancy I**	**Redundancy II**
Max. Equivalent Plastic Strain in the Main Girder	**Value**	No plastic strain	No plastic strain
	Location	-	-
Concrete Crushing	**Extent**	No concrete crushing	No concrete crushing
	Location	-	-
Stud Failing	**Value**	No stud failure	No stud failure
	Location	-	-
Max. Vert. Reaction Force	**Value**	1816 kips (LF) 1645 kips (RG)	1862 kips (LF) 1774 kips (RG)
	Location	S2B (C2 - 2HL-93) S3B (C3 - 2HL-93)	S2A (C2 - 3HL-93) S3A (C3 - 3HL-93)
Uplift at Supports	**Value**	No Uplift	
	Location		
Max. Hor. Displacement at Supports	**Value**	2.58 in.	3.76 in.
	Location	S4A (C3 - 2HL-93)	S4A (C3 - 3HL-93)
Max. Vertical Deflection Change	**Value**	Not Applicable	1.88 in. (C2) (LF) 2.16 in. (C3) (RG)

Notes:
- Strength bearing capacities for strength are 2830 kips (LF) and 2640 kips (RG)
- Shear capacity of the deck is checked.

For both Redundancy I and Redundancy II, the structure has adequate redundancy after the fracture of an exterior girder using the criteria for the strength and displacement requirements discussed above. The following were observed:

- Plastic strain is not reached in the steel tub girders.
- Crushing does not occur in the concrete deck.
- No haunch separation or shear stud failure is observed.
- The maximum vertical deflection change (difference between before fracture and after fracture stages) is 2.16 inches which is lower than L/50 (37.68 inches) and the maximum change in cross-slope is below 5%.

Summary of the redundancy evaluation is shown in Table 90.

Table 90 Summary of Redundancy failure criteria evaluation

Performance Requirement		Most Critical Analysis Case	Result	Acceptable?
Strength Requirements	**Steel Primary Members**	-	No component has strain larger than $5\varepsilon_y$ or 1%. Failure strain was not reached anywhere.	**YES**
	Concrete Crushing	-	No concrete crushing	**YES**
Serviceability Requirements	**Vertical Deflection Change**	C3. (Only Redundancy II DL considered).	Maximum deflection change is 2.2 in, which is lower than L/50 (37.7 in)	**YES**
	Cross-Slope Change	C3. (Only Redundancy II considered).	Maximum additional cross-slope is less than 5%.	**YES**
	Uplift	None.	No uplift.	**YES**

Notes:

- The analysis showed that the structure is capable of resisting an additional 15% of the applied factored live load.
- The horizontal displacement changes at support locations were lower than 6 in.

7.18.3 Summary

Analytical models have been developed to evaluate the structural redundancy of Ramp ES over Zoo Interchange (Structure ID B40-854-Unit2) in the state of Wisconsin. The girders are presently classified as Fracture Critical Members. A full depth fracture, including both webs and the top and bottom flange was simulated at four different locations in the exterior girder. The analysis confirms that the bridge satisfies the performance requirements for both Redundancy I and Redundancy II load combinations based on the failure criteria developed in NCHRP 12-87a [5]. Hence, the girders need not be classified as Fracture Critical Members (FCMs).

7.19 B40-854-Unit3 (3 Spans)

7.19.1 Background, geometry, and loading

The structural redundancy of Ramp ES over Zoo Interchange (Structure ID B40-854-Unit3 in Figure 138) was evaluated for the case where one of the two twin-tub-girders fails due to an assumed sudden full-depth failure. In the analysis, the outside girder was assumed to have fractured. The bridge is symmetric about the center of its midspan. In addition, the bridge is a new structure. Figure 139 shows that B40-854 was under construction in October 2016.

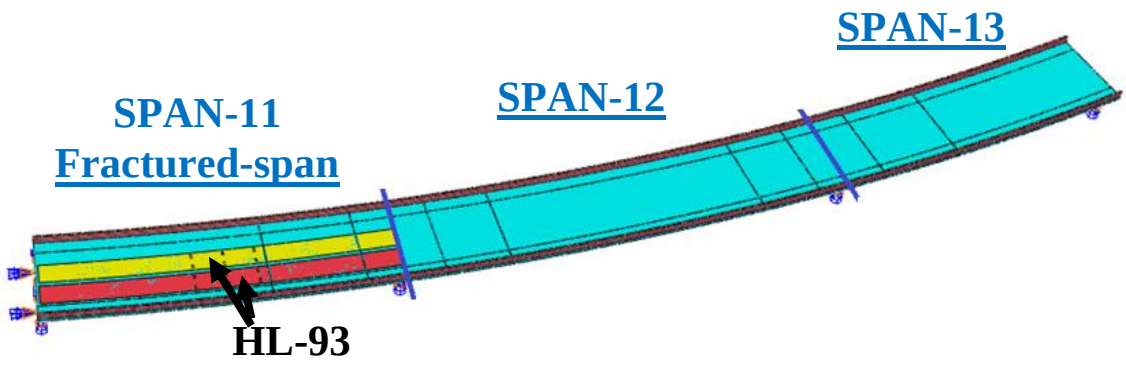

Figure 138 General Isometric View of B40-854-Unit3

Figure 139 B40-854 under construction in October 2016

Table 91 provides details related to the geometry and material properties associated with the structure.

Table 91 The bridge geometry and material properties

Bridge Details	
Bridge Name	B40-854-Unit3
Radius of Curvature	1493.75 ft. (measured from bridge centerline)
Span Lengths	157.0 - 220.0 - 157.2 ft.
Girder Details	
Girder Steel	ASTM A709 HPS 50WF ASTM A709 HPS 70WF (Top Flanges)
Box Girder Width (from the centers of interior top-flange to the center of exterior top-flange)	9.5 ft.
Girders Spacing (from the centers of the girders' bottom flanges)	23.0 ft.
Top Flange	Varies, 20.0 in. to 24.0 in. wide Varies, 0.875 in. to 2.0 in. thick
Web	84 in. high, 0.6875 in. thick
Bottom Flange	75 in. wide Varies, 1.0 in. to 2.25 in. thick
Diaphragms	Two full depth diaphragms
Internal Cross Frames	L6x6x1/2 (Top), L6x6x1/2 (Inclined)
Strut Braces	L6x6x1/2
Lateral Braces	WT7x30.5
Longitudinal Stiffeners on Bottom Flanges	-
Deck Details	
Concrete Material Strength	4 ksi (HPC)
Composite Deck	44.896 ft. wide, 10.5 in. thick 4 in. haunch thick
Transverse Reinforcement	No. 6 rebar with 7 in. spacing
Longitudinal Reinforcement	No. 4 & No. 6 rebar with 6. in. spacing
Overhang Reinforcement	No. 4 rebar with 7 in. spacing
Shear Studs	8 in. height. Longitudinal spacings are 14 to 16 in. Three shear studs spaced equally in the transverse direction
Parapet Type	42SS (Interior) – 42SS (Exterior)
Load Details	
Number of Lane	Two lanes traffic
Future Wearing Surface	20 lb/ft^2
Maximum Dead Load Displacement (before fracture)	L/750

Two different full-depth fractures were applied separately in each after-fracture performance analysis. Specifically, the tension flange, both webs, and both upper compression flanges were assumed to have failed in one of the girders for each scenario. The locations where the two fractures were assumed to have occurred is shown in Figure 140. The locations are as follows:

- Crack 1 (C1) just before 1st (D1) intermediate diaphragm after 1st (S1A) exterior support,
- Crack 2 (C2) between 1st (D1) and 2nd (D2) intermediate diaphragms.

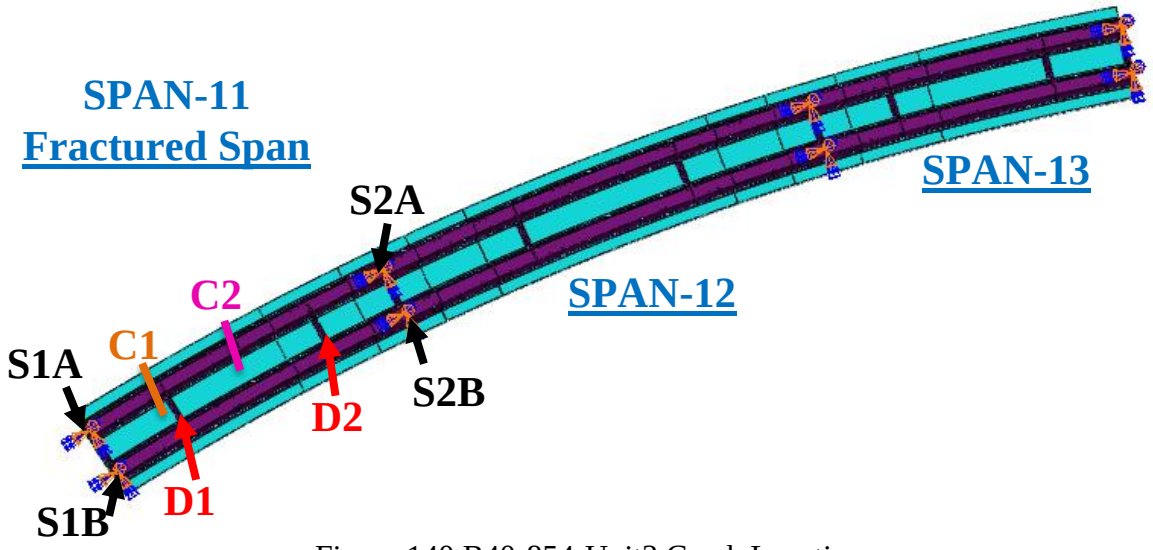

Figure 140 B40-854-Unit3 Crack Locations

The Redundancy I and Redundancy II load combinations require different positioning of traffic live loads. For analyses where only a single lane of live load is applied for the Redundancy I load combination, the HL-93 live load was positioned in the center of the exterior design (i.e., striped) traffic lane. In cases where two lanes of live load were considered, the HL-93 live loads were centered in the both design travel lanes. For the Redundancy II load combination, up to three HL-93 vehicular live loads were placed according to the procedure explained in Section 6.1.3. Full non-linear dynamic analysis was performed to determine the level of dynamic amplification that could be expected upon sudden failure of the tub girder. Based on this analysis, the dynamic amplification factor can conservatively be taken as 0.2 (i.e., 20%). Table 92 demonstrates the amount of total load applied in the Redundancy I (R1) and II (R2) load combinations.

Table 92 Total load applied on the fractured bridge

Type of Loading	Dead Load (1.05 * DA_R)	Future Wearing Surface (1.05 * DA_R)	Live Load (0.85 * m * DA_R)	Total Load (DA_R)
R1 1 HL-93	7057.20 (1.05 * 1.2)	565.19 (1.05 * 1.2)	211.12 (0.85 * 1.2 * 1.2) 242.16 (15% More LL)	7833.50 7864.55 (15% More LL)
R1 2 HL-93	7057.20 (1.05 * 1.2)	565.19 (1.05 * 1.2)	351.86 (0.85 * 1.0 * 1.2) 413.95 (15% More LL)	7974.24 8036.34 (15% More LL)

Type of Loading	Dead Load (1.05)	Future Wearing Surface (1.05)	Live Load (1.3 * m)	Total Load
R2 1 HL-93	5881.00 (1.05)	470.99 (1.05)	285.92 (1.3 * 1.2) * (15% more per HS-20 impact) 313.41 (15% More LL)	6637.90 6665.40 (15% More LL)
R2 2 HL-93	5881.00 (1.05)	470.99 (1.05)	476.53 (1.3 * 1.0) * (15% more per HS-20 impact) 531.51 (15% More LL)	6828.52 6883.50 (15% More LL)
R2 3 HL-93	5881.00 (1.05)	470.99 (1.05)	607.57 (1.3 * 0.85) * (15% more per HS-20 impact) 690.05 (15% More LL)	6959.56 7042.04 (15% More LL)

7.19.2 Results for B40-854-Unit3

The analysis has shown that Ramp ES over Zoo Interchange (Structure ID B40-854-Unit3) possesses considerable reserve strength in the faulted state and that the steel twin-tub-girders do not meet the definition of a fracture critical member when evaluated using the prescribed loading and failure criteria developed in NCHRP 12-87a [5]. Table 93 summarizes the results obtained from the redundancy analysis of the structure in faulted stage. The fracture case C2 was found to result in the most critical crack location, and hence the numerical values are presented in Table 93. The evaluation presents the results for the Redundancy I and II load combinations and compares the results to the minimum performance criteria discussed in CHAPTER 6.

Table 93 Results obtained for redundancy evaluation

Fracture Locations		**C1, C2**	
Load Combination		**Redundancy I**	**Redundancy II**
Max. Equivalent Plastic Strain in the Main Girder	**Value**	No plastic strain	No plastic strain
	Location	-	-
Concrete Crushing	**Extent**	No concrete crushing	No concrete crushing
	Location	-	-
Stud Failing	**Value**	No stud failure	No stud failure
	Location	-	-
Max. Vert. Reaction Force	**Value**	1690 kips	1591 kips
	Location	S2A (C2 - 2HL-93)	S2A (C2 - 3HL-93)
Uplift at Supports	**Value**	No Uplift	
	Location		
Max. Hor. Displacement at Supports	**Value**	1.33 in.	1.85 in.
	Location	S1A (C2 - 2HL-93)	S1A (C2 - 3HL-93)
Max. Vertical Deflection Change	**Value**	Not Applicable	1.20 in. (C2)

Notes:
- Strength bearing capacities for strength is 2640 kips.
- Shear capacity of the deck is checked.

For both Redundancy I and Redundancy II, the structure has adequate redundancy after the fracture of an exterior girder using the criteria for the strength and displacement requirements discussed above. The following were observed:

- Plastic strain is not reached in the steel tub girders.
- Crushing does not occur in the concrete deck.
- No haunch separation or shear stud failure is observed.
- The maximum vertical deflection change (difference between before fracture and after fracture stages) is 1.20 inches which is lower than L/50 (37.68 inches) and the maximum change in cross-slope is below 5%.

Summary of the redundancy evaluation is shown in Table 94.

Table 94 Summary of Redundancy failure criteria evaluation

Performance Requirement		Most Critical Analysis Case	Result	Acceptable?
Strength Requirements	**Steel Primary Members**	-	No component has strain larger than $5\varepsilon_y$ or 1%. Failure strain was not reached anywhere.	**YES**
	Concrete Crushing	-	No concrete crushing	**YES**
Serviceability Requirements	**Vertical Deflection Change**	C2. (Only Redundancy II DL considered).	Maximum deflection change is 1.2 in, which is lower than L/50 (37.7 in)	**YES**
	Cross-Slope Change	C2. (Only Redundancy II considered).	Maximum additional cross-slope is less than 5%.	**YES**
	Uplift	None.	No uplift.	**YES**

Notes:

- The analysis showed that the structure is capable of resisting an additional 15% of the applied factored live load.
- The horizontal displacement changes at support locations were lower than 6 in.

7.19.3 Summary

Analytical models have been developed to evaluate the structural redundancy of Ramp ES over Zoo Interchange (Structure ID B40-854-Unit3) in the state of Wisconsin. The girders are presently classified as Fracture Critical Members. A full depth fracture, including both webs and the top and bottom flange was simulated at two different locations in the exterior girder. The analysis confirms that the bridge satisfies the performance requirements for both Redundancy I and Redundancy II load combinations based on the failure criteria developed in NCHRP 12-87a [5]. Hence, the girders need not be classified as Fracture Critical Members (FCMs).

7.20 B40-856-Unit2 (6 Spans)

7.20.1 Background, geometry, and loading

The structural redundancy of Ramp WN over Zoo Interchange (Structure ID B40-856-Unit2) was evaluated for the case where one of the two twin-tub-girders fails due to an assumed sudden full-depth failure. In the analysis, the outside girder was assumed to have fractured. The bridge is not symmetric; therefore, two analyses were performed to investigate fracture behavior. The first analysis considered Span 8 to the centerline of Span 10 "LF" (Figure 141) and the second analysis considered the centerline of Span 11 through Span 13 "RG" (Figure 142). As discussed in Section 3.3 only first two and half span needs to be modeled.

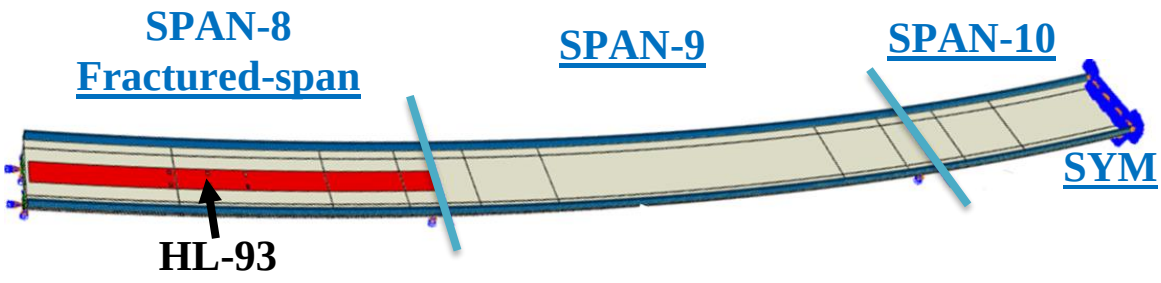

Figure 141 General Isometric View of B40-856-Unit2-LF (Span 8 to Half of Span 10)

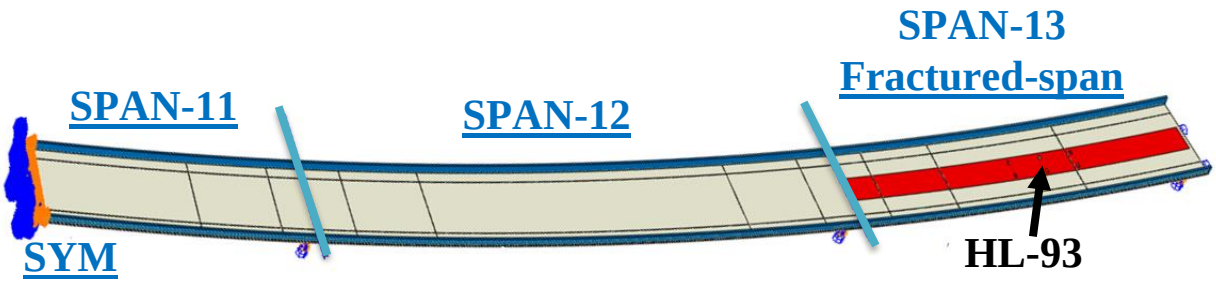

Figure 142 General Isometric View of B40-856-Unit2-RG (Half of Span 11 to Span 13)

Table 95 provides details related to the geometry and material properties associated with the structure.

Table 95 The bridge geometry and material properties

Bridge Details	
Bridge Name	B40-856-Unit2
Radius of Curvature	1401.5 ft. (measured from bridge centerline)
Span Lengths	LF: 151.0 - 220.0 - 110.0 ft. RG: 100.0 - 200.0 - 160.0 ft. Span 10 = 220.0/2 = 110.0 Span 11 = 200.0/ = 100.0
Girder Details	
Girder Steel	ASTM A709 HPS 50WF
Box Girder Width (from the centers of interior top-flange to the center of exterior top-flange)	8.0 ft.
Girders Spacing (from the centers of the girders' bottom flanges)	17.0 ft.
Top Flange	Varies, 20.0 in. to 26.0 in. wide Varies, 1.0 in. to 2.25 in. thick
Web	84 in. high Varies, 0.625 in. to 0.6875 in. thick
Bottom Flange	57 in. wide, Varies, 0.75 in. to 2.25 in. thick
Diaphragms	Two full depth diaphragms
Internal Cross Frames	L6x6x3/8 (Top), L6x6x1/2 (Inclined)
Strut Braces	L6x6x3/8
Lateral Braces	WT7x30.5
Longitudinal Stiffeners on Bottom Flanges	-
Deck Details	
Concrete Material Strength	4 ksi (HPC)
Composite Deck	33.896 ft. wide, 9.0 in. thick 4 in. haunch thick
Transverse Reinforcement	No. 5 rebar with 7 in. spacing
Longitudinal Reinforcement	No. 4 & No. 6 rebar with 7.5. in. spacing
Overhang Reinforcement	No. 4 rebar with 7.5. in. spacing
Shear Studs	6 in. height. Longitudinal spacing is 12 in. Three shear studs spaced equally in the transverse direction
Parapet Type	42SS (Interior) – 42SS (Exterior)
Load Details	
Number of Lane	One lane traffic
Future Wearing Surface	20 lb/ft^2
Maximum Dead Load Displacement	LF: L/880 – RG: L/550

Four different full-depth fractures were applied separately in each after-fracture performance analysis. Specifically, the tension flange, both webs, and both upper compression flanges were assumed to have failed in one of the girders for each scenario. The locations where the four fractures were assumed to have occurred is shown in both Figure 143 and Figure 144. The locations are as follows:

- Crack 1 (C1) just before 1st (D1) intermediate diaphragm after 1st (S1A) exterior support,
- Crack 2 (C2) between 1st (D1) and 2nd (D2) intermediate diaphragms,
- Crack 3 (C3) between 3rd (D3) and 4th (D4) intermediate diaphragms,
- Crack 4 (C4) just after 4th (D4) intermediate diaphragm before 4th (S4A) exterior support.

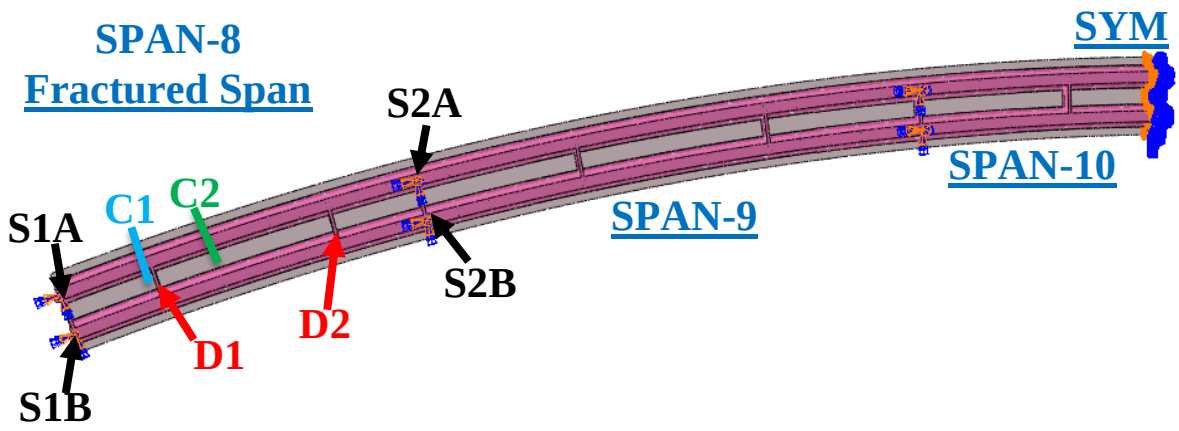

Figure 143 B40-856-Unit2-LF Crack Locations

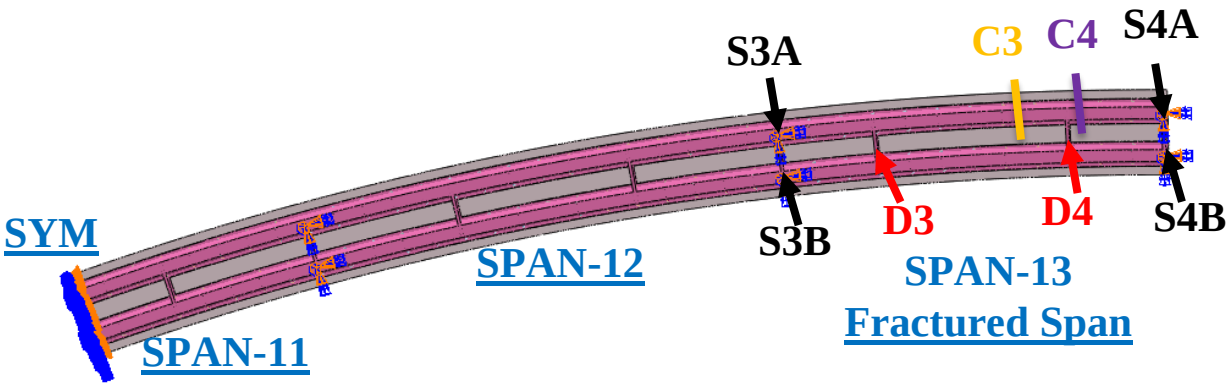

Figure 144 B40-856-Unit2-RG Crack Locations

The Redundancy I and Redundancy II load combinations require different positioning of traffic live loads. For analyses where only a single lane of live load is applied for the Redundancy I load combination, the HL-93 live load was positioned in the center of the exterior design (i.e., striped) traffic lane. In cases where two lanes of live load were considered, the HL-93 live loads were centered in the both design travel lanes. For the Redundancy II load combination, up to three HL-93 vehicular live loads were placed according to the procedure explained in Section 6.1.3. Full non-linear dynamic analysis was performed to determine the level of dynamic amplification that could be expected upon sudden failure of the tub girder. Based on this analysis, the dynamic amplification factor can conservatively be taken as 0.2 (i.e., 20%). Table 96 demonstrates the amount of total load applied in the Redundancy I (R1) and II (R2) load combinations.

Table 96 Total load applied on the fractured bridge

Type of Loading	**Dead Load (1.05 * DA_R)**	**Future Wearing Surface (1.05 * DA_R)**	**Live Load (0.85 * m * DA_R)**	**Total Load (DA_R)**
R1 1 HL-93	4644.00 (LF) 4452.00 (RG) (1.05 * 1.2)	374.98 (LF) 359.35 (RG) (1.05 * 1.2)	205.63 (LF) 213.47 (RG) (0.85 * 1.2 * 1.2) 235.87 (LF) (15% LL) 244.86 (RG) (15% LL)	5224.61 (LF) 5254.85 (15% More LL) - 5024.82 (RG) 5056.21 (15% More LL)

Type of Loading	**Dead Load (1.05)**	**Future Wearing Surface (1.05)**	**Live Load (1.3 * m)**	**Total Load**
R2 1 HL-93	3870.00 (LF) 3710.00 (RG) (1.05)	312.48 (LF) 299.46 (RG) (1.05)	278.93 (LF) 288.91 (RG) (1.3 * 1.2) * (15% more per HS-20 impact) 305.75 (LF) (15% LL) 316.69 (RG) (15% LL)	4461.41 (LF) 4488.23 (15% More LL) - 4298.37 (RG) 4326.15 (15% More LL)
R2 2 HL-93	3870.00 (LF) 3710.00 (RG) (1.05)	312.48 (LF) 299.46 (RG) (1.05)	464.88 (LF) 481.52 (RG) (1.3 * 1.0) * (15% more per HS-20 impact) 518.52 (LF) (15% LL) 537.08 (RG) (15% LL)	4647.36 (LF) 4701.00 (15% More LL) - 4490.98 (RG) 4546.54 (15% More LL)

7.20.2 Results for B40-856-Unit2

The analysis has shown that Ramp WN over Zoo Interchange (Structure ID B40-856-Unit2) possesses considerable reserve strength in the faulted state and that the steel twin-tub-girders do not meet the definition of a fracture critical member when evaluated using the prescribed loading and failure criteria developed in NCHRP 12-87a [5]. Table 97 summarizes the results obtained from the redundancy analysis of the structure in faulted stage. The fracture case C3 was found to result in the most critical crack location, and hence the numerical values are presented in Table 97. The evaluation presents the results for the Redundancy I and II load combinations and compares the results to the minimum performance criteria discussed in CHAPTER 6.

Table 97 Results obtained for redundancy evaluation

Fracture Locations		**C1, C2, C3, C4**	
Load Combination		**Redundancy I**	**Redundancy II**
Max. Equivalent Plastic Strain in the Main Girder	**Value**	No plastic strain	No plastic strain
	Location	-	-
Concrete Crushing	**Extent**	No concrete crushing	No concrete crushing
	Location	-	-
Stud Failing	**Value**	No stud failure	No stud failure
	Location	-	-
Max. Vert. Reaction Force	**Value**	1187 kips (LF) 1169 kips (RG)	1179 kips (LF) 1165 kips (RG)
	Location	S2B (C2 - 1HL-93) S3B (C3 - 1HL-93)	S2A (C2 - 2HL-93) S3A (C3 - 2HL-93)
Uplift at Supports	**Value**	No Uplift	
	Location		
Max. Hor. Displacement at Supports	**Value**	2.28 in.	3.37 in.
	Location	S4A (C3 - 1HL-93)	S4A (C3 - 2HL-93)
Max. Vertical Deflection Change	**Value**	Not Applicable	1.68 in. (C2) (LF) 2.47 in. (C2) (RG)

Notes
- Strength bearing capacities for strength are 1910 kips (LF) and 1860 kips (RG)
- Shear capacity of the deck is checked.

For both Redundancy I and Redundancy II, the structure has adequate redundancy after the fracture of an exterior girder using the criteria for the strength and displacement requirements discussed above. The following were observed:

- Plastic strain is not reached in the steel tub girders.
- Crushing does not occur in the concrete deck.
- No haunch separation or shear stud failure is observed.
- The maximum vertical deflection change (difference between before fracture and after fracture stages) is 2.47 inches which is lower than L/50 (38.4 inches) and the maximum change in cross-slope is below 5%.

Summary of the redundancy evaluation is shown in Table 98.

Table 98 Summary of Redundancy failure criteria evaluation

Performance Requirement		**Most Critical Analysis Case**	**Result**	**Acceptable?**
Strength Requirements	**Steel Primary Members**	-	No component has strain larger than $5\varepsilon_y$ or 1%. Failure strain was not reached anywhere.	**YES**
	Concrete Crushing	-	No concrete crushing	**YES**
Serviceability Requirements	**Vertical Deflection Change**	C3. (Only Redundancy II DL considered).	Maximum deflection change is 2.5 in, which is lower than L/50 (38.4 in)	**YES**
	Cross-Slope Change	C3. (Only Redundancy II considered).	Maximum additional cross-slope is less than 5%.	**YES**
	Uplift	None.	No uplift.	**YES**

Notes:

- The analysis showed that the structure is capable of resisting an additional 15% of the applied factored live load.
- The horizontal displacement changes at support locations were lower than 6 in.

7.20.3 Summary

Analytical models have been developed to evaluate the structural redundancy of Ramp WN over Zoo Interchange (Structure ID B40-856-Unit2) in the state of Wisconsin. The girders are presently classified as Fracture Critical Members. A full depth fracture, including both webs and the top and bottom flange was simulated at four different locations in the exterior girder. The analysis confirms that the bridge satisfies the performance requirements for both Redundancy I and Redundancy II load combinations based on the failure criteria developed in NCHRP 12-87a [5]. Hence, the girders need not be classified as Fracture Critical Members (FCMs).

7.21 B40-868 (2 Spans)

7.21.1 Background, geometry, and loading

The structural redundancy of HWY 100 Ramp SL over IH94 (Structure ID B40-868 in Figure 145) was evaluated for the case where one of the twin-tub-girders fails due to an assumed sudden full-depth fracture. In the analysis, the outside girder was assumed to have fractured.

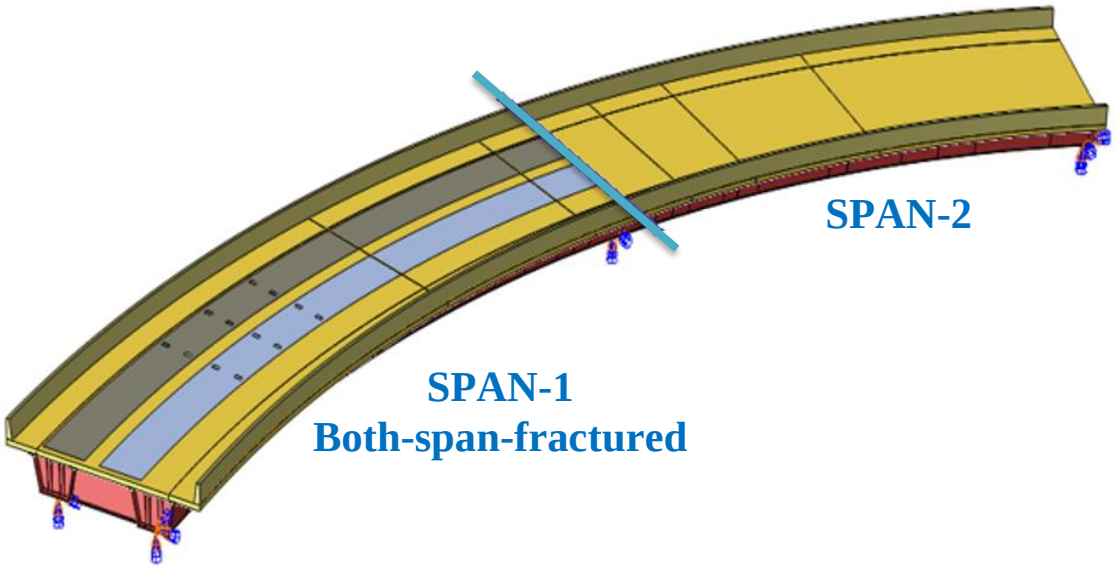

Figure 145 General Isometric View of B40-868

Table 99 provides details related to the geometry and material properties associated with the structure.

Table 99 The bridge geometry and material properties

Bridge Details	
Bridge Name	B40-868
Radius of Curvature	284.5 ft. (measured from bridge centerline)
Span Lengths	123.5 – 150.0 ft.
Girder Details	
Girder Steel	ASTM A709 HPS 50W
Box Girder Width (top flange center-to-center)	9.625 ft.
Girder Spacing (interior girder to exterior girder center)	23.5ft
Top Flange	Varies, 20 in. to 22 in. wide Varies, 0.875 in. to 2.75 in. thick
Web	69 in. high Varies, 0.6875 in. to 0.75 in. thick
Bottom Flange	84 in. wide Varies, 1.0 in. to 2.0 in. thick
Intermediate Diaphragms	Two full depth diaphragms in 1st span Three full depth diaphragms in 2nd span
Internal Cross Frames	2L6x6x1/2 (Top), 2L7x4x3/8 (Inclined)
Strut Braces	2L6x6x1/2
Lateral Braces	WT868xA-BC
Longitudinal Stiffeners on Bottom Flanges	-
Deck Details	
Concrete Material Strength	4 ksi (HPC)
Composite Deck	45.896 ft. wide, 11 in. thick 4 in. haunch thick
Transverse Reinforcement	No. 6 rebar with 7 in. spacing
Longitudinal Reinforcement	No. 4 & No. 6 rebar with 5 in. spacing
Overhang Reinforcement	No. 4 rebar with 7 in. spacing
Shear Studs	8 in. height. Longitudinal spacing is 9 in. Three shear studs spaced equally in the transverse direction
Parapet Type	42SS
Load Details	
Number of Lane	Two lanes of traffic
Future Wearing Surface	20 lb/ft^2
Maximum Dead Load Displacement (before fracture)	L/210

Six different full-depth fractures were applied separately in each after-fracture performance analysis. Specifically, the tension flange, both webs, and both upper compression flanges were assumed to have failed in one of the girders for each scenario. The locations where the six fractures were assumed to have occurred is shown in Figure 146. The locations are as follows:

- Crack 1 (C1) just before 1st (D1) intermediate diaphragm after 1st (S1A) exterior support,
- Crack 2 (C2) between 1st (D1) and 2nd (D2) intermediate diaphragms,
- Crack 3 (C3) between 3rd (D3) and 4th (D4) intermediate diaphragms,
- Crack 4 (C4) just after 4th (D4) intermediate diaphragms,
- Crack 5 (C5) just before 5th (D5) intermediate diaphragm, and
- Crack 6 (C6) just after 5th (D5) intermediate diaphragm before 3rd (S3A) exterior support.

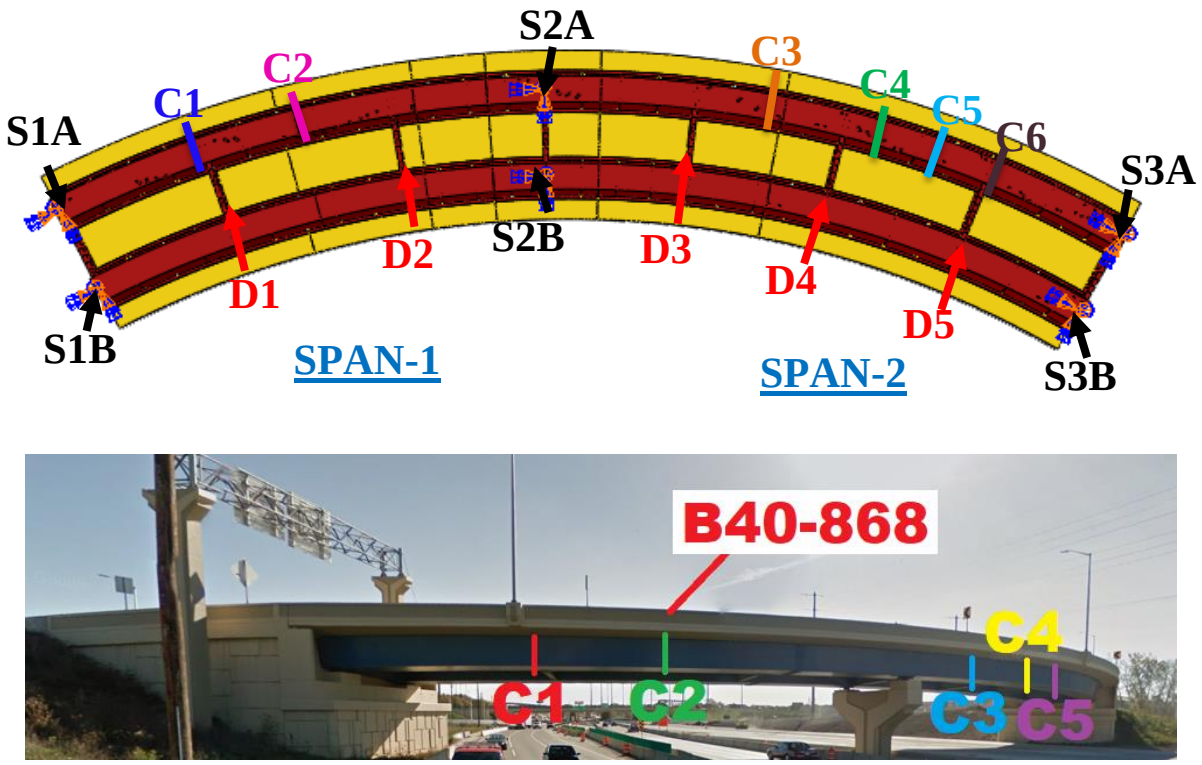

Figure 146 B40-868 Crack Locations

The Redundancy I and Redundancy II load combinations require different positioning of traffic live loads. For analyses where only a single lane of live load is applied for the Redundancy I load combination, the HL-93 live load was positioned in the center of the exterior design (i.e., striped)

traffic lane. In cases where two lanes of live load were considered, the HL-93 live loads were centered in the both design travel lanes. For the Redundancy II load combination, up to three HL-93 vehicular live loads were placed according to the procedure explained in Section 6.1.3. Full non-linear dynamic analysis was performed to determine the level of dynamic amplification that could be expected upon sudden failure of the tub girder. Based on this analysis, the dynamic amplification factor can conservatively be taken as 0.2 (i.e., 20%). Table 100 demonstrates the total load applied in the Redundancy I (R1) and II (R2) load combinations.

Table 100 Total load applied on the fractured bridge (fracture on span-2)

Type of Loading	**Dead Load (1.05 * DA_R)**	**Future Wearing Surface (1.05 * DA_R)**	**Live Load (0.85 * m * DA_R)**	**Total Load (DA_R)**
R1 1 HL-93	3852.00 (1.05 * 1.2)	308.83 (1.05 * 1.2)	205.63 (0.85 * 1.2 * 1.2) 235.87 (15% More LL)	4366.46 4396.70 (15% More LL)
R1 2 HL-93	3852.00 (1.05 * 1.2)	308.83 (1.05 * 1.2)	342.72 (0.85 * 1.0 * 1.2) 403.20 (15% More LL)	4503.55 4564.03 (15% More LL)

Type of Loading	**Dead Load (1.05)**	**Future Wearing Surface (1.05)**	**Live Load (1.3 * m)**	**Total Load**
R2 1 HL-93	3210.00 (1.05)	257.36 (1.05)	278.93 (1.3 * 1.2) * (15% more per HS-20 impact) 305.75 (15% More LL)	3746.28 3773.10 (15% More LL)
R2 2 HL-93	3210.00 (1.05)	257.36 (1.05)	464.88 (1.3 * 1.0) * (15% more per HS-20 impact) 518.52 (15% More LL)	3932.24 3985.88 (15% More LL)
R2 3 HL-93	3210.00 (1.05)	257.36 (1.05)	592.72 (1.3 * 0.85) * (15% more per HS-20 impact) 673.18 (15% More LL)	4060.08 4140.54 (15% More LL)

7.21.2 Results for B40-868

The analysis has shown that HWY 100 Ramp SL over IH94 (Structure ID B40-868) possesses considerable reserve strength in the faulted state and that the steel twin-tub-girders do not meet the definition of a fracture critical member when evaluated using the prescribed loading and failure criteria developed in NCHRP 12-87a [5]. Table 101 summarizes the results obtained from the redundancy analyses of the structure in faulted stages. The fracture case C5 and C6 were found to result in the most critical crack location, and hence the numerical values are presented in Table 101. The evaluation presents the results for the Redundancy I and II load combinations and compares the results to the minimum performance criteria discussed in CHAPTER 6.

Table 101 Results obtained for redundancy evaluation

Fracture Locations		**C1, C2, C3, C4, C5, C6**	
Load Combination		**Redundancy I**	**Redundancy II**
Max. Equivalent Plastic Strain in the Main Girder	**Value**	0.004 (C6)	0.02 (C6)
	Location	Very localized yielding Intermediate diaphragm "D5" flange & Intact girder bottom flange next to D5	
Concrete Crushing	**Extent**	Localized Crushing (C5)	Localized Crushing (C5)
	Location	Only over fracture zone (Figure 147)	Only over fracture zone (Figure 147)
Stud Failing	**Value**	No stud failure	Few stud failure (C6)
	Location	-	Over exterior girder - interior top flange - next to fracture
Max. Vert. Reaction Force	**Value**	1649 kips	1512 kips
	Location	S2B (C5 - 2HL-93)	S2A (C5 - 3HL-93)
Uplift at Supports	**Value**	No Uplift	
	Location		
Max. Hor. Displacement at Supports	**Value**	2.97 in.	4.61 in.
	Location	S3A (C5 - 2HL-93)	S3A (C5 - 3HL-93)
Max. Vertical Deflection Change	**Value**	Not Applicable	7.5 in. (C5)

Notes:
- Design bearing capacity for strength is 2320 kips.
- Shear capacity of the deck is checked.

For both Redundancy I and Redundancy II, the structure has adequate redundancy after the fracture of an exterior girder using the criteria for the strength and displacement requirements discussed above.

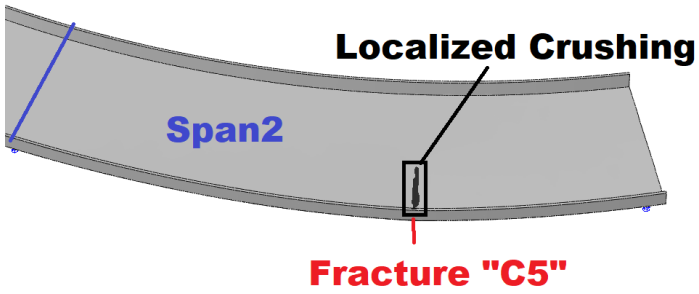

Figure 147 RI & RII Localized concrete crushing

The following were observed:

- Some localized plastic strain is not higher than 0.02 in D5's flanges.
- Only localized insignificant crushing occurs in the concrete deck.
- Few shear studs failure is observed in Redundancy II analysis.
- The maximum vertical deflection change (difference between before fracture and after fracture stages) is 7.5 inches which is lower than L/50 (36.0 inches) and the maximum change in cross-slope is below 5%.

A summary of the redundancy evaluation is shown in Table 102.

Table 102 Summary of Redundancy failure criteria evaluation

Performance Requirement		Most Critical Analysis Case	Result	Acceptable?
Strength Requirements	**Steel Primary Members**	C6. Redundancy I and II.	No component has strain larger than $5\varepsilon_y$ or 1%. Failure strain was not reached anywhere.	**YES**
	Concrete Crushing	C5. Redundancy I and II.	Localized concrete crushing	**YES**
Serviceability Requirements	**Vertical Deflection Change**	C5. (Only Redundancy II DL considered).	Maximum deflection change is 7.5 in, which is lower than L/50 (36.0 in)	**YES**
	Cross-Slope Change	C5. (Only Redundancy II considered).	Maximum additional cross-slope is less than 5%.	**YES**
	Uplift	None.	No uplift.	**YES**

Notes:

- The analysis showed that the structure is capable of resisting an additional 15% of the applied factored live load.
- The horizontal displacement changes at support locations were lower than 6 in.

When the C5 crack location and three HL93 traffic loads were applied in the Redundancy II load combination, the maximum nominal longitudinal stresses at the bottom flange of the fractured girder at the pier and at the bottom flange section change closest to the pier are 27.3 and 16.3 ksi, respectively. This is the most critical combination of loading and fracture location. This stress is lower than the bottom flange buckling capacity at the same locations which are equal to 37.2 and 17.3 ksi in the design calculations from Highway Structures Information System (HSI) [36].

7.21.3 Summary

Analytical models have been developed to evaluate the structural redundancy of HWY 100 Ramp SL (Structure ID B40-868) over IH94 in the state of Wisconsin. The girders are presently classified as Fracture Critical Members. A full depth fracture, including both webs and the top and bottom flange was simulated at six different locations in the exterior girder. The analysis confirms that the bridge satisfies the performance requirements for both Redundancy I and Redundancy II load combinations based on the failure criteria developed in NCHRP 12-87a. [5]. Hence, the girders need not be classified as Fracture Critical Members (FCMs).

7.22 UT Twin-tub-girder Test Bridge (1 Span)

7.22.1 Background, geometry, and loading

The structural redundancy of the UT Twin-tub-girder Test Bridge (details about the bridge are presented in CHAPTER 5) was evaluated for the case where one of the twin-tub-girders fails due to an assumed sudden full-depth fracture using the NCHRP 12-87a assessment criteria and the FEA methodology developed herein. In the analysis, the outside girder was assumed to have fractured. The structure did not satisfy the strength or performance criteria for the failure of the exterior tub girder. In fact, the structure was not able to sustain the required factored live load.

The Redundancy I and Redundancy II load combinations require different positioning of traffic live loads. For analyses where only a single lane of live load is applied for the Redundancy I load combination, the HL-93 live load was positioned in the center of the design (i.e., striped) traffic lane. For the Redundancy II load combination, up to two HL-93 vehicular live loads were placed according to the procedure explained in Section 6.1.3. Full non-linear dynamic analysis was performed to determine the level of dynamic amplification that could be expected upon sudden failure of the tub girder. Based on this analysis, the dynamic amplification factor can conservatively be taken as 0.35 (i.e., 35%).

7.22.2 Results for UT Bridge

The crack is located in the mid-span. Once failure if the exterior girder is introduced in the FEA, extended shear stud failure takes place along the exterior girder causing it to drop and completely detach from the bottom of the slab. As the exterior girder drops, it rotates leading to distortion of the end diaphragms, see Figure 148. In the end, the bridge becomes unstable and "flips" towards the exterior (radial outward direction), see Figure 149.

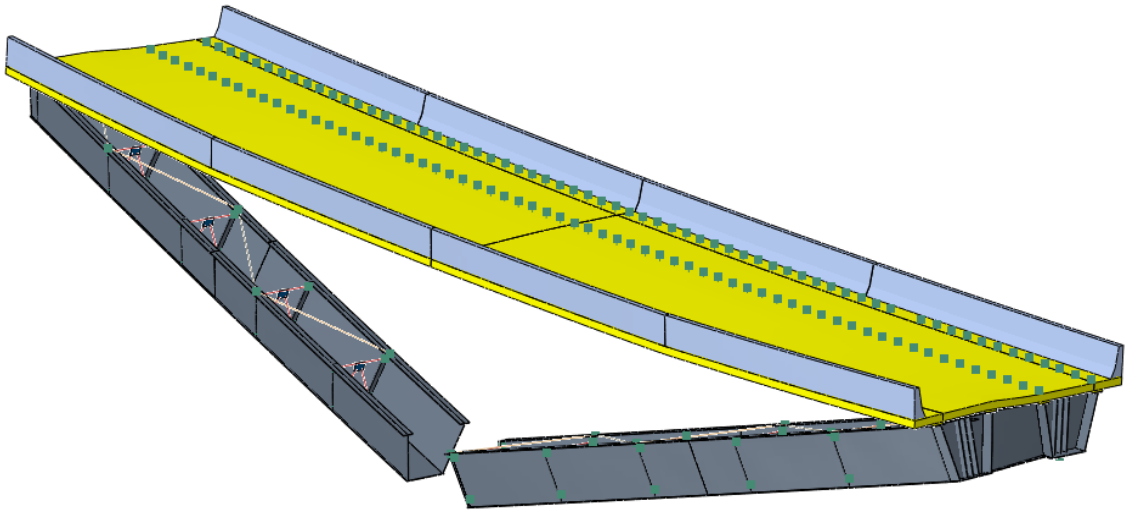

Figure 148 Shear stud failure along the exterior girder and detachment of exterior girder from the slab.

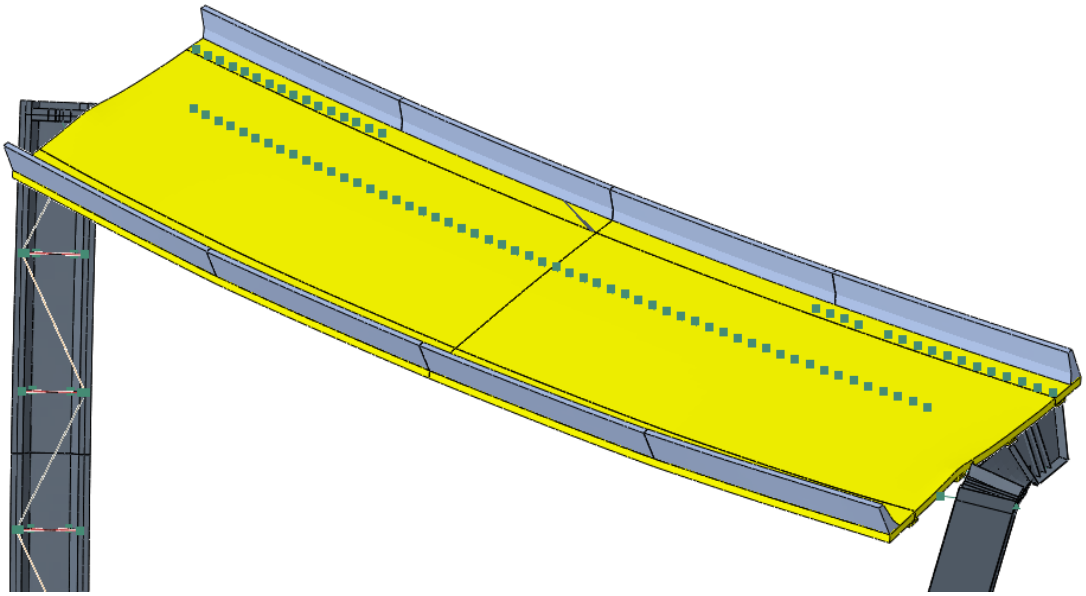

Figure 149 Distortion of end diaphragms due to fall and rotation of exterior tub girder.

Table 103 summarizes the results obtained from the redundancy analysis of the structure in faulted stage. The evaluation presents the results for the Redundancy I and II load combinations and compares the results to the minimum performance criteria discussed in CHAPTER 6. A summary of the redundancy evaluation is shown in Table 104 Summary of Redundancy failure criteria evaluation.

Table 103 Results obtained for redundancy evaluation

Fracture Locations		At the mid span	
Load Combination		**Redundancy I**	**Redundancy II**
Max. Equivalent Plastic Strain in the Main Girder	**Value**	Rupture of end diaphragms takes place under factored dead load only.	
	Location		
Concrete Crushing	**Extent**	Extensive concrete crushing with development of hinging mechanism between the tub girders.	
	Location		
Stud Failing	**Value**	Extensive shear stud failure	
	Location		
Max. Vert. Reaction Force	**Value**	Bridge becomes unstable and falls from supports.	
	Location		
Uplift at Supports	**Value**	Bridge becomes unstable and falls from supports.	
	Location		
Max. Hor. Displacement at Supports	**Value**	Bridge becomes unstable and falls from supports.	
	Location		
Max. Vertical Deflection Change	**Value**	Not Applicable	Unstable, non-computable

Table 104 Summary of Redundancy failure criteria evaluation

Performance Requirement		Most Critical Analysis Case	Result	Acceptable?
Strength Requirements	**Steel Primary Members**	RI and RII.	Rupture of end diaphragms takes place under factored dead load only.	**NO**
	Concrete Crushing	RI and RII.	Extensive concrete crushing with development of hinging mechanism between the tub girders.	**NO**
Serviceability Requirements	**Vertical Deflection Change**	Only RII DL considered	Bridge becomes unstable and falls from supports.	**NO**
	Cross-Slope Change	Only RII considered	Maximum additional cross-slope is more than 5%.	**NO**
	Uplift	RI and RII.	Bridge becomes unstable and falls from supports.	**NO**

7.22.3 Summary

A full depth fracture, including both webs and the top and bottom flange was simulated at the mid-span in the exterior girder. The analysis shows that the UT Tub Girder Bridge would not meet the proposed performance requirements for system analysis based on the failure criteria developed in NCHRP 12-87a. [5].

7.23 Simple-Span-1Lane-128ft (1 Span)

7.23.1 Background, geometry, and loading

The structural redundancy of typical 1 lane simple span bridge in Figure 150 was evaluated for the case where one of the twin-tub-girders fails due to an assumed sudden full-depth fracture. In the analysis, the outside girder was assumed to have fractured.

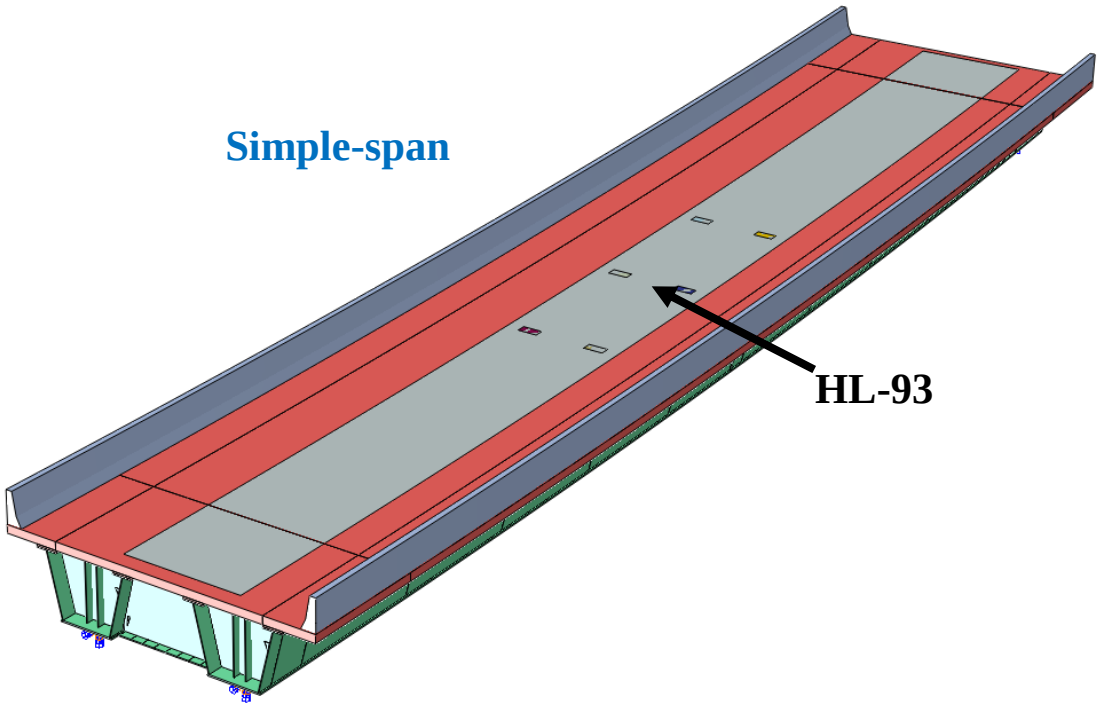

Figure 150 General Isometric View of Existing Bridge 1

Table 105 provides details related to the geometry and material properties associated with the structure.

Table 105 The bridge geometry and material properties

Bridge Details	
Bridge Name	Existing Bridge 1
Radius of Curvature	2864.8 ft. (measured from bridge centerline)
Span Length	128 ft.
Girder Details	
Girder Steel	ASTM A709 Grade 50
Box Girder Width (from the centers of interior top-flange to the center of exterior top-flange)	6.67 ft.
Girders Spacing (from the centers of the girders' bottom flanges)	12.8 ft.
Top Flange	20 in. wide 1.25 in. thick
Web	60 in. high 0.625 in. thick
Bottom Flange	53.5 in. wide 1.5 in. thick
Diaphragms	-
Internal Cross Frames	L5x3-1/2x1/2 (Top), L5x3-1/2x1/2 (Inclined)
Strut Braces	-
Lateral Braces	WT7x26.5
Longitudinal Stiffeners on Bottom Flanges	-
Deck Details	
Concrete Material Strength	4 ksi
Composite Deck	26.417 ft. wide 8.0 in. thick 3 in. haunch thick
Transverse Reinforcement	No. 5 rebar with 6.5 in. spacing
Longitudinal Reinforcement	No. 5 rebar with 8.5. in. spacing
Overhang Reinforcement	-
Shear Studs	6 in. height. Longitudinal spacing is 12 in. Three shear studs spaced equally in the transverse direction
Parapet Type	T501 (Interior) – T501 (Exterior)
Load Details	
Number of Lane	One lane traffic
Future Wearing Surface	-
Maximum Dead Load Displacement (before fracture)	L/460

7.23.2 Results for Existing Bridge 1

The crack is located in the mid-span. The Redundancy I and Redundancy II load combinations require different positioning of traffic live loads. For analyses where only a single lane of live load is applied for the Redundancy I load combination, the HL-93 live load was positioned in the center of the design (i.e., striped) traffic lane. For the Redundancy II load combination, up to two HL-93 vehicular live loads were placed according to the procedure explained in Section 6.1.3. Full non-linear dynamic analysis was performed to determine the level of dynamic amplification that could be expected upon sudden failure of the tub girder. Based on this analysis, the dynamic amplification factor can conservatively be taken as 0.35 (i.e., 35%). In Redundancy II, once failure if the exterior girder is introduced in the FEA, extended shear stud failure takes place along the exterior girder causing it to drop and completely detach from the bottom of the slab. The stud failures (Figure 151) are followed by parapet crushing, deck reinforcement yielding (Figure 152), and lateral brace failing. These failures cause flat or negative slope of the load-deflection curve.

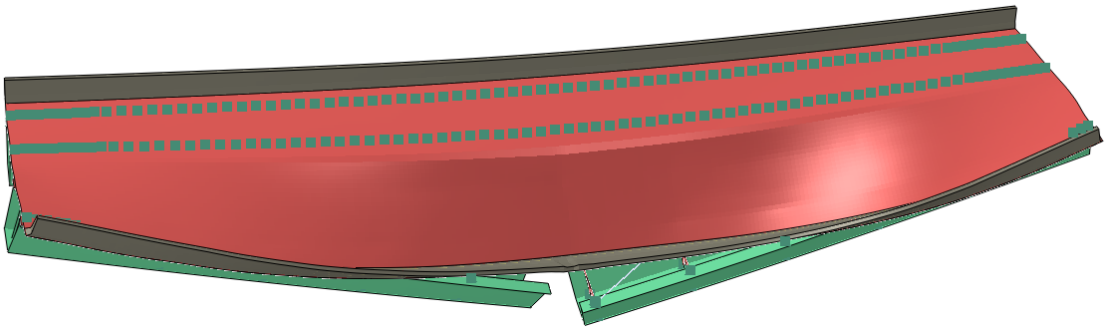

Figure 151 All stud failure over fractured girder

Table 106 shows the results obtained from the redundancy analysis of the structure in faulted stage. The evaluation presents the results for the Redundancy I and II load combinations and compares the results to the minimum performance criteria discussed in CHAPTER 6. A summary of the redundancy evaluation is shown in Table 107.

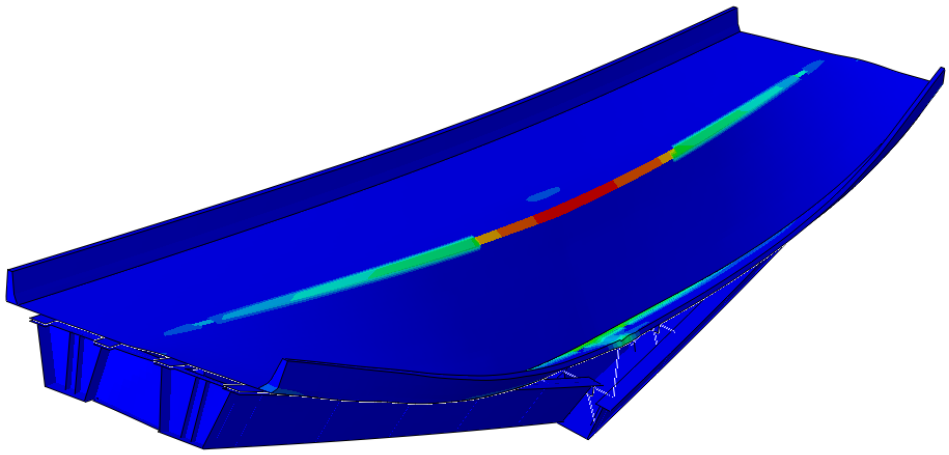

Figure 152 Deck reinforcement yielding

Table 106 Results obtained for redundancy evaluation

Fracture Locations		Mid-Span	
Load Combination		Redundancy I	Redundancy II
Max. Equivalent Plastic Strain in the Main Girder	**Value**	0.005	Rupture of end diaphragms Buckling of lateral bracing. Yielding on intact girder interior top flange Brace connection failure
	Location	End diaphragms	
Concrete Crushing	**Extent**	-0.013	Concrete crushing with development of hinging mechanism between the tub girders.
	Location	Some concrete crushing over top flange of fractured girder in transverse direction	
Stud Failing	**Value**	No stud failure	Stud failure along the exterior girder
	Location	-	Over fractured girder
Max. Vert. Reaction Force	**Value**	380 kips	Bridge becomes unstable with excessive dynamic effects.
	Location	Over fracture girder (at abutment)	
Uplift at Supports	**Value**	No Uplift	
	Location		
Max. Hor. Displacement at Supports	**Value**	1.67 in.	16.72 in.
	Location	Over fracture girder (at abutment)	Over fractured girder (at abutment)
Max. Vertical Deflection Change	**Value**	Not Applicable	3.635 (Only DL considered)

Table 107 Summary of Redundancy failure criteria evaluation

Performance Requirement		Most Critical Analysis Case	Result	Acceptable ?
Strength Requirements	**Steel Primary Members**	Redundancy II	Rupture of end diaphragms Buckling of lateral bracing. Yielding on intact girder interior top flange Brace connection failure	**NO**
	Concrete Crushing	Redundancy II	Concrete crushing with development of hinging mechanism between the tub girders.	**NO**
Serviceability Requirements	**Vertical Deflection Change**	(Only Redundancy II DL considered).	Maximum deflection change is 3.6 in, which is lower than L/50 (30.8 in)	**YES**
	Cross-Slope Change	(Only Redundancy II considered).	Maximum additional cross-slope is less than 5%.	**YES**
	Uplift	None.	No uplift.	**YES**

Notes:

- The analysis showed that the structure is not capable of resisting an additional 15% of the applied factored live load.
- The horizontal displacement changes at support locations were more than 6 in.

7.23.3 Summary

A full depth fracture, including both webs and the top and bottom flange was simulated at the mid-span in the exterior girder. The analysis shows that the Simple-Span-1Lane-128ft would not meet the proposed performance requirements for system analysis based on the failure criteria developed in NCHRP 12-87a. [5].

7.24 Simple-Span-2Lane-204ft (1 Span)

7.24.1 Background, geometry, and loading

The structural redundancy of typical simple-span 2 lanes bridge in Figure 153 was evaluated for the case where one of the twin-tub-girders fails due to an assumed sudden full-depth fracture. In the analysis, the outside girder was assumed to have fractured.

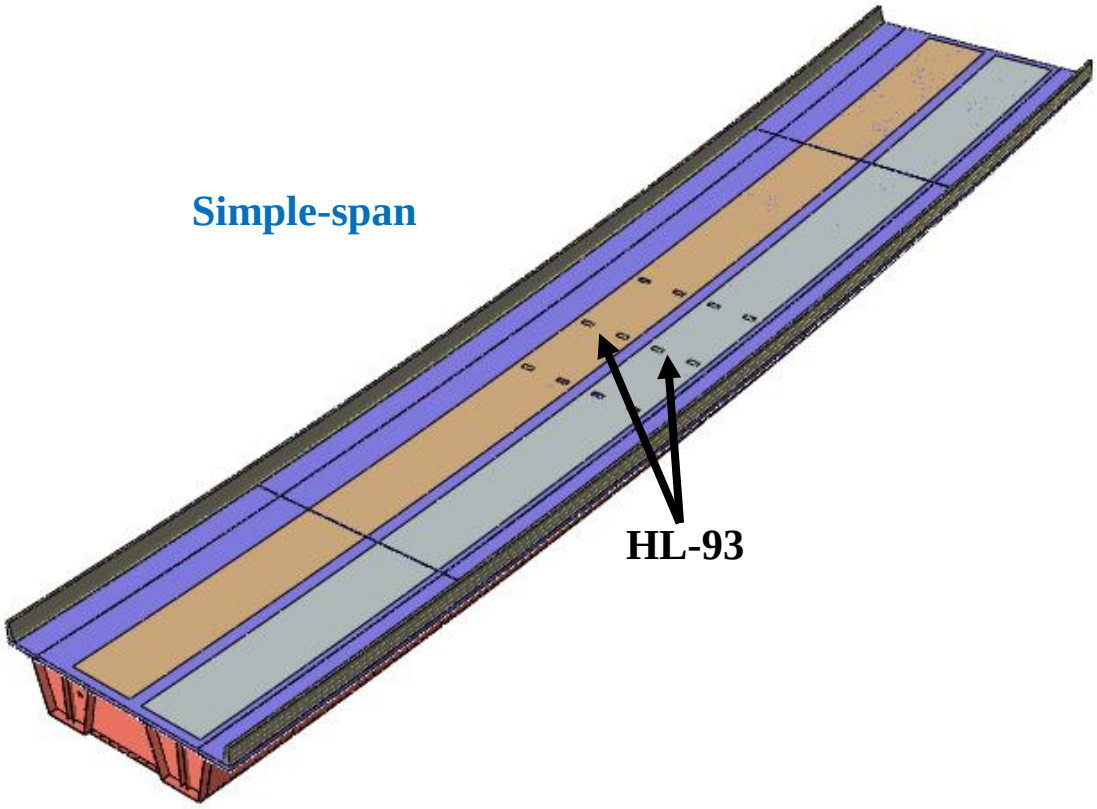

Figure 153 General Isometric View of Existing Bridge 1

Table 108 provides details related to the geometry and material properties associated with the structure.

Table 108 The bridge geometry and material properties

Bridge Details	
Bridge Name	Existing Bridge 1
Radius of Curvature	Straight (measured from bridge centerline)
Span Length	204 ft.
Girder Details	
Girder Steel	ASTM A709 Grade 50
Box Girder Width (from the centers of interior top-flange to the center of exterior top-flange)	10.0 ft.
Girders Spacing (from the centers of the girders' bottom flanges)	20.0 ft.
Top Flange	24 in. wide Varies, 1.25 in. to 1.5 in. thick
Web	90 in. high 0.625 in. thick
Bottom Flange	79 in. wide Varies, 1.25 in. to 1.5 in. thick
Diaphragms	-
Internal Cross Frames	L5x3-1/2x1/2 (Top), L5x3-1/2x1/2 (Inclined)
Strut Braces	-
Lateral Braces	WT8x33.5
Longitudinal Stiffeners on Bottom Flanges	-
Deck Details	
Concrete Material Strength	4 ksi
Composite Deck	38.417 ft. wide 8.0 in. thick 4 in. haunch thick
Transverse Reinforcement	No. 5 rebar with 5 in. spacing
Longitudinal Reinforcement	No. 5 rebar with 9 in. spacing
Overhang Reinforcement	-
Shear Studs	7 in. height. Longitudinal spacing is 15 in. Three shear studs spaced equally in the transverse direction
Parapet Type	T501 (Interior) – T501 (Exterior)
Load Details	
Number of Lane	Two lanes traffic
Future Wearing Surface	-
Maximum Dead Load Displacement (before fracture)	L/210

7.24.2 Results for Existing Bridge 2

The crack is located in the mid-span. The Redundancy I and Redundancy II load combinations require different positioning of traffic live loads. For analyses where only a single lane of live load is applied for the Redundancy I load combination, the HL-93 live load was positioned in the center of the exterior design (i.e., striped) traffic lane. In cases where two lanes of live load were considered, the HL-93 live loads were centered in the both design travel lanes. For the Redundancy II load combination, up to three HL-93 vehicular live loads were placed according to the procedure explained in Section 6.1.3. Full non-linear dynamic analysis was performed to determine the level of dynamic amplification that could be expected upon sudden failure of the tub girder. Based on this analysis, the dynamic amplification factor can conservatively be taken as 0.35 (i.e., 35%).

In Redundancy I and II, once failure if the exterior girder is introduced in the FEA, the bridge exhibits significant shear stud failures (See Figure 154) after fracture occurred. The stud failures are followed by parapet crushing (Figure 155), deck reinforcement yielding (Figure 156) lateral brace failing (Figure 157), and torsional buckling in their intact girders (Figure 158). These failures cause flat or negative slope of the load-deflection curve.

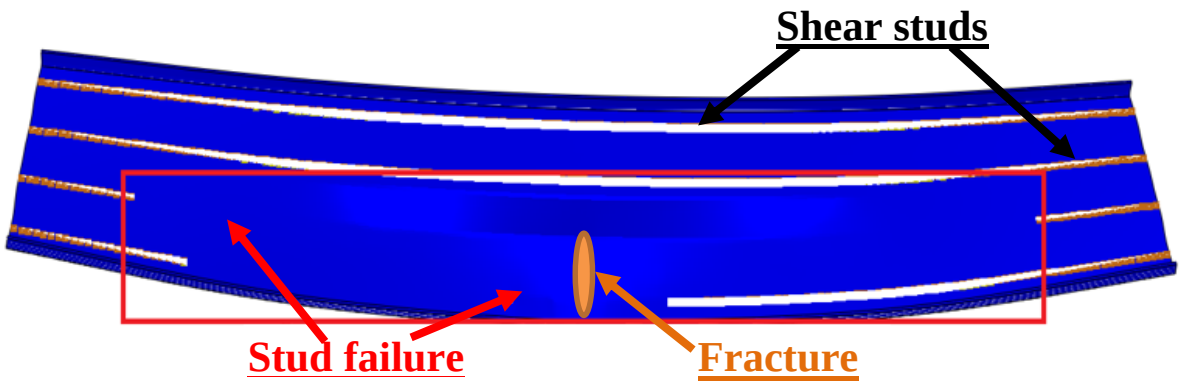

Figure 154 Stud failure of typical simple span bridge (top view)

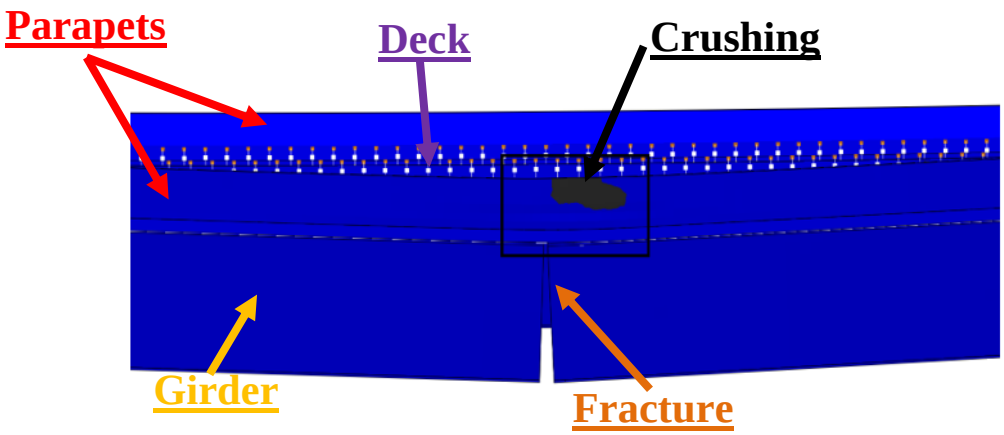

Figure 155 Parapet crushing in the typical simple span bridge (side view)

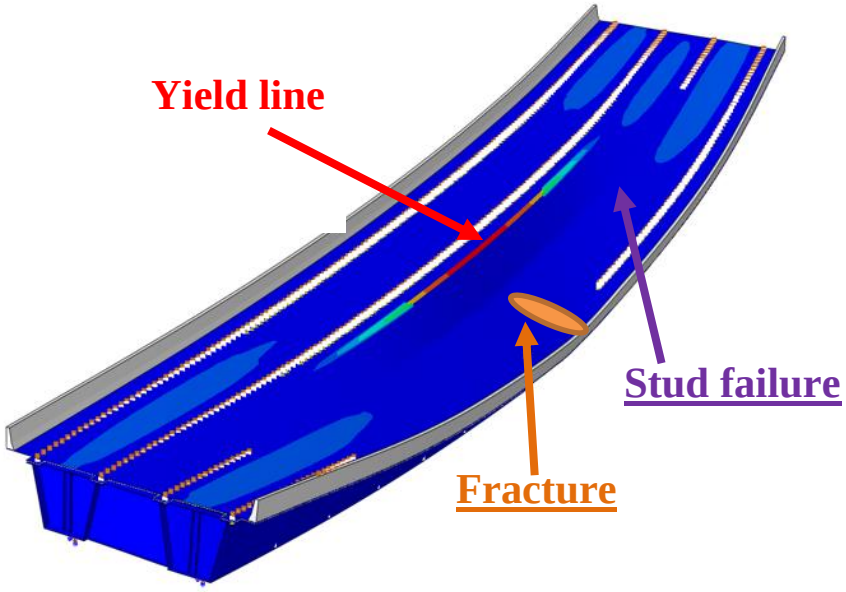

Figure 156 Deck reinforcement yielding in the typical simple span bridge (top view)

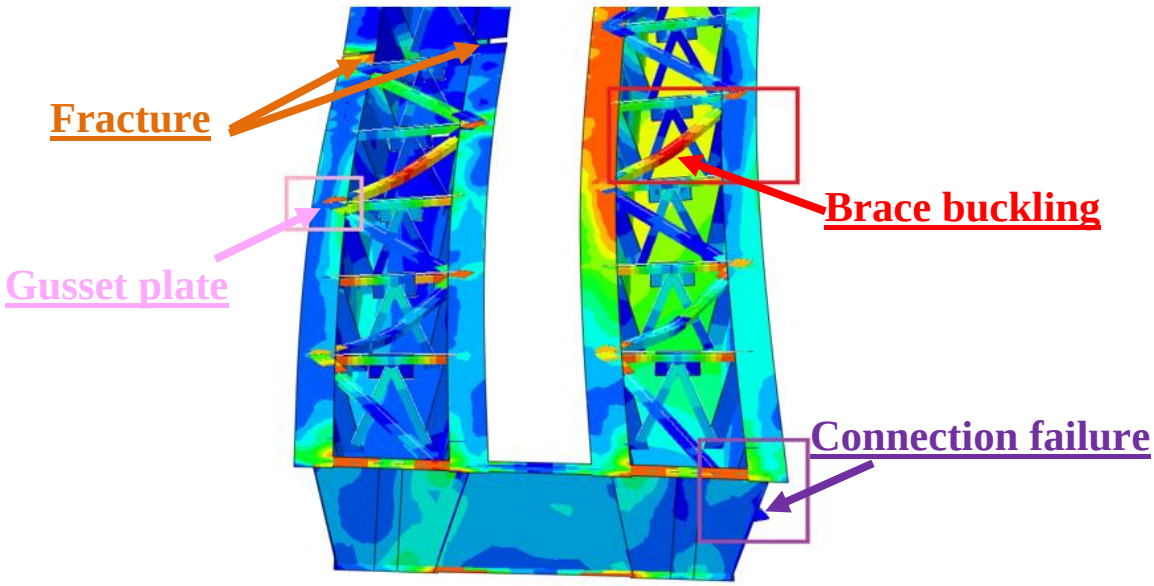

Figure 157 Lateral brace failure in the typical simple span bridge

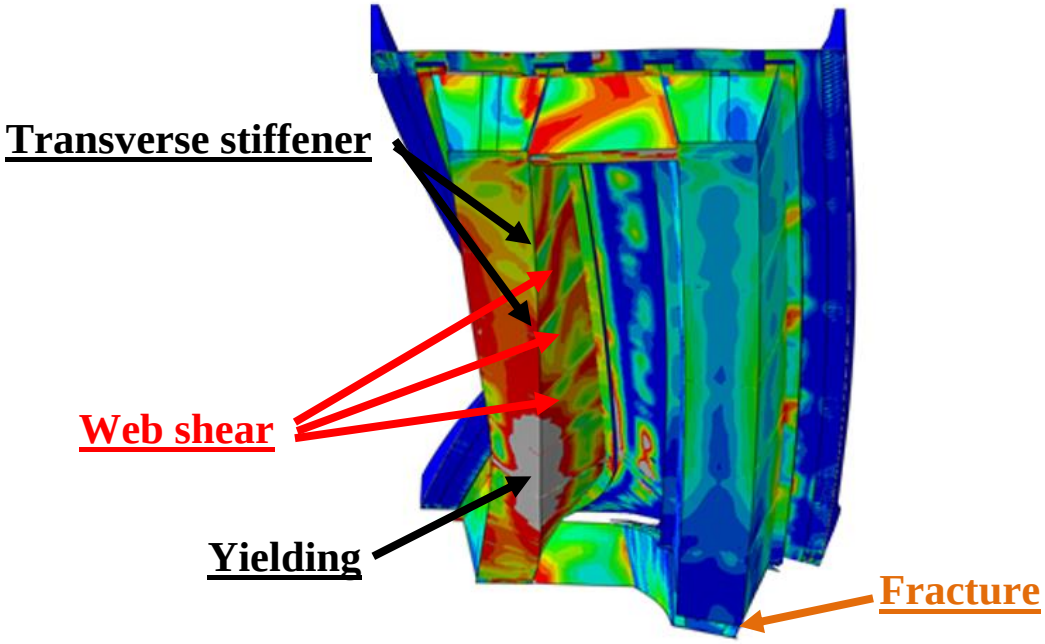

Figure 158 Intact girder torsional buckling and diaphragm shear buckling in the typical simple span bridge

Table 109 shows the results obtained from the redundancy analysis of the structure in faulted stage. The evaluation presents the results for the Redundancy I and II load combinations and compares the results to the minimum performance criteria discussed in CHAPTER 6. A summary of the redundancy evaluation is shown in

Table 109 Results obtained for redundancy evaluation

Fracture Locations		**Mid-Span**	
Load Combination		**Redundancy I**	**Redundancy II**
Max. Equivalent Plastic Strain in the Main Girder	**Value**	>0.05	>0.05
	Location	Lateral Brace Failure Yielding and buckling over intact girder	Lateral Brace Failure Yielding and buckling over intact girder
Concrete Crushing	**Extent**	Significant concrete crushing with development of hinging mechanism between the tub girders.	Concrete crushing with development of hinging mechanism between the tub girders.
	Location		
Stud Failing	**Value**	Significant stud failure	More than 50% studs failing over fractured girder
	Location	Over fractured girder	Over fractured girder
Max. Vert. Reaction Force	**Value**	Bridge becomes unstable and not converge in the analysis	
	Location		
Uplift at Supports	**Value**	Bridge becomes unstable and not converge in the analysis	
	Location		
Max. Hor. Displacement at Supports	**Value**	Bridge becomes unstable and not converge in the analysis	
	Location		
Max. Vertical Deflection Change	**Value**	Not Applicable	69.2 (Only DL considered)

Table 110 Summary of Redundancy failure criteria evaluation

Performance Requirement		Most Critical Analysis Case	Result	Acceptable?
Strength Requirements	**Steel Primary Members**	Redundancy II	Lateral Brace Failure Some Yielding over intact girder interior top flange	**NO**
	Concrete Crushing	Redundancy II	Concrete crushing with development of hinging mechanism between the tub girders.	**NO**
Serviceability Requirements	**Vertical Deflection Change**	(Only Redundancy II DL considered).	Maximum deflection change is 69.2 in, which is lower than L/50 (49.0 in)	**NO**
	Cross-Slope Change	(Only Redundancy II considered).	Maximum additional cross-slope is more than 5%.	**NO**
	Uplift	None.	Bridge becomes unstable and not converge in the analysis	**NO**

7.24.3 Summary

A full depth fracture, including both webs and the top and bottom flange was simulated at the mid-span in the exterior girder. The analysis shows that Simple-Span-2Lane-204ft would not meet the proposed performance requirements for system analysis based on the failure criteria developed in NCHRP 12-87a. [5].

CHAPTER 8 DISCUSSION OF RESULTS

Calibrated FE analytical models have been developed to evaluate the structural redundancy of multiple twin-tub-girder bridges from the existing inventory of the Wisconsin Department of Transportation (WisDOT) and three other simple span twin-tub-girder bridges that are representative of designs commonly used by other owners. The loading and assessment criteria are based on those proposed in NCHRP 12-87a [5]. The girders are presently classified as Fracture Critical Members. A full depth fracture, including both webs and the top and bottom flanges, was modelled in one of the girders. In Table 111, the evaluations showed that all the analyzed bridges from WisDOT satisfy the performance requirements for both Redundancy I and Redundancy II in the faulted state. Hence, those girders need not be classified as FCMs. In contrast, the "typical" simple span configurations do not possess sufficient reserve strength in the faulted state and should remain classified as FCMs. The most significant implications for future design and analysis of twin-tub-girder bridges are discussed below in the following sections.

Table 111 Summary of results of analyzed bridges

Bridge	Year Built	Name	Units	# of Spans	End-Span Length (ft.)	Dead Load Deflection (Before-Fracture)	Full-Depth Intermediate Diaphragms Provided?	Fracture - Critical?
B05-658 Wisconsin	2014	Ramp FEN over NB USH 41 to WB STH 29	Unit-1 Unit-2	4 6	170.0 199.2	L/630 L/415	**YES**	**NO**
B05-660 Wisconsin	2014	Ramp FNW over NB USH 41 to WB STH 29	Unit-1 Unit-2 Unit-3	3 5 7	168.2 211.0(LF)-148.2(RG) 128.2(LF)-100.0(RG)	L/560 L/325(LF)-L/925(RG) L/1420(LF)- L/2500(RG)	**YES**	**NO**
B05-661 Wisconsin	2012	Ramp FSW USH 41 SB to STH 29 WB	-	2	187	L/375	**YES**	**NO**
B05-678 Wisconsin	2015	Ramp IHB over IH 43 to USH 41 SB	Unit-3 Unit-4 Unit-5	4 4 5	137.2(LF)-180.3(RG) 176.0 151.2	L/1140(LF)-L/545(RG) L/610 L/2160	**YES**	**NO**
B05-679 Wisconsin	2015	Ramp NIH over IH 43 to USH 41 SB	Unit-1 Unit-2	5 5	170.0 180.9	L/940 L/650	**YES**	**NO**
B40-776 Wisconsin	2014	Watertown Plank Road Ramp WH over USH 45	-	3	105.8	L/365	**YES**	**NO**

Table 111 continued

B40-783 Wisconsin	2014	Watertown Plank Road Ramp WF over USH 45	-	3	119.0	L/410	**YES**	**NO**
B40-786 Wisconsin	2018	Zoo Interchange Ramp WS	Unit-1 Unit-2	4 4	160.0 146.0	L/570 L/770	**YES**	**NO**
B40-834 Wisconsin	2011	Ramp TF (S-W) over IH 43/894	-	3	116.6	L/350	**YES**	**NO**
B40-837 Wisconsin	2010	Ramp TH over IH 43/894	-	2	100.0	L/1250	**YES**	**NO**
B40-854 Wisconsin	2018	Zoo Interchange Ramp ES	Unit-1 Unit-2 Unit-3	5 5 3	146.0(LF)-136.0(RG) 164.5(LF)-157.0(RG) 157.0	L/1120(LF)-L/850(RG) L/685(LF)-L/680(RG) L/750	**YES**	**NO**
B40-856 Wisconsin	2018	Zoo Interchange Ramp WN	Unit-2	6	151.0(LF)-160.0(RG)	L/880(LF)-L/550(RG)	**YES**	**NO**
B40-868 Wisconsin	2014	HWY 100 Ramp SL over IH 94	-	2	150.0	L/210	**YES**	**NO**
UT Test Texas	-	Interchange between IH10 and Loop 610		1	120	L/240	**NO**	**YES**
Existing-1 Other Owner	-	-	-	1	128	L/460	**NO**	**YES**
Existing-2 Other Owner	-	-	-	1	204	L/210	**NO**	**YES**

8.1 The Advantages of Full-Depth Intermediate Diaphragms and Bridge Continuity

All the WisDOT twin-tub-girder bridges analyzed in this research have multiple full-depth intermediate diaphragms and continuous spans. These features provide additional load paths and help to make the bridges redundant thereby avoiding many failure modes which simple span bridges and bridges without full depth intermediate diaphragms commonly experienced. To illustrate the benefits of continuous spans and the full-depth diaphragms, two "representative" simple span bridges were analyzed (in Section 7.23 and 7.24) using the procedures described herein.

Those results have shown that in general, simple span bridges without intermediate diaphragms can be expected to more than 50% of shear studs over fractured girder failed (See Figure 154) after fracture occurred. The stud failures are followed by parapet crushing (Figure 155), deck reinforcement yielding (Figure 156) lateral brace failing (Figure 157), and torsional buckling in their intact girders (Figure 158). These failures cause flat or negative slope of the load-deflection curve. Furthermore, additional analyses were also performed for two "representative" simple span bridges (more details in Section 7.23 and 7.24), by adding intermediate diaphragms in order to investigate the advantages of diaphragms in the faulted state for simple span bridges.

For the first bridge "Simple-Span-1Lane-128ft" (in Section 7.23), two intermediate diaphragms was placed on the 30% of its span length (as shown in Figure 159). The web of the new diaphragms was assumed to be 0.5-inch thick and their flanges are 16 inch wide and 0.75 inch thick. (These component sizes are based the those typically used in the WisDOT designs previously evaluated.) The Redundancy II analysis is more critical than the Redundancy I for this bridge. In Redundancy II, noticeable crushing was observed in both transverse and longitudinal directions in the deck and the parapet. However, the amount of crushing did not lead to collapse and the bridge met the NCHRP 12-87a [5] performance criteria.

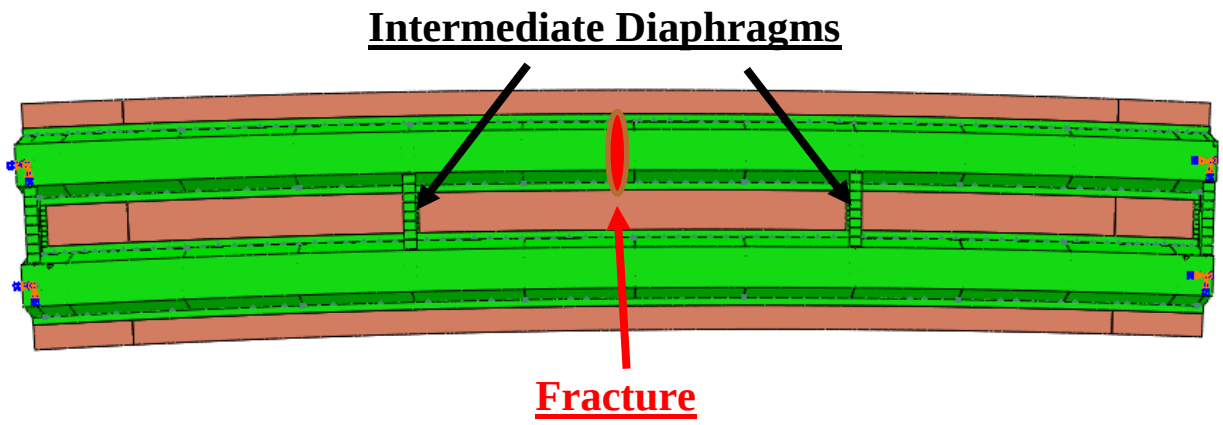

Figure 159 The location of two new intermediate diaphragms

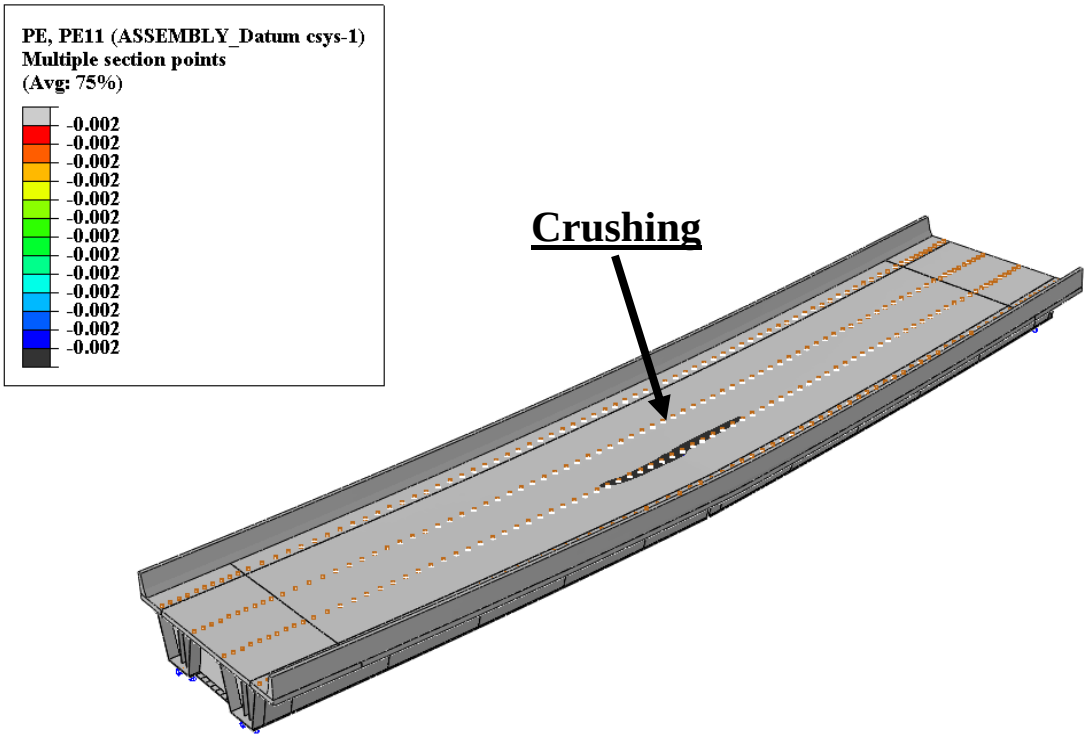

Figure 160 Concrete crushing in deck in transverse direction

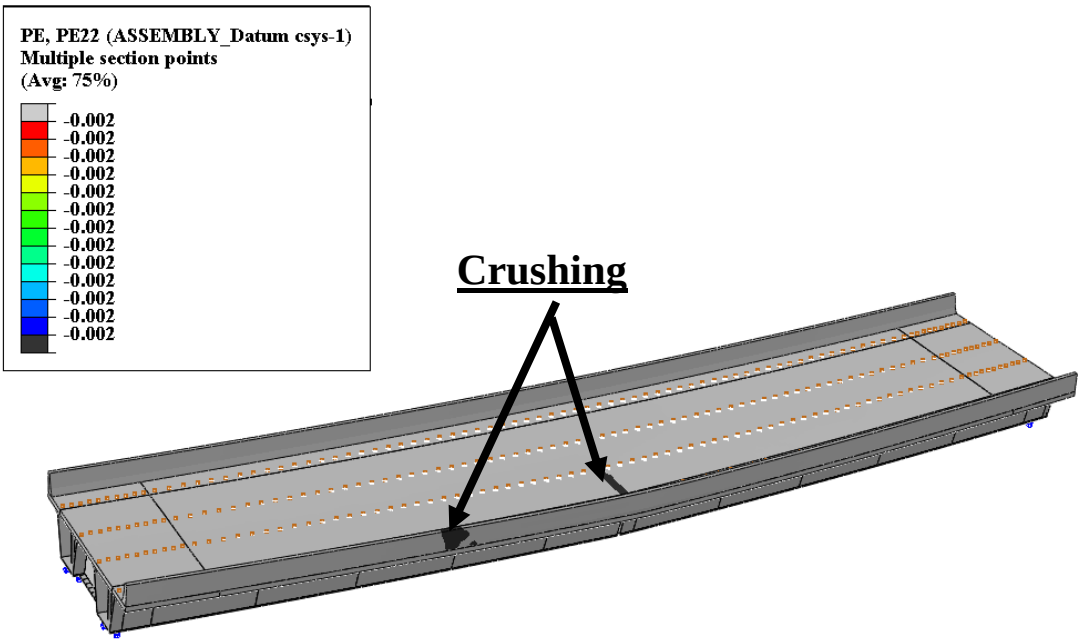

Figure 161 Concrete crushing in deck and parapet in longitudinal direction

For the second bridge "Simple-Span-2Lane-204ft" (in Section 7.24), three intermediate diaphragms were placed at the quarter points (as shown in Figure 162). The web of the new diaphragms is 0.75-inch thick and their flanges are 20 inches wide and 1.0 inch thick. In both the Redundancy I and II analyses, the bridge was not able to carry the applied loads. The bridge was not stable after the placement of truck loads, it can be seen more than 150 in. displacement in Figure 163 and torsional stresses in their intact girders. The analysis shows that the Simple-Span-2 Lane-204ft with intermediate diaphragms would not meet the proposed performance requirements for system analysis based on the failure criteria developed in NCHRP 12-87a. [5].

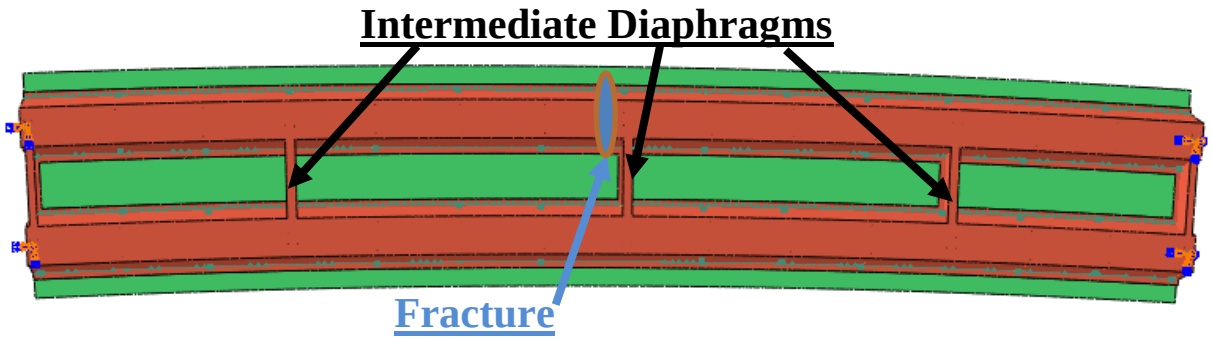

Figure 162 The location of three new intermediate diaphragms

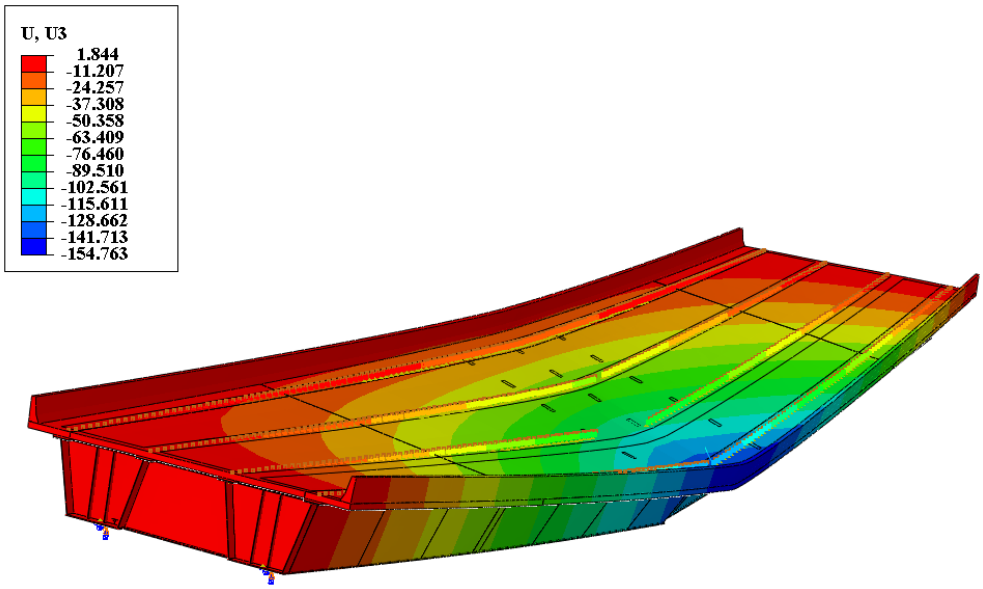

Figure 163 More than 150 in. displacement

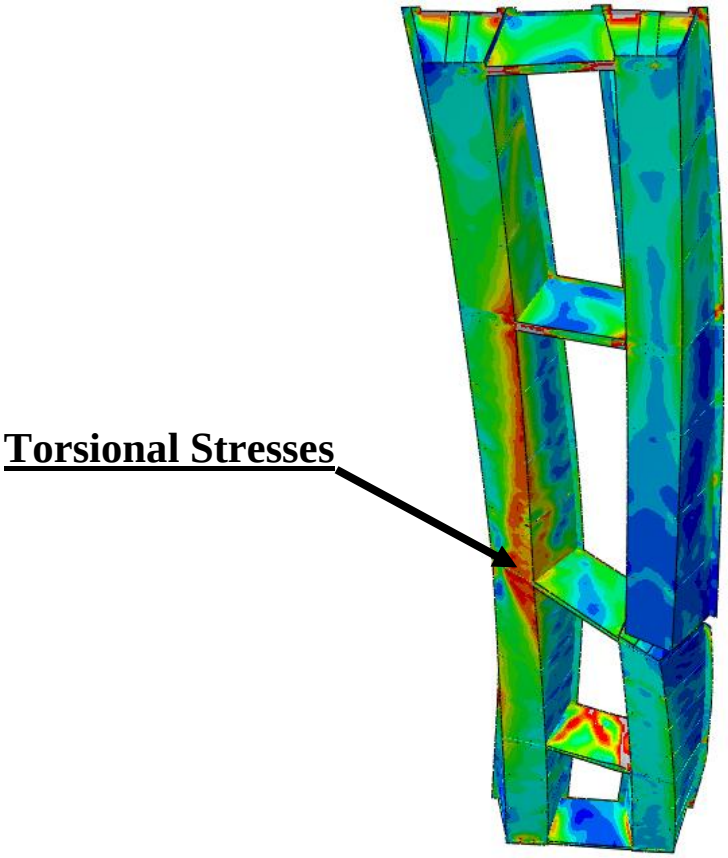

Figure 164 Intact girder torsional stresses

The intermediate diaphragms commonly used by WisDOT provide additional load paths and prevent many failure modes, such as failures in the deck due to concrete crushing, yield line, shear stud failures, etc. The torsional stability of the bridge is also improved significantly by the diaphragms. Additional analyses were also performed for B40-868 (more details about B40-868 in Section 7.21), ignoring the intermediate diaphragms, in order to investigate the advantages of intermediate diaphragms in the faulted state for continuous bridges. For B40-868, four different full-depth fractures were separately applied in its 150 ft. span. Specifically, the tension flange, both webs, and both upper compression flanges were assumed to have failed in one of the girders for each scenario. The locations where the four fractures were assumed to have occurred are shown in Table 112.

Table 112 B40-868 crack locations

Crack Name	**Distance from the pier**
C1	0.3 L
C2	0.5 L
C3	0.65 L
C4	0.75 L
Note: L is the second span length (150 ft.)	

The crack location "C4" is the most critical when the diaphragms are removed. Although there was couple of shear studs failed; deck reinforcement yielding, concrete crushing and concrete cracking, shown in Figure 165 and Figure 166, occurred under both Redundancy-1 and Redundancy-2 load combinations. These causes negative slope in load-displacement curves. When C3 was applied, there was some concrete crushing but it was not as significant as C4. When C1 or C2 were assigned, the bridge has remaining capacity in the faulted state. C4 is the most critical location due to its proximity to the discontinuous end of the bridge. Figure 167 shows the behavior of the same bridge with intermediate diaphragms when C4 was applied. It is noted that C1 to C4 do not correspond to same locations in Section 7.21.

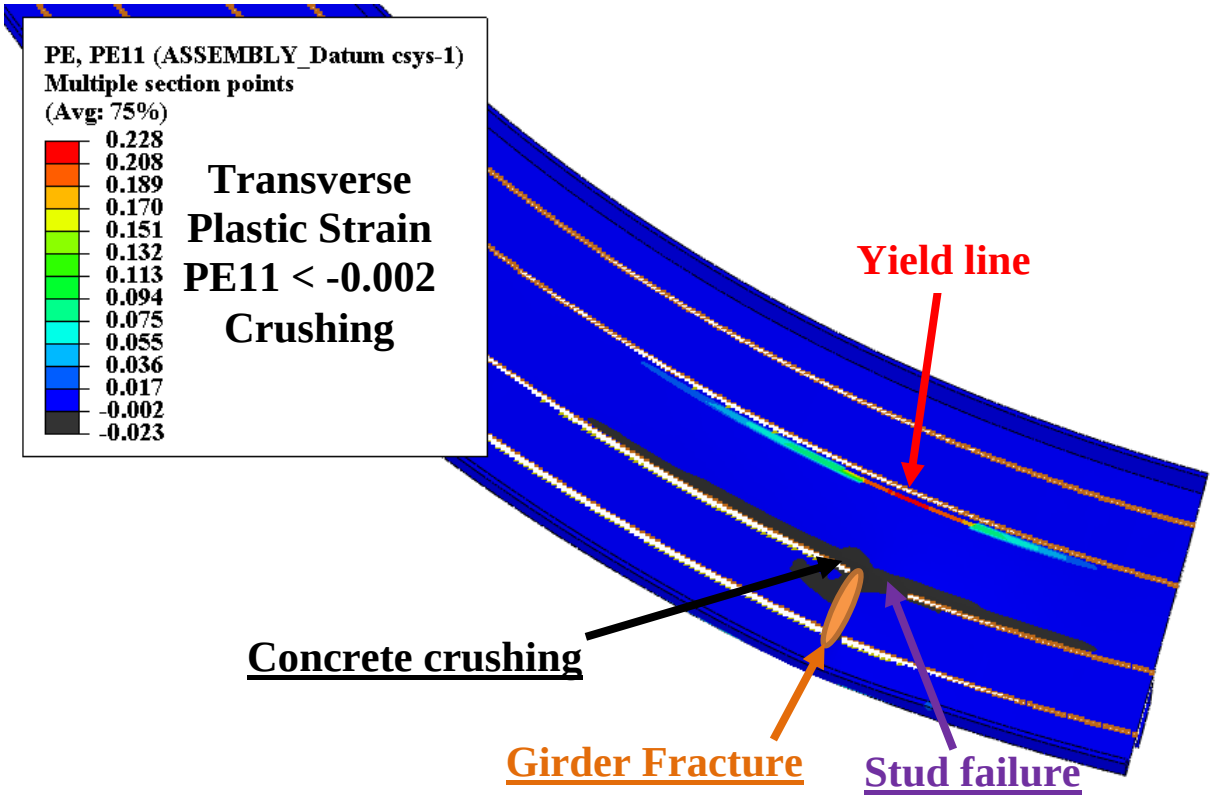

Figure 165 Concrete crushing and cracking in B40-868 without intermediate diaphragms (top view)

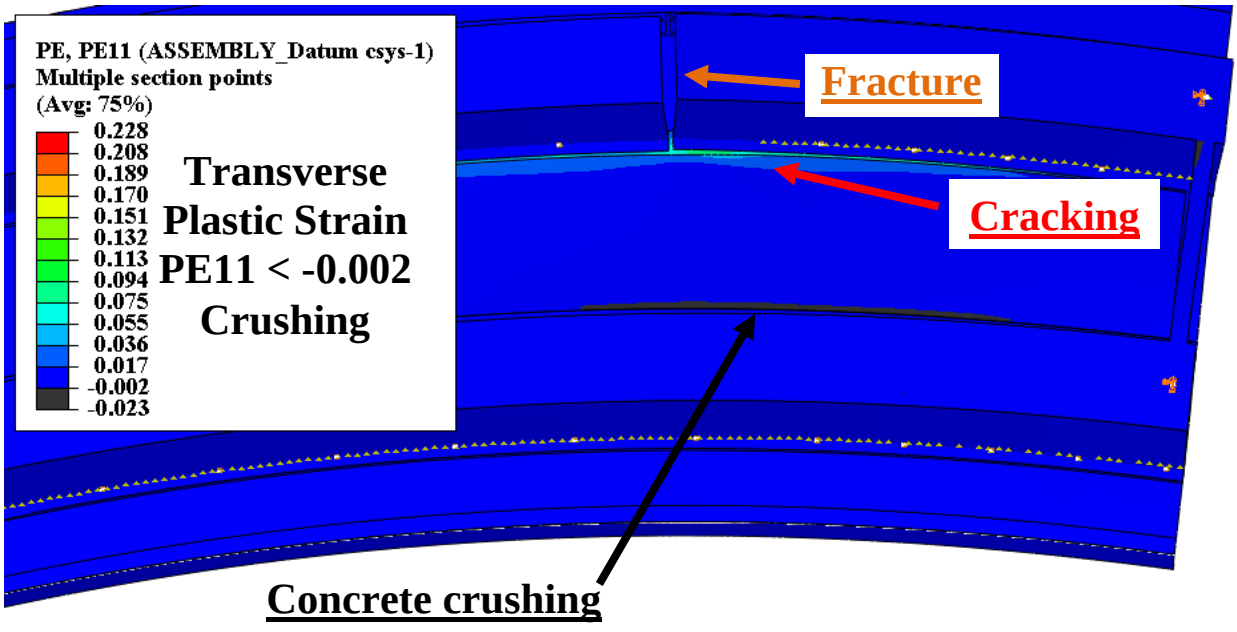

Figure 166 Concrete crushing and cracking in B40-868 without intermediate diaphragms (bottom view)

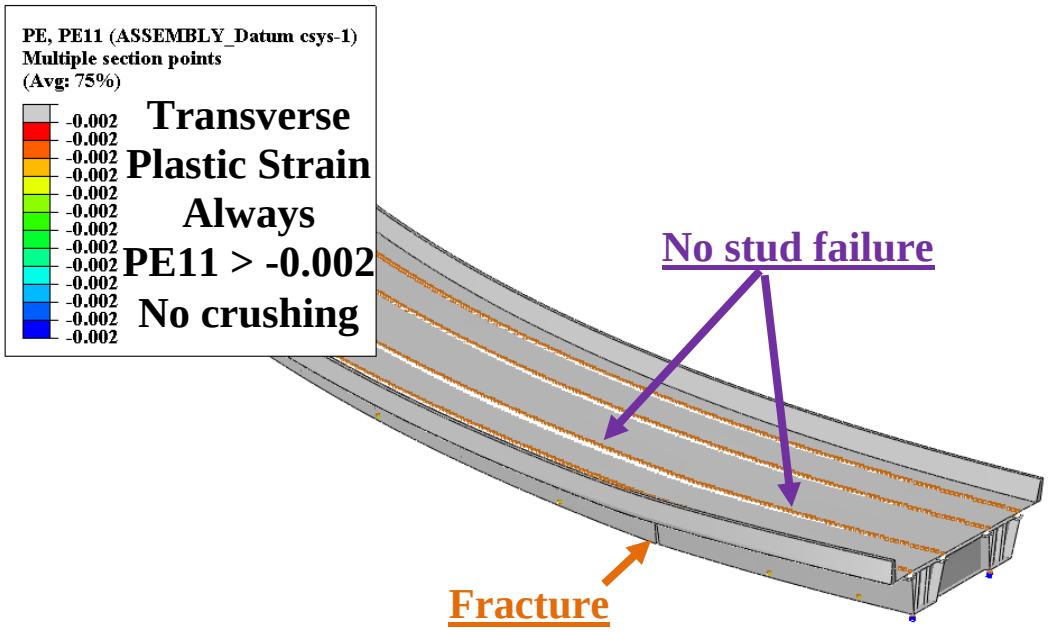

Figure 167 No concrete crushing in B40-868 with intermediate diaphragms (top view)

The addition of intermediate diaphragms significantly improves the after-fracture performance of the twin-tub-girder bridges analyzed in this research. Although some of the WisDOT bridges (such as B40-868, B05-661 etc.) exhibited some minor plasticity in the flanges of the intermediate diaphragms, the level of plasticity is localized and not significant.

In summary, the full depth intermediate diaphragms and bridge continuity appear to reduce the likelihood associated with the failure modes observed in the simple span bridge example discussed above. A small pilot study was performed to evaluate to benefits of full depth diaphragms in simple span configurations. In general, it appears that providing intermediate diaphragms may not be capable insuring sufficient performance in the faulted state in simple span configuration. For this reason, it is strongly recommended to use these features for future designs in order to significantly improve after-fracture performance. In the bridges analyzed for WisDOT, two or three intermediate diaphragms were used for the end spans. In general, two intermediate diaphragms were used in end spans under 120 ft., while three diaphragms were used in end spans longer than 120 ft. For more than 80% of these bridges, the first intermediate diaphragm was located no more than 30% of its end span length (L) and no more than 40 ft. It is also noted that bridges that had a maximum dead load displacement before-fracture of no more than L/500 did not experience plasticity in the first intermediate diaphragm. All of these details with typical diaphragm sizes are shown in Table 113

Table 113 Intermediate diaphragm details in Wisconsin bridges

Bridge	Units	End Span Length (L) (ft.)	Dead Load Deflection (Before-Fracture)	Deck Width (ft.)	Girder Spacing (ft.)	Web Height (in.)	Number of Diaph.	Location (/L)	Location (ft)	Diaph. Web-Thick. (in.)	Diaph. Top And Bottom Flange Sizes (in.)	Minor Yielding in Some Locations?
B05-658	Unit-1 Unit-2	170.0 199.2	L/630 L/415	35.896	19.0	86	3 3	20% 17%	34 33	0.75	20x7/8	N Y
B05-660	Unit-1 Unit-2(LF) Unit-2(RG) Unit-3(LF) Unit-3(RG)	168.2 211.0 148.2 128.2 100.0	L/560 L/325 L/925 L/1420 L/2500	44.896	25.0	86	3 3 3 3 2	20% 23% 22% 38% 33%	34 49 33 48 33	0.75	20x1	N Y N N N
B05-661	-	187	L/375	35.896	19.0	72	3	27%	51	0.75	20x7/8	Y
B05-678	Unit-3(LF) Unit-3(RG) Unit-4 Unit-5	137.2 180.3 176.0 151.2	L/1140 L/545 L/610 L/2160	44.896	25.0	86	3 3 3 3	25% 20% 20% 20%	34 36 35 30	0.75	20x1	N N N N
B05-679	Unit-1 Unit-2	170.0 180.9	L/940 L/650	44.896	25.0	86	3 3	20% 20%	34 36	0.75	20x1	N N
B40-776	-	105.8	L/365	41.896	21.0	60	2	30%	32	0.5	16x3/4	Y
B40-783	-	119.0	L/410	31.896	16.0	60	2	33%	40	0.5	16x3/4	Y
B40-786	Unit-1 Unit-2	160.0 146.0	L/570 L/770	44.896	23.0	84	2 2	25% 25%	40 37	0.625	16x1	N N

Table 113 continued

Bridge	Units	End Span Length (L) (ft.)	Dead Load Deflection (Before-Fracture)	Deck Width (ft.)	Girder Spacing (ft.)	Web Height (in.)	Number of Diaph.	Location (/L)	Location (ft)	Diaph. Web-Thick. (in.)	Diaph. Top And Bottom Flange Sizes (in.)	Minor Yielding in Some Locations?
B40-834	-	116.6	L/350	41.896	21.0	60	2	25%	35	0.5	16x3/4	Y
B40-837	-	100.0	L/1250	29.896	16.0	60	2	38%	38	0.5	16x3/4	N
B40-854	Unit-1(LF) Unit-1(RG) Unit-2(LF) Unit-2(RG) Unit-3	146.0 136.0 164.5 157.0 157.0	L/1120 L/850 L/685 L/680 L/750	44.896	23.0	84	2 2 2 2 2	33% 30% 25% 25% 25%	49 41 41 39 39	0.625	16x1	N N N N N
B40-856	Unit-2(LF) Unit-2(RG)	151.0 160.0	L/880 L/550	33.896	17.0	84	2 2	25% 25%	38 40	0.625	16x1	N N
B40-868	-	150.0	L/210	45.896	23.5	69	3	25%	38	0.5	16x3/4	Y

In the following Figure 168, one of the typically used intermediate diaphragm detail of B05-661 from the design plans was shown.

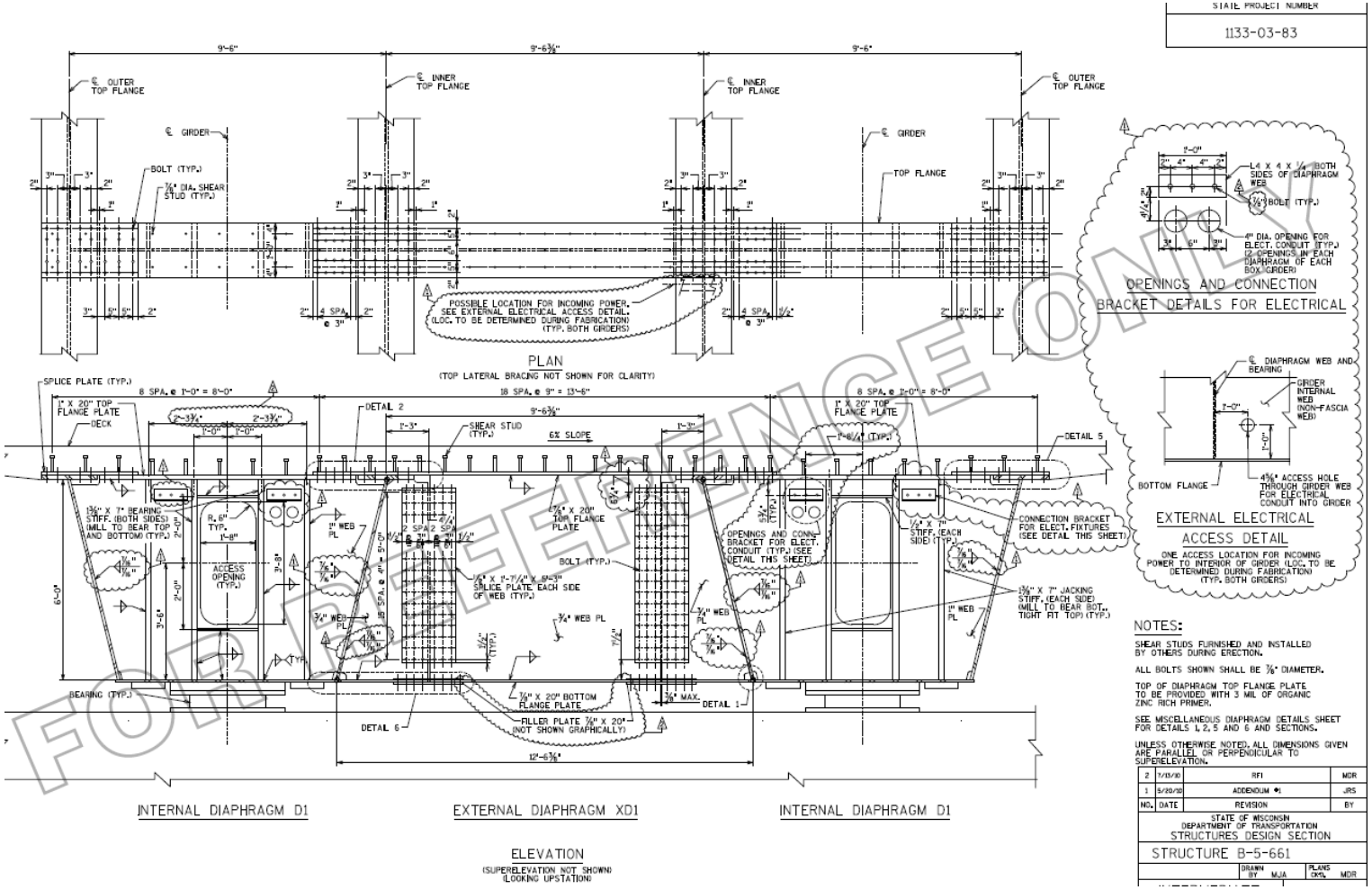

Figure 168 Bridge B05-661 intermediate diaphragm details from URS (2010) [38]

8.2 Expected Failure Mode of Analyzed Bridges

Additional analyses were also performed for B05-661 and B40-834 with higher live load factors in order to investigate the expected failure mode that would result in collapse. Generally, twin-tub-girder bridges designed in the state of Wisconsin have non-compact or slender bottom flanges in the negative moment region. Hence, in the faulted state, these flanges would be expected to buckle before the average stress in the flange reaches the yield strength. For both bridges at elevated live loads, the observed failure mode is local bottom flange buckling followed by web shear buckling at the pier in the fractured girder (shown in Figure 169 and Figure 170).

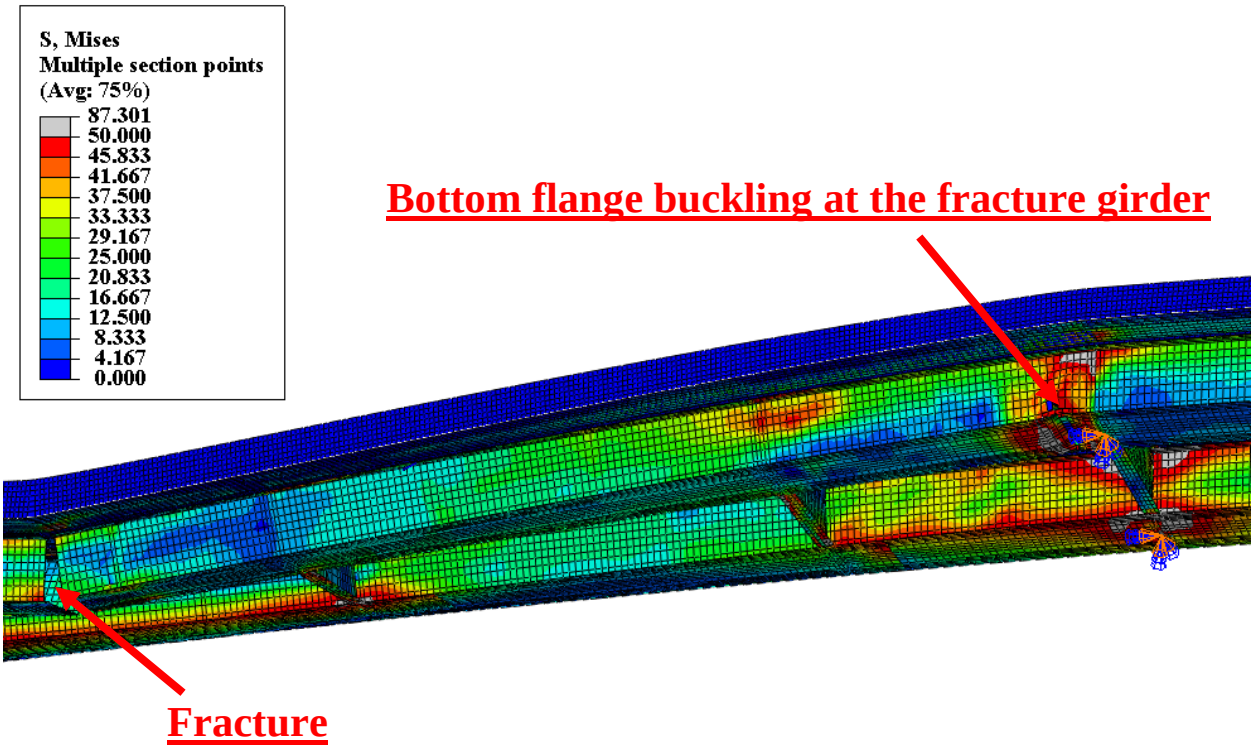

Figure 169 Fractured girder local bottom flange buckling next to pier (B05-661)

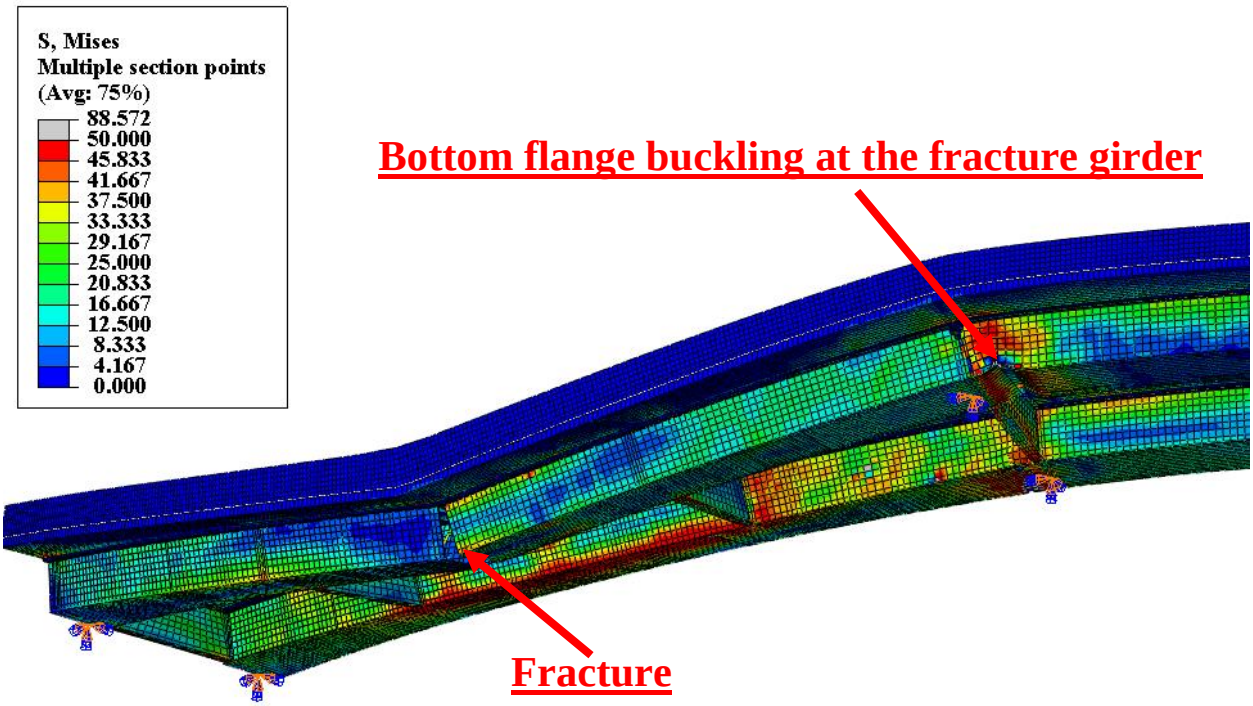

Figure 170 Fractured girder local bottom flange buckling next to pier (B40-834)

The design local buckling capacities and design stresses were also compared at the pier. For bridge B05-661, the local buckling capacity shown in the design plans (Highway Structures Information System (HSI) [38]) is 45.2 ksi in compression whereas, the design stress is 41.3 ksi in compression. The ratio of the design stress over the capacity is 0.91. On the other hand, for the bridge B40-834, the local buckling capacity and the design stress shown on the plans (Highway Structures Information System (HSI) [44]) are 39.7 and 30.4 in compression respectively, and the ratio is 0.79. A similar analysis, in which the live load was increased, was performed for B05-661. The total load and displacement at the fracture location were also compared for B05-661 in Figure 171 and B40-834 in Figure 172. The figures show the load-displacement behavior after the bridge fractured but before live load was applied on the bridges. Only HL-93 live loads are demonstrated in the curves. For the B05-661 bridge, the maximum live load capacity is 46% more than Redundancy II live load. For the B40-834 bridge, the maximum live load capacity is 150% more than Redundancy II live load.

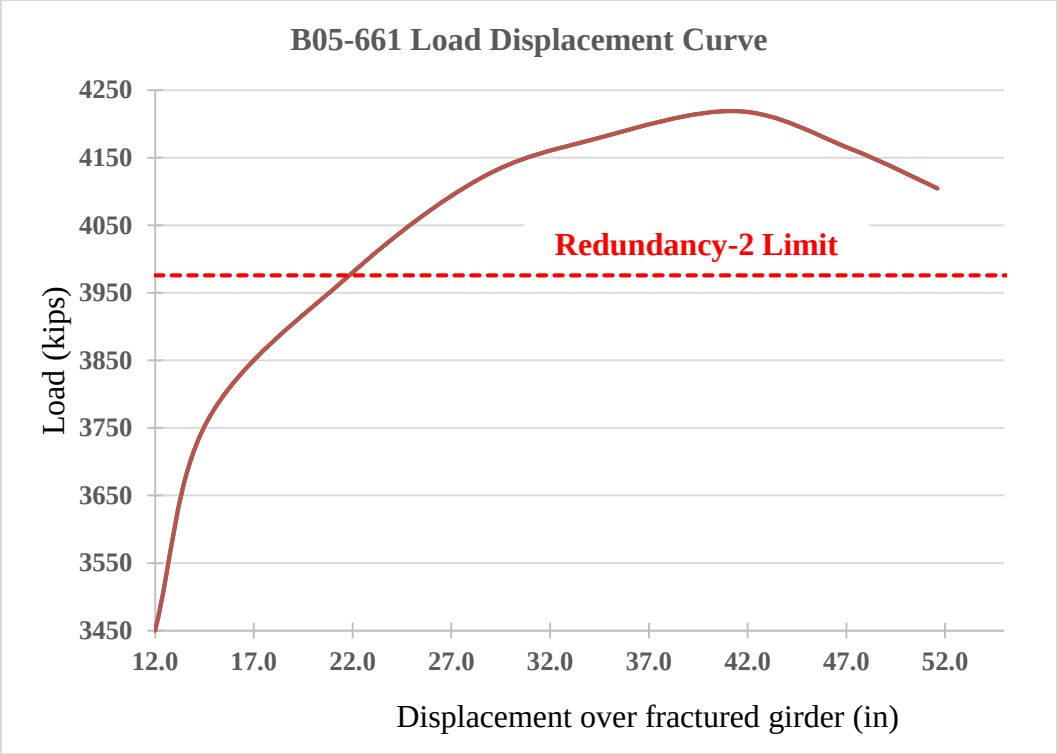

Figure 171 Load displacement curve of B05-661 up to the buckling

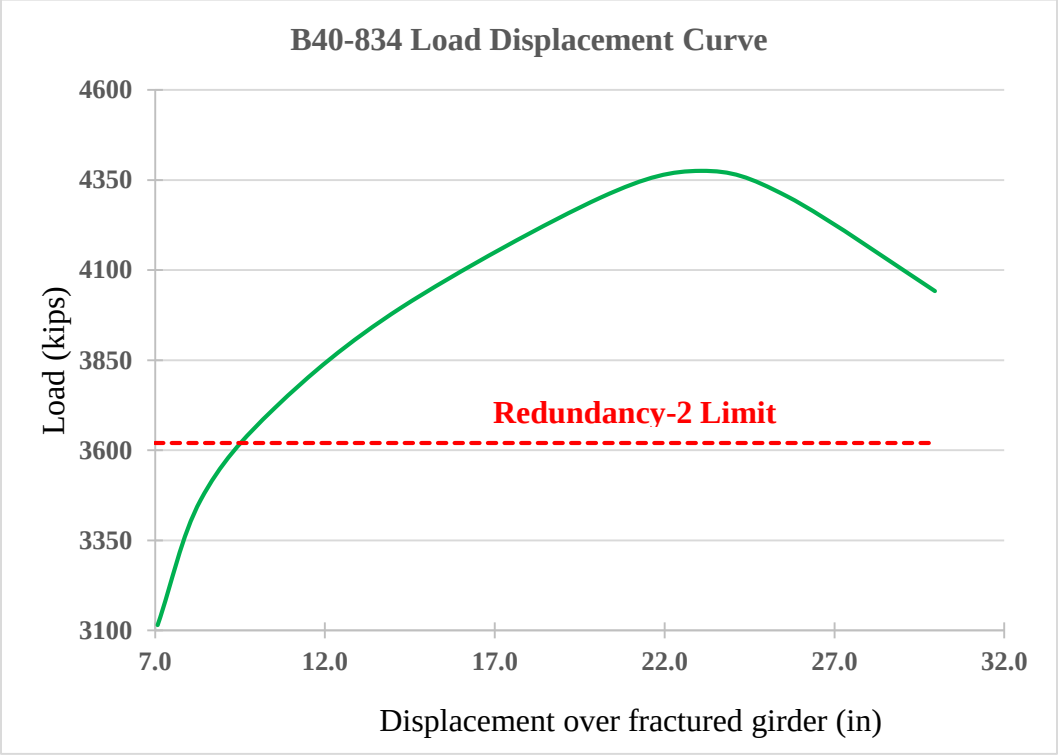

Figure 172 Load displacement curve of B40-834 up to the buckling

In this dissertation, additional analysis to maximize the negative moment over the pier was also performed in accord with AASHTO LRFD [13]. For this loading, the span adjacent to fractured span was also loaded with 90% of HL-93 in Redundancy II load combination (as shown in Figure 173).

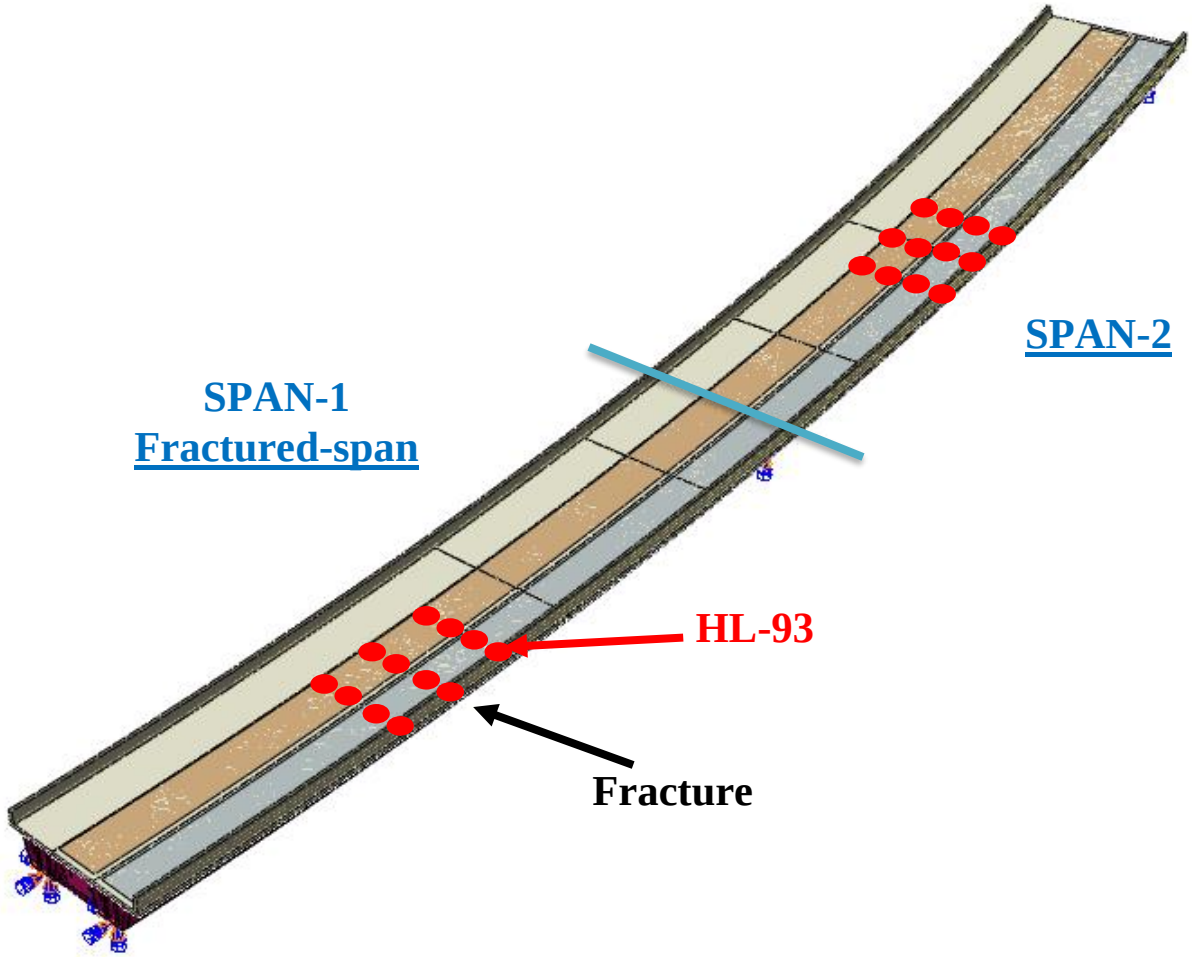

Figure 173 General Isometric View of B05-661

The local buckling capacities, the longitudinal stresses from design calculations, and the maximum nominal longitudinal stresses from the FEA were compared at the center of the bottom flange of the fractured girder at the pier (shown in Table 114) and at the bottom splice closest to the pier (shown in Table 115). According to Table 115, at the pier, the longitudinal stresses in the design calculations are always higher than FEA stresses; hence, local bottom flange buckling at the pier is unlikely in the faulted state. The main reason for this is that the negative moments generated in strength design is greater than those produced during the redundancy analysis. However, as shown

in Table 115, at the bottom flange thickness transition closest to the pier, some longitudinal stresses in the design calculations are slightly lower than those predicted FEA stresses. At the bottom flange splices, the thickness of the bottom flange generally changes. Due to this section change, the maximum stress in the FEA can be higher than the calculated buckling capacity because the thicker plate constrains the thinner plate. This is typically ignored in the calculation of the buckling capacity as most designers conservatively assume the thinner plate extends the past this region. In addition, non-uniform stresses in the bottom flange section and the contribution of the web stiffeners are other constraints which increase the actual local buckling capacities but are not accounted for in the design capacity calculations. Therefore, it is also unlikely to have the local bottom flange buckling at the bottom splice in the faulted state.

Table 114 Local buckling capacities and longitudinal stresses at the bottom flange at the pier

Bridge	**Units**	**Local Flange Buckling Capacities (ksi) from HSI Design Plans**	**Design Compression Stresses (ksi) from HSI Design Plans**	**Compression Stresses (ksi) From FEA (After Fracture)**
B05-658	Unit-1 Unit-2	40.9 47.2	37.8 44.3	29.5 35.0
B05-661	-	45.2	41.1	35.4
B40-868	-	43.2	36.8	35.5

Table 115 Local buckling capacities and longitudinal stresses at the bottom flange at the bottom section change location closest to the pier

Bridge	**Units**	**Local Flange Buckling Capacities (ksi) from HSI Design Plans**	**Design Compression Stresses (ksi) from HSI Design Plans**	**Compression Stresses (ksi) From FEA (After Fracture)**
B05-658	Unit-1 Unit-2	26.9 37.3	26.7 35.8	20.0 30.9
B05-661	-	27.3	24.8	25.6
B40-834	-	35.9	28.6	32.8

8.3 Impact of Results to Future Designs

The intermediate diaphragms commonly used by WisDOT provide additional load paths and prevent many failure modes. If similar intermediate diaphragms are provided, in the faulted state, the expected failure mode is local flange buckling in the negative moment region before the average stress in the flange reaches the yield strength. The results of analyzing a large family of WisDOT bridges suggests that the design characteristics for intermediate diaphragms and local buckling presently used by WisDOT appear to ensure adequate behavior in the faulted state. In other words, while there were no specific design criteria used for the design of the diaphragms and buckling in the faulted state, the designs which have been evaluated have sufficient reserve strength in the faulted state. Thus, it seems reasonable that for future designs, if one were to stay within the "box" of design characteristics (i.e., geometry, number of lanes, spans, etc.) currently used by WisDOT and utilized the same design philosophies, one would expect a bridge to meet the NCHRP 12-87a [5] criteria should a full system analysis be performed.

The basic design characteristics of the WisDOT bridges analyzed to date are as follows:

1) End span length is between 100 ft. and 210 ft.,
2) Number of traffic lanes is one or two,
3) Web height is from 60 in. to 86 in.,
4) Girder spacing between the center of the bottom flanges is from 16ft. to 25 ft.,
5) Girder spacing between the center of the interior top flanges is from 8 ft. to 13.875 ft.
6) Maximum span length ratio for two spans is 0.8.
7) Maximum recommended ratio of end spans over adjacent span for more than two span bridges is 1.0.
8) Maximum ratio of radius over the end span length is 0.54.
9) Average shear stud configuration:
    a. 6 in. high, spaced 12 in. longitudinally and spaced equally in the transverse direction.
    b. 7 in. high, spaced 14 in. longitudinally and spaced equally in the transverse direction.
    c. 8 in. high, spaced 16 in. longitudinally and spaced equally in the transverse direction.

As stated, the intermediate diaphragms commonly used by WisDOT provide additional load paths and prevent many failure modes. At present, there are no standard design criteria for the design of the typical WisDOT intermediate diaphragms. However, the analyzed bridges for WisDOT utilize "typical" and similar diaphragm details. Two or three intermediate diaphragms were used for the end spans. In general, two intermediate diaphragms were used in end spans under 120 ft., while three diaphragms were used in end spans longer than 120 ft. For more than 80% of these bridges, the first intermediate diaphragm was located no more than 30% of its end span length (L) and no more than 40 ft. Bridges that had a maximum dead load displacement before-fracture of no more than L/500 did not experience plasticity in the first intermediate diaphragm. Details of the typical diaphragm sizes used in the bridges analyzed are shown in Table 116.

Table 116 Typical diaphragm sizes from WisDOT bridges

Web Height (inch)	**Thickness (inch)**	**Flange sizes (inch x inch)**
84	0.75	20x1
72	0.625	16x1
60	0.5	16x3/4

If intermediate diaphragms with similar design characteristics are provided, the next expected failure mode will be the local bottom flange buckling with higher live load factors. However as shown in Table 114 and Table 115, the Redundancy I and Redundancy II load factors result in lower longitudinal stresses at the pier in the faulted state than shown in the design plans at pier in the unfaulted for Strength I or Strength II. Therefore, local bottom flange buckling is believed to be highly unlikely in the faulted state for the Redundancy load combinations. As a result, one can just assume that continuous composite twin-tub-girder bridges with full depth intermediate diaphragms which have similar design features noted above as WisDOT bridges may not need to be classified as having fracture critical members in future designs.

CHAPTER 9 CONCLUSION AND RECOMMENDATIONS

Today (2018), all twin-tub-girder bridges are automatically classified as having FCMs; hence, twin-tub-girder bridges are subjected to very expensive hands-on field inspection every two years. Furthermore, in the US, there are more than 500 twin-tub-girder bridges as of 2017 from the NBI database [6].

In this dissertation, a calibrated FE methodology was developed to investigate the response of the twin-tub-girder bridges for the case where one of the two tub girders fails due to brittle fracture. Throughout this study, a comprehensive shear stud damage FE modeling methodology was developed; and a simplified guidance was provided to estimate the shear stud strength, stiffness, and ductility and to apply shear stud damage behavior in the large bridge FE models.

Twenty-one (21) multi-span twin-tub-girder bridge units from the existing inventory of the Wisconsin Department of Transportation (WisDOT) and three other simple span representative designs were analyzed to evaluate if the steel tub girders could be classified as System Redundant Members (SRMs). The load models and the failure criteria described in NCHRP Project 12-87a [5] were utilized for this evaluation process. All bridges analyzed from WisDOT inventory possess considerable reserve strength in the faulted state and therefore the steel tub girders do not meet the definition of a fracture critical member. All WisDOT bridges have multiple full-depth intermediate diaphragms and continuous spans. These features provide additional load paths and help to make the bridges redundant thereby avoiding many failure modes which simple span bridges and bridges without full depth intermediate diaphragms commonly experience. None of the simple span bridges analyzed had sufficient reserve capacity in the faulted state.

The full-depth intermediate diaphragms used by WisDOT also appear to reduce the likelihood of shear stud failures, parapet crushing, deck reinforcement yielding, lateral brace failing, and torsional buckling in the intact girders. Although some of the WisDOT bridges exhibited minor plasticity in the flanges of the intermediate diaphragms and a few shear stud failures, the level of plasticity is localized and number of failed studs is not significant.

Additional analyses were also performed for two bridges with higher load factors (i.e., higher than proposed in NCHRP 12-87a [5]) in order to investigate the expected failure mode. For both bridges, the observed failure mode was local bottom flange buckling followed by web shear buckling in the fractured girder. However, in the faulted state, the Redundancy I and Redundancy II load factors result in lower longitudinal stresses in the negative moment region than the stresses shown in the design plans in the unfaulted condition for Strength I or Strength II.

The results also indicated that in general, bridges designed using the approaches specified by WisDOT, including the use of continuous spans and full-depth intermediate diaphragms may not need to be classified as having FCMs. The characteristics of the bridges considered were summarized in this study; hence, if met, one would have a very high confidence that the structure would satisfy the performance requirements of NCHRP 12-87a [5]. These characteristics include overall geometric limits, detailing and locating intermediate diaphragms, shear stud configurations, pre-fracture dead load displacement, and geometric limits for specific bridge components.

9.1 Recommendation for Future Work

The simple guidance in this dissertation is believed to be sufficient to classify continuous composite twin-tub-girder bridges which have similar features with WisDOT bridges described above as having SRMs. Therefore, there is no need for detailed 3D nonlinear FEA. However, there is no guidance to improve after-fracture system performance for the bridges without intermediate diaphragms. Simplified design criteria can possibly be developed to show that a given continuous twin-tub-girder bridge without intermediate diaphragms need not be classified as having FCMs. By following FE methodology developed in this dissertation, it may be possible to develop basic design rules and guidance on performing a few simple additional checks to show that a twin-tub-girder without diaphragms is not an FCM without the need to perform full 3D nonlinear FEA.

Furthermore, WisDOT routinely utilized full-depth and full-width diaphragms in all of their twin-tub-girder bridges. These diaphragms were shown to be very effective in transferring load in the faulted condition and significantly contributed to the excellent system performance of the bridges in the Wisconsin inventory. However, there is no specific guidance on how to design the

diaphragms to ensure the desired performance in the faulted state. Thus, a simple design methodology for the diaphragms can be developed in a future project for the bridges which would not fall within the typical parameters of the WisDOT bridges which were analyzed. For example, bridges with longer spans and wider decks.

As was discussed above regarding simple span bridges, simply adding diaphragms does not in itself guarantee the bridge will possess adequate strength in the faulted state, as was shown by the two simple span cases studies. Thus, it is recommended that future work, specifically focused on improving the load redistribution characteristics of simply span bridges be performed.

Properly designed and detailed studs have also been shown to be critical in the after-fracture performance of twin-tub-girder bridges. Although the diaphragm typically used by WisDOT generally prevent issues with shear stud concrete break-out, specific guidance on how to best detail and layout shears studs can be studied in a future project.

REFERENCES

[1] Connor, R. J., Dexter, R., and Mahmoud, H. (2005). *Inspection and management of bridges with fracture-critical details*. NCHRP Synthesis 354, National Academy Press, Washington, DC.

[2] Connor, R. J., Kaufmann, E. J., Fisher, J. W., and Wright,W. J. (2007). *Prevention and mitigation strategies to address recent brittle fractures in steel bridges.* J. Bridge Eng., 10.1061/(ASCE)1084-0702(2007) 12:2(164), 164–173.

[3] Neuman, B. J. (2009). *Evaluating the redundancy of steel bridges: Full scale destructive testing of a fracture critical twin box-girder steel bridge.* M.S. thesis, Univ. of Texas at Austin, Austin, TX.

[4] Diggelmann, L. M., Connor, R. J., & Sherman, R. J., (2013) *Evaluation of member and load-path redundancy on the US-421 bridge over the Ohio River*, FHWA Publication No. FHWA-HRT-13-104

[5] Connor, R. J., Bonachera M., F. J., Varma, A. H., Lai, Z., & Korkmaz, C. (2017). *Fracture-critical system analysis for steel bridges (NCHRP Project 12-87a).* Washington, D.C.: Transportation Research Board.

[6] National Bridge Inventory (NBI) Database. Retrieved September 9, 2017, from https://www.fhwa.dot.gov/bridge/nbi.cfm.

[7] *Recording and Coding Guide for the Structure Inventory and Appraisal of the Nation's Bridges.* (1995). Report No. FHWA-PD-96-001. Office of Engineering Bridge Division Bridge Management Branch Washington, D.C.

[8] Milwaukee Transportation Partners (2005). *Redundancy of Box Girder Steel Bridges—A Study for the Marquette Interchange HPS Twin Box Girder Structures.* Project ID 1060-05-1222.

[9] Highway Structures Information System (HSI) Retrieved January 18, 2018, from https://www.fhwa.dot.gov/bridge/nbi.cfm.

[10] Connor, R. J., & Korkmaz, C. (2016). *Evaluation of the Fracture Critical Status of Ramp TH over Interstate 43/894 in Milwaukee, Wisconsin.* Purdue University S-BRITE Center

[11] American Concrete Institute (ACI) Committee 318. (2014). *Building code requirements for structural concrete and commentary.* ACI 318-14 and ACI 318R-14, Farmington Hills, MI.

[12] Mouras, J. M., Sutton, J. P., Frank, K. H., and Williamson,E. B. (2008). *The tensile capacity of welded shear studs.* Univ. of Texas at Austin, Austin, TX.

[13] AASHTO. (2014). *AASHTO LRFD Bridge Design Specifications*. American Association of State Highway and Transportation Officials, Washington, DC.

[14] Cooper, J. D., (2001). *Hoan Bridge failure investigation*, Federal Highway Administration

[15] Hunley, C. A. (2008). *Structural redundancy of twin steel box girder bridges*. Ph.D. dissertation, University of Kentucky.

[16] Ghosn, M., and Moses, F., (1988). *Redundancy in Highway Bridge Superstructures, NCHRP Report 406*. National Cooperative Highway Research Program, 1988.

[17] Kim, J., & Williamson, E. B. (2015). *Finite-Element Modeling of Twin Steel Box-Girder Bridges for Redundancy Evaluation*. J. Bridge Eng. Journal of Bridge Engineering, 20(10), 04014106. doi:10.1061/(asce)be.1943-5592.0000706

[18] Bonachera M., F. J. (2016). *FEA methodology for system level redundancy evaluation: application to non-composite steel bridges.* Dissertation, Purdue University, West Lafayette, IN.

[19] Bernard, T., Hovell, C. G., Sutton, P. J., Mouras, J. M., Neuman, B. J., Samaras, V. A., Kim, J., Williamson, E. B., & Frank, K. H., (2010). *Modeling the Response of Fracture Critical Steel Box-Girder Bridges*. Report No. FHWA/TX-10/9-5498-1, Texas Department of Transportation

[20] Popovics, S. (1973). A numerical approach to the complete stress-strain curve of concrete. *Cement and Concrete Research*, 583-599.

[21] Hillerborg, A., Modéer, M., & Petersson, P. (1976). *Analysis of crack formation and crack growth in concrete by means of fracture mechanics and finite elements*. Cement and Concrete Research,6(6), 773-781. doi:10.1016/0008-8846(76)90007-7

[22] *Model code 2010: final draft.* (2012). Lausanne, Switzerland: International Federation for Structural Concrete (fib).

[23] Genikomsou, A. S., and Polak, M. A. (2015). *Finite element analysis of punching shear of concrete slabs using damaged plasticity model in ABAQUS*. Engineering Structures, 98, 38-48. doi:10.1016/j.engstruct.2015.04.016

[24] *Abaqus 2017 Documentation*. (2016) Velizy-Villacoublay, France: Dassault Systemes.

[25] Lubliner,J., Oliver, J., Oller, S., and Oñate, E., (1989) "A Plastic-Damage Model for Concrete," International Journal of Solids and Structures, vol. 25, no.3, pp. 229–326.

[26] Wang, W. (2013). *A study of stiffness of steel bridge cross frames (PhD Dissertation).* Austin, TX: The University of Texas at Austin.

[27] *Eurocode 3: design of steel structures.* (2005). Brussels, Belgium: European Committee for Standardization.

[28] Ocel, J. M. (2013). *Guidelines for the load and resistance factor design and rating of riveted and bolted gusset-plate connections for steel bridges (NCHRP Report 12-84).* Washington, D.C.: Transportation Research Board.

[29] ACI, "Committee 355 ACI UT IWB Tension Database for Cast-in and Expansion Anchors." Retrieved May 2017.

[30] Ollgaard, J. G., Slutter, R. G., & Fisher, J. W. (1971). *Shear strength of stud connectors in lightweight.* Bethlehem, PA: Fritz Laboratory Reports, Lehigh University.

[31] Lai, Z., Varma, A. H., & Zhang, K. (2014). *Noncompact and slender rectangular CFT members: Experimental database, analysis, and design*. Journal of Constructional Steel Research, 101, 455-468. doi:10.1016/j.jcsr.2014.06.004

[32] Fuchs, W., Eligehausen, R., Breen, J. (1995). *Concrete Capacity Design (CCD) Approach for Fastening to Concrete*. ACI Structural Journal. Vol 92, No. 1, pp 73-94.

[33] Eligehausen, R., Bouska, P., Cervanka, V., and Pukl, R., (1992). *Size Effect of the Concrete Cone Failure Load of Anchor Bolts*, In: Z.P. Bazant, (Editor), Fracture Mechanics of Concrete Structures, pp. 517-525.

[34] Bounds, W., (2010). *Design of Blast-Resistant Buildings in Petrochemical Facilities*, Reston: ASCE.

[35] Bode, H., and Roik, K., (1987). *Headed Studs-Embedded in Concrete and Loaded in Tension*. American Concrete Institute.

[36] HNTB, (2013). *Design Calculations for B-40-868: Ramp SL Over IH 94 and Ramp WS. State Project No: 1060-33-75.* from WisDOT Highway Structures Information System (HSI), Retrieved February 1, 2018, from https://www.fhwa.dot.gov/bridge/nbi.cfm.

[37] URS, (2009). *USH 41 Flyover Structures: USH 41 - STH 29 Interchange Design Calculations for Structure No. B-5-658 Project No: 25688353.* from WisDOT Highway Structures Information System (HSI), Retrieved February 1, 2018, from https://www.fhwa.dot.gov/bridge/nbi.cfm.

[38] URS, (2010). *WisDOT Project I.D. 1133-03-82 USH 41 Early Structure/Early Fill B-05-661: Design Computations.* from WisDOT Highway Structures Information System (HSI), Retrieved February 1, 2018, from https://www.fhwa.dot.gov/bridge/nbi.cfm.

[39] URS, (2011). *USH 41 Flyover Structures: USH 41 – IH 43 Interchange Design Calculations for Structure No. B-5-678 Project No: 25688353.* from WisDOT Highway Structures Information System (HSI), Retrieved February 1, 2018, from https://www.fhwa.dot.gov/bridge/nbi.cfm.

[40] URS, (2011). *USH 41 Flyover Structures: USH 41 – IH 43 Interchange Design Calculations for Structure No. B-5-679 Project No: 25688353.* from WisDOT Highway Structures Information System (HSI), Retrieved February 1, 2018, from https://www.fhwa.dot.gov/bridge/nbi.cfm.

[41] CH2MHILL, (2012). *Zoo IC - Watertown Plank Interchange: Watertown Plank Road Ramp WH over USH 45 B-40-776 Structure Calculations, State Project No: 1060-33-72.* from WisDOT Highway Structures Information System (HSI), Retrieved February 1, 2018, from https://www.fhwa.dot.gov/bridge/nbi.cfm.

[42] CH2MHILL, (2012). *Zoo IC - Watertown Plank Interchange: Watertown Plank Road Ramp WH over USH 45 B-40-783 Structure Calculations, State Project No: 1060-33-72.* from WisDOT Highway Structures Information System (HSI), Retrieved February 1, 2018, from https://www.fhwa.dot.gov/bridge/nbi.cfm.

[43] CH2MHILL, (2014). *Zoo IC - Core Phase 2: Ramp WS over Hank Aaron State Trail & Ramp GD B-40-786 Structure Computations, State Project No: 1060-33-81.* from WisDOT Highway Structures Information System (HSI), Retrieved February 1, 2018, from https://www.fhwa.dot.gov/bridge/nbi.cfm.

[44] CH2MHILL, (2009). *I-94 North-South Freeway: College AV to Howard AV State Project No: 1030-20-72, Structure Calculations for Ramp TF (S-W) over IH 43/894 Str. B-40-834.* from WisDOT Highway Structures Information System (HSI), Retrieved February 1, 2018, from https://www.fhwa.dot.gov/bridge/nbi.cfm.